



DEVELOPMENT OF ANDROGRAPHOLIDE ANALOGUE (3A.1)-LOADED
NANOCARRIERS AND 3A.1 NANOSUSPENSIONS FOR CANCER THERAPY



A Thesis Submitted in Partial Fulfillment of the Requirements
for Doctor of Philosophy (PHARMACEUTICAL TECHNOLOGY)
Department of PHARMACEUTICAL TECHNOLOGY
Graduate School, Silpakorn University

Academic Year 2020

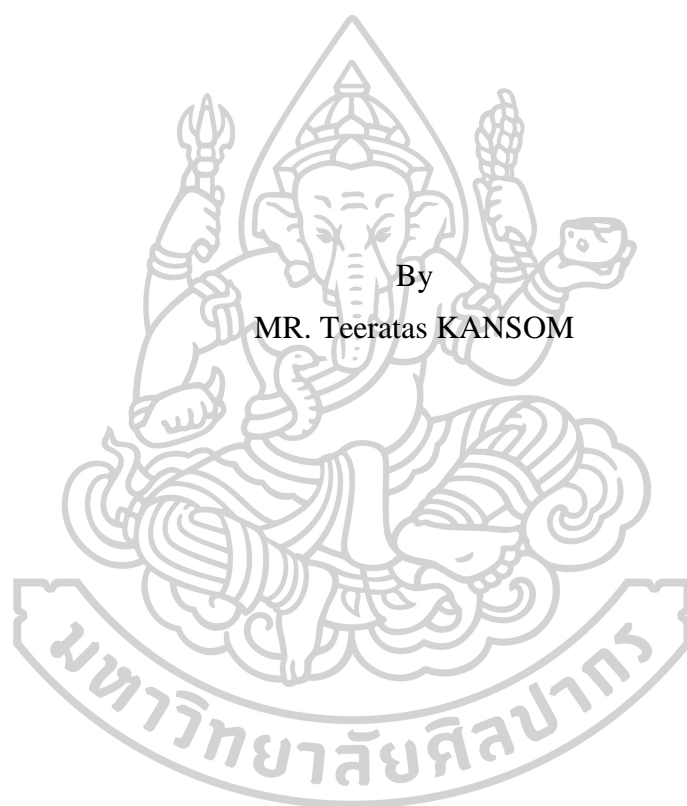
Copyright of Graduate School, Silpakorn University

การพัฒนาตัวพายาระดับนาโนบรรจุอนุพันธ์แอนโดรกราโฟไลต์ (3A.1) และยาแขวน
ตะกอนระดับนาโนของ 3A.1 เพื่อการรักษาโรคมะเร็ง



วิทยานิพนธ์นี้เป็นส่วนหนึ่งของการศึกษาตามหลักสูตรปรัชญาดุษฎีบัณฑิต
สาขาวิชาเทคโนโลยีเกษตรกรรม แบบ 1.2 ปรัชญาดุษฎีบัณฑิต
ภาควิชาเทคโนโลยีเกษตรกรรม
บัณฑิตวิทยาลัย มหาวิทยาลัยศิลปากร
ปีการศึกษา 2563
ลิขสิทธิ์ของบัณฑิตวิทยาลัย มหาวิทยาลัยศิลปากร

DEVELOPMENT OF ANDROGRAPHOLIDE ANALOGUE (3A.1)-
LOADED NANOCARRIERS AND 3A.1 NANOSUSPENSIONS FOR
CANCER THERAPY



By
MR. Teeratas KANSOM

A Thesis Submitted in Partial Fulfillment of the Requirements
for Doctor of Philosophy (PHARMACEUTICAL TECHNOLOGY)
Department of PHARMACEUTICAL TECHNOLOGY
Graduate School, Silpakorn University
Academic Year 2020
Copyright of Graduate School, Silpakorn University

Title Development of andrographolide analogue (3A.1)-loaded
nanocarriers and 3A.1 nanosuspensions for cancer therapy
By Teeratas KANSOM
Field of Study (PHARMACEUTICAL TECHNOLOGY)
Advisor Professor PRANEET OPANASOPIT , Ph.D.

Graduate School Silpakorn University in Partial Fulfillment of the
Requirements for the Doctor of Philosophy

.....Dean of graduate school
(Associate Professor Jurairat Nunthanid, Ph.D.)

Approved by

.....Chair person
(Associate Professor TANASAIT NGAWHIRUNPAT ,
Ph.D.)

.....Advisor
(Professor PRANEET OPANASOPIT , Ph.D.)

.....Co advisor
(Assistant Professor Prasopchai Patrojanasophon , Ph.D.)

.....Co advisor
(Associate Professor Arthit Chairoungdua , Ph.D.)

.....External Examiner
(Assistant Professor Rungnapha Saeeng , Ph.D.)

58353802 : Major (PHARMACEUTICAL TECHNOLOGY)

Keyword : Andrographolide analogue, Nanocarriers, Nanosuspensions, Cancer therapy

MR. TEERATAS KANSOM : DEVELOPMENT OF ANDROGRAPHOLIDE ANALOGUE (3A.1)-LOADED NANOCARRIERS AND 3A.1 NANOSUSPENSIONS FOR CANCER THERAPY THESIS ADVISOR : PROFESSOR PRANEET OPANASOPIT, Ph.D.

In this study, 19-*tert*-butylsilyldiphenyl-8,17-epoxy andrographolide (3A.1)-loaded nanocarriers and 3A.1 nanosuspensions were developed for improving its aqueous solubility and antitumor efficacy. First, the pH-sensitive amphiphilic chitosan derivatives, i.e. *N*-naphthyl-*N,O*-succinyl chitosan (NSC), *N*-octyl-*N,O*-succinyl chitosan (OSC), *N*-benzyl-*N,O*-succinyl chitosan (BSC) and folate-conjugated NSC (Fol-NSC), were synthesized and were formulated polymeric micelles (PMs) for 3A.1 incorporation. The influence of entrapment methods, hydrophobic parts of copolymers, and initial amount of drug on physicochemical characteristics were investigated. Second, 3A.1 was entrapped into liposomes (LPs) including LPs and PEGylated LPs. The effect of lipid components and initial amount of drug on physicochemical properties was studied. Third, 3A.1 nanosuspensions (NSs) were fabricated by an anti-solvent technique, using NSC, OSC, and BSC as surface stabilizers. The effect of drug to polymer ratios and types of stabilizer on physicochemical properties was observed. The 3A.1-loaded PMs based on CS derivatives at 40%wt to polymer, prepared by dropping method provided the highest value of % entrapment efficiency (%EE) and loading capacity (LC). These PMs were in nanometer scale (<200 nm) and had spherical shape with highly negative charge. The release behaviors of 3A.1 from 3A.1-loaded PMs displayed a delayed release. The 3A.1-loaded LPs and PEGylated LPs showed the maximum values of %EE and LC at the initial drug content of 3.0 mmol. These LPs had vesicle size in nanometer range (<150 nm) with spherical shape and mildly negative charge. The release profile of PEGylated LPs was slower than that of LPs and drug solution. The 3A.1-NSs at an optimal drug to polymer ratio of 1.5:1 w/w had spherical shape with particle size in a nanoscale (<500 nm) with negative charge. To keep physical and chemical stability at least 6 months, the 3A.1-loaded PMs, 3A.1-loaded LPs, and 3A.1-NSs were stored at 4°C. The 3A.1-loaded PMs, LPs, and 3A.1-NSs showed a significant increase in the anticancer activity against colorectal cancer (CRC) cells with dose- and time-dependent manners, compared to free drug. In addition, these nanocarriers induced CRC cell apoptosis. Interestingly, the Fol-NSC PMs entrapped 3A.1 had greater suppression of cancer growth than the unconjugated NSC PMs due to enhancing cellular uptake via receptor-mediated endocytosis. The *in vitro* cell migration showed that free 3A.1 and both 3A.1-loaded PMs and LPs inhibited cell motility in CRC and oral cancer cells, compared with untreated cells. Moreover, the *in vivo* antitumor efficacy indicated that the effective 3A.1 dose of 40 mg/kg/day in group of 3A.1-NSs yielded higher inhibition of tumor growth rate and lower toxicity than that of free drug solution and blank NSs. Therefore, these nanocarriers and nanosuspensions could be great potential as drug delivery of 3A.1 for cancer treatment.

ACKNOWLEDGEMENTS

It would not be possible to accomplish this thesis dissertation without the helpful support from every people around me. First and foremost, I would like to express the deepest appreciation to my supervisor, Prof. Dr. Praneet Opanasopit for her excellent guidance, encouragement, motivation, patient, and providing me with warm atmosphere for doing research. I also would like to express my gratitude to my co-advisors, Assoc. Prof. Dr. Arthit Chairoungdua and Asst. Prof. Dr. Prasopchai Patrojanasophon for valuable advice, support, and kindness throughout the course of this research.

I wish to acknowledge my thesis committees, Assoc. Prof. Dr. Tanasait Ngawhirunpat and Asst. Prof. Dr. Rungnapha Saeeng for valuable time, insightful comments and suggestions, but also for the hidden issues which inspired me to think from various viewpoints.

My special appreciation goes to Dr. Waruyuth Sajomsang, National Nanotechnology Center (NANOTEC), National Science and Technology Development Agency (NSTDA) for kind giving me the amphiphilic chitosan derivatives used in this research, Asst. Prof. Dr. Rungnapha Saeeng, Faculty of Science, Burapha University for synthesis of 3A.1 analogue, and Dr. Somrudee Reabroi, Faculty of Science, Mahidol University for training me throughout doing *in vivo* testing.

I would like to give special thanks to members of the Pharmaceutical Development of Green Innovation Group (PDGIG) for good cooperation and course of friendship, especially Mrs. Areerut Sripattanaporn, for good laboratory technique and support. I would like to extend my special thanks to Assoc. Prof. Dr. Sunhapas Soodvilai and Asst. Prof. Dr. Sirima Soodvilai for their laboratory support at Research Center of Transport Protein for Medical Innovation, Faculty of Science, Mahidol University for training me to achieve part of cell culture.

In addition, I would like to recognize the generous assistance throughout my project provided by laboratory technician and staff at the Faculty of Pharmacy, Silpakorn University. I also would like to thank Graduate Affairs, Faculty of Pharmacy, Silpakorn University and Graduate School of Silpakorn University for all registration and examination process during my Ph.D program.

In particular, I wish to express thankfulness to the Commission of Higher Education (Thailand), the Thailand Research Sciences and Innovation (TSRI) through the Royal Golden Jubilee Ph.D. program (Grant No. PHD/0077/2558) and the International Research Network (IRN58W0004) as well as Faculty of Pharmacy, Silpakorn University for facility support, scientifically instrumental support and partial financial support.

I would like to express my gratitude to Prof. Dr. Robert D. Arnold, for giving me a great opportunity to conduct a research at Department of Drug Discovery and Development, Harrison School of Pharmacy, Auburn University, Alabama, USA. He gave the excellent ideas, precious suggestion and supported me everything in USA. I also would like to express my sincere appreciation to Dr. Tarawsi Mitra Ghosh and Dr. Suman Mazumder for excellent guidance and laboratory technique, Arnold's lab members for their helping and caring during my living in USA.

I cannot forget to thank my friends for all the unconditional support and encouragement which push me to pass the tough situations.

Last but not the least, I would like to express the deepest gratefulness to my parents, my family and my relatives for their spiritual support, beautiful smile, understanding and believing in me.

For any mistake or inadequate information that may still in this dissertation, certainly, I sincerely apologize for these points and the responsibility is entirely my own.

Teeratas KANSOM

TABLE OF CONTENTS

	Page
ABSTRACT.....	D
ACKNOWLEDGEMENTS.....	E
TABLE OF CONTENTS.....	G
LIST OF TABLES.....	N
LIST OF FIGURES.....	P
LIST OF ABBREVIATIONS.....	1
CHAPTER 1 INTRODUCTION.....	5
1.1 Statement and significance of the research problem.....	5
1.2 Aims and objectives.....	9
1.3 The research hypothesis.....	10
CHAPTER 2 LITERATURE REVIEW.....	11
2.1 Cancer disease.....	11
2.1.1 Colorectal cancer (CRC).....	12
2.1.2 Treatment of CRC.....	13
2.2 Plant-based anticancer drugs.....	14
2.2.1 Andrographolide.....	15
2.2.2 Semi-synthetic andrographolide (3A.1 analogue).....	16
2.3 Nanocarriers for cancer therapy.....	18
2.4 Tumor targeting strategies.....	20
2.4.1 Passive targeting.....	20
2.4.2 Active targeting.....	21

2.5 Polymeric micelles (PMs)	24
2.5.1 Definition	24
2.5.2 Types of polymer used.....	27
2.5.3 Advantages and limitations	28
2.5.4 Methods for micelle preparation	29
2.5.5 Factor influencing the properties of PMs.....	31
2.5.6 Characterizations of micellar system	33
2.5.7 Application of PMs in cancer therapy	34
2.6 Liposomes (LPs).....	35
2.6.1 Definition	36
2.6.2 Basic components in liposomes	36
2.6.3 Advantages and limitations	39
2.6.4 Classification of liposomes	39
I. Conventional liposomes (First generation).....	40
II. Stealth liposomes or PEGylated liposomes (Second generation)	41
III. Ligand targeted liposome	42
IV. Stimuli-responsive liposomes.....	43
2.6.5 Methods for liposome preparation	44
2.6.6 Characterization of liposomes.....	47
2.6.7 Stability of liposomes	48
2.6.8 Application of LPs in cancer therapy.....	49

2.7 Nanosuspensions (NSs).....	52
2.7.1 Definition	54
2.7.2 Physicochemical properties of drug nanocrystals.....	55
2.7.3 Advantages and limitations.....	56
2.7.4 Methods for nanosuspension preparation	57
2.7.4.1 Top-down or disintegration method.....	57
2.7.4.2 Bottom-up or nanoprecipitation method.....	60
2.7.4.3 Combination technologies.....	61
2.7.5 Particle stabilization.....	62
2.7.6 Characterization of nanosuspensions.....	64
2.7.7 Stability of nanosuspensions.....	67
2.7.8 Application of NSs in cancer therapy	69
2.8 Chitosan (CS) and chitosan derivatives.....	73
CHAPTER 3 MATERIALS AND METHODS	76
3.1 Materials	76
3.1.1 Drugs and pharmaceutical excipients	76
3.1.2 Cell lines and culture reagents	77
3.1.3 Animal experiment	78
3.2 Equipments	79
3.3 Methods.....	83
3.3.1 Preparation of 3A.1-loaded polymeric micelles (PMs)	83
3.3.1.1 Dialysis method	83
3.3.1.2 O/W emulsion method.....	83
3.3.1.3 Dropping method.....	83

3.3.1.4 Evaporation and sonication method	83
3.3.2 Preparation of 3A.1-loaded liposomes (LPs).....	84
3.3.3 Preparation of 3A.1 nanosuspensions (NSs)	84
3.3.4 Entrapment efficiency and loading capacity of 3A.1-loaded PMs and LPs ...	85
3.3.5 Drug content of 3A.1 NSs	86
3.3.6 HPLC analysis	86
3.3.7 Characterization of 3A.1-loaded PMs, 3A.1-loaded LPs and 3A.1 NSs	87
3.3.7.1 pH	87
3.3.7.2 Morphology	87
3.3.7.3 Particle size, size distribution, and zeta potential	87
3.3.7.4 Other physicochemical properties of 3A.1 NSs	88
3.3.7.4.1 Reconstitution test	88
3.3.7.4.2 Differential scanning calorimetry (DSC)	88
3.3.7.4.3 Powder X-ray diffraction (PXRD)	88
3.3.7.4.4 Fourier transform infrared spectrophotometry (FT-IR).....	88
3.3.7.4.5 Saturation solubility.....	89
3.3.8 <i>In vitro</i> drug release study	89
3.3.8.1 3A.1-loaded PMs	89
3.3.8.2 3A.1-loaded LPs	89
3.3.9 Stability study	90
3.3.10 <i>In vitro</i> anticancer activity	90
3.3.11 Induction of cell apoptosis	91
3.3.12 <i>In vitro</i> cell migration	92
3.3.12.1 Scratch wound healing assay	92
3.3.12.2 Transwell migration assay (Boyden chamber)	92
3.3.13 <i>In vitro</i> cellular uptake	93
3.3.14 <i>In vivo</i> antitumor efficacy	94
3.3.14.1 Establishment of tumor xenograft models of CRC	94

3.3.14.2	Investigation of anticancer efficacy of the drug NSs compared with free 3A.1 in CRC xenograft models.....	96
3.3.15	Statistical analysis.....	98
CHAPTER 4	RESULTS AND DISCUSSION.....	99
4.1	Polymeric micelles with or without 3A.1 analogue.....	99
4.1.1	Effects of physical entrapment methods.....	99
4.1.2	Effects of initial 3A.1 and hydrophobic cores	103
4.1.2.1	Particle size and zeta potential	103
4.1.2.2	Micellar morphology	104
4.1.2.3	Entrapment efficiency and loading capacity	105
4.1.3	<i>In vitro</i> drug release.....	107
4.1.4	Short-term stability.....	108
4.1.5	<i>In vitro</i> anticancer activity.....	110
4.1.6	Induction of cell apoptosis.....	111
4.1.7	<i>In vitro</i> anti-migratory activity	113
4.1.8	<i>In vitro</i> cellular uptake.....	114
4.1.9	Folate-conjugated NSC polymeric micelles as a delivery system of 3A.1 for active tumor targeting.....	115
4.1.9.1	Preparation and physicochemical properties of 3A.1-loaded micelles.....	115
4.1.9.2	<i>In vitro</i> drug release.....	116
4.1.9.3	<i>In vitro</i> anticancer activity.....	117
4.1.9.4	Induction of cell apoptosis	118
4.2	Formulation screening of liposomes with or without 3A.1 analogue.....	119
4.2.1	Effect of initial drug molar ratios	120
4.2.1.1	Particle size and zeta potential	120
4.2.1.2	Drug loading capacity	123
4.2.1.3	Visual appearance.....	123
4.2.1.4	Morphology	124
4.2.2	<i>In vitro</i> drug release.....	125
4.2.3	Short-term stability	126

4.2.4 <i>In vitro</i> anticancer activity	128
4.2.5 Induction of cell apoptosis	131
4.2.6 <i>In vitro</i> anti-migratory effect	133
4.2.6.1 Wound-healing assay	133
4.2.6.2 Transwell migration assay	134
4.3 Nanosuspensions with or without 3A.1 analogue.....	135
4.3.1 Effect of drug to polymer ratios and the hydrophobic parts of their polymers	136
4.3.1.1 Particle size and zeta potential	136
4.3.1.2 Drug content.....	139
4.3.1.3 Visual appearance.....	140
4.3.2 Comparison of the use of chitosan derivatives and surfactants	140
4.3.3 Reconstitution test	141
4.3.4 Morphological analysis.....	142
4.3.5 DSC.....	143
4.3.6 PXRD.....	145
4.3.7 FT-IR	145
4.3.8 Solubility.....	146
4.3.9 Short-term stability	147
4.3.10 <i>In vitro</i> anticancer activity	149
4.3.11 <i>In vivo</i> anticancer efficacy	151
4.3.11.1 Establishment of HCT116 tumor-bearing nude mice.....	151
4.3.11.2 <i>In vivo</i> antitumor efficacy of drug NSs	152
CHAPTER 5 CONCLUSION.....	155
5.1 Development of 3A.1-loaded polymeric micelles (PMs)	155
5.2 Development of 3A.1-loaded liposomes (LPs).....	155
5.3 Development of 3A.1 nanosuspensions (NSs).....	156
REFERENCES	157
APPENDIX.....	170

APPENDIX A..... 171
APPENDIX B 175
APPENDIX C 182
APPENDIX D..... 193
VITA..... 199



LIST OF TABLES

	Page
Table 1 Various tumor molecules and specific ligands for active targeting [96]	23
Table 2 Current clinical status of polymeric micelle formulations for intravenous administration [24,104].....	26
Table 3 Different methods for polymeric micelle characterization [105,106]	33
Table 4 Different methods for liposome preparation [145,147].....	46
Table 5 Different techniques for liposome characterization [145,147]	48
Table 6 List of marketed liposomal products used in cancer therapy [38,83].....	51
Table 7 Available marketed pharmaceutical nanosuspension products [170].....	72
Table 8 The physicochemical properties of 3A.1-loaded polymeric micelles with 20 wt% initial drug added (NSC, OSC, and BSC) prepared using four physical entrapment methods. Each value represents the mean \pm standard deviation from three independent experiments.	100
Table 9 The particle size, PDI, and zeta potential of 3A.1-loaded polymeric micelles prepared using the dropping method at the different drug to polymer weight ratios. All data represent the mean \pm standard deviation (n = 3).	101
Table 10 The effect of different pH of dispersion vehicle on particle size and zeta potential of 3A.1-loaded polymeric micelles with 40 wt% initial drug added prepared using the dropping method. All data represent the mean \pm standard deviation (n = 3).	102
Table 11 The physicochemical properties of 3A.1-loaded polymeric micelles with and without 40 wt% initial drug added (NSC vs. Folate-conjugated NSC) prepared using the dropping method. All data represent the mean \pm standard deviation (n = 3).....	102
Table 12 The influence of liposome formulations encapsulated different 3A.1 molar ratios on vesicle size, PDI and zeta potential, %encapsulation efficiency (%EE), and loading capacity (LC). All data represent the mean \pm standard deviation (n=3).....	121
Table 13 The IC ₅₀ values of free 3A.1, 3A.1-loaded Con LP and 3A.1-loaded 0.25-PEG LP against HCT116 and HT29 after 24- and 48-h treatment were determined using GraphPad Prism 5.01 software. Each value was derived from three different experiments in sextuplicate wells and reported as mean \pm standard error of mean (n=3). *, p<0.05 compared with free 3A.1 group; #, p<0.05 compared with 3A.1-loaded Con LP group.	130

Table 14 The influence of drug to stabilizers ratios on the particle size, PDI, and zeta potential of 3A.1 nanosuspensions prepared by a nanoprecipitation method. All data represent the mean \pm standard deviation (n=3).....	138
Table 15 The properties of 3A.1 nanosuspensions with and without cryoprotectant after the process of lyophilization.....	144
Table 16 The IC ₅₀ values of free 3A.1 and 3A.1 nanosuspensions against HCT116 after 24- and 48-h treatment were determined using GraphPad Prism 5.01 software. Each value was derived from three different experiments in sextuplicate wells and reported as mean \pm standard error of mean (n=3). *, p<0.05 compared with free 3A.1 group.	150



LIST OF FIGURES

	Page
Figure 1 Clinical stages of colorectal cancer growth according to the American Cancer Society; See more details in ref. [52,56]	13
Figure 2 Chemical structure of (a) andrographolide and (b) semi-synthetic andrographolide (3A.1). The illustration was written by ChemDraw Pro 12.0.....	15
Figure 3 Photograph of fresh herb of <i>A. paniculata</i> (Fah-Ta-Lai-Chon, Nakorn Pathom, Thailand).....	16
Figure 4 Schematic representation of numerous nanocarriers used in targeted drug delivery under preclinical and clinical development [83].....	18
Figure 5 Schematic illustration of NC-mediated drug delivery through systemic administration. After injecting nanocarriers into the body, these delivery systems carrying anticancer drugs should target at cancer site without rapid clearance by the immune system and then specific release drugs with sufficient concentration at the target site [85].	20
Figure 6 Schematic illustration of tumor-targeting approaches. (a) Passive targeting: transport drug NCs through defective and fenestrated blood vessels into the tumoral interstitium surrounding the solid tumors by convection and passive diffusion. Small molecules can freely move in and out of the tumor capillaries whereas drug-loaded NCs can retain at interstitial fluid without diffusion back into blood circulation due to their large size. (b) Active targeting: specific recognition process is involved with ligands attached at the carrier's surface selectively bind to receptor overexpressed at the target site (tumor cells or endothelial cells) via sufficient affinity. Adapted from ref. [91]	21
Figure 7 Structure of amphiphilic copolymer and polymeric micelles structure. Generally, linear diblock copolymers of A-B type or linear triblock copolymers (2 types of polymer, AB; 3 types of polymer, ABC) or non-linear/grafted copolymers are often used to design PMs. PMs are self-assembled by amphiphilic copolymers consisting of hydrophilic and hydrophobic parts at/or above critical micelle concentration (CMC) in aqueous solution. Adapted from ref. [24].....	25
Figure 8 Different physical entrapment methods for the preparation of drug-loaded polymeric micelle; (a) dialysis, (b) O/W emulsion followed by evaporation, (c) solvent casting, and (d) freeze-drying. Adapted from ref. [105]	29

Figure 9 Schematic presentation of the interaction among hydrophobic drugs, copolymers, and water molecules: (a) stronger hydrophilicity polymer (b) hydrophilic-hydrophobic balance (c) stronger hydrophobic polymer. Adapted from ref. [110]	32
Figure 10 Basic structure and classification of liposomes: small unilamellar vesicles (SUV), large unilamellar vesicles (LUV), and multilamellar vesicles (MLV). Adapted from ref. [122].....	36
Figure 11 Chemical structure of common liposomal lipid constituents: (a) phosphatidylcholine (b) cholesterol and (c) DSPE-PEG2000. The length and degree of saturation in the carbon chain can vary in each class of phospholipids. [128].....	38
Figure 12 Type of liposomes based on components in the formulation: (a) conventional liposomes are made of phospholipids, (b) PEGylated/stealth liposomes are composed of coating of polyethylene glycol at liposome surface, (c) targeted liposomes contain a specific targeting ligand to target cells at tumor environment, and (d) multifunctional liposomes. Adapted from ref. [37].....	40
Figure 13 Pictorial representation of liposome preparation by lipid thin-film hydration followed by vortex or manual stirring. Adapted from ref. [145].....	46
Figure 14 Schematic illustration of top-down techniques: wet ball milling and high-pressure homogenization. Adapted from ref. [170].....	58
Figure 15 Schematic illustration of bottom-up techniques. Adapted from ref. [170].	61
Figure 16 Chemical structure of chitin and chitosan. [193].....	73
Figure 17 Schematic diagram of synthesis of amphiphilic chitosan derivatives [28].	75
Figure 18 Protocol for CRC implantation in athymic nude mice	95
Figure 19 Protocol for drug treatments in athymic nude mice	96
Figure 20 TEM images of polymeric micelles prepared by dropping method: (a) blank NSC PMs, (b) 3A.1-loaded NSC PMs, (c) 3A.1-loaded OSC PMs, and (d) 3A.1-loaded BSC PMs. The scale bars in all images are 100 μm	105
Figure 21 Effects of the initial amount of drug added (5-40 wt% to polymer) on (a) the entrapment efficiency and (b) the loading capacity of 3A.1-loaded NSC PMs (\blacklozenge), 3A.1-loaded OSC PMs (\blacksquare), and 3A.1-loaded BSC PMs (\blacktriangle) prepared by a dropping method. Data are expressed as the mean \pm standard deviation (n= 3).....	106
Figure 22 In vitro release profiles of free 3A.1 (\times) and 3A.1-loaded polymeric micelles prepared by a dropping method; NSC (\blacklozenge), OSC (\blacksquare), and BSC (\blacktriangle), in simulated gastric fluid (SGF; pH 1.2, 0–2 h), simulated intestinal fluid (SIF; pH 6.8, 2–8 h) followed by simulated colonic fluid (SCF; pH 7.4, 8–12 h). These data are	

expressed as mean \pm standard deviation ($n = 3$). *Statistically significant difference compared with OSC PMs ($p < 0.05$); **Statistically significant difference compared with BSC PMs ($p < 0.05$)..... 108

Figure 23 The short-term stability of 3A.1-loaded polymeric micelles stored under long-term condition (left) compared with under accelerated condition (right) for 6 months; (a,d) particle size of NSC PMs (black bar), OSC PMs (dark gray bar), and BSC PMs (light gray bar); (b,e) zeta potential of NSC PMs (black bar), OSC PMs (dark gray bar), and BSC PMs (light gray bar); (c,f) the amount of 3A.1 remaining in NSC PMs (\blacklozenge), OSC PMs (\blacksquare), and BSC PMs (\blacktriangle). All data are presented as the mean \pm standard deviation ($n = 3$)..... 110

Figure 24 The percentage of cell viability (y-axis) of HT29 cells after being exposed to various concentrations of 3A.1-loaded polymeric micelles or free 3A.1 (x-axis) for 36-h treatment, and the IC₅₀ values ($\mu\text{g/mL}$) were included. 111

Figure 25 3A.1-loaded PMs induce HT29 cancer cell apoptosis examined by flow cytometry: (a) HT29 cells treated with 3A.1-loaded PMs, free 3A.1 (at the equivalent 3A.1 concentration of $3.8 \mu\text{g/mL}$), and Triton-X[®] for 24 h which are presented in four quadrants (Q) with dot plot. The number of necrosis cells, late apoptosis cells, early apoptosis cells, and living cells are displayed on Q1, Q2, Q4, and Q3, respectively. (b) Percentage of cell apoptosis rate of the cells after being treated with 3A.1-loaded PMs, free drug, and Triton-X[®]. *Statistically significant difference from free 3A.1 group ($p < 0.05$). 112

Figure 26 The anti-migratory effect of free 3A.1 and 3A.1-loaded PMs prepared by a dropping method on head and neck (HN22) cancer cells presented as the (a) wound images taken by a microscope ($40\times$ magnification) at 0 and 24 h, (b) cell migration rate and (c) % wound closure after 24-h treatment exposure. *Statistically significant difference from the untreated control group ($p < 0.05$); NS, no significantly different from free 3A.1 group ($p > 0.05$). 114

Figure 27 Fluorescent images of HT29 cells that were exposed to 40 wt% Dox-loaded NSC PMs, compared with free Dox for 12-h and 24-h treatment. The scale bars in all images are $200 \mu\text{m}$ 115

Figure 28 Drug uptake from 40 wt% Dox-loaded NSC PMs and free Dox in HT29 cells determined by flow cytometry; (a) histogram of fluorescent events and (b) mean fluorescent intensity of Dox. *Statistically significant difference compared with free Dox ($p < 0.05$)..... 115

Figure 29 TEM images of (a) 3A.1-loaded NSC PMs and (b) 3A.1-loaded Fol-NSC PMs prepared by a dropping method with drug loading of 40 %wt to polymer. The scale bars in all images are $100 \mu\text{m}$ 116

- Figure 30 In vitro release patterns of free 3A.1 (×) and 3A.1-loaded polymeric micelles prepared by a dropping method; NSC (◆) vs. Fol-NSC (●), in simulated gastrointestinal fluid. All data are expressed as mean ± standard deviation (n=3). *Statistically significant difference compared with NSC PMs (p<0.05)..... 117
- Figure 31 Dose-response curve of the 3A.1-loaded NSC PMs and the 3A.1-loaded Fol-NSC PMs against HT29 cancer cells for 36 h, compared with free 3A.1. Each bar graph is presented as the mean ± standard deviation (n = 3). 118
- Figure 32 Analysis of HT29 cell apoptosis by flow cytometry after treatment with 3A.1-loaded NSC PMs and Fol-NSC PMs at the equivalent 3A.1 concentration of 3.8 µg/mL for 24 h. (a) Fluorescent dot-plot and (b) rate of cell apoptosis. Data are presented as mean ± standard deviation (n=3). *, p<0.05 vs. free 3A.1 group; NS, no statistically significant difference vs. 3A.1-loaded NSC PMs..... 119
- Figure 33 The appearance of liposomal formulations prepared by a thin film hydration and probe-sonication method: (a) blank Con LP, (b) 3A.1-loaded Con LP, (c) blank PEG LP, and (d) 3A.1-loaded PEG LP 124
- Figure 34 TEM images of liposomal formulations prepared by a thin film hydration and probe-sonication method: (a) blank Con LP, (b) 3A.1-loaded Con LP, (c) blank PEG LP, and (d) 3A.1-loaded PEG LP. The scale bar in each image is equal to 100 nm. 125
- Figure 35 In vitro release profiles of 3A.1 from 3A.1 solution (×), 3A.1-loaded Con LP (◆), and 3A.1-loaded 0.25-PEG LP (▲) in PBS solution (pH 7.4) at 37°C for 24 h. *, p<0.05 compared to free drug; #, p<0.05 compared to Con LP. 126
- Figure 36 The short-term stability of 3A.1-loaded liposomes stored under long-term condition (left) compared to under accelerated condition (right) for 180 days: (a,d) vesicle size; (b,e) zeta potential of the 3A.1-loaded Con LP (black bar) and the 3A.1-loaded PEG LP (gray bar); (c,f) the relative drug remaining of the 3A.1-loaded Con LP (black line) and the 3A.1-loaded PEG LP (red line). All data are represented as the mean ± standard deviation (n=3). 128
- Figure 37 In vitro anticancer activity of 3A.1 solution (×), 3A.1-loaded Con LP (◆), and 3A.1-loaded PEG LP (▲) against HCT116 cell line for (a) 24 h and (b) 48 h and HT29 cell line for (c) 24 h and (d) 48 h. The data are shown as the mean ± standard deviation of three independent replicates. 131
- Figure 38 Apoptosis inductive effect of HCT116 cancer cells after treatment with free 3A.1 and 3A.1-loaded liposomes (at the equivalent 3A.1 concentration of 3.8 µg/mL) in vitro. (a) Flow cytometry analysis of dot plot in groups of control, free 3A.1, and 3A.1- encapsulated liposomes. (b) Percentage of cell apoptosis rate of HCT116 cells after being exposed to free 3A.1 and 3A.1-loaded liposomes for 24-h treatment. *,

$p < 0.05$ compared to free drug; NS, no statistically significant difference compared to free drug.....	132
Figure 39 Inhibition effect of free 3A.1 and 3A.1-loaded liposomes on cell migration of HN22 cancer cells was measured by scratch assay. (a) Photographs of wound area captured by an inverted microscope (40× magnification) at 0, 6, and 18 h. (b) Cell migration rate and (c) % wound closure after 18-h treatment in each experimental group. *, $p < 0.05$ compared to free drug; #, $p < 0.05$ compared to Con LP; NS, no statistically significant difference, compared to Con LP.	134
Figure 40 Anti-migratory effect of free 3A.1 and 3A.1-loaded liposomes on HCT116 cancer cells after 24-h incubation was investigated using a transwell migration assay. (a) Photographs of migrated cancer cells stained with the purple color of crystal violet in each treatment group under an inverted microscope. (b) The number of migrated cancer cells was counted and reported as the percentage of control. *Statistically significant difference ($p < 0.05$) compared to free drug; NS, no statistically significant difference compared to the Con LP.	135
Figure 41 Effects of the drug to stabilizer weight ratios on (a) 3A.1 concentration and (b) percentage yield of 3A.1 NSs stabilized by NSC (◆), OSC (■), and BSC (▲). Data are represented as the mean ± standard deviation (n=3).	139
Figure 42 The appearance of (a) 3A.1 coarse suspension without stabilizer and 3A.1 nanosuspensions stabilized by CS derivatives; (b) NSC, (c) OSC, and (d) BSC at a drug to polymer ratio of 1.5:1 (w/w)	140
Figure 43 TEM images of nanosuspensions with a drug to polymer ratio of 1.5:1 (w/w) prepared by a nanoprecipitation method: (a) 3A.1 NS-NSC, (b) 3A.1 NS-OSC and (c) 3A.1 NS-BSC. SEM images of (d) 3A.1 coarse powder and (e) freeze-dried 3A.1 NS-NSC powder.	142
Figure 44 (a) Differential scanning calorimetry (DSC) patterns and (b) X-ray diffraction (XRD) patterns of bulk 3A.1 powder, excipient of CS derivatives, physical mixtures of 3A.1/CS derivatives, and lyophilized 3A.1 NSs (1.5:1, w/w).....	143
Figure 45 Fourier transform infrared spectra of bulk 3A.1 powder, excipient of CS derivatives, physical mixtures of 3A.1/CS derivatives, and lyophilized 3A.1 NSs (1.5:1, w/w).....	146
Figure 46 Solubility data of bulk 3A.1 (striped bar) and 3A.1 NSs stabilized by NSC (black bar), OSC (dark gray bar), and BSC (light gray bar) in various types of solvent. All bar graphs are presented as the mean ± standard deviation (n=3). UP, undetectable peak of 3A.1 in HPLC chromatogram.	147

Figure 47 The short-term stability of 3A.1 nanosuspensions stored under long-term condition (left) compared to under-accelerated condition (right) for 6 months; (a,d) particle size; (b,e) zeta potential of 3A.1 NS-NSC (black bar), NS-OSC (gray bar) and NS-BSC (light gray bar); (c,f) the drug remaining of 3A.1 NS-NSC (◆), NS-OSC (■) and NS-BSC (▲). All data are expressed as the mean \pm standard deviation (n=3).

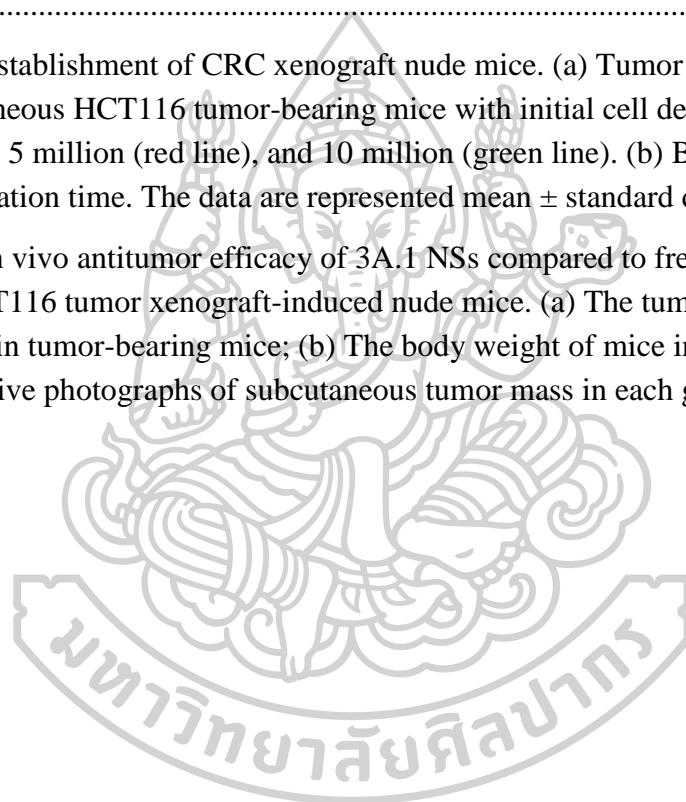
..... 149


Figure 48 In vitro anticancer activity of 3A.1 solution (×) and 3A.1 NS-NSC (◆), NS-OSC (■), and NS-BSC (▲) against HCT116 cell line for (a) 24 h and (b) 48 h. The data are shown as the mean \pm standard deviation of three independent replicates.

..... 151


Figure 49 Establishment of CRC xenograft nude mice. (a) Tumor growth curves of the subcutaneous HCT116 tumor-bearing mice with initial cell density of 1 million (black line), 5 million (red line), and 10 million (green line). (b) Body weight of mice over observation time. The data are represented mean \pm standard deviation (n = 2). 152

Figure 50 In vivo antitumor efficacy of 3A.1 NSs compared to free 3A.1 solution against HCT116 tumor xenograft-induced nude mice. (a) The tumor growth curves of each group in tumor-bearing mice; (b) The body weight of mice in each group; (c) Representative photographs of subcutaneous tumor mass in each group..... 154

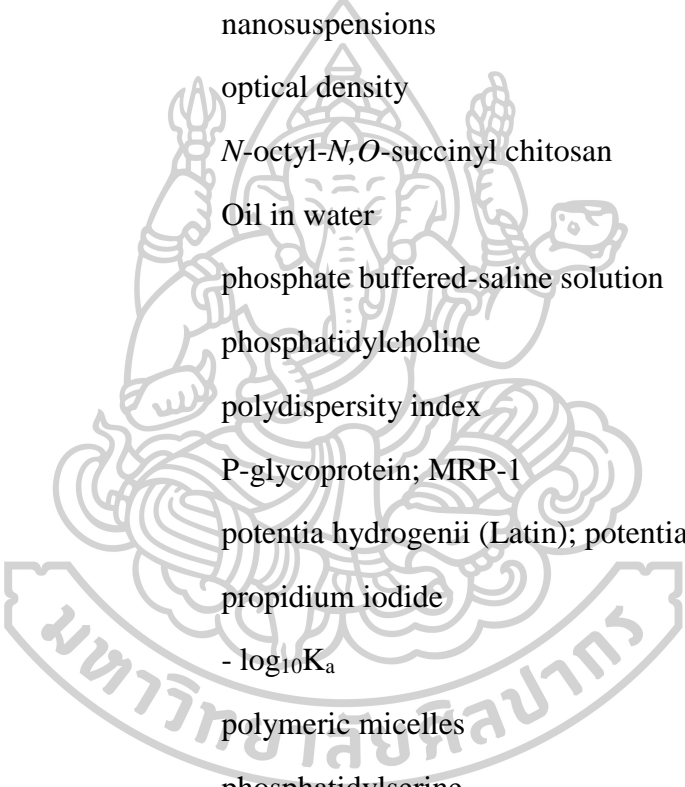


LIST OF ABBREVIATIONS

3A.1	19- <i>tert</i> -butyldiphenylsilyl-8,17-epoxy andrographolide
5-FU	5-fluorouracil
AG	andrographolide
ANOVA	analysis of variance
BSC	<i>N</i> -benzyl- <i>N,O</i> -succinyl chitosan
cm ⁻¹	wave number
CMC	critical micelle concentration
CO ₂	carbon dioxide
conc.	concentration
CRC	colorectal cancer
CS	chitosan
DCM	dichloromethane
DDA	degree of deacetylation
DDS	drug delivery system
DLS	dynamic light scattering
DMEM	Dulbecco's modified Eagle's medium
DMF	dimethylformamide
DMSO	dimethyl sulfoxide
Dox	doxorubicin
DSC	differential scanning calorimetry
EE	entrapment efficiency
e.g.	exempli gratia (Latin); for example
Eq	equation
et al.	and others
etc.	et cetera (Latin); and other things/ and so forth
FBS	fetal bovine serum



Fol-NSC	folic-conjugated <i>N</i> -naphthyl- <i>N,O</i> -succinyl chitosan
FITC	fluorescein isothiocyanate
FT-IR	fourier-transform infrared spectroscopy
g	gram(s)
GI	gastrointestinal
h	hour(s)
HCl	hydrochloride
HPLC	high performance liquid chromatography
IC ₅₀	half-maximal inhibitory concentration
i.e.	id est (Latin); that is
i.p.	intraperitoneal injection
i.v.	intravenous injection
kDa	kilodalton
KH ₂ PO ₄	potassium dihydrogen phosphate
LC	loading capacity
LPs	liposomes
M	molarity
MEM	Minimum essential media
meq	milliequivalents
mg	milligram(s)
min	minute(s)
mL	milliliter(s)
mm	millimeter(s)
mm ³	cubic millimeter(s)
mmol	millimole
MTT	3-(4,5-Dimethylthiazol-2-yl)-2,5 diphenyltetrazolium bromide, a tetrazole
mV	millivolt(s)



MW	molecular weight
NaBH ₄	sodium borohydride
NaOH	sodium hydroxide
NCs	nanocarriers
nm	nanometer(s)
NMs	nanomedicines
NSC	<i>N</i> -naphthyl- <i>N,O</i> -succinyl chitosan
NSs	nanosuspensions
OD	optical density
OSC	<i>N</i> -octyl- <i>N,O</i> -succinyl chitosan
O/W	Oil in water
PBS	phosphate buffered-saline solution
PC	phosphatidylcholine
PDI	polydispersity index
P-gp	P-glycoprotein; MRP-1
pH	potentia hydrogenii (Latin); potential for hydrogen
PI	propidium iodide
pK _a	- log ₁₀ K _a
PMs	polymeric micelles
PS	phosphatidylserine
PXRD	powder X-ray diffraction
RH	relative humidity
rpm	revolutions per minute
s	second(s)
SCF	simulated colonic fluid
SD	standard deviation
SDS	sodium dodecyl sulfate
SEM	scanning electron microscopy

SGF	simulated gastric fluid
SIF	simulated intestinal fluid
TEM	transmission electron microscopy
vs	versus
v/v	volume by volume
w/v	weight by volume
w/w	weight by weight
μg	microgram(s)
μL	microliter(s)
μm	micron; micrometer(s)
μM	micromolar(s)
%	percentage(s)
™	trademark
®	registered trademark
°C	degree Celsius
>	more than
<	less than
~	approximately
π	pi
θ	theta

CHAPTER 1 INTRODUCTION

1.1 Statement and significance of the research problem

Cancer is the most common cause of death around the world. The global burden is expected to rise to 21.7 million new cancer cases and 13 million cancer deaths in 2030 [1,2]. Among them, the cancer of the gastrointestinal tract is ranked as the top five common cancer-related deaths in both men and women [3]. Colorectal cancer (CRC), disease emanating from the epithelium cells lining the colon or rectum of the gastrointestinal tract, is the most common malignant tumor with high mortality and morbidity rates worldwide. The major risk factors for CRC include dietary or environmental factors, inflammatory bowel disease, and genetics [4]. CRC is initially developed as colorectal polyps before invading the surrounding muscular and lymph nodes, then metastasize to distant organs. Signs and symptoms of CRC are not specific, including weakness, weight loss, bloody stool, abdominal pain, and constipation; therefore, most CRC patients are diagnosed in the advanced stages. The standard treatment for stages I-IIIC is surgical excision. Patients diagnosed in advanced stages (IIIA-IV) will be treated with surgical excision combination with chemo-radiotherapy. The prognostic is good only in the patient diagnosed with early-stage; however, the survival rate is low in the advanced stages due to acquired drug resistance and metastasis. Moreover, fluctuations in plasma drugs level can trigger the development of drug resistance in the cancer cells. Therefore, the utilization of effective screening devices and tumor-specific anticancer agents with reduced side effects for the screening and treatment of cancer is recommended to achieve the best clinical outcomes. To date, there are many strategies for CRC therapy that focus on cure or palliation, especially chemotherapy is the major part of CRC treatment. Nevertheless, the use of conventional anticancer agents is limited by their undesirable properties, such as poor solubility, narrow therapeutic window, cytotoxicity to normal tissues, and nonspecific biodistribution, which may be the cause of failure in cancer treatment [5]. To obtain improved therapeutic efficacy, new strategies like nanotechnologies are required.

Developing a drug targeting system (DTS) is a current approach to overcome the complicated regulating molecular mechanisms of cancer. DTS is designed to

administer pharmaceutical agents as an alternative form to increase safety and efficacy while remained therapeutic potentials. There are varieties of the systems, including beads, polymeric micelles, liposomes, nanosuspensions, and nanoparticulate systems [6]. Nanocarriers, generally 10 to 1000 nm in size, have been designed with attracting properties using specific materials in order to carry and transport particular drugs to specific target cancer sites [7]. Numerous reports have shown that small nanocarriers with the size ranging from 20-200 nm tended to accumulate in tumor cells because they have a longer circulatory residence time and slower extravasation from normal capillaries [8]. The drug-encapsulated nanocarriers can be accumulated in tumor tissue through an enhanced permeation and retention effect (EPR) and avoiding clearance by the reticuloendothelial system (RES) [9,10]. Hence, they are able to circulate in the bloodstream for a longer period to achieve the desired therapeutic concentration through the property of passive tumor targeting.

Moreover, drug delivery via nanocarriers is also able to solve the solubility problems of poorly water-soluble drugs by incorporating the drug into the hydrophobic core of the carriers and optimize the surface charge of the drug before entering into the sites of the disease using adventitious-coating polymers. Generally, nanocarriers should have a hydrophilic surface to increase solubility and excellent ability to escape from macrophages in the mononuclear phagocyte system (MPS). Thus, coating the surface of nanocarriers with a hydrophilic polymer, such as polyethylene glycol (PEG), creates a steric side chain which can protect the nanocarriers from being opsonized by macrophage [11]. Moreover, generating nanocarriers from block copolymers with hydrophilic and hydrophobic components, such as the combination between poly (lactic acid) (PLA), poly (lactic-co-glycolic acid) (PLGA), and PEG polymers, can provide “stealth properties” to the nanocarriers leading to more remarkable ability to target tumor sites [12]. Currently, several data have shown the applications of nanocarriers for cancers targeting such as Doxil (liposomal doxorubicin), Abraxane (Nab-paclitaxel), and Genexol-PM (polymeric micelle) [13-15].

Many approved anticancer drugs were derived from natural sources, especially from plants. Plant-derived antitumor compounds have been developed to treat cancer such as vinblastine, vincristine, etoposide, teniposide, paclitaxel, vinorelbine,

docetaxel, camptothecin, topotecan, and irinotecan [16]. *Andrographis paniculata* (Berm. F.) Nees belongs to the Acanthaceae family. It has been used as a traditional herbal medicine in many countries, including in India, China, and Southeast Asia countries (Thailand, Malaysia, Indonesia, and Philippines). This herb is official in Thai herbal pharmacopoeia. The isolated compounds from this plant have been reported to have a wide spectrum of pharmacological effects including anti-diarrheal, anti-inflammatory, anti-hyperglycemia, anti-microbial, anti-HIV, anti-hepatitis and hepatoprotective effect [17]. Andrographolide (AG, C₂₀H₃₀O₅) is a major *ent*-labdane diterpenoid that demonstrates many pharmacological activities including cytotoxic activity. It exhibited both direct and indirect effects on cancer cells by inhibiting cancer cell proliferation, promoting cell-cycle arrest, and inducing apoptosis and necrosis cell death [18]. However, AG lacks selectivity and potency toward several cancer cell lines. To improve the cytotoxic activity and to be used as a potential anticancer drug, many researchers have attempted to chemically modify AG based on its structure-activity relationships (SAR). A series of novel analogues of AG were semi-synthesized and evaluated for antitumor activity against different cancer cells [19]. Among them, 19-*tert*-butyldiphenylsilyl-8,17-epoxy andrographolide (3A.1, C₃₆H₄₈O₆Si) possesses high cytotoxic activity against several cancer cells including hepatocellular carcinoma, cervical carcinoma, and human breast carcinoma [20]. In addition, this analogue has higher cytotoxic activity than the parent compound in the CRC cell line. Thus, this analogue could be a potential semisynthetic anticancer drug in the future. However, the administration of cytotoxic drugs remains far away from optimal. It is limited by poor aqueous solubility (<1 µg/mL at 37°C) and high systemic toxicity to nonspecific organs. Therefore, the development of a drug delivery system for improving therapeutic efficacy and minimizing the side effect is necessary. Utilization of nanotechnology in various biomedical applications, including drug delivery system has attracted increasing interest. Therefore, the delivery of hydrophobic 3A.1 with nanocarrier platforms including polymeric micelles, liposomes, and nanosuspensions will be investigated in the current study [21,22].

Polymeric micelles (PMs) are nano-sized, spherical shape carriers, with a core-shell architecture composed of hydrophobic segments as the internal core and

hydrophilic segments as the surrounding corona in the aqueous medium. Micelles can enhance the aqueous solubility of an anticancer drug by incorporating the drug into the core of the micelles. Simultaneously, the hydrophilic shell helps maintain colloidal stability and protect the particles from being opsonized in the bloodstream, leading to prolonged circulation time [23-25]. Most polymeric micelles are formed from various synthetic copolymers. The structure of chitosan (CS) is usually modified to obtain amphiphilic chitosan derivatives. The amphiphilic chitosan derivatives, *N*-naphthyl-*N,O*-succinyl chitosan (NSC), *N*-octyl-*N,O*-succinyl chitosan (OSC) and *N*-benzyl-*N,O*-succinyl chitosan (BSC) were synthesized by introducing hydrophobic (naphthyl, octyl, benzyl group) and hydrophilic pH-sensitive moiety (succinyl group) into the chitosan backbone. These derivatives demonstrate pH-sensitive properties that have been employed for carrying various compounds such as curcumin [26], meloxicam [27,28], and silymarin [29].

Liposomes (LPs) are naturally occurring phospholipid-based amphipathic nanocarriers. They are self-assembled circular vesicles composed of a phospholipid bilayer that can encapsulate both hydrophilic and hydrophobic drugs. Cholesterol is commonly added to the structure of liposomes to increase stability [30-32]. However, conventional liposomes have many problems, such as low drug loading, faster drug release, and short half-life in the bloodstream. To overcome these problems, PEGylation is used to help liposomes escape from RES, leading to an increase in blood circulation time [33,34]. Moreover, novel liposomes are also developed to precisely deliver an anticancer drug to the targeted sites by conjugating a specific ligand on the surface of liposomes, which can bind to the overexpressed receptors of the cancer cells. This approach leads to an increase in the anticancer efficacy and reduced toxicity [35-37]. Nowadays, many commercial liposome products contain anticancer drugs such as doxorubicin, paclitaxel, vincristine [38,39].

Nanosuspensions (NSs) are submicron colloidal dispersions composed of drug nanocrystals (<1000 nm), stabilizing agents (e.g., surfactants and/or polymeric stabilizers), and a liquid dispersion medium, especially water. The particle size of the drug crystals can be reduced, which leads to an increase in the total surface area and an eventual upsurge in the solubility, dissolution profile, and the bioavailability of the drug

[40-43]. To prevent the particle aggregation or crystal growth which is the principal instability of the formulations, the appropriate stabilizers are usually added to stabilize the nanocrystals via electrostatic and/or steric effect [44,45].

In this study, we aimed to develop three drug delivery nanosystems (polymeric micelles, liposomes and nanosuspensions) containing an anticancer drug 3A.1 for improving the solubility and anticancer activity against CRC cells. First, 3A.1-loaded pH-sensitive amphiphilic chitosan polymeric micelles were formulated using different physical preparation methods and chitosan derivatives (NSC, OSC, and BSC) and various amount of drug. For active tumor targeting, the folate-conjugated *N*-naphthyl-*N,O*-succinyl chitosan (Fol-NSC) was also synthesized and formulated 3A.1-loaded Fol-NSC PMs. Second, 3A.1-loaded liposomes (conventional and PEGylated liposomes) were produced to encapsulate drug using different lipid compositions and various amount of drug. Third, 3A.1 nanosuspensions stabilized by stabilizers were prepared through nanoprecipitation method with different amphiphilic chitosan derivatives, stabilizers (sodium dodecyl sulfate (SDS), Tween[®] 80, and Poloxamer 188) and various drug to stabilizer ratios. The physicochemical properties (i.e. particle size, size distribution, zeta potential, morphology) and drug loading (or drug concentration) of the two nanocarrier systems and the nanosuspensions were examined. Other properties including solubility and degree of crystallinity of the nanosuspensions were also investigated. In addition, the *in vitro* drug release of the two nanocarriers and short-term stability of the nanosystems were evaluated along with the *in vitro* anticancer activity, apoptosis induction and anti-migratory effect. Furthermore, *in vivo* antitumor efficacy of the optimal nanosystems (nanosuspensions) were also evaluated in CRC xenograft nude mice model.

1.2 Aims and objectives

1. To synthesize pH-responsive amphiphilic chitosan derivatives and folate-conjugated chitosan derivatives
2. To formulate 3A.1-loaded polymeric micelles (PMs), 3A.1-loaded liposomes (LPs), and 3A.1 nanosuspensions (NSs)

3. To evaluate the factors affecting the particle size, size distribution, zeta potential, morphology, drug content, drug release, and physical stability of 3A.1-loaded PMs, 3A.1-loaded LPs, and 3A.1 NSs
4. To investigate the *in vitro* anticancer activity, apoptosis induction, and anti-migratory activity of 3A.1-loaded PMs, 3A.1-loaded LPs, and 3A.1 NSs
5. To examine the *in vivo* antitumor efficacy of 3A.1 NSs

1.3 The research hypothesis

1. The amphiphilic chitosan derivatives can be successfully synthesized and can be used to formulate 3A.1-loaded PMs and 3A.1 NSs.
2. Folate-conjugated chitosan derivatives can be synthesized and can be employed for the formulation of PMs for active tumor targeting.
3. The entrapment methods, types of amphiphilic chitosan derivatives, and initial amounts of drug influence the physicochemical properties, entrapment efficiency, loading capacity, *in vitro* drug release, and physical stability of the 3A.1-loaded PMs.
4. The lipid compositions and initial amounts of the drug affect the physicochemical characteristics, entrapment efficiency, and loading capacity, *in vitro* drug release, and physical stability of the 3A.1-loaded LPs.
5. The drug to stabilizers ratios and type of amphiphilic chitosan derivatives affect the physicochemical characteristics, solubility, and physical stability of the 3A.1 NSs.
6. The 3A.1-loaded PMs, 3A.1-loaded LPs and 3A.1 NSs can increase the anticancer activity, apoptosis induction, and anti-migratory activity.

CHAPTER 2

LITERATURE REVIEW

2.1 Cancer disease

Cancer remains the second leading cause of mortality worldwide, accounting for 9.6 million cancer-related deaths in 2018. According to the updated cancer fact sheet reported by World Health Organization (WHO), annual cancer cases are expected to rise to 13 million within the next decade (2030) [1,2]. Generally, about 1 in 6 dead people is due to cancer. The five most common types of cancer are lung, breast, colorectal, prostate, and skin cancers. Cancer (malignant tumor or neoplasm) is a pathologically heterogeneous group of diseases that rapidly progressive abnormal cells to an uncontrollable stage after onset [46]. In daily lifestyle, humans are exposed to several risk factors of cancer such as consumption of alcohol, tobacco, unhealthy nutrition with low fiber intake, obesity, physical inactivity, ultraviolet radiation, infections from viruses, bacteria or parasites, etc. These principle risk factors can induce usual cells in the body to undergo genetic transformation and defection, leading to the development of cancer cells. The genetic mutation often occurs in the upregulation of oncogenes or downregulation of tumor-suppressor genes [47]. As is known to all, cancer-related death dramatically increased in the past few decades, but due to advanced early detection and sufficient management, cancer mortality can currently be reduced and the annual economic cost of cancer is also saving. Different cancer types and stages require specific management with single or combination approaches including immune, photothermal, photodynamic, gene, and hormone therapy that have the promising killing effect of cancer in preclinical studies. However, surgical operation, radiotherapy, and chemotherapy continue to be the first option treatment for most common cancers [48]. Although the efficiency of each cancer management varies according to the tumor's type, stages, and different locations, the important goals of cancer treatment are to cure cancer disease or to extend the patient's survival time and improve the patient's quality of life with supportive or palliative care and psychological support [49]. However, these focused treatment strategies fail to manage "metastasis" tumors that cancer cells have spread from the original site to distant organs. The metastasis stages are very harmful to a cancer patient because of incurable clinical

outcomes and the major cause of death from cancer. Despite the advancement of modern medicine in diagnostic and therapeutic tools, cancers remain a major health concern and a leading cause of mortality and morbidity globally [50].

2.1.1 Colorectal cancer (CRC)

CRC, originating from the abnormal growth of the inner wall of the epithelial cells lining at the colon or rectum of the GI tract, is the third-most-common malignant tumor and is associated with high morbidity and mortality worldwide, both in developed and developing countries [51]. In 2019, an estimated 145,600 new cases were diagnosed with colon and rectum cancer with an estimated 51,020 deaths, making colorectal cancer the third leading cause of cancer-related deaths in the United States. Overall, colon and rectal cancers make up approximately 8-9% of all cancer diagnoses in men and women in the United States. The incidence rate of colorectal cancer in men is approximately 1.2 times greater than observed in women [52,53]. The cancer cases reported by the National Cancer Institute (NCI) of Thailand showed that CRC was ranked to be the first (n=245) and the third (n=191) frequent new cases in men and women population [54,55]. Age seems to be the major risk factor for the development of colorectal cancer with 70% of cases diagnosed in adults older than 65 years of age. In addition to age, dietary or environmental factors, life habits, inflammatory bowel disease, and genetic susceptibility increase the risk of CRC. As patient age, abnormal cells accumulate on the surface epithelium and protrude into the stream of fecal matter, their contact with mutagens can lead to further cell mutations and eventual adenoma formation [56]. The development of a colorectal neoplasm is a multi-step process of several genetic and phenotypic alterations of normal bowel epithelium leading to unregulated cell growth, proliferation, and tumor development. Commonly, CRC first develops as colorectal adenomatous polyps (grape-like growth), which are abnormal growths in the inner lining of the bowel/ intestinal tract. Then, carcinoma invades muscular and the nearby lymph nodes, and ultimately they spread to other organs. The signs and symptoms include fatigue, blood in the stool, constipation, tenesmus, rectal bleeding, abdominal pain, and weight loss.

The clinical presentation can be extremely varied and nonspecific. However, CRC patients at an early stage mostly are asymptomatic clinical signs [4].

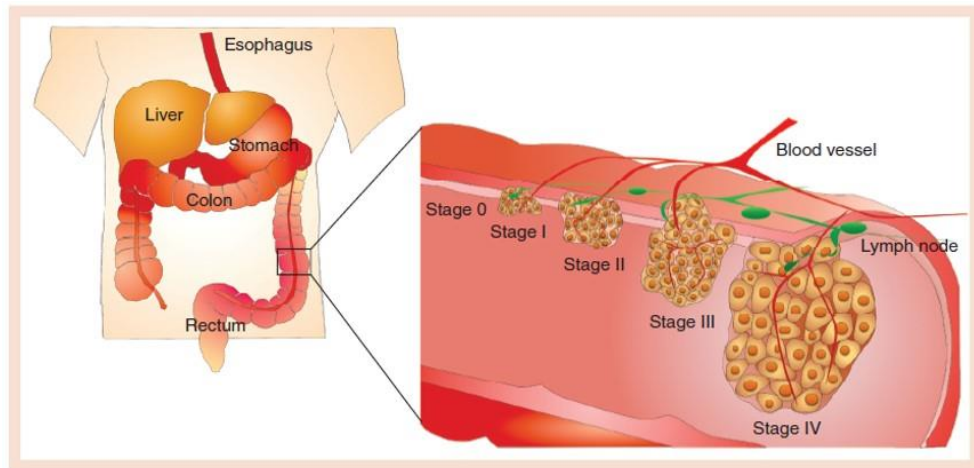


Figure 1 Clinical stages of colorectal cancer growth according to the American Cancer Society; See more details in ref. [52,56]

Tumor recurrence and distant metastasis are critical survival-influencing factors of CRC. CRC survival is primarily dependent on the stage of the disease. The 5-year survival rate in patients with a localized stage was very high (~90%), in contrast, the survival rate was dropped to 65% in patients diagnosed for distant metastasis. The relative survival rate is inversely related to stages of tumor development at the time of detection. The prognosis is mainly predicted by the stage of the disease and the prognosis of patients with an initial stage (I or II) is better at detection time [53]. The US Centers for Disease Control and Prevention (CDC) recommends that adults age 50 to 75 should start to be screened for precancerous lesions of CRC using accurate and sensitive tools such as sigmoidoscopy and colonoscopy [57].

2.1.2 Treatment of CRC

The treatment of CRC commonly depends on the tumor size, the local microenvironment, and the range of cancer metastasis. The primary goal of the CRC treatment approach is curative care for localized disease (stage I, II, and III), while is palliative care for metastasis cancer (stage IV). In the early stage of colon cancer, surgical resection is the primary option to remove tumors and

lymph nodes for curative effects in these patients. Other treatment options available for CRC treatment include radiation therapy, chemotherapy, stem cell transplant, and targeted immunotherapy [58].

Currently, chemotherapy as a pharmacological intervention is still the most commonly used and effective strategy for the treatment of CRC, especially in the metastatic phase. Chemotherapeutic drugs that are approved by the US Food and Drug Administration (FDA) for CRC therapy include 5-fluorouracil (5-FU), oxaliplatin, irinotecan, capecitabine, etc. The other drugs for CRC therapy mostly consist of cytotoxic drugs, monoclonal antibodies, and their combinations (see more details in ref. [59]). To achieve efficient chemotherapy, drug concentration in plasma should be balanced between the minimum therapeutic level and the maximum tolerable level for a prolonged time interval. However, cancer treatment using conventional chemotherapy is highly non-specific in targeting the drugs to the cancer cells causing undesirable side effects to the healthy cells/tissues [60].

2.2 Plant-based anticancer drugs

Natural products are a great source of novel therapeutic agents for drug discovery and development in the pharmaceutical industry and a number of new chemical anticancer drugs originating from herbal plants are currently used in the clinic for treatments of different types of cancer [16]. We believed that they are contemplated to be safe and low risk to the human body's normal cells as they have been used to treat patients for over the centuries and it is hopeful that their natural compounds would be extensively beneficial to remedy suffering symptoms and also improve physical and mental quality of life. Recently, many semi-synthetic compounds from plant products have been proved to strongly improve anticancer activities *in vitro* and *in vivo* experimental tests [61,62]. Therefore, chemical modification of plant-based lead candidates could be a better approach to receive a new class of chemotherapeutic drugs with potential anticancer efficacy. Many approved plant-derived chemotherapeutic agents have been developed to treat cancer such as vincristine, vinblastine, etoposide, paclitaxel, docetaxel, topotecan, and irinotecan [63].

2.2.1 Andrographolide

Andrographolide (AG, Figure 2a) is the major bioactive component present in *Andrographis paniculata* (Burm. f.) Nees (family Acanthaceae), a medicinal plant that has been widely used in complementary medicine, especially in China, India, Southeast Asia countries including Thailand [64,65]. This herbal plant, commonly known as “king of bitters”, is traditionally used in Ayurvedic medicine for a long time and is also preferred to treat a variety of diseases including sore throat, flu, upper respiratory infections, fever, and common cold. Therefore, these curative effects make it expressed as a “natural antibiotic” [17]. It is officially recorded in the Thai Herbal Pharmacopoeia (THP) in the name of Fah-Ta-Lai-Chon for treatment of common cold, laryngitis, and diarrhea [66]. Moreover, AG can be isolated in a large quantity (~2%) from the methanolic extract of dried whole plant but most concentrated in the leaves (Figure 3) [67]. The natural compounds extracted from dried aerial parts of *A. paniculata* are mainly diterpenoids, flavonoids, and sterols [68]. Various phytoconstituents are reported to have a broad range of pharmacological effects, such as anti-inflammatory, anti-viral, anti-malarial, anti-diabetic, anti-hypertensive, hepatoprotective, immunostimulatory, and anti-cancer activity [69].

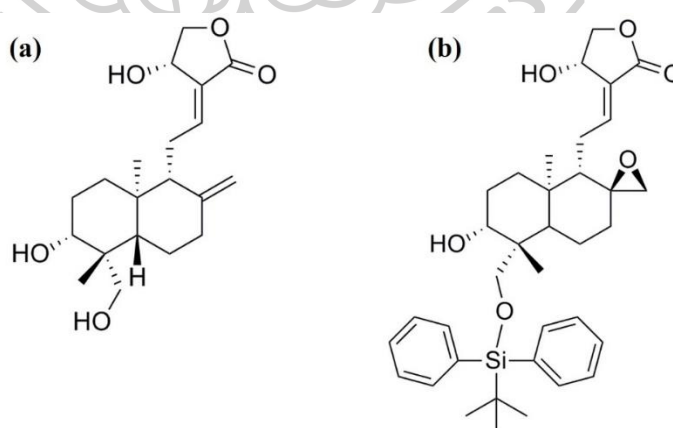


Figure 2 Chemical structure of (a) andrographolide and (b) semi-synthetic andrographolide (3A.1). The illustration was written by ChemDraw Pro 12.0.



Figure 3 Photograph of fresh herb of *A. paniculata* (Fah-Ta-Lai-Chon, Nakorn Pathom, Thailand).

In recent years, many researchers have revealed that AG and its derivatives possess anticancer activity both *in vitro* and *in vivo* experiments. The mechanism of antitumor actions against several solid tumors (cervical, breast, prostate, liver, colon cancer, etc.) has been extensively studied and established by a lot of research groups. The results reported that the molecular mechanisms are mainly through induction of cell cycle arrest and promotion of apoptosis in several cancer cells by attenuating various cell signaling pathways, induction of intracellular reactive oxygen species (ROS), induction of tumor suppressor proteins p53 and p21 leading to inhibition of cancer cell proliferation, survival, invasion, metastasis, and angiogenesis [70,71].

2.2.2 Semi-synthetic andrographolide (3A.1 analogue)

Many previous studies suggested that AG is an interesting pharmacophore with potent anticancer activity and hence has the potential to be developed as a new anticancer entity. Nowadays, several semi-synthetic compounds from medicinal herbs have been shown impressive anticancer profiles in both efficacy and safety in various cancer cells [72]. Based on the chemical structure of AG ($C_{20}H_{30}O_5$, MW: 350.4 g/mol), it contains three major moieties including (1) an α,β -unsaturated γ -butyrolactone ring, (2) two olefin bonds ($\Delta^{8,17}$ and $\Delta^{12,13}$) and (3) three hydroxyl groups at C3 (secondary), C-14 (allylic) and C-19 (primary) [18,73,74]. Being a bipolar compound, with the tendency to form hydrogen bonds, AG elicits biological responses by binding to receptors via its hydroxyl group terminus [75]. However, the development of

AG formulations to treat cancer in the clinic is restricted by low water solubility, lack of selectivity, and low potency leading to poor oral bioavailability [76]. Therefore, numerous AG analogues have been designed and synthesized by modifying each important moieties of its structure to improve its potency and selectivity. Many of these analogues exhibit superior anticancer activity over the parent compound and the potential AG analogues would be approved to become a novel class of anticancer agents for clinical use in the foreseeable future [19]. The basic knowledge to modify AG structure through structure-activity relationship (SAR) stated that (1) an intact γ -butyrolactone ring, (2) the C₁₂=C₁₃ and C₈=C₁₇ double bonds, and (3) C-14 hydroxyl group play a crucial role in the cytotoxic activity [77]. In previous reports, it revealed that the conversion of exocyclic C-8 and C-17 double bond to an epoxide through epoxidation do not affect the cytotoxic activity [75,78]. Furthermore, the introduction of high lipophilic groups such as aromatic derivatives on the hydroxyl group provided a stronger cytotoxic activity than the parent compound. This effect could be explained that these bulky functional groups with lipophilic property allow AG analogues to pass the cell membrane by passive diffusion and protect adjacent hydroxyl groups [79,80].

In our earlier studies, we have attempted to synthesize a lot of derivatives and to evaluate their anticancer potential as well as modes of action to find out a better lead. We found that one of the semi-synthetic AG analogue, 3A.1 (19-*tert*-butyldiphenylsilyl-8,17-epoxy andrographolide; C₃₆H₄₈O₆Si, MW: 604.8 g/mol) (Figure 2b), can suppress the growth of several cancer cell lines including cholangiocarcinoma (CCA) and colorectal cancer (CRC) and exhibits higher anticancer activity than the parent compound. This analogue was chemically modified the AG molecule by coupling C-19 hydroxyl group with aromatic silyl ether as a bulky lipophilic moiety through the silylation process [20,81]. For CRC, this analogue has previously been reported to inhibit cell proliferation and to induce apoptosis in HT29 and HCT116 cells through inhibition of Wnt/ β -catenin signaling [82].

2.3 Nanocarriers for cancer therapy

The utilization of nanotechnology in various biomedical and pharmaceutical fields is an emerging therapeutic platform that uses nanocarriers (NCs) for the detection, diagnosis, and treatment of cancer. The use of nanomedicines (NMs) as a targeted drug delivery system is regarded as one of the potential devices for cancer therapy [6]. NCs (also called as colloidal drug carriers) are utilized in cancer therapy due to their unique size, i.e. in general 1-1000 nm, or preferably in the range of 20-200 nm suitable for drug delivery applications. The nano-ranged size, large surface area to volume ratios, and the ability for surface modification/functionalization play a crucial role in its biodistribution and therapeutic efficacy *in vivo* [7]. Currently, NCs for transporting anticancer drugs are divided into several types of formulations such as polymer-based NCs (polymeric micelles, polymeric nanoparticles, dendrimers), lipid-based NCs (liposomes, lipid nanoparticles, microemulsions, nanoemulsions), drug conjugates, and inorganic nanoparticles (Figure 4) [83].

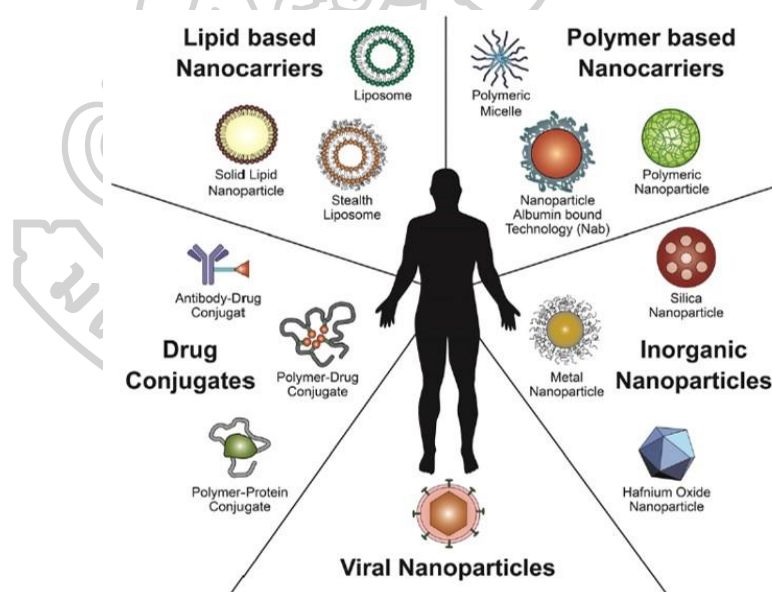


Figure 4 Schematic representation of numerous nanocarriers used in targeted drug delivery under preclinical and clinical development [83].

NCs provide distinct advantages for cancer therapy beyond free drug administration of conventional chemotherapy as follow;

- 1) Improve the therapeutic index of the loaded anticancer medication compared to the drug delivered via conventional dosage forms.
- 2) Increase drug efficacy by achieving steady-state therapeutic levels of drugs over an extended period or prolonged half- life in blood circulation.
- 3) Lower drug toxicity due to controlled drug release and improve drug's pharmacokinetic by increasing the drug's solubility (poorly soluble compounds are solubilized/encapsulated in the hydrophobic compartment) and stability as well as reducing premature drug release [35,83].

The ideal drug delivery system should be able to carry chemotherapeutic drugs and then precisely release the encapsulated drug at pathological tumor sites, control drug level which is not too low to be inefficient therapy or is not too high to have serious side effects and protect the drugs from the environment degradation during systemic circulation and excretion. In addition, the drugs should selectively kill cancer cells, increasing the therapeutic efficacy, and reducing harmful side effects simultaneously (Figure 5) [84,85]. There are basic two strategies for tumor targeting: passive targeting has arisen from the enhanced permeability and retention (EPR) phenomenon in solid tumors, while active targeting is related to specific binding between ligand grafted on the carrier system and overexpressed receptors on the cell surface, like a guided missile. Moreover, they can be applied by external or internal stimuli for selective drug release at a target site only [86].

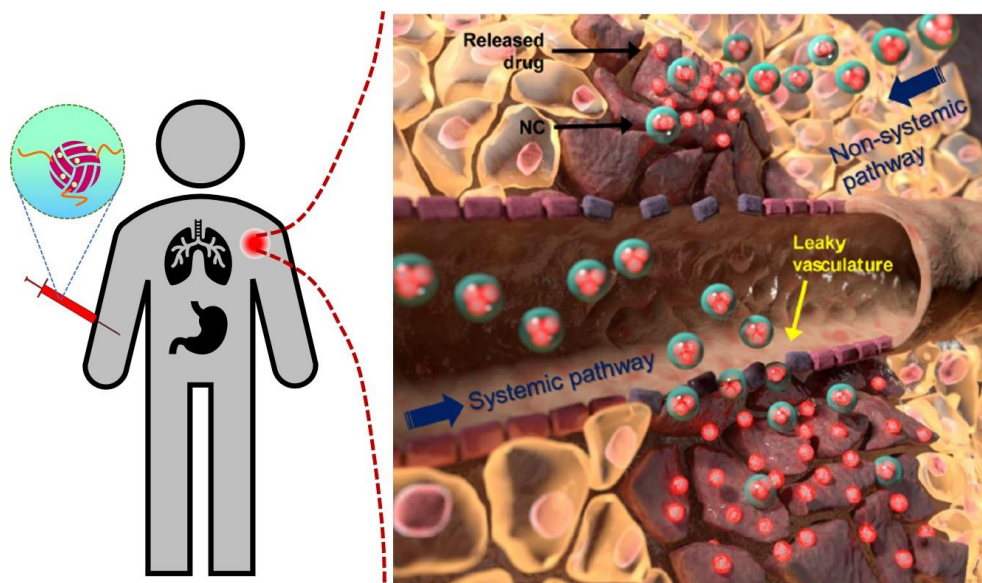


Figure 5 Schematic illustration of NC-mediated drug delivery through systemic administration. After injecting nanocarriers into the body, these delivery systems carrying anticancer drugs should target at cancer site without rapid clearance by the immune system and then specific release drugs with sufficient concentration at the target site [85].

2.4 Tumor targeting strategies

2.4.1 Passive targeting

The schematic representation of different targeting approaches of a nanosized vehicle is illustrated in Figure 6. Typically, due to the leaky tumor vasculatures and the poor lymphatic drainage system in most solid tumors, the NCs can passively target the tumor sites through the EPR effect. The spontaneous penetration of NCs into the tumoral interstitium relies on convection (which is the movement of molecules across large pores within interstitial fluids) or diffusion (which is the transportation of molecules across cell membranes based on concentration gradient without energy requirement). Many factors affect the correlation of the EPR effect and properties of the NCs so that NCs must be designed to achieve maximum targeting and therapeutic efficacy. NCs with the size range of 20-200 nm can easily extravasate through the walls of poorly formed microvessels in the angiogenic tumor. The particle's surface charge is electrically neutral or anionic for the avoidance of renal

elimination. Even though the EPR phenomenon can facilitate the extravasation of NCs to the tumoral interstitium via passive retention mechanism, the main challenge is the heterogeneity of EPR capability in each tumor mass and lower accumulation of NCs in the central zone of the metastatic solid tumor. Nowadays, there is more potential to improve the tumor targetability of NCs by adopting active targeting strategies in various cancers [87-90].

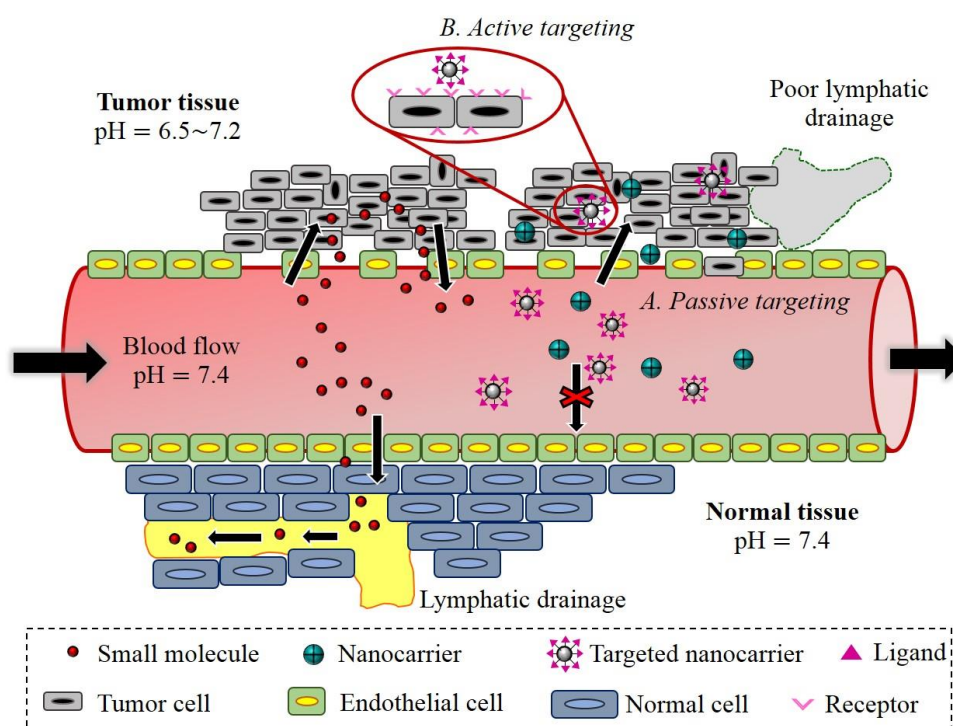


Figure 6 Schematic illustration of tumor-targeting approaches. (a) Passive targeting: transport drug NCs through defective and fenestrated blood vessels into the tumoral interstitium surrounding the solid tumors by convection and passive diffusion. Small molecules can freely move in and out of the tumor capillaries whereas drug-loaded NCs can retain at interstitial fluid without diffusion back into blood circulation due to their large size. (b) Active targeting: specific recognition process is involved with ligands attached at the carrier's surface selectively bind to receptor overexpressed at the target site (tumor cells or endothelial cells) via sufficient affinity. Adapted from ref. [91]

2.4.2 Active targeting

The active targeting of NCs toward specific tumor tissues has been developed to solve the weakness of passive targeting by conjugation/decoration

of ligand to the surface's NCs (Figure 6). The active targeting aims to increase the drug delivery to the pathological target and reduce off-target delivery by the attachment of NCs with a wide range of targeting ligands including (1) antibodies and their fragments (2) proteins and peptides-transferrin, RGD (3) carbohydrates-sugar (4) vitamin-folic acid (5) other small molecules [92,93]. The ligands (single or multiple moieties) can be chemically and physically decorated onto NCs due to the high surface area to volume ratio of NCs. These targeting ligands can enhance biologically specific binding to the receptors which are overexpressed on the "tumor cell surface" or "tumor vasculature/ microenvironment", as concluded in Table 1, improving the retention and cellular uptake of NCs.

Fundamental selection of specific ligand to couples with NCs is based on the overexpression of receptors on the target cell surface with a low level of expression in normal tissues [94]. Generally, cellular internalization of NCs occurs through receptor-mediated endocytosis [95]. Targeting the cancer cell is the direct eradication of tumor cells in a specific type of cancer. It differs from targeting the tumor vasculature that involves the inhibition of angiogenesis surrounding tumor tissue, leading to blocking oxygen and nutrient supply and consequent induction of indirect killing tumor cells. Compared to NCs without ligand attachment or unconjugated form, this technique helps entry of the nanocarrier system into the cells, enhances therapeutic efficacy, and minimizes toxic effects to healthy tissues or organs by improving specific biodistribution [96].

Table 1 Various tumor molecules and specific ligands for active targeting [96]

Target site	Target molecule or receptor (cell marker)	Ligand
Tumor vasculature/ microenvironment	Vascular endothelial growth factor receptor (VEGFR)	Anti-VEGFR antibody, Pegaptanib
	Vascular cell adhesion molecule (VCAM)	Anti-VCAM antibody
	Matrix metalloproteinase (MMP)	Anti-MMP antibody
	Integrin ($\alpha_v\beta_3$) receptor	Cyclic arginine-glycine- aspartic acid (cRGD)
Tumor cell	Folate receptor (FR)	Folic acid
	Transferrin receptor (TfR)	Transferrin
	Epidermal growth factor receptor (EGFR)	EGF antibody
	Estrogen receptor (ER)	Estrone
	Asialoglyco-protein receptor CD44 receptor	Lectin Hyaluronic acid

To obtain optimal cancer-targeted NCs, several factors including ligand biocompatibility, cell specificity, binding affinity, ligand surface density, and arrangement must be carefully considered to receive optimal characteristics for the achievement of sufficient internalization and avoidance of recognition by the reticuloendothelial system (RES). The actively targeted NCs should deliver chemotherapeutic drugs to specific tumor sites. The better properties of ligand-conjugated NCs possess great therapeutic potential at both preclinical and clinical development [97].

2.5 Polymeric micelles (PMs)

Currently, treatment of cancer using classic chemotherapeutic drugs still faces major delivery drawbacks including lack of selective drug delivery, low therapeutic activity, and serious side effect toward normal tissues. Due to these limitations, a large number of nanocarriers have been designed and developed for the delivery of an anticancer drug to specific tumor sites. Many pieces of research showed that these NCs are able to improve therapeutic efficacy and potency along with reducing harmful toxicity. PMs, which belong to polymer-based nanocarriers, have gained a lot of attention in the area of anticancer drug delivery [98].

2.5.1 Definition

PMs are submicron colloidal particles (10-1000 nm in diameter) with a spheroidal structure formed by the self-assembly process of amphiphilic copolymers (di-block, tri-block, or grafted copolymer) as a building unit [99]. Amphiphilic molecules, composing of hydrophilic and hydrophobic segments, possess the unique property of self-assembly when exposed to an aqueous solvent at above critical micelle concentration (CMC) or critical aggregation concentration (CAC) [100]. The polar parts of the copolymer are attracted to the solvent, while hydrophobic parts orient away from the solvent. In this way, the hydrophobic parts form an inner core, whereas hydrophilic parts set up an outer shell (corona) to build a direct or regular micelle, depicted in Figure 7. By contrast, when amphiphilic molecules are exposed to an organic solvent, they are conversely oriented to form a reverse micelle [101]. The core-shell structure of PMs allows the entrapment of hydrophobic drug molecules inside the cavity through interaction between hydrophobic core and drug molecules, while the outer shell of PMs helps to stabilize the hydrophobic core, controls *in vivo* pharmacokinetics, and is compatible with the aqueous environment [102]. Besides, the outer shell also protects the loaded drugs from interaction with the blood components and recognition by the RES which results in prolonged circulation of nanosized micelles in the blood followed by passive accumulation in tumor area [24].

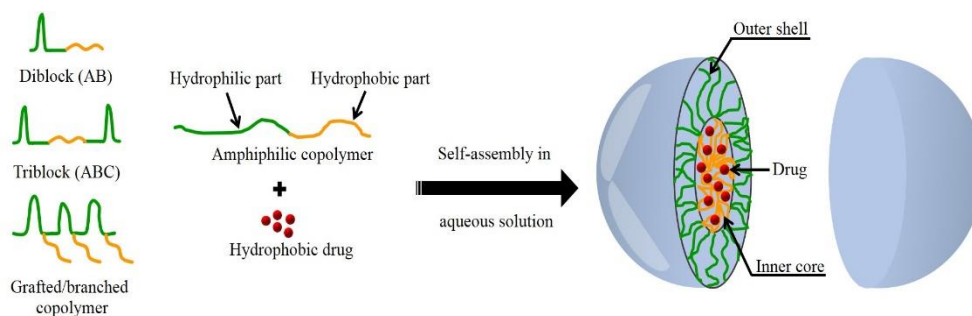


Figure 7 Structure of amphiphilic copolymer and polymeric micelles structure. Generally, linear diblock copolymers of A-B type or linear triblock copolymers (2 types of polymer, AB; 3 types of polymer, ABC) or non-linear/grafted copolymers are often used to design PMs. PMs are self-assembled by amphiphilic copolymers consisting of hydrophilic and hydrophobic parts at/ or above critical micelle concentration (CMC) in aqueous solution. Adapted from ref. [24]

At the present, many anticancer drugs including doxorubicin, paclitaxel, camptothecin loaded into PMs are being tested in clinical trials for the treatment of several types of solid tumors (Table 2). However, there are only a few approved products on the market. Genexol-PM[®] comprised of an amphiphilic diblock copolymer (mPEG-PDLLA) and paclitaxel is approved for the treatment of breast and lung cancer. This micellar product can enhance antitumor activity and maximum tolerated dose, compared to conventional formulation [103,104].

1 **Table 2** Current clinical status of polymeric micelle formulations for intravenous administration [24,104]

Product name	Composition of copolymer	Active compound	Loading method	Purpose	Therapeutic indication
Genexol®-PM (phase IV)	mPEG-PDLLA	Paclitaxel	Physical entrapment	Solubilization	Breast and lung cancer
NK105 (phase III)	PEG-b-poly(aspartic acid)	Paclitaxel	Physical entrapment	Solubilization	Breast and gastric cancer
NK911 (phase II)	PEG-P(Asp)-Dox	Doxorubicin	Physical entrapment	Targeting	Solid tumors
SP1049C (phase III)	Pluronic L61 and F127	Doxorubicin	Physical entrapment	Anti-MDR	Adenocarcinoma of the esophagus
NC-6300 (phase I)	PEG-b-poly(aspartate-hydrazone)	Epirubicin	Chemical conjugation	Targeting	Breast and liver cancer
NC-4016 (phase I)	PEG-b-poly(L-glutamic acid)	Oxaliplatin	Coordinate bonding	Targeting	Solid tumors
NC-6004 (phase III)	PEG-b-poly(L-glutamic acid)	Cisplatin	Coordinate bonding	Targeting	Pancreatic cancer

2.5.2 Types of polymer used

Typically, amphiphilic copolymer molecules that are used to create PMs should contain two basic sections, namely hydrophilic block, and hydrophobic block.

- 1) Hydrophilic block: it is the very important exterior of the micelle surface that can be designed to achieve the desired physicochemical properties. Polyethylene glycol (PEG) is one of the utilized hydrophilic polymers for the development of various NCs because of its hydrophilic, electrically neutral, less toxic, and flexibility. The hydrophilic property at the particle surface through the PEGylation process facilitates stealth nature in the bloodstream, circumvent uptake by RES, and prolongs their circulation time. Due to the perfect properties of PEG, it has been used to make the outer cloud shell of micelles for the prevention of protein adsorption in plasma and recognition by MPS along with micellar aggregation or precipitation via steric hindrance. Other hydrophilic polymers that are used to form hydrophilic portions include chitosan, poly (ethylene oxide) (PEO), poly (N-vinyl pyrrolidone) (PVP), and pNIPAAm [23,105].
- 2) Hydrophobic block: it represents the major interior of the inner cavity of the micelle's core-shell structure that can entrap the hydrophobic drug molecules via physical entrapment technique or conjugate with drugs through chemical attachment. The inner core is normally made up of polyesters, polyethers, and poly (amino acids) such as poly (propylene oxide) (PPO), Pluronics, polycaprolactone (PCL), poly (L-lactide) (PLA), poly (D, L-lactide-co-glycolide) (PLGA), poly (L-histidine) (pHis), poly (L-aspartate) (pAsp), poly (L-glutamate) (pGlu). In addition to these polymers, lipid derivatives such as stearic acid, distearoyl phosphatidylethanolamine (DSPE) are selected to be a hydrophobic part as well [23,106].

2.5.3 Advantages and limitations

PMs are widely made of biocompatible, biodegradable, low toxic, and low immunogenicity copolymer. The nanosized particle (10-200 nm) of micelles provides high loading capacity and protects the entrapped drug from exposure to the outer aqueous environment [107]. The useful advantages of micelles are further explained below:

- 1) Enhance water solubility of poorly aqueous soluble and hydrophobic drugs by entrapment/ solubilization of drugs within the hydrophobic core of micelles in order to improve drug absorption and bioavailability
- 2) Increase blood circulation time by concealing from clearance of PMs by recognition of macrophages in RES
- 3) Improve drug localization, targeting efficiency, biodistribution (pharmacokinetic profile), and therapeutic outcome of anticancer drugs by surface modification such as specific ligand-conjugation onto micelle surface for site-specific drug delivery
- 4) Control release of encapsulated drug at tumor sites
- 5) High thermodynamic stability because the CMC value of PMs can be reduced up to the millimolar range (10^{-3} to 10^{-4} mM), which lower than low molecular weight surfactants (10^3 to 10^4 M). They are durable to dilute in a large volume of vehicles. [23,108]

Furthermore, the other advantages of micelles are their simple, easy, and reproducible manufacturing procedure, ease of sterilization by simple filtration for injectable preparation [109]. Although PMs possess many beneficial properties over other NCs, the limitations of micelles remain. After systemic administration, the micelles will be extremely diluted in biological fluid and may be disrupted the equilibrium between micelle and blood. The premature drug release or drug leakage and unstable structure of micelles limit the capability of drug delivery to the target site causing ineffective cancer treatment and toxicity to normal tissues. Another drawback of micelles is the incapacity to load hydrophilic drugs or macromolecules. In some cases, improper hydrophobic drug loading may cause precipitation of drug while micelles are

diluted with aqueous media, leading to drug aggregation-related embolism in blood capillaries. The way to improve drug loading capacity is to match the good compatibility between drug and copolymer and to optimize the strong cohesive forces between hydrophobic drug and micelle's core as well [110,111].

2.5.4 Methods for micelle preparation

The drugs can be either loaded into the PMs via physical entrapment method or chemical conjugation method. The selection of methods for micelle preparation depends on the physicochemical characteristics, especially solubility of copolymer and drug [112,113]. In this context, only the physical entrapment method (Figure 8) is briefly explained below:

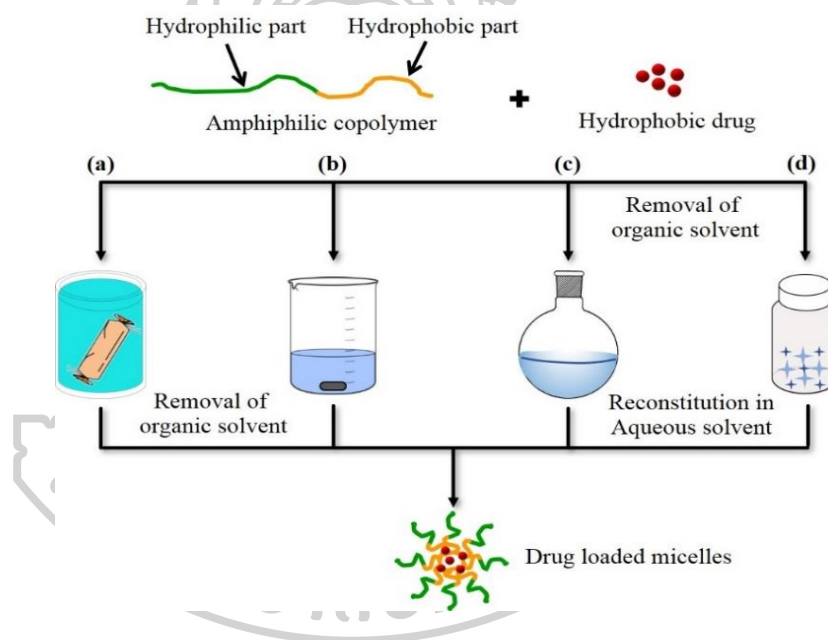


Figure 8 Different physical entrapment methods for the preparation of drug-loaded polymeric micelle; (a) dialysis, (b) O/W emulsion followed by evaporation, (c) solvent casting, and (d) freeze-drying. Adapted from ref. [105]

- 1) Dialysis: this method is applicable for amphiphilic copolymers that cannot readily dissolve in an aqueous medium. Both the copolymer and hydrophobic drugs are separately soluble in a water-miscible organic solvent such as dimethylsulfoxide (DMSO), *N,N*-dimethylformamide (DMF), acetone, acetonitrile, dimethylacetamide, and ethanol. The mixture solution of drug and copolymer is filled into a dialysis

membrane tube and dialyzed against water for several days for removing the organic solvent. During the solvent exchange, water goes inside the tube but the organic solvent moves out from the tube, resulting in micelle formation in the aqueous system.

- 2) Oil in water (O/W) emulsion: when copolymer cannot dissolve in aqueous solution, this method is another option to produce micelles. The drug is physically encapsulated through an O/W emulsification process. Both the copolymer and hydrophobic drugs are dissolved in a water-immiscible organic solvent such as dichloromethane (DCM), tetrahydrofuran, ethyl acetate, chloroform. Then, the mixture solution (organic phase) was gradually mixed in water (aqueous phase) to form O/W emulsion and the organic solvent is then removed by continuous stirring. During the evaporation of the organic solvent, the drug-loaded micelles are spontaneously formed in aqueous solution.
- 3) Solvent casting: initially, both polymer and drugs are dissolved in the organic solvent to obtain a clear homogenous solution. The organic solvent is evaporated to yield polymeric thin film at the bottom of the container. The evaporation of organic solvent favors polymer-drug interactions. The thin film is then hydrated with the aqueous solution under heat and stirring to form drug-loaded micelles.
- 4) Freeze drying: this is a single-step method employed for the preparation of drug-loaded micelles. Both the copolymer and hydrophobic drugs are dissolved in the mixture of water/tert-butanol (TBA). Owing to the high vapor pressure of TBA, it can accelerate the rate of sublimation during the lyophilization process. TBA induces the formation of fine ice crystals that quickly sublime during the freeze-drying step. The reconstitution of freeze-dried cake with the vehicle spontaneously forms drug-loaded micelles [102,109].

The encapsulation of hydrophobic drugs into the inner core of micelles is related to cohesive interactions such as hydrophobic, π - π interactions, van der Waals, hydrogen bonding, and electrostatic interaction, depending on the

nature of copolymers. Most hydrophobic anticancer drugs interact with the hydrophobic core of copolymer via hydrophobic interaction as the main attractive force and these drugs are loaded at sufficient loading capacity and formed micelles having physical stability [105,114]. In addition to these non-covalent interactions, the ionic copolymers with the opposite charge of the drug can form micelles by electrostatic interaction, which is called polyion complex (PIC) micelles. PIC micelles could be a potential polymer-based nanocarrier for the delivery of charged macromolecules (proteins, nucleic acids) [115].

2.5.5 Factor influencing the properties of PMs

1) The ratio of hydrophilic/hydrophobic part

Both particle size, conformation, and drug loading of micelles are affected by the hydrophilic-hydrophobic balance of copolymers. Copolymers with different hydrophobic modifications show three types of patterns in the aqueous system upon the addition of hydrophobic drugs as schematically described in Figure 9. Copolymers with “strong hydrophilicity” have better compatibility with water molecules and tend to form micelles separated from hydrophobic drugs. Although it can still entrap hydrophobic drugs, the loaded drugs into micelles are very low with less structural stability. When a large number of hydrophobic drugs are added in the formulation, the copolymers do not possibly hold the whole drug in micelles and the system becomes nanosuspensions. On the contrary, copolymers with “strong hydrophobicity” may occur aggregation or precipitation in the system due to good compatibility of hydrophobic drug and polymer. Hence, copolymers with suitable hydrophilic-hydrophobic ratio can be formed PMs with desirable properties because of equilibrated interaction among drug, polymer, and water molecules. The size of micelles is governed by both polymer chain length and hydrophilic-hydrophobic block ratio. The increase in the hydrophobic region leads to higher hydrophobic bonding and forms closely compacted, resulting in the maintenance of a stable micellar system [106,110].

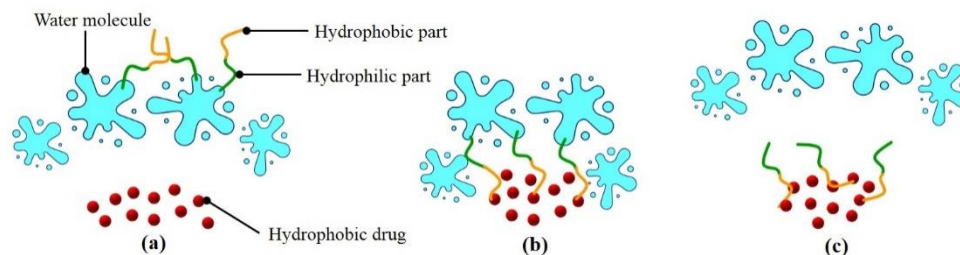


Figure 9 Schematic presentation of the interaction among hydrophobic drugs, copolymers, and water molecules: (a) stronger hydrophilicity polymer (b) hydrophilic-hydrophobic balance (c) stronger hydrophobic polymer. Adapted from ref. [110]

2) Concentration of the copolymer

At a very low concentration (below CMC), the copolymers only exist as monomers dispersed in a solvent. An increase in copolymer concentration until reach the CMC value, the monomers become saturation at the air/ water interface and the polymer chains start to arrange monolayer, associate, and form spherical micelles. If increasing the copolymer concentration above the CMC point, the micelles tend to change their shapes to cylinder, bilayer, or vesicle causing larger particle size with higher aggregation. Generally, low CMC value indicates the ability of a polymer to form micelle at a low concentration of polymers and it offers higher stability of the micellar structure. Their CMC values mainly depend on the hydrophilic-hydrophobic balance of copolymers, chemical characteristics, compatibility between polymers and drugs, and mean molecular weight. It was found that an increase in the length of the hydrophobic block can decrease its CMC value [105,116]. CMC value can be measured by observation in physicochemical changes during micelle formation. Commonly used methods include surface tension, electrical conductivity, voltammetry, calorimetry, luminescence probe, light scattering, spectroscopy (UV, visible, or fluorescence). The frequently used technique is fluorescence spectroscopy using pyrene (non-polar polyaromatic molecule) as a fluorescent probe [117].

3) Drug loading and drug loading method

Entrapment of hydrophobic drugs into micelles may increase the “hydrophobic interaction” of drugs with the hydrophobic segment of the copolymer, leading to tightly packed and smaller cores of the micelles. For amphiphilic copolymer, with an increase in the drug amount loaded into the hydrophobic cores, the particle size of the micelles decreased. After the administration of micelles, the loaded drug was gradually released from the micelles, which can be explained by the dissociation of micelles. The drug loading method is another main factor affecting micelles property. Hydrophobic drugs can be encapsulated into micelles by chemical conjugation, or physical entrapment such as dialysis, O/ W emulsion with solvent evaporation, sonication, solvent casting methods. This indicates that the compatibility between the anticancer drug and the hydrophobic core remarkably influences drug loading capacity [116,118].

2.5.6 Characterizations of micellar system

The physicochemical properties of PMs can be determined during the production process, storage, and administration using different techniques which are listed in Table 3 [24,105,106].

Table 3 Different methods for polymeric micelle characterization [105,106]

Characteristics	Methods
<i>Synthesized polymer</i>	
Structure and composition	Nuclear magnetic resonance (¹ H-NMR) associated with Fourier-transform infrared spectroscopy (FT-IR)
CMC value	Fluorescence spectroscopy (pyrene probe)
<i>Micelle formulation</i>	
Size and size distribution	Static and dynamic light scattering
Surface charge (zeta potential)	Photon correlation spectroscopy (PCS) associated with electrophoretic mobility
Morphology	Microscopy (light, TEM, SEM, AFM, CLSM)
Solid state analysis/crystallinity	Differential scanning calorimetry (DSC)

Drug encapsulation	Spectrophotometry, fluorescence spectroscopy, HPLC and electrochemical techniques
<i>In vitro</i> drug release	Dialysis diffusion method in specified release medium that mimic the physiological fluid
<i>In vitro</i> structural stability	Size exclusion chromatography (SEC) and gel permeation chromatography (GPC)
<i>In vitro</i> cytotoxicity	Tetrazolium dye (MTT) assay, flow cytometry analysis

CMC, critical micelle concentration; TEM, transmission electron microscope; SEM, scanning electron microscope; AFM, atomic force microscopy; CLSM, confocal laser scanning microscope.

2.5.7 Application of PMs in cancer therapy

Advances in polymer modification and the versatility of PMs forming copolymers make them an attractive carrier in cancer therapy. The leaky endothelium of the tumor vasculature and poor function of the lymphatic drainage system leads to the retention of the micelles with a smaller size (between 10-200 nm) in the tumoral interstitium. The passive targeting through the EPR effect can enhance drug accumulation with higher concentration at certain tumor tissue, compared to healthy tissues. Ideally, the micelle size should not smaller than 10 nm to avoid quick glomerular filtration and not bigger than ~200 nm to escape removal from the plasma by liver and spleen after i. v. administration. The high surface charge (zeta potential > - 30 mV) helps to improve physical stability through electrostatic repulsion. Nevertheless, the permeability of fenestrated tumor endothelium fluctuates depending on the tumor's type and stage, anatomical area of the tumor [119]. For actively targeted cancer cells via active targeting, different types of ligands namely, folic acid, peptides, carbohydrates, antibodies are decorated on the micelle surface for the development of the site-specific drug nanoparticles. These ligands enable to specifically bind overexpressed receptors/ antigens on targeted cells with high biological affinity. The surface modification is proceeded by coupling the targeting ligands at the distal end of the hydrophilic block. The actively targeted micelles exhibit better drug delivery to the tumor area and cellular internalization, compared with passively targeted micelles relying on the EPR

effect [23]. In addition, stimuli-sensitive micelles are constructed from a modified polymer that is responsive to internal stimuli (low pH at tumor microenvironment, higher temperature due to inflammation process, redox reaction, higher production of enzymes) or external stimuli (local hyperthermia, light energy, ultrasound, magnetic field). When stimuli-sensitive polymers in micelles are locally exposed with a signal, the micellar structure suddenly destabilizes or transforms to release the payload of anticancer drugs at the right concentration at a specific diseased site [120]. The drug-loaded micelles with the behavior of site-specific drug delivery improve therapeutic efficacy along with decrease side effects [121].

2.6 Liposomes (LPs)

In the past few decades, liposomes were first published by Alec Bangham in 1964. Later, the word “liposomes” was denominated by Gerald Weissman (lipos = fat; soma = body) [122]. This lipid-based nanocarrier has been used to carry various drugs i.e. antibiotics, antifungals, and cytotoxic agents. It's well known that chemotherapeutic drugs can inhibit the growth of both cancer and normal cells, especially in fast-proliferating healthy cells (epithelial in oral, GI tract, a hair follicle), thereby it needs to be careful during treatment with these chemotherapeutic drugs to balance between the anticancer efficacy and system toxicity in cancer patient [35,123]. Liposomes have been utilized to improve current cancer treatment due to unique features including increased solubility of low aqueous soluble anticancer drugs and encapsulation of both hydrophobic and hydrophilic compounds. The development of optimal liposomal formulations is intended to achieve sufficient therapeutic efficacy and the minimization of side effects. The liposomes can be modified to decrease the carrier clearance by mononuclear phagocyte system's (MPS) uptake using long-circulating liposomes which support a passive targeting toward the solid tumors and they have a potential to be greater drug accumulation into targeted tumor site via active targeting strategies, coupling specific ligands to the liposome surface. The combination of this lipid-based nanocarrier and drug transport mechanisms facilitate to increase drug bioavailability, improve therapeutic efficacy, and/or lessen system toxicity [36,37].

2.6.1 Definition

Liposome, belonging to a type of lipid-based nanocarriers, is a vesicular structure entirely enclosed by one or more membranous lipid bilayers or lamellae that encapsulate both hydrophilic and lipophilic compounds (Figure 10). The concentric lipid bilayers are separated by aqueous compartments [124]. The basic molecular building block of a typical liposomal membrane is a phospholipid which is similar to the phospholipid cell membrane. In an aqueous environment, phospholipids orient to a thermodynamically stable structure called a “bilayer”. This flat sheet of lipids then curves into a spherical liposomal structure [39,125].

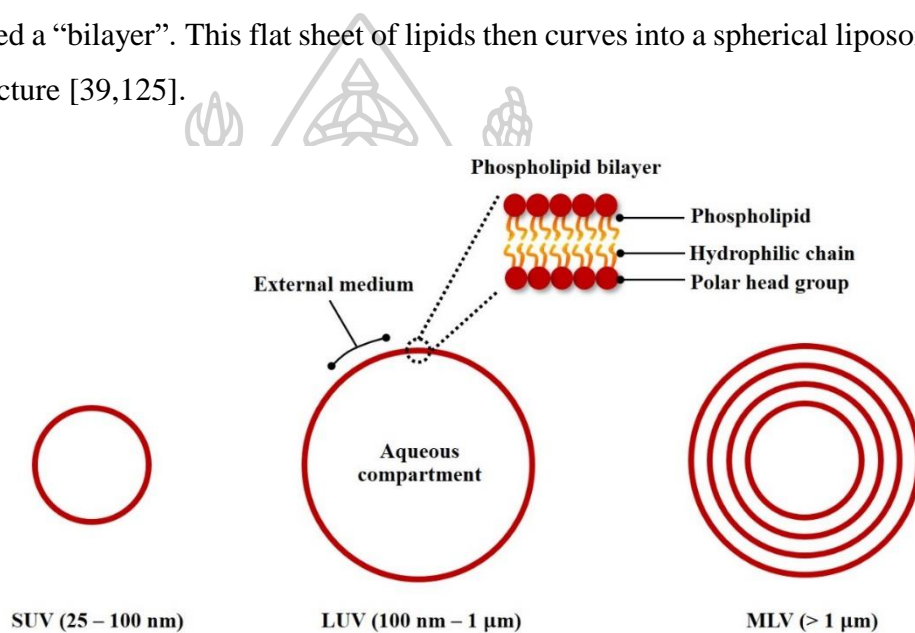


Figure 10 Basic structure and classification of liposomes: small unilamellar vesicles (SUV), large unilamellar vesicles (LUV), and multilamellar vesicles (MLV). Adapted from ref. [122]

2.6.2 Basic components in liposomes

The function of phospholipid in liposomes

Generally, the amphiphilicity of phospholipid molecules contains two elemental parts: polar phosphate head groups (water-soluble hydroxy) connected with the hydrophobic (non-polar) backbone, as presented in Figure 10 [126]. The spontaneous formation of liposomes can be explained that when phospholipid is dispersed in an aqueous medium, the hydrophilic interaction of the lipid head groups with aqueous environment conduces to organize

themselves for forming an aqueous cavity (hydrophilic compartment), whereas the hydrocarbon tails (saturated or unsaturated fatty acid) are repelled by the water molecules and arrange in the opposite direction. The head groups of the inner layer orient inside the intravesicular liposome and the outer layer point to an aqueous medium. According to its structure, liposomes can encapsulate “lipophilic drugs” within the lipid bilayer, at the same time, their aqueous cavity is reserved for loading “hydrophilic drugs” [127].

Currently, many derivatives of phospholipids have been used to prepare liposomes such as phosphatidylcholine (PhC, zwitterionic), phosphatidylserine (PhS), phosphatidylglycerol (PhG), phosphatidylinositol (PhI, negative charge), DOTAP, DOTMA (positive charge), and sphingomyelin (SM), etc. The suitable properties of phospholipids should be biodegradability, biocompatibility, non-toxicity, and low immunogenicity. The natural phospholipids consist of a mixture of various lipid components while synthetic phospholipids are uniform and pure fatty acyl chains. Among these lipids, phosphatidylcholine or lecithin (Figure 11a) is the most frequently used because of its proper stability in the biological environment. The surface charges of liposomes are neutral, positive or negative charge, depending on the polar head charge of used phospholipids [128].

The function of cholesterol in liposomes

Despite certain stability of liposomes formed by a single type of phospholipid, the flip-flop movement (rotational freedom) and imperfect packing of phospholipid molecules remain and make the drug leakage from liposomes [38]. The chemical structure of cholesterol (Chol) is presented in Figure 11b. Cholesterol, hydrophobic and water-insoluble steroid backbone, is added into liposomal formulations as a function of co-lipid to (1) increase their stability of bilayer membrane in the biological fluids, (2) enhance rigidity's lipid bilayer membrane, (3) improve packing capacity between the phospholipid molecules, and (4) reduces the permeability of water-soluble molecules through the membrane. Thus, most liposomes delivering various types of drugs including chemotherapeutic agents need to be put into during liposomal

production [129]. The polar part of cholesterol is aligned with the polar head of phospholipids in the lipid bilayer. Due to hydrophobic chains of cholesterol, it resides in the interior portion of lipid bilayers and serves to fill the gap between phospholipids, leading to the prevention of flip-flop movement of lipid membrane [130]. The percentage of cholesterol used in liposomal formulations affects the phase transition temperature of the lipid bilayer. Furthermore, the effect of cholesterol on size is found that an increase in cholesterol concentration leads to an increase in liposomal size and shape transition. The molar percentage of cholesterol varying from 30-45% of total lipid components serves the balance of lipid membrane fluidity and rigidity while the molar percentage of phospholipids varying from 55-100% of total lipid constituents is the main lipidic membrane of a liposome. In some cases, the inclusion of cholesterol can decrease drug loading into the liposomal structure because it hinders drug penetration in the bilayer. By contrast, liposomes without cholesterol tend to react with blood proteins such as albumin, transferrin, and macroglobulin, resulting in the destabilization and reduced utility of liposomes as a drug delivery system [122,131].

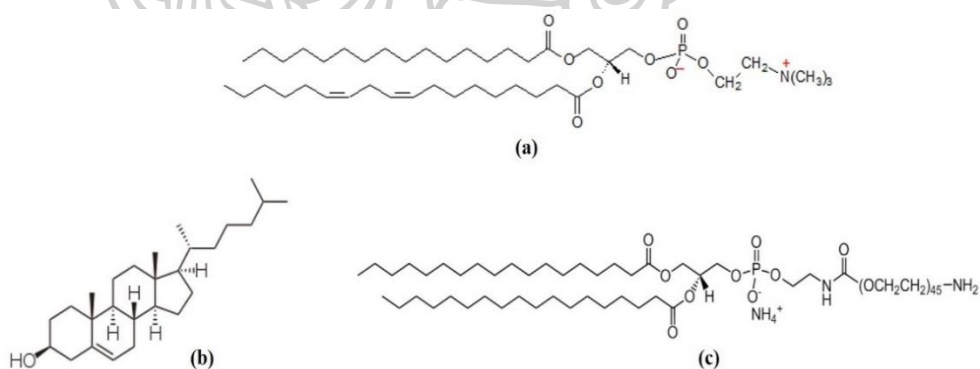


Figure 11 Chemical structure of common liposomal lipid constituents: (a) phosphatidylcholine (b) cholesterol and (c) DSPE-PEG2000. The length and degree of saturation in the carbon chain can vary in each class of phospholipids. [128]

2.6.3 Advantages and limitations

Nowadays, the liposomal formulations have a lot of unique characteristics over the conventional dosage form, as described hereafter:

- 1) Deliver various types of active compounds: hydrophilic compounds (proteins, peptides, carbohydrates, nucleic acids) are entrapped within the aqueous core, lipophilic compounds are inserted inside the lipid bilayer and amphiphilic molecules are located in both the aqueous cavity and lipid bilayer.
- 2) Improve water solubility and bioavailability of poorly water-soluble drugs
- 3) Protect the payload drug from the loss and degradation such as an acidic level in the GI tract, chemical degradation (hydrolysis or photolysis) during preparation, storage and drug transport, and the biological barrier such as MPS uptake in the liver and spleen
- 4) Improve pharmacokinetic and pharmacodynamic profiles of a therapeutic drug by surface modification/functionalization
- 5) Promote the controlled and sustained release of drug from liposomal vesicles and reduce drug leakage before reaching to target tumors
- 6) Biocompatibility, biodegradability, low toxicity, lack of immune system activation in the human body due to the cell-like structure of liposome
- 7) Lower systemic toxicity and side effects, compared to traditional chemotherapeutic regimen [21,35-37]

2.6.4 Classification of liposomes

Liposomes are mainly categorized based on size (small, intermediate, or large), the number of lipid bilayers (uni- and multi-lamellar), phospholipid charges (neutral, anionic, and cationic), lipid composition, and mechanism of drug delivery. Liposomal vesicles vary in size between 0.025 μm to 2.5 μm [39]. Unilamellar vesicles consisting of a single phospholipid bilayer are subdivided into small unilamellar vesicles (SUV) with a mean diameter vesicle ranging from 25 to 100 nm and large unilamellar vesicles (LUV) with size ranging from 100 to 1000 nm [126]. Multilamellar vesicles (MLV) are made of

multiple lipid bilayers (≥ 2) that are separated by the layers of aqueous, with size in the micron range (1-5 μm). Their lamellae mimic an onion-like structure (Figure 10). Both the size and number of lamellae in the liposomes are considered to be the most crucial factors influencing the vesicle half-life in plasma. As considered the composition and purpose of drug delivery, the liposomes are classified into conventional liposomes, stealth liposomes, ligand-conjugated liposomes, and triggered release liposomes (pH-sensitive, thermo-sensitive), as shown in Figure 12 [132].

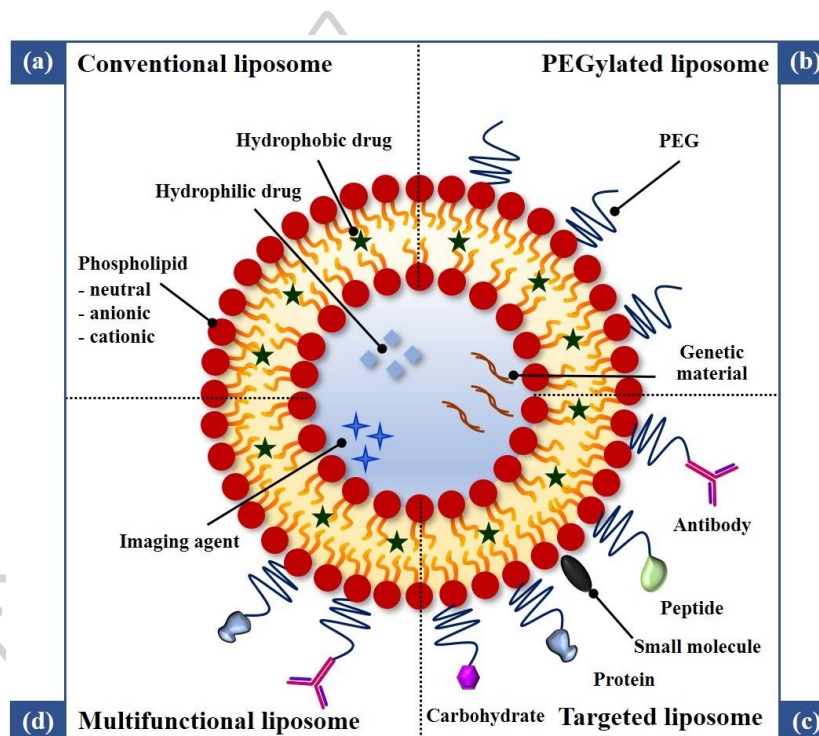


Figure 12 Type of liposomes based on components in the formulation: (a) conventional liposomes are made of phospholipids, (b) PEGylated/ stealth liposomes are composed of coating of polyethylene glycol at liposome surface, (c) targeted liposomes contain a specific targeting ligand to target cells at tumor environment, and (d) multifunctional liposomes. Adapted from ref. [37]

I. Conventional liposomes (First generation)

The basic components of conventional liposomes are phospholipids and cholesterol. Despite the valuable advantages of liposomes, one of the major hindrances of conventional liposomes is their instability in the biological fluid.

They have a short half-life in the bloodstream after i. v. injection due to quick phagocytosis and rapid clearance by macrophage cells in MPS. To overcome this weakness, the surface coating of liposome with inert hydrophilic materials have been developed to achieve long-circulating liposomes. The introduction of a 5-10% (molar ratio) of PEG lipid-derivatives prevents opsonization because the PEG layer at the surface of liposomes provides high hydrophilicity and steric hindrance between liposomes and blood proteins (serum opsonin, complements) leading to the reduction in protein adsorption. Owing to the leaky property of tumor neovascular, nanocarriers including liposomes can penetrate across the gap between endothelium and enter the interstitial space [133]. In addition, solid tumors have impairment of the lymphatic drainage system lead to the retention of nanocarriers in tumor sites for a longer period. This phenomenon has been well-known as the EPR effect. In other words, passive targeting of liposomes takes place by moving them from capillaries into the tumoral interstitium. The nanocarriers of not more than 200 nm have been reported for effective extravasation into tumors. The composition and charge on the liposome surface affect the passive targeting. The anionic or neutral liposomes can escape from renal clearance while the cationic liposomes seem to interact with anionic species in the blood, leading to rapid clearance by the RES [21].

II. Stealth liposomes or PEGylated liposomes (Second generation)

The insertion of polyethylene glycol (PEG) molecules in the bilayer membrane via PEGylation can significantly enhance longevity in the blood of liposomes, compared to traditional liposomes. PEG polymer can improve stealth property in liposomes due to desirable properties such as high solubility in an aqueous medium, inert, flexible, nonionic, biocompatibility, and it is approved by US FDA as a safe material [134]. The 1,2-diastearoyl-sn-glycero-3-phosphoethanolamine (DSPE) (Figure 11c) is often used to covalently conjugated other hydrophilic polymers like PEG. The grafting of PEG to the liposome surface mimics the glycoprotein on the cell surface in the human body. The long-circulation property is directly related to the amount and length of the grafted PEG chain (molecular weight). The long-chain PEG has better

pharmacokinetic behaviors than a short-chain. The DSPE-PEG2000 has been proven to provide extended blood circulation and ligand binding *in vivo* [135]. Normally, the addition of PEG lipid derivatives during mixing lipid components can prevent opsonization from RES due to an increase in surface hydrophilicity, promoting repulsive interactions between polymer-coated liposomes and blood components. Moreover, PEG can form a protective hydrophilic layer on the liposome surface and prevent vesicle aggregation through the steric stabilization effect. However, the hydrophilic layers on the surface of stealth liposomes may hinder the fusion of liposomal lipid membrane into the tumor cell membrane, leading to a decrease in drug cellular uptake. Moreover, some side effects are still caused by the non-specific drug distribution in the body of PEGylated liposomes [33]. Furthermore, Lee et al. reported that the sterically-stabilized liposomes with a slightly negative zeta potential had longer blood circulation times and higher tumor accumulation than stealth liposomes with highly negative zeta potentials [136]. Some reports revealed that the PEG-lipid derivatives in liposome can induce an antibody response (anti-PEG IgG and IgM) against the PEG chain, leading to accelerated clearance of liposomes by macrophages in the liver and spleen. This phenomenon is called accelerated blood clearance (ABC) [36,137,138].

III. Ligand targeted liposome

This liposomal system brings the improvement of tumor accumulation and therapeutic efficacy and reducing the adverse effects, arisen from the non-specific distribution of drug carriers in the human body. Liposomes can be functionalized with specific targeting ligands such as monoclonal antibodies, aptamers, proteins (transferrin), peptides (RGD), carbohydrates (sugar), or small molecules (folic acid) using different surface engineering strategies. These ligands can recognize and bind on specific macromolecules or receptors on the cell surface (cancer cells or tumoral endothelium) with high biological affinity. It may be called as active targeting liposomes or targeted liposomes or decorated liposomes [37]. This liposome is capable of direct delivery to the region of solid tumors and enhances the internalization of liposomes in tumor

cells, via mainly receptor-mediated endocytosis, in a process called active targeting. The liposome surface can be modified by attachment to these ligands via a covalent bond, electrostatic, and hydrophobic interaction. The ligands can be linked to the distal ends of PEG chains or grafted on the liposome surface. Furthermore, the liposomes that are conjugated with antibodies on the surface can be named as immunoliposomes (ILPs) [36]. It can selectively bind with targeting receptors that overexpressed on the surface of tumor cells (epidermal growth factor receptor, EGFR; folate receptor, FR; transferrin receptor, TfR; etc.) or endothelial cells and other cells in tumor vasculature (vascular endothelial growth factor, VEGF; vascular cell-adhesive molecule, VCAM; $\alpha_v\beta_3$ integrin; matrix metalloproteases, MMPs; etc.). Many studies reported that it could have greater targeting efficiency if the antibody is attached to a spacer arm rather than directly linked to the liposome surface [35,127].

Multifunctional liposomes are the delivery systems that combine the surface modification with a variety of functional groups such as two ligands-grafted liposomes (dual-functional liposomes) or two compounds-encapsulated liposomes (theranostic liposomes that contain an imaging and therapeutic agent, etc) [36]. Another type of liposomes is cationic liposomes that are made of positive charge lipids such as DOTAP, DOTMA. It can encapsulate DNA and RNA in the aqueous core for delivery into targeted cells. The positively charged lipid can bind negatively charged nucleic acid through electrostatic interactions. These are called lipoplexes [139].

IV. Stimuli-responsive liposomes

Liposomes can be modified to be a triggered release of therapeutic payloads utilizing pathophysiological differences in the tumor's microenvironment. Moreover, many liposomal systems containing appropriate lipid components can be responded by various internal or external stimulation such as pH, redox reaction, a proteolytic enzyme, ultrasound, heat, or light offering controlled drug release at a diseased site [140,141]. A pH-responsive liposome maintains a stable structure at physiological pH (pH 7.4) but can dissociate and release the loaded drugs under mildly acidic conditions in tumor

tissues [142]. A thermal-sensitive liposome is made of thermo-sensitive phospholipids that are stable at body temperature (37°C). When it is stimulated by local heating at a temperature above the lipid phase transition temperature, the entrapped drugs are readily released from the liposome and accumulated at the tumor sites. For instance, Thermodox[®] (commercially liposomal doxorubicin formulation) contains DPPC (dipalmitoylphosphatidylcholine), MSPC (myristoylphosphatidylcholine), and DSPE-PEG2000. After i.v. injection followed by the hyperthermia process (temperature range of 37°C to 42°C), the entrapped drug is released from liposomes with higher drug concentration at target tumors [143,144].

2.6.5 Methods for liposome preparation

The types of preparation methods influence the properties of liposomes, including their shape, size, stability, and drug loading efficiency. Liposomes are mainly prepared by the passive- or active-loading procedure. The passive-loading method is performed by mixing the drug before or during the liposome formation, whereas the active- or remote-loading method is accomplished by loading the drug into premade liposomes. There are several passive loading methods for the preparation of liposomes such as mechanical dispersion (thin-film hydration or membrane extrusion), solvent dispersion (solvent injection, or reverse-phase evaporation), detergent removal, and emulsion removal [145]. Liposomes are spontaneously self-assembled colloidal vesicles formed by hydration of phospholipids with aqueous buffer solution under shaking or stirring. The organization of phospholipids is driven by the entropy of water molecules and by hydrophobic interactions between the fatty acyl chains. Generally, each liposome preparation involves three steps: vesicle formation, vesicle size reduction, and purification, as summarized in Table 4. The lipophilic drugs are co-dissolved with other lipids in an organic solvent and added in the first step, whereas the hydrophilic drugs are dissolved in an aqueous medium and added in the step of film hydration [102,146].

The lipid film-hydration method is the first described and most commonly used method for liposome preparation. Lipid hydration followed by

vortex or stirring, also known as “Bangham’s method” (Figure 13). Briefly, the lipid components are dissolved in a suitable organic solvent such as chloroform and/or methanol mixture. The concentration of lipids is typically in the range of 10-20 mg/mL depending on the solubility of lipids in the organic solvent. The lipid solvent is subsequently removed by a rotary evaporator under low pressure or flow of nitrogen gas (N₂) to produce a thin film of the lipids. Next, the dry lipid film is hydrated with an aqueous buffer medium, which has a similar osmolarity to the physiological medium, under the temperature above the phase transition temperature (T_c) of the lipids. After that, vortex or shaking is applied to produce multiple bilayers (MLV) liposomes. Despite the simple method to form a vesicle, the drug loading is not sufficient to encapsulate the hydrophobic drugs because of the small captured volume in MLV liposomes. For reducing the vesicle size of MLV to form SUV, sonication using a probe or bath sonicator is generally introduced into liposomal dispersion. The temperature of the water is maintained above the T_c of lipids. To avoid degradation of the drugs and lipids, it needs to keep the lipid dispersion in an ice bath during the sonication with high energy. Sonic wave can disrupt the outer layers of giant liposomes and reorganize the lamellae into uniform SUV, thereby the hydrophobic drugs can easily translocate across the lipid bilayer to obtain higher drug encapsulation efficiency. The final size of liposomes not only depends upon the sonication time, energy input, and the number of cycling but also upon other factors, including lipid composition, concentration, and dispersion volume. Alternatively, the liposomes are also pass through the extrusion process using a polycarbonate membrane of actual size under high pressure and at a temperature above T_c of lipids. This process which is done in several cycling can provide only nanometer vesicle size and takes the larger one out. Hence, the size of the extruded liposomes tends to be close to the filter pore size with unimodal size distribution. After the formation of SUV vesicles, the excess lipid components, untrapped drugs, and traces of titanium from the probe sonicator have to be removed through a purification process [146-148].

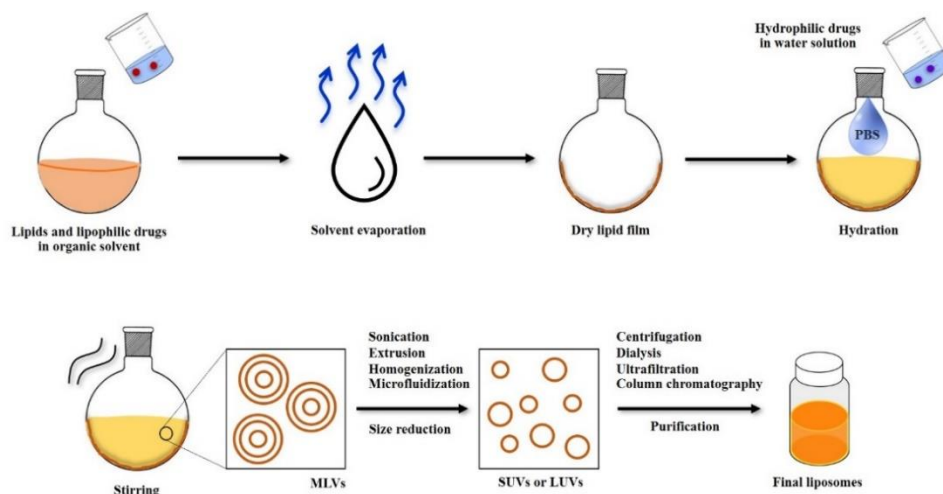


Figure 13 Pictorial representation of liposome preparation by lipid thin-film hydration followed by vortex or manual stirring. Adapted from ref. [145]

Table 4 Different methods for liposome preparation [145,147]

Step 1: vesicle formation	Type of final liposomes
Lipid hydration and shaking	MLV
Reverse-phase evaporation	MLV, LUV
Organic solvent injection	MLV, LUV, SUV
Freeze-thawing	MLV, SUV
pH gradient	LUV, SUV
Dehydration-rehydration	MLV
Detergent analysis	MLV, LUV
Step 2: vesicle size reduction	
Sonication	SUV
Microfluidization	SUV
Extrusion through membranes	LUV, SUV
High-pressure homogenization	LUV, SUV
Step 3: purification	
Centrifugation, dialysis, column chromatography separation, ultrafiltration	

Selection of phospholipids

The type, molar percentage, surface charge, and packing orientation of phospholipids determine the physicochemical properties of liposomes. The T_c of phospholipids is also an important criterion to select phospholipids for liposome preparation. The T_c is defined as the temperature required to prompt a change in the lipid physical state from an ordered gel phase where the fatty acyl chains are tightly packed, to a disorganized liquid crystalline phase, where the hydrocarbon chains are loosely oriented and fluid-like [149]. The T_c of phospholipids depends on hydrocarbon chain length, unsaturation, charge, and head group series. As the hydrocarbon length is increased, van der Waals interactions become stronger requiring more energy to destroy the well-ordered packing, thus the phase transition temperature increases. Likewise, introducing a cis double bond into the acyl group puts a kink in the hydrocarbon chain which requires much lower temperatures to receive an ordered packing arrangement. The formation of liposome using phospholipids with higher T_c provides more stability and reduces the risk of premature drug release. As the satisfactory release behavior, the drug molecules will be released from liposomes once they reach the tumor sites. On the contrary, when liposomes are formed from too high T_c of phospholipids, the entrapped drug may be denatured during the loading step. Therefore, the optimum T_c of phospholipids in a liposomal formulation is preferred for minimizing drug leakage and releasing the drug at the right diseased sites [150]. Moreover, the vesicle size, lipid composition, surface coating, surface charge, and interaction of liposome and plasma protein affect drug plasma concentration and clearance process of liposomes in the whole body [151].

2.6.6 Characterization of liposomes

The different techniques employed for the characterization of liposomes are listed in Table 5. Physicochemical characterization comprises of measurement of size, surface charge, morphology, and lamellarity of liposomes. The drug release profile is also studied in different media. Chemical characterization is measured for percentage encapsulation, which is the ratio between the actual quantity of drugs inside the liposomes and the quantity of

initial drug added to the liposomal formulation. Another term is loading capacity, which is the ratio between the loaded drug within the liposomes and the total lipids of the liposomal formulation [120,152].

Table 5 Different techniques for liposome characterization [145,147]

Characteristics	Methods
Phospholipid quantification	Lipid phosphorus content (Bartlett method)
Vesicle size and size distribution	Static and dynamic light scattering, size-exclusion chromatography
Surface charge	Photon correlation spectroscopy associated with electrophoretic mobility
Morphology	Microscopy techniques (light, electronic and atomic force)
Drug encapsulation	Spectrophotometry, fluorescence spectroscopy, HPLC and electrochemical techniques
Lamellarity	Nuclear magnetic resonance (^{31}P -NMR), electron microscopy, small angle X-ray scattering
Lipid phase-transition temperature	Differential scanning calorimetry and nuclear magnetic resonance (^1H -NMR)

2.6.7 Stability of liposomes

The physical and chemical stability of the liposomes is the main restriction for the development of an effective delivery system. Physical instabilities of liquid dispersions of liposomes such as aggregation, flocculation, fusion, and coalescence are usually found during storage. These events can change vesicle size and size distribution and lose the encapsulated drugs from the phospholipid bilayers. Accordingly, it is more preferable to keep liposomal preparations in solid form. Several techniques are available for conversion of the colloidal dispersions of liposomes to dry powders, such as freeze-drying, spray drying, and supercritical fluid [30,37]. The liposomal aggregation can be prevented by electrostatic repulsion between the vesicles arisen from the use of the ionic polar head group's phospholipids. The higher electrostatic repulsive

forces may be optimized by an increase in surface charge density and a decrease in ionic strength stability. Other repulsive interactions, van der Waals is the minimum requirement for helping to reduce aggregation as well. Chemical degradation of liposomes often occurs at the phospholipid bilayer membranes; (1) hydrolysis of the ester bonds between fatty acids and glycerol backbone in the presence of water. The chemical reaction generates lysophospholipids, which reduce rigidity's lipid membrane, enhance permeability, and destabilize the liposomal structure (2) lipid peroxidation of unsaturated fatty acyl chain's phospholipid tends to produce free radical species. From these instabilities, the saturated, short/medium-chain lipids are developed to form a better stable liposome [38,39]. Several factors that affect liposomal stability include liposomal composition, fatty acid side-chains, polar head, chain length, and degree of saturation. Additionally, "phospholipid to cholesterol molar ratio" is also essential for stoutness' bilayers and control of drug release [153]. To maintain the stability of liposomes, it is recommended that liposomes should be stored in a refrigerator [132].

2.6.8 Application of LPs in cancer therapy

The chemotherapeutic drugs are used in single or combination treatment for standard interventions in cancer patients. Most of them are restricted in clinical application because of several issues including narrow therapeutic index, off-target systemic toxicity arisen from poor specific drug distribution, development of multidrug resistance. These problems can lead to failure in cancer therapy. Several anticancer drugs loaded in liposomal formulations have been developed to solve the limitations of conventional chemotherapies to achieve effective therapeutic outcomes with less toxicity toward normal cells by specific delivery of drugs at targeted tumor sites. More importantly, good lipid carriers having desirable properties should not only enhance high cytotoxicity against malignant tumors but also improve patients' quality of life and extend survival time. Liposomes are the first nanocarrier systems to be approved for use in humans in 1995, in the tradename of Doxil[®]. Some liposomal formulations of anticancer drugs approved by US FDA/ other regulatory

authorities were commercially launched in the market and plenty of liposomes are being tested in clinical trials, as listed in Table 6. Most of all products are administered via i. v. route. When anticancer drugs are encapsulated in liposomal structures, they help to reduce the risk of drug exposure with normal tissues, resulting in reducing side effects as well as improving their therapeutic index [122,154,155].



Table 6 List of marketed liposomal products used in cancer therapy [38,83]

Clinical products (Approval year)	Anticancer drug (Administration)	Lipid components	Therapeutic indication	Company
Doxil® / Caelyx® (1995)	Doxorubicin (Intravenous)	HSPC/Chol/DSPE- PEG2000 (56:39:5 molar ratio)	AIDS-related Kaposi's sarcoma, refractory ovarian cancer, metastatic breast cancer, and multiple myeloma	Janssen Pharmaceuticals, USA
DaunoXome® (1996)	Daunorubicin (Intravenous)	DSPC/Chol (2:1 molar ratio)	AIDS-related Kaposi's sarcoma	Galen Ltd., UK
DepoCyt® (1999)	Cytarabine (Spinal)	DOPC/DPPG/Chol/ Triolein	Neoplastic meningitis	Sky Pharma Inc., USA
Myocet® (2000)	Doxorubicin (Intravenous)	EPC/Chol (55:45 molar ratio)	Metastasis breast cancer (in combination with cyclophosphamide)	Elan Pharmaceutical, USA
Marqibo® (2012)	Vincristine (Intravenous)	Sphingomyelin/Chol (60:40 molar ratio)	Acute lymphoblastic leukemia	Talon Therapeutics, USA
Onivyde® (2015)	Irinotecan (Intravenous)	DSPC:mPEG- 2000:DSPE (3:2:0.015 molar ratio)	Metastatic pancreatic cancer (in combination with 5-FU and leucovorin)	Merrimack Pharmaceutical Inc., USA
Lipusu® (2003)	Paclitaxel (Intravenous)	DSPC/Chol	Ovarian cancer, breast cancer and non- small cell lung cancer	Luye Pharmaceutical Co. Ltd. China

2.7 Nanosuspensions (NSs)

The drug discovery process based on up-to-date technologies such as combinatorial chemistry, computer-aided drug design, and high throughput screening have boosted an increase in a vast [156] number of drug candidates possessing satisfiable efficacy profile over the decades but it is estimated that ~40% of new chemical entities (NCEs) are poorly soluble in water. The huge challenge for pharmaceutical development is to formulate special formulations and drug delivery systems to overcome the issue of practically insoluble (< 0.1 mg/mL) of these drugs which are also related to poor bioavailability, especially when the drug is administered through the oral route [157]. The dissolution rate and intestinal permeability are important factors for prediction of the bioavailability, particularly for oral administration. Thus, the two main parameters are chosen to classify chemical drugs into 4 classes, based on the biopharmaceutical classification system (BCS). Poorly soluble drugs belong to either class II (low aqueous solubility with high intestinal permeability) or class IV (low aqueous solubility with low intestinal permeability). Despite high permeability, the poor solubility of drugs with a low concentration gradient between the gut lumen and blood vessels may result in the restriction of drug absorption. The term “solubilization techniques” refers to a tool that enhances the dissolution velocity (dc/dt) and ideally also the saturation solubility (C_s), which may improve the bioavailability of drugs [158]. There are many conventional approaches for the solubilization of poorly water-soluble drugs. Excipients including organic solvents, surfactants, and macromolecules are used in different methods. Overall, they may be called as a solubilizer or solubilizing agent [159].

Co-solvency: co-solvents such as ethanol, isopropanol, propylene glycol (PG), polyethylene glycol (PEG) are widely used in liquid dosage form, especially for parenteral products. Systemic adverse effects resulting from these co-solvents should be considered in the selection of co-solvents [160].

Salt formation: if a drug molecule (weak base or weak acid) can dissociate to form an ionized molecule, it can be coupled with appropriate salt of its acid or base (counterion) via ionic interaction. The ionizable form of the drug in aqueous has a higher water solubility compared to the neutral one [161].

Micellar solubilization: use of low molecular weight surfactants is to reduce surface tension and solubilize drugs by an increase in wetting of hydrophobic compound and assembly of micelle structure that reserves hydrophobic molecule within micelles [162].

Complexation: cyclodextrins (cyclic oligosaccharides) as a complexing agent, can form a reversible, non-covalent bonding with poorly soluble drugs to solubilize them. It can be described that the hydrophobic drug molecules (known as a guest) are inserted into the cavity of cyclodextrin (known as a host) at a suitable ratio of drug to cyclodextrin. Another drawback of this technique is the high excipient level of the resulting product [163].

Unfortunately, the use of some solubilizing agents/ excipients or residual organic solvent can cause toxicities and side effects, for example, allergic reactions, hypersensitivity reactions, nephrotoxicity, neurotoxicity, and neutropenia. Therefore, it is essential to intensively develop special formulations that can deliver poorly water-soluble drugs, including chemotherapeutic drugs [164].

Attempting reach to target tumors, anticancer drugs are commonly designed and formulated into several NCs including liposomes, micelles, solid lipid nanoparticles, polymeric nanoparticles, and dendrimers. Most of all, hydrophobic drug molecules are solubilized, dispersed, and/or entrapped by carrier materials [35]. The US FDA approved a few nanocarrier products of anticancer drugs, for example, liposomal formulations, Doxil[®] (doxorubicin), and Daunosome[®] (daunorubicin); albumin-bound nanoparticles, Abraxane[®] (paclitaxel) [165]. There are many factors that restrict the potential use of NCs in the clinical setting including physical instability, structure deformation, drug leakage during storage and/or *in vivo* performance, resulting in less efficacy, complexation in preparation and synthesis, high manufacturing cost, and difficulty in scaling-up [83]. The NCs with an optimal size range of 100 to 300 nm could fully take advantage of the EPR effect (tumor's leaky vasculature and ineffective lymphatic drainage system) when these delivery systems have to be stable in a physiological environment, high drug loading, capable of sustained release of drug molecules at tumor sites [84]. Among various solubility enhancement strategies, nanocrystal formulations have been considerably interested in the delivery of poorly

aqueous soluble drugs. Marketed nanocrystal-based products are mainly for the oral delivery route, formulated mostly by the top-down approach. Nanocrystals have been used for other routes as well, including parenteral, transdermal, mucosal, ocular, and pulmonary since it can reduce the use of chemical solubilizers, employ simple preparation techniques, and is possible of industrial scale-up [166].

The micronization of drugs is processed to increase the surface area. Increasing the surface area will directly increase the dissolution rate and diffusion rate (drug absorption). Micronization means the transformation of coarse drug powder to micrometer particles under mechanical forces. The mean diameter of micronized drug particles is in the range of approximately 2 to 5 μm . Size reduction of a particle using micronization fails to improve the saturation solubility of the drug compound and is not sufficient to enhance bioavailability. For this reason, nanonization of drugs which makes particle size in the nanometer range is developed to apply instead of the previous method. It further increases the surface area, leading to an increase in aqueous solubility and dissolution rate [42]. Nanocrystals were firstly invented in the 1990s and the first marketed products were quickly launched in the year 2000. This strategy is a rather simple, effective, and universal method that is applied to all poorly water-soluble drugs because these drugs can be cracked into the nanometer range [43].

2.7.1 Definition

Drug nanocrystals are pure solid drug particles with a mean diameter below 1000 nm. Drug nanosuspensions are defined as very finely colloid, biphasic, dispersed drug nanocrystals that are stabilized by stabilizers (surfactants and/or polymers) in a liquid dispersion medium (water, aqueous solution, or nonaqueous medium). This is prepared by suitable methods and used for pharmaceutical drug delivery via various routes of administration. Furthermore, the term “drug nanocrystals” represents a crystalline form of drug particles. In fact, the polymorphism of drug depends on the production method, they can be partially or fully amorphous form [167]. The obvious difference between nanocarriers and nanocrystals can be explained that the main component of nanocrystals is drug powder that is stabilized by few quantities of stabilizers, whereas the nanocarriers contain a small amount of drug that is

dispersed, entrapped, or incorporated by a higher amount of carrier materials [158].

Crystalline vs. Amorphous

Although an active substance has the same chemical formula, there are two polymorphic states of drug solid particles that characterized by three-dimensional arrangement (molecules or atoms): crystalline form is well-defined edges and surfaces, regularly ordered arrangements of components with characteristic X-ray diffraction patterns, and specific melting point, density, and saturation solubility, whereas amorphous form is irregular or curved surfaces, randomly packed arrangements and wide range of melting temperature. The crystalline state is more stable but is lower water solubility and dissolution rate. Moreover, it readily becomes a spontaneous phase transition and recrystallization, resulting in a change in physicochemical properties. In other words, the drug nanocrystals in the amorphous form possess higher saturation solubility compared to drug nanocrystals in crystalline form. To obtain the maximum saturation solubility, dual properties of a nanometer size range and amorphous state are preferable to prepare nanosized drug particles. However, the use of amorphous form in pharmaceutical formulations should be aware that the amorphous form can be maintained throughout the shelf life [40,167].

2.7.2 Physicochemical properties of drug nanocrystals

Drug nanocrystals possess outstanding properties that address the solubility problems including an increase in saturation solubility, an increase in dissolution rate, and an increase in mucoadhesion to the cells. Particle size reduction down to the nanometer range can increase the solubility by increased surface area.

1) Increase in saturation solubility (C_s)

Saturation solubility depends on the physicochemical properties of the compound, dissolution medium, and temperature. This meaning is only valid for drug particles in the micrometer size range. Surprisingly, the saturation

solubility of the particle would increase when particle size is decreased to below 1000 nm due to an extreme increase in surface area.

2) Increase in dissolution velocity

The increased dissolution velocity of nanocrystals can be described by the “Noyes-Whitney equation”.

$$dc/dt = (DA/h) \times (C_s - C_t) \quad \text{Eq.1}$$

where dc/dt is the dissolution velocity, D is the diffusion coefficient, A is the surface area of drug particle, h is the diffusional distance, C_s is the saturation solubility of the drug, C_t is the concentration surrounding the drug particles.

The increase in dissolution velocity (dc/dt) of drug nanocrystal arises from the greater surface area (A) and the increase in saturation solubility (C_s) of the compound (see equation 1). Moreover, the nanometer size range of drug nanocrystals can promote permeation and absorption by passive diffusion because an increase in saturation solubility leads to an increase in concentration gradient between the gut lumen and blood circulation.

3) Augmentation of biological mucoadhesion

The nanometer dimension of drug nanocrystals that have very high contact surface areas helps to enhance adhesiveness to surface/ cell membranes/ tissues, leading to the enhancement of oral bioavailability of poorly soluble drugs [41,168,169].

2.7.3 Advantages and limitations

As above described in the previous section, the drug NSs also have other advantages over other drug delivery systems. When lipophilic drugs are produced in NSs, the resultant formulations with smaller particle sizes in the nanometer range can enhance drug dissolution, diffusion, and absorption rate, enhance the bioavailability, reduce variability, and reduce fed/fasted effect. Due to very small particle size with high surface area, NSs can be easily applied and penetrated for topical drug formulations. There is research reported that they can be applied for reasons of task-masking in oral formulations. NSs are easy

to manufacture and more cost-effective than other nano-drug delivery platforms [42,167]. Despite the many benefits, the technology for producing drug NSs still has some limitations. First, the smaller size of drug nanoparticles can enter any cells of the human body via pinocytosis and lead to further nanotoxicity. Next is the advanced new technique needs an expensive instrument, increasing the cost for the final pharmaceutical products. Moreover, this technique still cannot be considered as a universal approach for all drugs. Finally, the preparation and stability of different drug NSs vary based on the molecular structure of drugs and stabilizers. There are several marketed nanosuspension products for oral drug delivery but none of the FDA- approved nanosuspension containing anticancer drugs has been launched to the market [158].

2.7.4 Methods for nanosuspension preparation

Nowadays, there are two basic techniques for the production of drug nanocrystals including (1) top-down process which is the diminution of large particles into smaller pieces while (2) bottom-up process which is the precipitation of drug solution to form nanoparticles dispersed in a liquid vehicle.

2.7.4.1 Top-down or disintegration method

Typically, the top-down method is involved with size reduction through different technologies (Figure 14). There are two major particle size reduction techniques related to the top-down process; media milling (MM) that is divided into wet milling (NanoCrystals[®]) and dry co-grinding while high-pressure homogenization (HPH) that is categorized into microfluidizer (IDD-P[®]) and piston gap homogenizer using aqueous media (DissoCubes[®]) and non-aqueous media (Nanopure[®]). These methods can generate high thermal energy during the running of the process. Thus, cooling jacket systems are required to control proper temperature without exceeding heating and prevent degradation of heat-labile drugs and alteration of polymorphism [41,170].

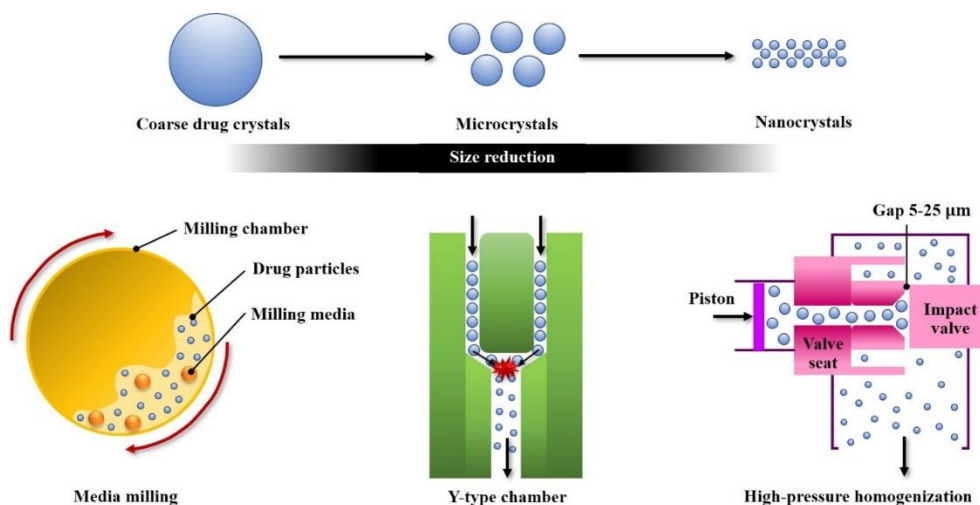


Figure 14 Schematic illustration of top-down techniques: wet ball milling and high-pressure homogenization. Adapted from ref. [170]

1) Media milling

The large particles are physically comminuted into smaller particles via mechanical forces and impactions. Drug particles are dispersed and wetted by an aqueous stabilizer solution in a milling chamber and then subjected to grinding and shearing by operating mechanical instruments, such as milling machines, at a very high shear rate under controlled temperature. To control the appropriate properties of nanocrystals, we should consider several factors that affect the particle size and size distribution of nanocrystals including milling time, speed of rotation, number of running cycles. During rotation of the milling chamber, the milling media (balls or pearls) rollover, crush together and break the drug micronized particles into fine powder until the particle size is reduced to obtain particles with nanosized diameter. The milling media consist of glass, ceramics, stainless steel, zirconium oxide, or highly cross-linked polystyrene resin. The process can be worked in both batch-to-batch (discontinuous mode) and recirculation (continuous mode), depending on the scale. Even though this method is preferred because of its simple scalability and less batch-to-batch variations, main problem is contamination from the corrosion of metal surface's milling media. The residues generated during the milling step are not more than 0.005% w/w in the final product. The use of polymer-coated metal beads (e.g.

polystyrene resin derivatives) may minimize the erosion in order to reduce the unexpected side effects caused by their impurities. The disadvantages of this technique include high energy requirement, time consumption (varies from hours to days), and expensive cost of the machine. This technique is an effective particle size reduction process that has been applied to produce several marketed products such as Rapamune[®], Emend[®], Tricor[®], and Megace ES[®] (see Table 7). These products on the market prove that the media milling is the acceptance and applicability [171]. Another type of media filling is dry cogrinding or dry milling. This method is used to produce NSs by mixing poorly soluble drugs with surface-active agents such as sodium lauryl sulfate (SLS), polyvinylpyrrolidone (PVP), polyvinyl alcohol (PVA) in a liquid medium. Dry milling can reduce particles to the submicron levels without any use of organic solvents [167,170].

2) High-pressure homogenization (HPH)

It is another attrition technique which based on jet-stream microfluidization. Two fluid streams of drug suspension vigorously attack in a Y-shaped or a Z-shaped chamber, leading to particle collision and consequent particle fracture under high pressure up to 1700 bar. An example of a marketed product produced by this technique is Triglide[®] (see Table 7). Piston-gap homogenizers are also used to manufacture nanosized drug particles by forcing the drug suspension with a piston through a small orifice under high pressure. The cavitation forces, high shear forces, and turbulent flow help to fracture the drug particles. The capacity of size reduction, in terms of particle size and size distribution, depends on many factors, including the power of homogenization, pressure level, and numbers of the cycles. The process is generally composed of three steps: (1) drug powders are dispersed in stabilizer solution (2) particle size is reduced using high-speed homogenization under low pressure (3) high-pressure homogenization is applied to obtain the desirable particle size and size distribution [41].

2.7.4.2 Bottom-up or nanoprecipitation method

Drug particles in nanometer size can be formed by a bottom-up process which is related to two important steps, nucleation and crystal growth (Figure 15). This method may be called the “classical precipitation method” (known as via *humida paratum*). In brief, a poorly water-soluble drug is dissolved in an organic medium that is water-miscible (e.g. ethanol, methanol, acetone, dimethyl sulfoxide). When this drug solution (molecular level) is poured into a nonsolvent/an anti-solvent, such as water/buffer solution, the drug molecules are precipitated to form finely dispersed drug NSs because of the supersaturation of the drug solution. The mixing of the drug solution and anti-solvent can be performed in batch-to-batch or continuous mode [41]. The main drawback of this technique is that the fine particles tend to grow up, driven by a phenomenon called “Oswald ripening” and become an aggregation of particle clusters [172]. The major limitation of this method is that the drug can be dissolved/ solubilized in at least one solvent and the solvent needs to be miscible with a nonsolvent. Other bottom-up methods include sonocrystallization, supercritical fluid technology (SCF), high gravity controlled precipitation (HGCP) technology, confined impinging liquid jet (CLIJ) technology, and multi-inlet vortex mixing. Before using the final nanosuspension products, the organic solvent has to be carefully removed, leading to the high cost of production. Therefore, the bottom-up techniques have not been used for the manufacturing of commercial products. NSs produced by the bottom-up technique are more suitable for i.v. injection of anticancer drugs, owing to low generating energy and contamination of fewer impurities. Nonetheless, no approved parenteral commercial products using this technique has reached the market [41,173].

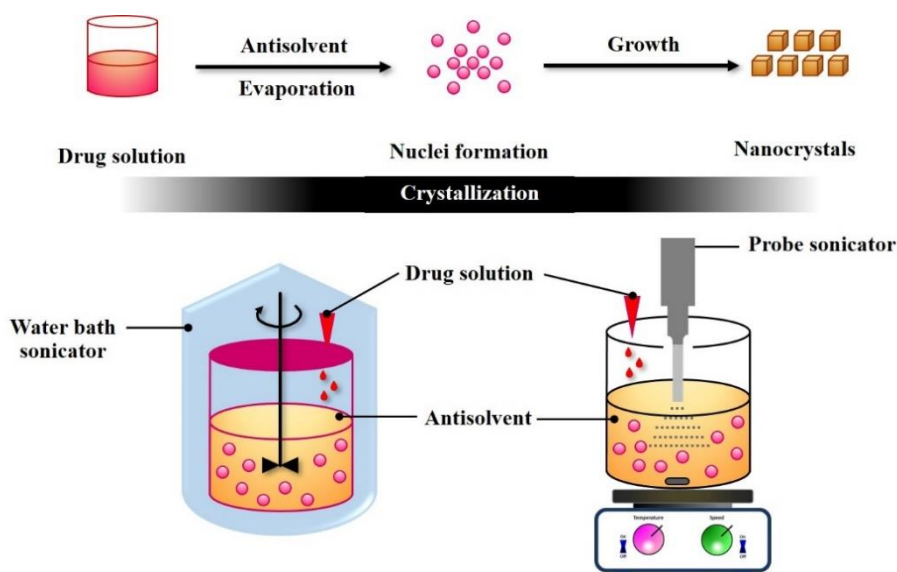


Figure 15 Schematic illustration of bottom-up techniques. Adapted from ref. [170]

2.7.4.3 Combination technologies

Currently, there is a combination of previously mentioned techniques to significantly improve the capacity of particle size reduction and other benefits such as faster manufacturing, improved physical stability. The NanoEdge™ owned by Baxter shows that nanocrystals can be produced by two steps: nanoprecipitation technique followed by high-pressure homogenization. Starting from a uniform suspension is created by mixing hydrophobic drug solution in an organic solvent into an aqueous solution containing a stabilizer under vigorous stirring. The drug compounds become drug microparticles dispersed in an aqueous medium. For additional size reduction, they are homogenized under high-energy input using a high-pressure homogenizer to yield the drug particles with nanometer range, usually found to be 400 nm to 2 μm. Next technologies, SmartCrystal® technology is a useful tool for various multiple processes e. g. H42 (spray-drying with HPH), H69 (parallel flow precipitation with HPH), H96 (lyophilization with HPH), PLH (precipitation-lyophilization-homogenization) [41,174].

2.7.5 Particle stabilization

Nanocrystals and nanosuspensions often require stabilizers (surfactants and polymers) to be physically adsorbed onto the surface of each particle, provide sufficient interaction between drug molecules and stabilizers to prevent the particle aggregation or agglomeration during production, storage, and administration [172]. Particle aggregation arises from Ostwald ripening and eventually does not return to normal system (irreversible process), resulting in larger particles and precipitate formation. Ostwald ripening is a phenomenon that coarse particles grow at the expense of fine particle re-dissolving. The small sizes which are more soluble than bigger ones, occur mass transferring from the fine to the coarse particles, leading to the formation of microparticles. It needs to add surfactant into nanocrystal formulations if the surface of nanocrystals is uncharged and neutral particles. Normally, polymers are widely used to provide a steric barrier between each particle; in the case of using ionic surfactants or polymers, electrostatic repulsion also inhibits particle aggregation. Povidones, polysorbates, Pluronics or Poloxamers, and cellulose derivatives are the most frequently used stabilizers. Some stabilizing molecules originated from natural sources such as lecithin, chitosan are utilized as well. For instance, hydroxypropyl methylcellulose (HPMC), methylcellulose (MC), sodium carboxymethylcellulose (NaCMC), sodium alginate (NaAlg) produce terrible stabilizing performance because of their high viscosity. Stabilizer with lower viscosity including linear synthetic polymers (PVP K30 and K90) and synthetic copolymers (Poloxamer 188) show better stabilizing capabilities, especially at higher concentrations. Tween[®] 80 and TPGS (D- α -tocopheryl polyethylene glycol succinate) containing hydrophobic tail and hydrophilic head in the same molecular structure gave more stabilizing performance [175]. Lecithin is considered the stabilizer of choice when NSs are intended for the parenteral products as their sterilization can be achieved with heat. Interestingly, TPGS is a very good stabilizer that provides dual properties; stabilizing effect, and P-gp inhibition effect, so it can be used to solve multidrug resistance (MDR) of anticancer drugs [176]. The novel stabilizers with appropriate functions have been studied for stabilizing the dispersion system of nanocrystals or

nanosuspensions. The good stabilizers should have sufficient adsorption on the particle surface and introduce proper repulsive force (electrostatic and/or steric hindrance) between each particle. The other properties of stabilizers are expected to be compatible, safe, and low toxicity [44].

The selection of stabilizers is considered in the types and concentration of the stabilizers. Excess amounts of surfactants do not always lead to better prevention of particle aggregation because the surfactant molecules tend to form micelles in an aqueous medium when their concentration above the critical micelle concentration (CMC). The drug to stabilizer ratio, generally vary from 1:20 to 20:1, needs to be optimized to archive the desired nanosuspension formulation [41]. In general, stabilizers are commonly mixed along with the microparticle materials before the process of particle size reduction to maintain the original form of drugs. Nowadays, no systematic guidelines for using proper stabilizers is well-published, so the way to find out one of suitable stabilizer for stabilizing each hydrophobic drug is usually proven by trial and error. Alternatively, nanocrystal products may be transformed to dry state via solidification (freeze-drying, spray drying, electrospraying, or pelletization), in case the stabilizers cannot maintain the stability of nanocrystals in liquid form for long-term storage. Additionally, the dry powder of drug NSs can be formulated with pharmaceutical excipients to obtain finished products such as tablets, capsules, pellets, etc [44]. NSs for the parenteral route are often sterilized by moist heat sterilization using autoclave, membrane filtration as well as gamma radiation. NSs can be stored as liquid suspension or lyophilized solid form [45]. Some nanosuspension products are also added with some other additives such as salts, buffering agent, osmotic agent, antioxidant. These additives should be considered in the issues of compatibility with drug and route of administration [177,178].

Role of stabilizer

During nanosuspension production, when drug particles are reduced in diameter, leading to increased surface area with a significant increase in Gibb's free energy of the system. From Gibb's free energy equations as shown below,

the high interfacial tension becomes a thermodynamically unstable system. Thus, the system tends to reduce total free energy by undergoing particle aggregation/agglomeration.

$$\Delta G = \gamma \Delta A - T \Delta S \quad \text{Eq.2}$$

where ΔA is the change in surface area, γ is the interfacial tension, T is the absolute temperature (Kelvin), and ΔS is the change in entropy.

Adding the stabilizers into NSs causes a reduction in the interfacial tension between the particles and dispersion medium leading to free energy minimization (see equation 2). Stabilizers also act as a wetting agent by reducing the contact angle. It is suggested that stabilizers should be mixed at the initial stage of the production process to fully maintain stability. The mechanisms of preventing physical instability of NSs involve electrostatic repulsion from the electrical charge of the particles and steric hindrance due to the bulky moieties of the stabilizers. Many reviews reported that a combination utilization of electrostatic and steric stabilizers usually exhibited a better effective stabilizing effect in drug NSs [44,177].

2.7.6 Characterization of nanosuspensions

There are many parameters of NSs that affect their stability, saturation solubility, dissolution profile, safety, as well as their *in vivo* performance. These characteristic topics including particle size and size distribution; surface charge; crystallinity; dissolution rate, are described below.

1) Particle size

Photon correlation spectroscopy (PCS) is mostly used for particles ranging from 3 nm to 3 μm . The particle size from this technique is light intensity weighted. PCS is a good, accurate, and fast technique for measurement of particle size and size distribution. For particle size $> 3 \mu\text{m}$, laser diffractometry (LD) is mostly utilized to determine the diameter of drug microparticles. This method gives particle size data based on volume. Both methods operate well for spherical-like particles. In the case of non-spherical particles, the size may significantly deviate from actual size. Another method

that can be used to measure actual morphology, surface feature and diameter size is electron microscopy (scanning electron microscope; SEM and transmission electron microscope; TEM). The size distribution is indicated by the “polydispersity index” (PDI), which indicates the breadth of particle size distribution. A PDI value of 0.1-2.5 represents a narrow size distribution while a PDI > 0.5 indicates a broad size distribution. To maintain long-term physical stability, it is necessary to monitor the PDI value as low as possible. The change of the mean particle size of drugs leads to variation in saturation solubility and dissolution rate. Bear in mind, when nanocrystal formulation is administered via i.v. route, it is essential to assure that the particle size is not bigger than the cavity of capillaries ($\sim 5 \mu\text{m}$) to circumvent the capillary blockade or embolism [179,180].

2) Surface charge

Charging on the electrical surface's particle is important for considering the physical stability of nanocrystals in liquid form. According to the DLVO theory, the stability of the colloidal system depends on the balance between two basic forces; attractive (van der Waals) and repulsive (electron double layer). The electrical double layer enclosing a particle has an inner region (Stern layer, counterions are strongly attached to the particle) and an outer region (diffuse layer, counterions are attached with low affinity). Within the diffuse layer, the “slipping plane” separates counterions that move along with the particle. The electrokinetic potential difference at the slipping plane versus a point in the bulk medium is defined as the “zeta potential (ζ)”. In other words, it is a function of electrolyte concentration or ionization of stabilizer molecules that are adsorbed onto the particle surfaces. This parameter can be determined by light scattering to monitor the “electrophoretic mobility” when the colloidal dispersion system is subjected to an electric field. Moreover, the pH of the medium, conductivity of the liquid, and its composition can affect the distributions of counterions surrounding the interface and thereby the zeta potential [180]. Generally, at least $\pm 30 \text{ mV}$ is the appropriate value of zeta potential that can stabilize the nanosuspension system without aggregation via electrostatic repulsion. For

particles with low zeta potentials, stabilizers may be needed to provide further steric repulsions. A minimum zeta potential of 20 mV is desirable for a combined electrostatic and steric stabilization. The positively charged nanoparticles caused higher hemolytic activity due to strong electrostatic interactions between the particles and the anionic cell membrane and they accumulated in the liver proportionally to the positive charge density; in contrast, negatively charged nanoparticles were not hemolytic. Highly charged nanoparticles had a much higher uptake than neutral or slightly charged nanoparticles of the same size, by opsonization of RES, largely in the liver and spleen [41,181].

3) Crystallinity

Crystallinity is often assessed by X-ray diffraction (XRD), augmented by differential scanning calorimetry (DSC). The drugs pseudopolymorphs in form of hydrates or solvates are evaluated by thermogravimetric analysis (TGA) to know any weight loss during heating. These instruments can indicate the polymorphic form of nanocrystal formulation; crystalline or amorphous materials. These data help to understand polymorphic changes of drug particles when they are subjected to the step of nanosizing [180].

4) *In vitro* dissolution study

The dissolution rate for NSs can be defined as drug quantity in solution per time under standard conditions of liquid/ solid interface, temperature, and type of media (e. g. simulated gastric fluid, simulated intestinal fluid, or physiological media). Normally, their dissolution profiles can be examined by USP dissolution apparatus 2 (paddle) or modified similar methods. Before quantitative analysis of the dissolved drug, the insoluble drug particles should be removed by membrane filtration or ultracentrifugation. With the presence of high concentration stabilizers, the solubility of a drug may be increased, likely due to micellar solubilization of the drug. It must be noted that although the dissolution rate of nanocrystal formulation is improved due to the increase in surface area, the increasing level of saturation solubility seems less. For a poorly soluble drug, the absolute increase in the dissolution rate of its nanocrystal

formulation is still marginal. Similarly, saturation solubility can predict the change in biological performances such as plasma drug concentration and bioavailability. NSs are supposed to improve the saturation solubility of the insoluble compound. The determination of saturation solubility of NSs is simultaneously performed in accordance with specified procedures in a solvent at a specified temperature [182].

5) Resuspendability

Prior to the administration of nanosuspension products, the colloidal heterogenous liquid should be easily resuspended by hand-shaking to obtain uniform distribution of dispersed drug particles. It makes sure that each delivered volume of NSs contains precise and constant concentration of drug. When the gravity of drug particles becomes larger their buoyancy force provided by colloidal dispersion system, the sedimentation occurs. For long-term physical stability testing, the coarse suspension or nanosuspensions of poorly water-soluble drug are monitored in sedimentation phenomenon. The NSs will be good stability when sedimentation rate is very low [183].

6) Others

NSs are expected to have a specific appearance such as color, turbidity, viscosity. In addition, pH is also an important factor that influences the physical stability and solubility of the drug [180].

2.7.7 Stability of nanosuspensions

Even though an increase in the surface area of drug particles bring their unique characteristic and biopharmaceutical behavior, it remains thermodynamically unstable and promotes agglomeration and crystal growth. The high surface energy of a nanosized particle is reduced by decreasing the surface area by forming a bigger particle size (known as Ostwald ripening phenomenon). Similarly, the process of flocculation or crystal growth during the preparation or shelf life of NSs directly influences the dissolution and *in vivo* performance. These obstacles might retard formulation development and their applications in the pharmaceutical industries [184].

1) Aggregation

The use of inappropriate stabilizers causes lasting instability in NSs and eventually aggregation during the storage, preparation, or solidification process. Therefore, prevention of the particle aggregation is a principal parameter for the development of a stable and effective drug NSs. Amphiphilic polymers can be used to be adsorbed onto particle surfaces. The adsorbed chain molecules on surfaces help to prevent coalescence by repulsive entropic forces. The stabilizer having high viscosity in the aqueous phase, like a suspending agent, can reduce the particle growth and sedimentation rate. It also forms stereospecific blockade between the nanosuspension particles and inhibits the particle contacting [185].

2) Sedimentation and flocculation

NSs are colloidal dispersion having a particle size between true solutions (<1 nm) and coarse dispersions (>1000 nm). Sedimentation takes place in NSs like a coarse suspension when the gravity of the drug particle is greater than the buoyant force of the dispersion system. Flocculation, a type of sedimentation, is a disequilibrium condition of colloidal nanosuspensions, which is caused by an attractive force that is stronger than the repulsive force between drug particles. Multiple mechanisms are involved in polymer chain bridging, polymer surface complex formation, charge neutralization. When NSs are much diluted in a medium, floccules will be fractal structure. This instability in NSs can be prevented by optimizing the preparation process parameters, using the proper stabilizer, and also transforming NSs into dry powder [186].

3) Polymorphism and crystallinity

The full or partial amorphous state of the solid drugs is the potential to improve their dissolution velocity and is thermodynamically unstable, compared to their crystalline states. However, the amorphous form of drugs in NSs can transform into some specific crystalline form. This is an unrequired drawback being found during storage that directly affects solubility and dissolution rate. Thus, the conversion of liquid nanosuspensions to dry powder is an effective way to avoid the polymorphic transformation and keep the original form of drugs [44,180].

Solidification process

Some drugs NSs cannot be stored in an aqueous medium because the active compounds are degraded by hydrolysis or other chemical reactions. Hence, the post-production procedure of NSs needs to be done for the extension of storable time and prevention of particle aggregation. Even though various techniques are used to produce a dry powder such as spray drying and pelletization, freeze-drying is recommended and frequently used as it is a friendly method for heat-sensitive products. Freeze drying process (known as lyophilization) mainly consists of three steps: first, freezing is to transform the liquid nanosuspensions to solid form (ice crystals) in the freezer, followed by primary drying is to sublimate the solvent using a freeze dryer at low temperature and vacuum. Finally, secondary drying is to completely remove an unfrozen aqueous until obtaining resultant highly porous and dry powder of drug particles [187]. Cryoprotectants or protective agents are added into liquid nanosuspensions to avoid particle aggregation or caking during the lyophilization process. The mostly used cryoprotectants include sugar (sucrose, glucose, lactose, trehalose); sugar alcohol (sorbitol, mannitol); dextran; etc. Mannitol has been more widely used than other sugars. These protective materials should not affect the biological performance of the drug and the lyophilized products can provide original nanosuspensions when dry powders are re-dispersed/reconstituted in an aqueous vehicle. To reserve the biological activities of the drug, the content of nanocrystal products should be collected in the right packaging that protects the drug from chemical hazards, photolysis, and oxidation [188].

2.7.8 Application of NSs in cancer therapy

To date, the number of studies reported that the use of nanocrystals for cancer therapy is limited. In general, free drug molecules dissolved from nanocrystals enter cells through passive diffusion. Additionally, nanocrystals can be taken up cells via active transport process, including the clathrin- and caveolae-mediated endocytosis. The particle size of ≤ 200 nm is preferentially taken up by clathrin-coated pits, while particles between 200 and 500 nm are

taken up by the caveolae-mediated pathway. The maximum size of particles that can be internalized through the cell membrane is 500 nm [189].

NSs are a suitable therapeutic platform for targeted drug delivery systems. They attract lots of interest in site-specific drug delivery due to the ease in modification/ functionalization of surface properties, and scale-up. Optimized physicochemical properties of NSs containing anticancer agents are supposed to express a better antitumor efficacy against malignant tissues with lower toxicity toward normal tissues. However, nanocrystals with size in the submicron range in blood circulation will be recognized as exogenous elements by macrophage cells in MPS, which are found abundantly in the liver and spleen, conducting to passive accumulation in these cells but occurring low plasma concentration. It has been reported that more than 90% of the i. v. injected dose is transported to the liver and ~5% to the spleen within 5 min after injection [44]. To solve this problem, surface coating with biocompatible and hydrophilic materials such as polyethylene glycol (PEG) or Poloxamer helps to reduce the opsonization process resulting in prolong shelf life in blood circulation and promoting the accumulation of drug nanocrystals via the EPR effect. Generally, the EPR effect is not enough to specifically deliver to the tumor sites because the non-specific distribution of drugs throughout the body results in side effects, further limiting their clinical use [11,33].

An effective strategy for tumor targeting through ligand- conjugated nanocrystals may be used to selectively enhance drug accumulation in order to achieve good antitumor efficiency with low toxicity. Not only surface treatment using stabilizers can stabilize nanocrystals, but also surface attachment with further functional ligands can design nanocrystals with the purpose of active targeting or inhibition of MDR [190].

Although orally administered nanoformulations are more accepted, i. v. injection is still the preferable route for cancer therapy. This can be explained that some anticancer drugs have poor oral absorption and bioavailability, mainly due to their poor water solubility. Intravenously administered drug nanocrystals are expected to reach solid tumors via the EPR effect due to the nanoscale

dimension. Nanocrystals are not expected to dissolve rapidly in the plasma upon i.v. administration, leading to improved biodistribution, compared with the oral route [45]. The *in vivo* distribution of drug nanocrystals is affected by main factors including particle size, particle morphology, and surface properties as discussed below.

- 1) The smaller particles can dissolve quickly in the blood, escape from phagocytosis in MPS, whereas larger particles are more being phagocytosed than the small one, leading to reduced drug accumulation in the solid tumors.
- 2) Particle morphology also affects the biodistribution of nanocrystals.
- 3) Surface modification of nanocrystals can alter their biodistribution profiles. As mentioned already, the PEGylation of surface particles acting stealth property reduces the RES uptake. Moreover, ligand modification can improve the targeting efficiency for specific delivery of anticancer drugs nanocrystals as well. The attached ligands at the surface's particles specifically bind target receptors on tumor cells, leading to the induction of internalization to the cancer cell via receptor-mediated endocytosis [45,191].

However, ligand modification might not usually enhance the *in vivo* distribution behavior of drug nanocrystals. This situation can be explained that the specific ligands that are physically adsorbed onto nanocrystals surface cannot bind via adequate interaction, resulting in detachment of ligands from the surface (loss of balance between adsorption and desorption) in aqueous stabilizer solution. This instability can occur when the nanocrystals coupled with ligands are much diluted in biological fluid [192].

1 **Table 7** Available marketed pharmaceutical nanosuspension products [170]

Trade name/ Approval year	Generic drug/ Indication	Nanosuspension method	Dosage form	Company
Rapamune® (2000)	Sirolimus (Immunosuppressant)	Top-down (NanoCrystal® Elan system)	Oral tablet	Wyeth
Emend® (2003)	Aprepitant (Anti-emetic)	Top-down (NanoCrystal® Elan system)	Oral capsule	Merck
Tricor® (2004)	Fenofibrate (Hypercholesterolemia)	Top-down (NanoCrystal® Elan system)	Oral tablet	Abbott
Megace ES® (2005)	Megesterol acetate (Appetite stimulant)	Top-down (NanoCrystal® Elan system)	Oral suspension	Par Pharmaceutical
Ritalin® (2002)	Methyphenidate HCl (Antipsychotic)	Top-down (NanoCrystal® Elan system)	Oral tablet	Novartis
Triglide® (2005)	Fenofibrate (Hypercholesterolemia)	Top-down (IDD-P® Skyepharma)	Oral tablet	First Horizon Pharma
Invega Sustena (2009)	Paliperidone palmitate (Antidepressant)	Top-down (High-pressure homogenization)	Parenteral suspension	Johnson & Johnson
Cesamet® (2005)	Nabilone (Anti-emetic)	Bottom-up, Co-precipitation	Oral capsule	Lilly

2.8 Chitosan (CS) and chitosan derivatives

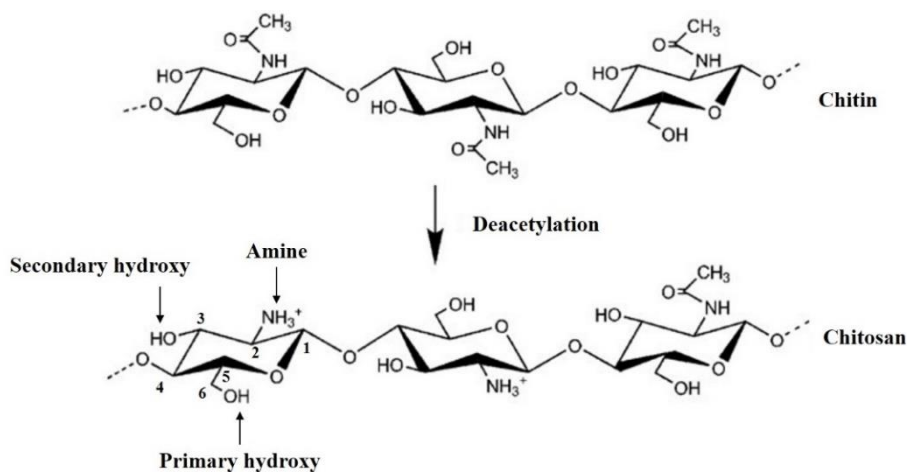


Figure 16 Chemical structure of chitin and chitosan. [193]

Chitosan, a linear cationic amino polysaccharide derivative, consists of N-acetyl-D-glucosamine (acetylated unit) and D-glucosamine (deacetylated unit) linked in a β (1→4) manner (Figure 16). This biopolymer originated from a natural source is generally produced by alkaline deacetylation of chitin which is a component found in the exoskeleton of crustaceans such as crabs and shrimps [193]. The USP officially indicated that its degree of deacetylation is in the range of 70.0% to 95.0% [194]. It has several useful properties including biocompatibility, biodegradability, bioadhesivity, non-toxicity, low immunogenicity, and low cost [195,196]. However, it cannot dissolve in neutral or alkaline solution and physiological fluid but solubilize in an acidic environment ($\text{pH} < 6.5$); consequently, it could be used to carry drugs through the body until reaching acidic tissue environments, such as in solid tumors [197,198]. Due to its attractive properties involved in pharmaceutical and biomedical applications, many researchers have been interested in the development of novel drug delivery systems based on chitosan and chitosan derivatives with a favorable profile. According to the structure of chitin- chitosan, it cannot form micelle itself because of a lack of amphipathicity in its molecule [199].

Currently, many researchers have designed and synthesized by connecting the hydrophobic parts on the chitosan backbone to generate plenty of amphiphilic chitosan derivatives with improved solubility and other demanded properties. Normally, the

chemical modification used for the synthesis of chitosan derivatives is based on the reductive amination of amino ($-NH_2$) groups at the C-2 position and esterification or etherification of hydroxyl ($-OH$) group at C-3 (secondary hydroxyl) or C-6 (primary hydroxyl) position [200]. The chitosan derivatives such as *N*-lauryl-carboxyl methyl chitosan [201], *N*-octyl-*O*-sulfate chitosan [202], PEG conjugated *N*-octyl-*O*-sulfate chitosan [203], *N*-octyl-*O*-glycol chitosan [204], stearyl chitosan oligosaccharide [205], *cis*-acetyl chitosan oligosaccharide [206], carboxymethyl chitosan-graft-polycaprolactone [207] have been successfully synthesized to form self-assembled polymeric micelles loaded with anticancer drugs.

In this research, various amphiphilic chitosan derivatives including *N*-naphthyl-*N,O*-succinyl chitosan (NSC), *N*-octyl-*N,O*-succinyl chitosan (OSC) and *N*-benzyl-*N,O*-succinyl chitosan (BSC) were synthesized by introducing hydrophobic (naphthyl, octyl, benzyl group) onto the primary amino groups on the CS backbone through N-amination, and grafting hydrophilic pH-sensitive moiety (succinyl group) onto primary amino and hydroxyl groups of CS backbone through *N,O*-succinylation (Figure 17). The critical micelle concentration (CMC) of NSC, OSC, and BSC was 0.0678, 0.0855, and 0.0575 mg/mL, respectively, as measured by fluorescence spectroscopy (hydrophobic pyrene probe). These CMC values of CS derivatives were lower than low MW surfactants. Moreover, the degree of N-hydrophobic substitution (DS) and degree of *N,O*-succinylation (DSS) calculated from the H-NMR and FT-IR spectra indicated that hydrophobic and succinyl group were successfully grafted onto CS backbone [27,28].

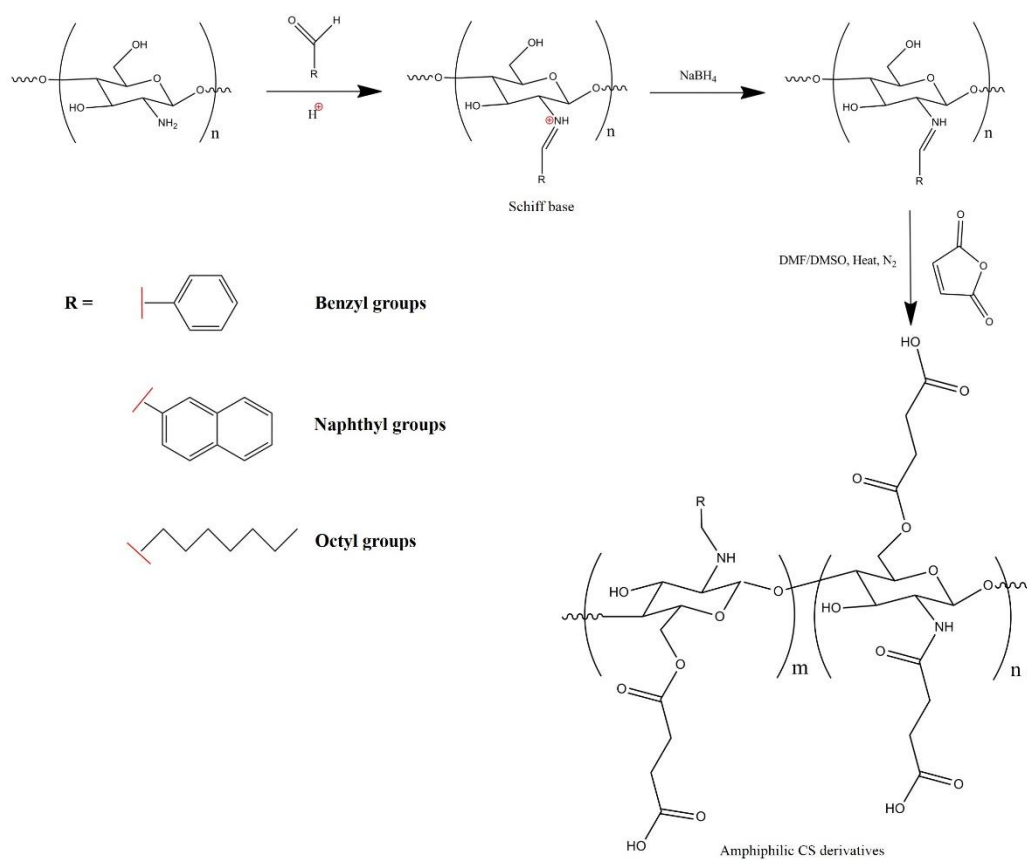
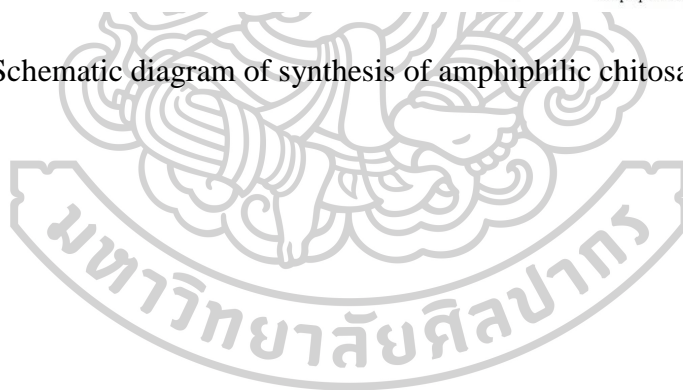


Figure 17 Schematic diagram of synthesis of amphiphilic chitosan derivatives [28].



CHAPTER 3

MATERIALS AND METHODS

3.1 Materials

3.1.1 Drugs and pharmaceutical excipients

- Acetone (QReC, Malaysia)
- Andrographolide analogue 3A.1 (19-tert-butyldiphenylsilyl-8,17-epoxy andrographolide) was gifted from Faculty of Science, Burapha University (Chonburi, Thailand)
- Annexin V-FITC apoptosis detection kit (BD Biosciences, NJ, USA)
- Benzaldehyde (Sigma Aldrich[®], St. Louis, MO, USA)
- CD₃COOD and DMSO-d₆ (Cambridge Isotope Laboratories, Inc., MA, USA)
- Chitosan (DDA 96%, MW 10-13 kDa) (OilZac Technologies Co., Ltd., Bangkok, Thailand)
- Chloroform (V.S. Chem House, Bangkok, Thailand)
- Cholesterol (Carlo Erba Reagenti, Ronado, Italy; purity 95%)
- Crystal violet (Microscopy grade, Loba Chemie Pvt. Ltd., Mumbai, India)
- Deionized water
- Deuterium oxide (D₂O) (MagniSolv[™], Merck, Switzerland)
- Dichloromethane (Merck, Germany; purity ≥ 99.8%)
- Dimethyl sulfoxide (DMSO) (Fisher Scientific, UK Limited, UK)
- Doxorubicin (Sigma Aldrich[®], St. Louis, MO, USA; purity ≥ 98%)
- Ethanol (Merck, Germany; purity ≥ 99.9%)
- Fluorouracil (5-FU) solution (Effcil[®], Boryung Pharmaceutical Co., Ltd., Seoul, Republic of Korea; 500 mg/10 mL)
- Folate-conjugated NSC (NANOTEC, Thailand)
- Formaldehyde solution (The Government Pharmaceutical Organization (GPO), Bangkok, Thailand; 34.5-38.0% w/w of CH₂O)
- Glacial acetic acid (Merck, Germany; purity ≥ 99.8%)
- Hydrochloric acid (Scharlau Chemie S.A., Spain; purity ≥ 99.8%)
- Mannitol (Chemipan Co., Ltd., Bangkok, Thailand)
- Methanol (Merck, Germany; purity ≥ 99.9%)

- 2-Naphthaldehyde (Sigma Aldrich[®], St. Louis, MO, USA)
- Na-salt of N-(carbonyl-methoxypolyethylene glycol-2000)-1,2-distearoyl-sn-glycero-3-phosphoethanolamine (PEG2000-DSPE) (Lipoid GmbH, Ludwigshafen, Germany)
- *N*-benzyl-*N,O*-succinyl chitosan (BSC) (NANOTECH, Thailand)
- *N*-naphthyl-*N,O*-succinyl chitosan (NSC) (NANOTECH, Thailand)
- *N*-octyl-*N,O*-succinyl chitosan (OSC) (NANOTECH, Thailand)
- Nitrogen gas (Masser Specialty Gas Co., Ltd., Nakorn Pathom, Thailand)
- *N,N*-dimethylformamide (DMF) (Brightchem Sdn Bhd, Malaysia; purity \geq 99.8%)
- Octaldehyde (Sigma Aldrich[®], St. Louis, MO, USA)
- Phosphatidylcholine (PC) (Phospholipon[®] 90G, Lipoid GmbH, Ludwigshafen, Germany)
- Poloxamer 188 (Lutrol F68) (VITA Co., Ltd., Thailand)
- Polyoxyethylene 20 sorbitan monooleate (Tween 80) (OmniPur[®], USA)
- Potassium bromide (KBr) (IR grade, Merck[®], Germany)
- Potassium chloride (KCl) (Ajax Finechem Australia, New Zealand)
- Potassium dihydrogen phosphate (KH₂PO₄) (Ajax Finechem Australia, New Zealand)
- Sodium borohydride (Sigma Aldrich[®], St. Louis, MO, USA)
- Sodium chloride (NaCl) (Sigma Aldrich[®], St. Louis, MO, USA)
- Sodium dihydrogen phosphate (Ajax Finechem Australia, New Zealand)
- Sodium dodecyl sulfate (SDS) (Fisher Scientific, UK Limited, UK)
- Sodium hydroxide (Ajax Finechem Australia, New Zealand)
- Succinic anhydride (Sigma Aldrich[®], St. Louis, MO, USA)
- Triton[®] X-100 (Amresco[®], Solon, Ohio, USA)
- The other reagents and chemicals were commercially available and used without further purification.

3.1.2 Cell lines and culture reagents

- Accutase enzyme solution (Accutase[™], Merck, Kenilworth, NJ, USA)

- 3-(4,5-dimethylthiazol-2-yl)-2,5-diphenyltetrazolium bromide (MTT) (Sigma Aldrich[®], St. Louis, MO, USA)
- Dulbecco's modified Eagle's medium (DMEM) (GIBCO[®], Grand Island, NY, USA)
- Fetal bovine serum (FBS) (GIBCO[®], Grand Island, NY, USA)
- Glutamax (GIBCO[®], Grand Island, NY, USA)
- Human colon adenocarcinoma (Caco-2) cell line (ATCC[®] HTB-37[™], Rockville, MD, USA)
- Human colorectal adenocarcinoma (HT29) cell line (ATCC[®] HTB-38[™], Rockville, MD, USA)
- Human colorectal carcinoma (HCT116) cell line (ATCC[®] CCL-247[™], Rockville, MD, USA)
- Human head and neck squamous cancer (HN22) cell line was provided from Faculty of Dentistry, Naresuan University (Phisanulok, Thailand)
- L-glutamine (GIBCO[™], NY, USA)
- Minimum essential media (MEM) (GIBCO[™], NY, USA)
- Non-essential amino acids (100X) (GIBCO[™], NY, USA)
- Penicillin-streptomycin antibiotics (GIBCO[®], Grand Island, NY, USA)
- Phosphate-buffered saline (PBS, pH 7.4)
- Sterile water for irrigation (Thai Otsuka Pharmaceutical Co., Ltd., Bangkok, Thailand)
- Trypan blue (0.4%) staining solution (GIBCO[®], Grand Island, NY, USA)
- Trypsin-EDTA (0.25 %) solution (GIBCO[®], Grand Island, NY, USA)

3.1.3 Animal experiment

- Nude mice (male, BALB/cAJcl-nu, 18±2 g, 5 weeks old) (Nomura Siam International Co., Ltd., Bangkok, Thailand)
- Adhesive tape
- Digital Vernier caliper (Syntex[®], Syntex Electronic Technology Co., Ltd., China)
- 70% Ethanol solution
- Fine forceps

- Hypodermic needle 23G × 0.5-inch, 26G × 0.5-inch (Nipro Co., Ltd., Bangkok, Thailand)
- Hypodermic needle 27G × 0.5-inch (Terumo Co., Tokyo, Japan)
- Medical scissor and scalpels
- Normal saline solution (A.N.B. Laboratories Co., Ltd., Bangkok, Thailand)
- Sterile gauze (United Medical Instruments Co., Ltd., Bangkok, Thailand)
- Sterile syringe 1 mL, 3 mL (Nipro Co., Ltd., Bangkok, Thailand)
- Surgical blade stainless steel (Feather Safety Razor Co., Ltd., Osaka, Japan)
- Xylinvet[®] injection (xylazine)
- Zoletil[®] injection (tiletamine/zolazepam)

3.2 Equipments

- 1.5, 2.0 mL microcentrifuge tube (Eppendorf[®], Corning Incorporated, NY, USA)
- 15, 50 mL centrifuge tubes-sterile (Biologix Research Company, KS, USA)
- Aluminum foil (Diamond[®], China)
- Analytical balance (Sartorius CP224S; Scientific Promotion Co., Ltd., Bangkok, Thailand)
- Automatic autoclave (Model: LS-2D; Scientific promotion Co., Ltd.)
- Automatic cell counting machine (TC10[™], Bio-Rad laboratories Inc., CA, USA)
- Bath sonicator (Transonic series 890/H, Elma Hans Schmidbauer GmbH, Germany)
- Beaker (Pyrex, USA)
- Cell culture flask 25 cm³, 75 cm³ (Corning[®], Corning Incorporated, NY, USA)
- Clock timer
- CO₂ Incubator (Heraeus HERA Cell 240, Heraeus Holding GmbH., Germany)
- Cylinder (Pyrex, USA)
- Desiccator
- Dialysis tube (Cellusep[®] T1 6000-8000 MWCO, Membrane Filtration Products, Seguin, TX, USA)
- Differential scanning calorimeter (DSC) (Model: 8000, Perkin Elmer Inc., Germany)

- Duran glass bottle 250, 500, 1000, 2000 mL
- Filter paper (Whatman™, GE Healthcare, UK)
- Flow cytometer (BD FACSCanto™, BD Bioscience, CA, USA)
- FlowJo software (BD Bioscience, FlowJo LLC, Ashland, Oregon, USA)
- Fluorescence spectrophotometer (RF 1501; Shimadzu, Kyoto, Japan)
- Fluorescence microscope (Olympus Co., Ltd., Tokyo, Japan)
- Fourier transform infrared spectrometer (FTIR) (Model: Nicolet 4700, Nicolet, USA)
- Freeze-dryer (Model: Freezone 2.5, LABCONCO, Kansas city, MO, USA)
- Freezer/Refrigerator -20 °C, -80 °C, 4 °C
- Fume hood (Wiwatsan Lab, Nonthaburi, Thailand)
- Glass bottom container
- Glass slide microscope and cover slip (Sail Brand, China)
- Gloves
- GraphPad Prism version 5.01 (GraphPad Inc., San Diego, CA USA)
- High performance liquid chromatography (HPLC) instrument (Agilent 1100 series, Agilent Technologies, USA)
- Hot air oven (WTB Binder, Germany)
- HPLC column (Phenomenex® C-18 column; 5 µm particle size; 250 × 4.6 mm)
- HPLC vial and septum
- Ice bath
- Incubated shaker (Model: KBLee 1001, Daiki sciences, Bio-Active, Bangkok, Thailand)
- Inverted microscope (Nikon® T-DH, Japan)
- ImageJ software (National Institute of Health, MD, USA)
- J MicroVision version 1.2.7
- Laminar air flow (BIO-II-A, Telstar Life Science Solutions, Spain)
- Magnetic stirrer (Framo, Germany) and magnetic bar
- Micropipette 0.1-2.5 µL, 2-20 µL, 20-200 µL, 100-1000 µL, 1-5 mL (Eppendorf® AG, Hamburg, Germany)
- Micropipette tips (Corning®, Corning Incorporated, NY, USA)

- Microcentrifuge (Microfuge 16[®], Model: A46473, Beckman Coulter Inc., Germany)
- Microplate reader (Multimode plate reader, Model: Victor Nivo[™], PerkinElmer, Hamburg, Germany)
- Multipoint pipettor with 8 channels aspiration manifold 30-300 μ L (Eppendorf[®] AG, Hamburg, Germany)
- Multispeed centrifuge (ALC[®], Model: PK121R, New Jersey, USA)
- Nylon membrane filter (diameter 13 mm, 47 mm, pore size 0.45 μ m, Filtrex[®])
- Parafilm (BEMIS[®], WI, USA)
- pH meter (Horiba compact pH meter B-212, Japan)
- pH meter (Mettler Toledo; Switzerland)
- Pipette aid (Powerpette Plus; Bio-Active Co., Ltd.)
- Powder X-ray diffractometer (Miniflex II, Rigaku, Japan)
- Probe-type sonicator (Model: CV 244, Sonics VibraCell[™], Newtown, CT, USA)
- Scanning electron microscope (SEM) (JSM-6400, JEOL Co., Ltd., Japan)
- Shaking incubator (Orbital shaking incubator Model: S14)
- Sterile measuring pipette 5 mL, 10 mL (Falcon[®], Corning Incorporated, NC, USA)
- Syringe 1 mL, 10 mL, 50 mL (Nipro Co., Ltd., Bangkok, Thailand)
- Test tube 10 mL (Pyrex, USA)
- Transmission electron microscope (TEM) (JEM-2100, JEOL Co., Ltd., Japan)
- Transwell plate with insert and polycarbonate membrane (8 μ m pore size, 6.5 mm diameter) (Costar[®], Corning Incorporated, ME, USA)
- Ultracentrifuge (Kendro[®], Multifuge 1S/1S-R, Germany)
- Vacuum pump connected suction line (Model: WP621 1560 Millipore, Billerica, MA, USA)
- Vertical mixer (Intelli-mixer RM-22, Germany)
- Volumetric flask (Pyrex, USA)
- Vortex mixer (Model: VM-10, DAIHAN Scientific Co., Ltd., Republic of Korea)

- Water bath (HETOFRIG CB60; Heto High Technology of Scandinavia, Brikerod, Denmark)
- Well-plate (6-, 24-, 96-well plate; flat clear bottom) (Corning®, Corning Incorporated, NY, USA)
- Zetasizer Nano ZS (Malvern Instruments Ltd., Malvern, UK)



3.3 Methods

3.3.1 Preparation of 3A.1-loaded polymeric micelles (PMs)

The blank and drug-loaded PMs were prepared using four different physical entrapment methods as follows:

3.3.1.1 Dialysis method

Overall, 5 mg of the amphiphilic copolymers (NSC, OSC, and BSC) and the drug (0-40 wt% to polymer) were dissolved in 2 mL of dimethyl sulfoxide (DMSO) in a glass bottom container. Then, the mixture was stirred at room temperature until completely dissolved before being transferred to a dialysis bag (6000-8000 MWCO). The solution was dialyzed against distilled water to remove the solvent. The distilled water was replaced every 4 h for 24 h. The solution was centrifuged at 1500 rpm for 2 min before the supernatant was collected for further studies.

3.3.1.2 O/W emulsion method

The copolymers (NSC, OSC, and BSC) were prepared as mentioned in dialysis method without adding the drug in order to obtain the blank polymeric micelles. Drug solution (0-40 wt% to polymer) which was dissolved in dichloromethane (DCM) was then injected into 2 mL of the blank micelle solution under regular stirring. After that, DCM was evaporated overnight by stirring at room temperature. The micelle solution was then centrifuged and collected for further studies.

3.3.1.3 Dropping method

Briefly, 5 mg of the copolymers and the drug (0-40 wt% to polymer) were dissolved in 0.5 mL of DMSO. The solution was gradually dropped into stirred water, and the mixed solution was stirred overnight. The final volume ratio of DMSO:water was 1:5. The mixture was then placed into a dialysis bag and dialyzed against distilled water overnight. The micelle solution was then centrifuged and collected for further studies.

3.3.1.4 Evaporation and sonication method

In brief, 5 mg of the copolymers and the drug (0-40 wt% to polymer) were dissolved in dimethylformamide (DMF) contained in a glass test tube.

The solution was mixed with acetone (1/3 volume of DMF) and stirred at room temperature under nitrogen gas flow in a laminar hood until the solvent was completely evaporated to form a thin-film. Afterward, 3 mL of distilled water was added, and the solution was sonicated using a probe-type sonicator (CV 244, Sonics VibraCell™, Newtown, CT, USA) in cycle with a sonication time of 5 min and a standby time of 5 min for 20 min under cold temperature (in an ice bath). The micelle solution was then centrifuged and collected for further studies.

3.3.2 Preparation of 3A.1-loaded liposomes (LPs)

The liposome formulations including conventional liposomes (LP) and PEGylated liposomes (PEG LP) were prepared using various amounts of phosphatidylcholine (PC), cholesterol (Chol) and 1,2-distearoyl-sn-glycero-3-phosphoethanolamine-N-(carbonyl-methoxypolyethylene glycol-2000) (DSPE-PEG2000) at the molar ratio of 10:2:0, 10:2:0.125, 10:2:0.25 and 10:2:0.50 mM. The amount of 3A.1 in the formulation was varied ranging from 0.5-4.0 mM. All liposomes were produced using a thin-film hydration and probe-sonication method. Briefly, PC, Chol, and DSPE-PEG2000 were dissolved in a mixture of chloroform and methanol (2:1, v/v) and mixed them in a glass test tube before 3A.1 solution was added. The solvent was then evaporated by nitrogen gas flow and the obtained thin-film was placed in a desiccator for 6 h to remove the residual organic solvent. The dry thin film of lipid was subsequently hydrated with PBS solution (pH 7.4). After that, the liposomes were properly vortexed and subsequently probe-sonicated by a probe-type sonicator (CV 244, Sonics VibraCell™, Newtown, CT, USA) in an ice bath for 30 min to reduce the vesicle size of the liposomes. The liquid liposome was centrifuged at 15000 rpm at 4°C for 15 min to remove the excess lipid compositions and traces of titanium from the probe sonicator. The supernatant was collected in glass bottle containers and kept at 4°C for further evaluations.

3.3.3 Preparation of 3A.1 nanosuspensions (NSs)

The 3A.1 nanosuspensions (3A.1 NSs) were prepared via a nanoprecipitation (bottom-up) method, using DMSO as a solvent and distilled water as an anti-solvent. The final volume ratio of DMSO:water was 1:5. Briefly,

the drug and copolymers (NSC, OSC, and BSC) (3.5 mg) were co-dissolved in DMSO in a 1.5 mL centrifuge tube at the different ratios of the drug to polymer (0.8:1 to 2:1, w/w). Next, the solution was slowly dropped with p200 into 3.5 mL of distilled water under magnetic stirring for 24 h, and then the suspension was transferred to a dialysis tube (6000-8000 MWCO) and dialyzed against distilled water to remove the organic solvent. The drug NSs was then centrifuged and the supernatant was collected for further studies. Moreover, three stabilizers i.e. sodium dodecyl sulfate (SDS), Tween[®] 80, and Poloxamer 188 (Lutrol F68) were selected to prepare drug NSs by the similar process. To obtain the formulation containing stabilizers, the drug solution was gradually dropped into 3.5 mL aqueous solution containing the stabilizers.

In order to improve the physical stability of the liquid NSs, 5% w/v mannitol was added as a lyoprotectant to reduce the expansion of the particles during freeze-drying process. The liquid samples were pre-frozen at 20°C for 72 h before being vacuumized using a freeze dryer instrument (FreeZone2.5, Labconco Co., Kansas City, MO, USA) at -48°C for 72 h to obtain NS powder.

3.3.4 Entrapment efficiency and loading capacity of 3A.1-loaded PMs and LPs

The quantitative determination of 3A.1 in the 3A.1-loaded PMs prepared using different methods were determined by dissolving the samples in a mixture of DMSO:water (9:1, v/v) while the 3A.1 contained in the 3A.1-loaded LPs were determined by dissolving the samples in 0.1% Triton[®] X-100 solution in PBS (pH 7.4), followed by centrifugation at 10000 rpm at 4°C for 10 min. The sample of micelle mixture and the supernatant of the liposome mixture were filtered through a syringe filter (0.45 µm pore size). The average amount of the drug loaded in the polymeric micelles or liposomes was determined in triplicate using a high performance liquid chromatography (HPLC). The entrapment efficiency (%EE) and loading capacity (LC) were calculated according to Eq.3 and Eq.4, respectively.

$$\%EE = \frac{\text{The amount of entrapped drug in PMs or LPs}}{\text{Initial amount of the drug added during preparation}} \times 100 \quad \text{Eq.3}$$

$$LC (\mu\text{g}/\text{mg}) = \frac{\text{The amount of entrapped drug in PMs or LPs}}{\text{Amount of the polymer or lipid used during preparation}} \quad \text{Eq.4}$$

For 3A.1-loaded PMs, the optimal preparation method showing the highest drug entrapment efficiency and loading capacity was selected for the preparation of the PMs using 3 different graft copolymers (NSC, OSC, and BSC).

For 3A.1-loaded PEG LP, the optimal initial drug amount and molar ratio of lipid compositions showing the highest drug entrapment efficiency and loading capacity was selected for further experiments and evaluations.

3.3.5 Drug content of 3A.1 NSs

The average content of 3A.1 in the 3A.1 NS formulations was determined by dissolving the samples in a mixture of DMSO:water (9:1, v/v), then the sample was filtered through a 0.45- μm filter prior to an HPLC analysis. The drug concentration ($\mu\text{g}/\text{mL}$) was calculated from the calibration curve while percentage yield was calculated as follows:

$$\text{Yield (\%)} = \frac{\text{The amount of drug in the NS formulation}}{\text{Initial amount of the drug added during preparation}} \times 100 \quad \text{Eq.5}$$

3.3.6 HPLC analysis

The amount of 3A.1 in the 3A.1-loaded PMs, 3A.1-loaded LPs and 3A.1 NSs was determined using a high performance liquid chromatography (HPLC, Agilent 1100 series, Agilent technologies, USA) connected with Phenomenex[®] C-18 column (5- μm particle size, 250 \times 4.6 mm) and diode array detector (DAD) set at 219 nm. The isocratic elution was performed with the mobile phase composed of methanol and ultrapure water at the volume ratio of 80:20 with the flow rate of 1.0 mL/min. The injection volume was set at 20 μL . The column temperature was set constantly at 25°C. Standard solution with different drug concentrations (10-200 $\mu\text{g}/\text{mL}$) in methanol was used to generate the calibrate curve (see Appendix A).

3.3.7 Characterization of 3A.1-loaded PMs, 3A.1-loaded LPs and 3A.1 NSs

3.3.7.1 pH

The pH of the freshly prepared 3A.1-loaded PMs, 3A.1-loaded LPs and 3A.1 NSs was measured in triplicate at 25°C using a pH electrical meter (HORIBA compact pH meter B-212, Japan).

3.3.7.2 Morphology

Surface morphologies of the blank and 3A.1-loaded PMs, 3A.1-loaded LPs and 3A.1 NSs were observed using a transmission electron microscope (TEM). The formulations were diluted with distilled water and dropped onto a formvar-coated copper grid. They were then negatively stained with 1% uranyl acetate solution and air dried at room temperature. Finally, the samples were scanned under TEM (Philips® Model TECNAI 20, Japan) at an accelerating voltage of 80 kV. Furthermore, a scanning electron microscope (SEM, JSM-6400, JEOL Co., Ltd., Japan) was also utilized to observe coarse 3A.1 powder and the freeze-dried 3A.1 NSs. In brief, the specimens of the freeze-dried powder were mounted onto an aluminum stub with conductive double-sided adhesive tape and then sputtered with a thin gold layer under vacuum. Finally, the morphological features of each sample were viewed at an accelerating voltage of 15 kV.

3.3.7.3 Particle size, size distribution, and zeta potential

Dynamic light scattering (DLS) (Zetasizer Nano ZS, Malvern Instruments, Malvern, UK) was employed to measure the mean particle size, polydispersity index (PDI), and zeta potential of blank nanocarriers, 3A.1-loaded PMs, 3A.1-loaded LPs and 3A.1 NSs. The samples were properly diluted with distilled water before the measurements. All measurements were determined in triplicate at 25°C. As pH-responsive polymers (NSC, OSC, and BSC) were used in the polymeric micelles, a dispersed vehicle with different pH values (pH 1.2, 6.8, and 7.4) was used to dilute the micelle formulations containing a drug to polymer ratio of 40 %wt to determine the effect of pH on the particle size and zeta potential of the 3A.1-loaded PMs.

3.3.7.4 Other physicochemical properties of 3A.1 NSs

3.3.7.4.1 Reconstitution test

A small amount of the freeze-dried NS powder with and without mannitol was added in a glass bottle container and re-dispersed greatly with 1 mL of distilled water. The mean particle size, PDI, and zeta potential of the dispersed 3A.1 NS was determined as described earlier.

3.3.7.4.2 Differential scanning calorimetry (DSC)

DSC thermogram was recorded using a differential scanning calorimeter (DSC8000, PerkinElmer Inc., Germany). The samples including 3A.1 coarse powder, all stabilizers, a physical mixture, and the freeze-dried sample of 3A.1 NS, were accurately weighed in a standard aluminum pan fitted with a perforated lid for thermal analysis. A heating rate of 10°C/min was used for the analysis in the range of 30-300°C, and an empty pan was used as the reference. The measurements were carried out under nitrogen gas flow, at a rate of 20 mL/min.

3.3.7.4.3 Powder X-ray diffraction (PXRD)

The PXRD analysis was performed to detect any change in physical properties and crystallinity of the 3A.1 coarse powder, all stabilizers, a physical mixture, and the freeze-dried 3A.1 NS by a powder X-ray diffractometer (Miniflex II, Rigaku, Japan) with a Cu radiation source. Samples were packed into a flat-type glass holder. The PXRD patterns were obtained at 40 kV and 25 mA. The scanning angle was set from $5^\circ < 2\theta < 50^\circ$, and the scanning rate is 2°/min.

3.3.7.4.4 Fourier transform infrared spectrophotometry (FT-IR)

FTIR spectra were recorded to investigate whether there is any degradation of the drug in the NS or any interaction between drug and auxiliary materials. The samples, including the bulk 3A.1, blank excipients, their physical mixture, and the freeze-dried 3A.1 NS, were grounded with KBr powder and pressed into round disc with a diameter

of 13 mm. The spectra were recorded at a wavenumber ranging from 400-4000 cm^{-1} using an FT-IR spectrometer (Nicolet 4700, USA).

3.3.7.4.5 Saturation solubility

The saturation solubility of the bulk 3A.1 and the 3A.1 NSs stabilized by NSC, OSC, and BSC was determined using a shaken flask method. An excess amount of all samples was added to a plastic microcentrifuge tube containing various solvents including distilled water, buffer medium pH 1.2, 6.8 and 7.4, and continuously shaken at 150 rpm using a shaking incubator for 48 h at $37 \pm 0.5^\circ\text{C}$ to ensure saturation. After equilibration, the samples were centrifuged at 10000 rpm for 30 min, and the supernatant was filtered through a 0.45- μm membrane filter, before being analyzed for the actual drug concentration using an HPLC. This experiment was carried out in triplicate.

3.3.8 *In vitro* drug release study

3.3.8.1 3A.1-loaded PMs

In brief, 100 μL of 3A.1-loaded PMs and 3A.1 coarse suspension (the drug powder dispersed in distilled water containing equivalent concentration of the drug to the 3A.1-loaded PMs) were added to 900 μL of release medium contained in a 1.5-mL microcentrifuge tube. A simulated gastric fluid (SGF) pH 1.2 was used as the medium for the first 2 h, followed by a simulated intestinal fluid (SIF) pH 6.8 for 6 h and a simulated colonic fluid (SCF) pH 7.4 for the further 4 h. The release study was conducted at $37 \pm 0.5^\circ\text{C}$ in a shaking incubator at a shaking speed of 150 rpm. The samples were collected at predetermined time points and filtered through a 0.45- μm membrane filter before the content determination via HPLC analysis. The release study was carried out in triplicate.

3.3.8.2 3A.1-loaded LPs

The *in vitro* release of the drug loaded in the liposome or free drug was investigated at $37 \pm 0.5^\circ\text{C}$ in a shaking incubator shaken at 150 rpm. The drug solution was prepared by dissolving the drug in DMSO. The liposome sample was diluted to 1 mL in a microcentrifuge tube containing

PBS buffer (pH 7.4) as the release medium, to obtain the equivalent drug concentration to the drug solution. At the predetermined time intervals up to 24 h, the amount of the drug released was determined by HPLC. The release experiment was performed in triplicate.

3.3.9 Stability study

The stability of 3A.1-loaded PMs, 3A.1-loaded LPs, and 3A.1 NSs was determined according to the ICH guideline section Q1A R2 [208]. The samples contained in a glass bottle clogged with a plastic cap were stored at $5 \pm 3^\circ\text{C}$, $60 \pm 5\% \text{RH}$ (long-term condition) and at $25 \pm 2^\circ\text{C}$, $60 \pm 5\% \text{RH}$ (accelerated condition) for 6 months. The particle size, zeta potential, and drug content remaining of the samples were evaluated after storage for 0, 30, 60, 120, and 180 days. All data were measured in triplicate.

3.3.10 *In vitro* anticancer activity

The anticancer activity of free 3A.1, 3A.1-loaded PMs, 3A.1-loaded LPs, and 3A.1 NSs against human colorectal cancer (CRC) cells was assessed by an MTT assay. Briefly, CRC cells (1×10^4 cells/well) were seeded into 96-well plates with Dulbecco's modified Eagle's medium (DMEM) supplemented with 10% FBS at pH 7.4 and cultured at 37°C in a humidified 5% CO_2 incubator. After 24-h incubation (60-70% confluence), various concentrations of the free drug and the selected drug nanocarriers were added to each well and further incubated for 24, 36, and 48 h. After treatment, the medium was removed and the cells were incubated with the fresh medium containing 1 mg/mL of MTT for 4 h. After that, the medium was removed again, and the formazan crystals formed in the living cells were dissolved by the addition of DMSO (100 μL). Afterward, the optical density (OD) of each well was analyzed using an automated microplate reader (Multimode plate reader, Model Victor NivoTM, PerkinElmer, Hamburg, Germany) operated at 550 nm. The percentage of cell viability was calculated following the equation:

$$\text{Cell viability (\%)} = \frac{\text{OD}_{\text{treated}} - \text{OD}_{\text{DMSO}}}{\text{OD}_{\text{untreated}} - \text{OD}_{\text{DMSO}}} \times 100 \quad \text{Eq.6}$$

Moreover, half-maximal inhibitory concentration (IC_{50}) values were estimated using GraphPad Prism version 5.01 (GraphPad Inc., USA). The cytotoxicity of the blank nanocarriers was also evaluated using the similar procedure.

3.3.11 Induction of cell apoptosis

An apoptosis and necrosis assay was performed using a flow cytometer (BD, FACSCanto, Becton Dickinson, CA, USA) with FITC-conjugated Annexin V/propidium iodide (PI) double-staining (BD Bioscience, USA). Briefly, CRC cells were seeded in 6-well plates and incubated until 60-70% confluence at 37°C in a humidified 5% CO₂ incubator. The cells were treated with 3A.1-loaded PMs, 3A.1-loaded LPs, and free 3A.1 in the fresh DMEM medium (the final drug concentration was fixed at the IC_{50} value of 3.8 µg/mL) at 37°C for 24 h. The detergent 1% (v/v) Triton[®] X-100 solution in culture medium, which is reported to damage cell membrane, was used as positive control for cell apoptosis and necrosis [209,210]. After the treatment, the cells were gently detached using Accutase enzyme solution (Accutase[™], Merck, Temecula, CA, USA) and carefully washed with the fresh medium. After that, the cells were centrifuged at 1400 rpm for 5 min, and the cell pellets were re-suspended in a cold PBS buffer (pH 7.4). The cell pellets were then re-suspended in 1x annexin V binding buffer. The cells were stained with Annexin V-FITC (5 µL) and PI (5 µL) for 15 min at room temperature in the dark, 400 µL of 1x annexin V binding buffer was subsequently added before being analyzed immediately using a flow cytometry with green fluorescence (FITC) measured at 530 nm, and red (PI) fluorescence at 575 nm. Concurrently, the untreated cells were considered as control. The data were evaluated using FACS diva software (BD Bioscience, USA). Both early apoptotic (Annexin V⁺/PI⁻) and late apoptotic (Annexin V⁺/PI⁺) cells were included in the cell apoptosis determination. Before data acquisition, the staining color compensation in flow cytometry was conducted to ensure accurate interpretation of data.

3.3.12 *In vitro* cell migration

3.3.12.1 Scratch wound healing assay

The effect of free 3A.1, 3A.1-loaded PMs, and 3A.1-loaded LPs on HN22 (human oral squamous cancer) cell motility was performed using a scratch wound healing assay. Briefly, HN22 cells were cultured in 6-well culture plates with DMEM containing 10% FBS at pH 7.4 to achieve confluent monolayer. A monolayer of the cell in each well was gently scratched with a sterile 200- μ L pipette tip to create three straight lines/well and rectangular cell-free spaces. Then, the culture medium was discarded and gently washed twice with PBS (pH 7.4) to remove debris and scratched cells. After that, the free drug and selected drug nanocarriers in fresh medium at a final 3A.1 concentration lower than IC₅₀ value (3.0 μ g/mL) were added into each well and cultured at 37°C in an incubator with humidified 5% CO₂ for 24 h. Culture medium without drug and DMSO was used as control. After scraping at 0, 6, 12, 18, and 24 h, the images (5 images/well) of the wound were captured at 40 \times magnification using an inverted microscope (Nikon® T-DH, Japan). The anti-migratory activity was assessed in triplicate. The wound gap and wound area were quantified using JMicroVision version 1.2.7 and calculated to determine the cell migration rate and percentage of wound closure using Eq.7 and Eq.8, respectively.

$$\text{Rate of cell migration } (\mu\text{m/h}) = \frac{\text{Initial wound gap} - \text{Final wound gap}}{\text{Observed time}} \times 100 \quad \text{Eq.7}$$

$$\text{Wound closure } (\%) = \frac{\text{Wound area at the starting time point} - \text{Wound area at the ending time point}}{\text{Wound area at the starting time point}} \times 100 \quad \text{Eq.8}$$

3.3.12.2 Transwell migration assay (Boyden chamber)

Transwell migration assay was also performed to determine the effect of the free 3A.1 and 3A.1-loaded LPs on HCT116 cell motility in vertical direction. In brief, HCT116 cells (5×10^4 cells/well) dispersed in a medium containing low level of FBS (1% v/v), were seeded in the upper

chamber of a transwell system in a 24-well plate clear flat bottom (Costar[®], Corning Incorporated, USA). The experimental study was carried out according to the manufacturer's procedures. Each drug treatment at a final 3A.1 concentration of 2.0 µg/mL, which was diluted in culture medium supplemented with high level of FBS (10%) as a chemotactic reagent, was added to the lower chamber and incubated in a humidified 5% CO₂ incubator at 37°C for 24 h. Subsequently, the culture medium in the upper insert was discarded, washed twice with PBS (pH 7.4), and cold 95% methanol was then added to fix the cells for 30 min. Then, the cells were washed with PBS (pH 7.4), and the non-migrated cells were wiped out using a cotton swab. The cells migrated through the pore of membrane from the upper side to the lower side were stained overnight with 2% crystal violet in methanol solution. After that, the part of insert was washed with PBS (pH 7.4), and the membrane was dried at room temperature. The images of the migrated cells in each treatment were captured under an inverted microscope at 4× and 10× magnification. The migrated cells that penetrated to the lower membrane were counted and then calculated to relative percentage of cell migration compared with control group under the same filed at the endpoint. Both assays of anti-migratory activity of the drug nanocarriers were conducted at least three replicates.

$$\text{No. of cell migration (\%)} = \frac{\text{The no. of migrated cells in the treatment group}}{\text{The no. of migrated cells in the control group}} \times 100 \quad \text{Eq.9}$$

3.3.13 *In vitro* cellular uptake

In this part, doxorubicin (Dox) which is a red fluorescent agent was selected to be incorporated into the polymeric micelles to generate drug-loaded micelles. The cellular uptake of Dox into HT29 cells was examined by a flow cytometric analysis. Briefly, HT29 cells at a density of 1×10^5 cells/well were grown in a 6-well plate and incubated overnight at 37°C. Later, the cells were treated with free Dox or the 40 wt% Dox-loaded NSC micelles (equivalent Dox concentration to 2.0 µM) in the fresh culture medium for 12 and 24 h. Afterward, the cells were rinsed twice with PBS (pH 7.4), to discard any free Dox or micelles, and were then

visualized by a fluorescence imaging system (Nikon DS-Ri2 camera connected with NIS element D4.60 software; Nikon, Japan) using 4× objective lens. Moreover, to confirm the extent of Dox in the cells, the cell suspensions in PBS (pH 7.4) of each treatment were analyzed by flow cytometer (BD Bioscience, USA). An excitation and emission wavelength at 488 nm and 575 nm were applied to detect the fluorescent intensity and fluorescent histogram of Dox. Typically, 30000 events were counted for each sample. Finally, the mean fluorescent intensity (MFI) of Dox from individual three detections were computed and reported as mean \pm SD.

3.3.14 *In vivo* antitumor efficacy

3.3.14.1 Establishment of tumor xenograft models of CRC

The tumor xenograft nude mouse model of colorectal cancer (CRC) should be established before the investigation of anticancer effect of the compound. Nude mice (male, BALB/cAJcl-nu/nu, 18 ± 2 g, 5 weeks old) were supplied from Nomura Siam International Co., Ltd., Thailand. The nude mice were immunodeficient characteristic as they lack of thymus gland (athymic) and T-cell function. All animal experiments and animal care were performed according to the Guidelines for Ethical and Regulatory for Animal Experiments as issued by Central Animal Facility, Faculty of Science, Mahidol University (MUSC-CAF), Thailand [211]. This *in vivo* experimental protocol was officially approved by MUSC-CAF with protocol number MUSC61-015-417. The mice were quarantined on a 12-h dark/light cycle, in an air-controlled room temperature at $25 \pm 1^\circ\text{C}$ and $55 \pm 5\%$ RH, under specific pathogen-free conditions at least 7 days before tumor implantation in the individual ventilated cages (IVC). The mice were provided with sterile RO water and diet ad libitum. HCT116 (human colorectal cancer) cells in the logarithmic growth curve were collected aseptically by trypsinization. The cells were washed twice and re-suspended with sterile PBS (pH 7.4). The cell viability and number were counted after staining with 0.4% trypan blue. For cancer cell implantation, the nude mice were randomly divided into 3 groups (2 mice/ group), disinfected skin at

injected position with 70% ethanol and then injected subcutaneously with the cell densities of 1×10^6 cells/200 μ L, 5×10^6 cells/200 μ L and 10×10^6 cells/200 μ L at the right lower flank with 1-mL syringes and 26G \times 0.5-inch long needle under sterile conditions (Figure 18). The tumor nodules became palpable at day 7 after cell inoculation (with cell density of 10×10^6 cells). The tumor size was determined twice a week using a digital Vernier caliper (Syntex[®], Syntex Electronic Technology Co., Ltd., China). Only HCT116 cell density that displayed the desirable tumor growth rate was chosen for investigation of *in vivo* antitumor efficacy of the free 3A.1 and the 3A.1 NSs.

Tumor growth was investigated for 4-6 weeks or until the size of tumor reached ~ 2000 mm³. The tumor size (mm) in two dimensions (length and width) and body weight (g) were recorded twice a week using a digital Vernier caliper, and the tumor volume (TV) was calculated according to the following formula:

$$TV \text{ (mm}^3\text{)} = L \times W^2 / 2 \quad \text{Eq.10}$$

where L and W refer to the length (range of major-axis) and width (range of minor-axis) of spherical tumors, respectively. If the tumor volumes reached over 2000 mm³ or the animals show any tumor necrosis, they were also sacrificed.

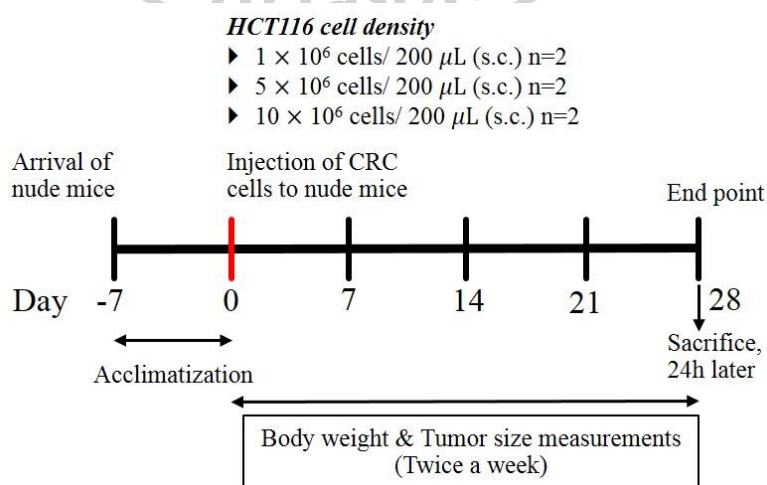


Figure 18 Protocol for CRC implantation in athymic nude mice

3.3.14.2 Investigation of anticancer efficacy of the drug NSs compared with free 3A.1 in CRC xenograft models

In vivo anticancer efficacy of the 3A.1 NSs and its free form was evaluated in HCT116 cell xenograft nude mice. After cell inoculation and tumor growing for 1-2 week until tumor volumes reached 100-150 mm³, xenograft nude mice were randomly divided into 7 groups (n=5 for each treatment group). All treatment groups administered via intraperitoneal (i.p.) injection two times per week for 18 days as follows (Figure 19):

- (1) Vehicle group (negative control): mixture of 5% DMSO and 5% Tween 80 in sterile normal saline (100 uL/mouse)
- (2) Positive control: 30 mg/kg 5-FU (100 uL/mouse)
- (3) Low dose of 3A.1 solution: 20 mg/kg 3A.1 (100 uL/mouse)
- (4) High dose of 3A.1 solution: 40 mg/kg 3A.1 (100 uL/mouse)
- (5) Low dose of 3A.1 NS-NSC: 20 mg/kg 3A.1 equivalent (100 uL/mouse)
- (6) High dose of 3A.1 NS-NSC: 40 mg/kg 3A.1 equivalent (100 uL/mouse)
- (7) Empty NS-NSC

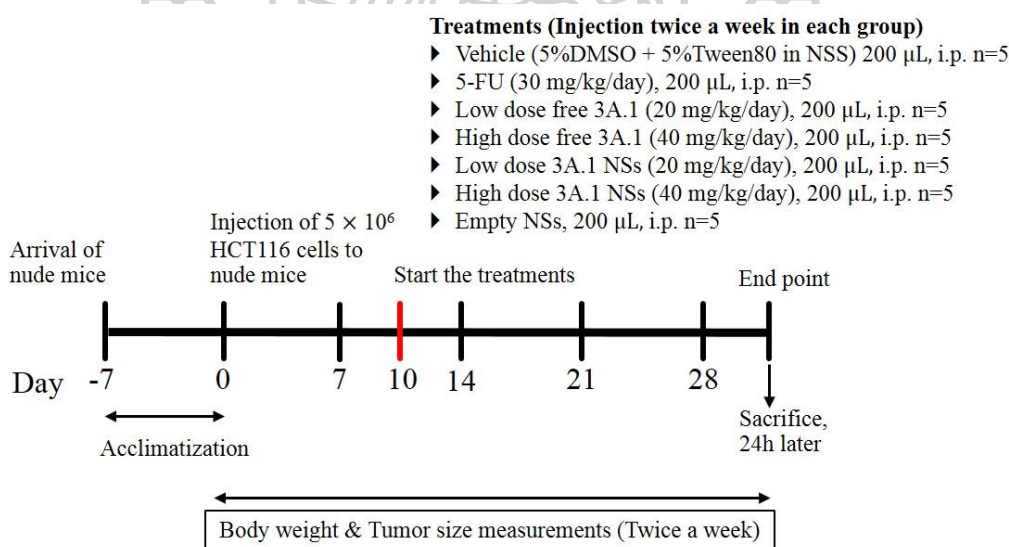


Figure 19 Protocol for drug treatments in athymic nude mice

Free 3A.1 was dissolved in a solvent mixture consisting of DMSO/Tween 80/PBS (5/5/90, v/w/v) achieving the final concentration for *in vivo* administration. The free 3A.1 was then sonicated for 30 min in a bath sonicator prior to i.p. injection. During the entire injectable period (with total of 6 doses), the body weight of each mouse was recorded, and the tumor size was measured two times per week using a digital Vernier caliper, and the tumor volume was then calculated using the Eq.10. All procedures related to drug administration were performed in a laminar airflow hood using aseptic techniques. TV was measured to evaluate the therapeutic effects of each treatment group. Tumor growth curves and body weight profiles were drawn to compare these results among treatments. The tumor volumes from the total number of survival mice in the control and treated groups that observed since the beginning to the end of the study were used to calculate the percentages of tumor growth inhibition (%TGI) following the Eq.11:

$$\%TGI = \left[1 - \left(\frac{T_t - T_0}{C_t - C_0} \right) \right] \times 100 \quad \text{Eq.11}$$

which T_t is the median TV (mm^3) of the treated mice at time t

T_0 is the median TV (mm^3) of the treated mice at time 0

C_t is the median TV (mm^3) of the vehicle control-treated mice at time t .

C_0 is the median TV (mm^3) of the vehicle control-treated mice at time 0.

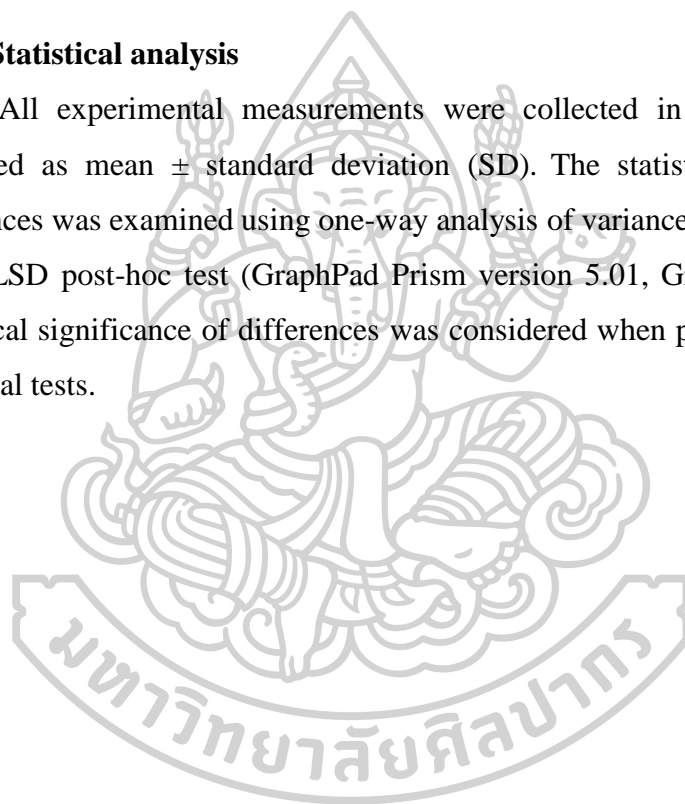
Tumor volume doubling time was measured over the linear growth range of the tumor. TGI of 50% over one tumor volume doubling time are considered an active anti-tumor response.

Furthermore, the common toxicities of free 3A.1 and the 3A.1 NSs were observed by monitoring the relative body weight loss throughout the experiments. At the end of treatments (18 days of post-treatment), the surviving mice were sacrificed by anesthesia via an i.p. injection of 5 mg/kg xylazine plus 50 mg/kg Zoletil using 26G \times 0.5-inch long needle with 1-mL syringe, followed by an aortic arch cutting. The fresh tumor masses were excised from the back of mice using scissors and scalpels, weighed

and photographed. The visceral organs including lung, liver, spleen, and kidney were also removed from each mouse to assess the adverse effect of the compound. The tumor tissues and visceral organs were cut for histopathological examination by staining with hematoxylin and eosin. Half section of tumor was fixed in 10% buffered formalin and embedded in paraffin wax in tissue cassettes for routine histopathology. These tissue paraffin samples (4 μm in thickness) were stained with haematoxylin and eosin (H&E) reagent for histopathological examination.

3.3.15 Statistical analysis

All experimental measurements were collected in triplicate. Data are presented as mean \pm standard deviation (SD). The statistical significance of differences was examined using one-way analysis of variance (ANOVA) followed by an LSD post-hoc test (GraphPad Prism version 5.01, GraphPad Inc., USA). Statistical significance of differences was considered when p-value < 0.05 for all statistical tests.



CHAPTER 4

RESULTS AND DISCUSSION

4.1 Polymeric micelles with or without 3A.1 analogue

The blank polymeric micelles and hydrophobic 3A.1-loaded polymeric micelles based on the three types of amphiphilic chitosan graft copolymers (NSC, OSC, and BSC) were prepared using different physical encapsulation techniques including dialysis, O/W emulsion, dropping, and evaporation followed by sonication method. These chitosan graft copolymers could generate core-shell structural nanomicelles which encapsulated the 3A.1 in the hydrophobic inner core by a self-assembly process. Overall, the pH of these micelles was in the ranges of 5.5-6.7, representing mildly acidic solution.

4.1.1 Effects of physical entrapment methods

The effects of different physical entrapment methods on the physicochemical properties of the 3A.1-loaded micelles were investigated at a fixed initial ratio of 20 wt% drug to polymer. The parameters considered when selecting the optimal drug-loading method were particle size, zeta potential, entrapment efficiency (%EE), and drug loading capacity (LC). All data are listed in Table 8. Among the four drug-loading methods with different grafted hydrophobic moieties, the micelles formed by the dropping method exhibited the smallest particle size with the diameter ranging from 90.33 to 165.63 nm, while the zeta potential values showed a highly negative surface charge (-24.97 to -28.40 mV) due to dissociation of carboxyl groups in hydrophilic moieties resulting in the diminished aggregation. On the other hand, the 3A.1-loaded micelles prepared by O/W emulsion method were found to be the biggest, with the lowest values of drug loading content. The %EE and LC of 3A.1-loaded micelles prepared by dropping method were 72.59 ± 8.61 to $80.13 \pm 5.01\%$ and 145.17 ± 17.21 to 160.27 ± 10.03 $\mu\text{g}/\text{mg}$, respectively. These high values of drug content indicated that this method could efficiently entrap the hydrophobic 3A.1 anticancer drug within the cores of the micellar particles. Therefore, dropping method was selected to formulate 3A.1-loaded micelles for further studies.

Table 8 The physicochemical properties of 3A.1-loaded polymeric micelles with 20 wt% initial drug added (NSC, OSC, and BSC) prepared using four physical entrapment methods. Each value represents the mean \pm standard deviation from three independent experiments.

Type of CS derivatives	Method	Particle size (nm)	Zeta potential (mV)	Entrapment efficiency (%)	Loading capacity ($\mu\text{g}/\text{mg}$)
NSC	Dialysis	136.07 \pm 1.43	(-) 25.10 \pm 0.22	66.70 \pm 2.57	133.39 \pm 5.13
	O/W emulsion	105.03 \pm 1.28	(-) 24.90 \pm 1.34	7.86 \pm 1.89	15.72 \pm 3.78
	Dropping	90.33 \pm 2.28	(-) 24.97 \pm 1.11	72.59 \pm 8.61	145.17 \pm 17.21
	Evaporation	348.50 \pm 9.48	(-) 21.97 \pm 0.49	5.34 \pm 1.12	10.68 \pm 2.24
OSC	Dialysis	287.00 \pm 3.81	(-) 29.60 \pm 0.33	62.88 \pm 1.58	125.77 \pm 3.17
	O/W emulsion	249.50 \pm 8.78	(-) 25.80 \pm 0.29	14.34 \pm 1.29	28.67 \pm 2.59
	Dropping	165.63 \pm 9.80	(-) 26.67 \pm 0.82	80.13 \pm 5.01	160.27 \pm 10.03
	Evaporation	251.17 \pm 2.95	(-) 28.73 \pm 0.09	3.26 \pm 1.33	6.52 \pm 2.66
BSC	Dialysis	242.67 \pm 2.23	(-) 26.77 \pm 0.46	65.31 \pm 1.89	130.62 \pm 3.77
	O/W emulsion	160.60 \pm 0.50	(-) 32.37 \pm 1.54	12.34 \pm 1.97	24.68 \pm 3.95
	Dropping	131.63 \pm 1.05	(-) 28.40 \pm 0.68	73.06 \pm 2.38	146.13 \pm 4.76
	Evaporation	441.20 \pm 8.78	(-) 24.67 \pm 0.12	4.27 \pm 1.45	8.54 \pm 2.90

Table 9 The particle size, PDI, and zeta potential of 3A.1-loaded polymeric micelles prepared using the dropping method at the different drug to polymer weight ratios. All data represent the mean \pm standard deviation (n = 3).

3A.1 to polymer (%)	NSC				OSC				BSC			
	Size (nm)	PDI	ζ (mV)	Size (nm)	PDI	ζ (mV)	Size (nm)	PDI	ζ (mV)	Size (nm)	PDI	ζ (mV)
0	66.26 \pm 1.21	0.300	(-) 30.50 \pm 1.93	132.33 \pm 6.61	0.131	(-) 17.67 \pm 1.57	111.11 \pm 1.05	0.160	(-) 29.33 \pm 0.34	111.11 \pm 1.05	0.160	(-) 29.33 \pm 0.34
5	75.23 \pm 1.35	0.164	(-) 26.77 \pm 0.97	150.43 \pm 6.70	0.181	(-) 29.24 \pm 3.42	112.27 \pm 0.67	0.138	(-) 26.23 \pm 0.61	112.27 \pm 0.67	0.138	(-) 26.23 \pm 0.61
10	82.12 \pm 3.55	0.185	(-) 28.80 \pm 2.32	161.81 \pm 5.27	0.194	(-) 27.02 \pm 0.22	127.06 \pm 2.32	0.185	(-) 27.35 \pm 1.51	127.06 \pm 2.32	0.185	(-) 27.35 \pm 1.51
20	90.33 \pm 2.28	0.255	(-) 24.97 \pm 1.11	165.63 \pm 9.80	0.185	(-) 26.67 \pm 0.82	131.63 \pm 1.05	0.208	(-) 28.40 \pm 0.68	131.63 \pm 1.05	0.208	(-) 28.40 \pm 0.68
40	102.53 \pm 0.60	0.162	(-) 22.23 \pm 5.27	170.67 \pm 1.72	0.192	(-) 32.07 \pm 3.07	153.97 \pm 1.20	0.195	(-) 26.07 \pm 0.42	153.97 \pm 1.20	0.195	(-) 26.07 \pm 0.42

3

4

5

6

7

8

9

Table 10 The effect of different pH of dispersion vehicle on particle size and zeta potential of 3A.1-loaded polymeric micelles with 40 wt% initial drug added prepared using the dropping method. All data represent the mean \pm standard deviation (n = 3).

Formulations	Buffer pH 1.2		Buffer pH 6.8		Buffer pH 7.4	
	size (nm)	ζ (mV)	size (nm)	ζ (mV)	size (nm)	ζ (mV)
3A.1 NSC PMs	2595.2 \pm 190.34	(+) 4.61 \pm 0.37	122.27 \pm 1.91	(-) 24.23 \pm 1.27	121.43 \pm 0.49	(-) 21.33 \pm 0.49
3A.1 OSC PMs	1407.67 \pm 93.20	(+) 1.90 \pm 0.54	132.80 \pm 3.92	(-) 26.60 \pm 0.51	129.80 \pm 0.57	(-) 19.43 \pm 0.21
3A.1 BSC PMs	1360.33 \pm 141.06	(+) 5.08 \pm 0.51	136.30 \pm 0.92	(-) 17.47 \pm 1.60	133.67 \pm 0.96	(-) 19.71 \pm 1.32

Table 11 The physicochemical properties of 3A.1-loaded polymeric micelles with and without 40 wt% initial drug added (NSC vs. Folate-conjugated NSC) prepared using the dropping method. All data represent the mean \pm standard deviation (n = 3).

Formulations	Particle size (nm)	PDI	ζ (mV)	Entrapment	
				efficiency (%)	Loading capacity (μ g/mg)
Blank NSC PMs	85.26 \pm 1.21	0.283	(-) 23.03 \pm 1.11	-	-
Blank Fol-NSC PMs	343.80 \pm 43.73	0.494	(-) 28.50 \pm 1.15	-	-
3A.1-loaded NSC PMs	110.17 \pm 1.13	0.170	(-) 26.17 \pm 1.44	90.84 \pm 7.43	363.35 \pm 29.74
3A.1-loaded Fol-NSC PMs	189.47 \pm 2.90	0.174	(-) 31.67 \pm 0.39	68.44 \pm 3.72	273.75 \pm 14.91

5

6

4.1.2 Effects of initial 3A.1 and hydrophobic cores

The effects of the initial amount of drug added (5-40 wt% drug to polymer) and hydrophobic functionalities (naphthyl, octyl, or benzyl groups) on the physicochemical properties of the amphiphilic nanomicelles were studied. All 3A.1-loaded micelles were prepared by the dropping method. The particle size, size distribution, and surface charge of the micelles were determined by dynamic light scattering (DLS), and the results are shown in Table 9.

4.1.2.1 Particle size and zeta potential

It was found that an increase in the initial amounts of drug added resulted in an increase in the mean particle sizes (75.23 ± 1.35 to 170.67 ± 1.72 nm), which were bigger than those of the blank micelles (66.26 ± 1.21 to 132.33 ± 6.61 nm). This might be due to the high amount of the drug molecule entrapped inside the micelles. However, it should be noted that some aggregations occurred as the initial amounts of drug added (wt% to polymer ratio) was increased to 80%. At the initially added drug to polymer ratio of 40 wt%, the mean particle sizes of the 3A.1-loaded micelles were ranked as follows: NSC (102.53 ± 0.60 nm) < BSC (153.97 ± 1.20 nm) < OSC (170.67 ± 1.72 nm). The 3A.1-loaded NSC micelles exhibited the smallest particle size compared with the other micelles. In addition, the polydispersity indices (PDI) of all micelles were lower than 0.3, indicating that the particle size distribution of these micelles was narrow. The surface charges were also presented to be negative (-22.23 ± 5.27 to -32.07 ± 3.07 mV) which may be resulted from the appearance of negatively charged succinyl moieties on the micelles that reduce micelles aggregation, stabilize the micelles in an aqueous medium, and display pH-sensitive feature.

According to the pH-sensitive polymers of amphiphilic CS derivatives used in the 3A.1-loaded micelles, the 3A.1-loaded micelles (NSC, OSC, and BSC) with 40 wt% initial drug added were dispersed in various pH of the dispersion medium. The results showed that the different pH of dispersion vehicles affected both particle size and zeta potential of 3A.1-loaded micelles, as presented in Table 10. When the micelles were

surrounded by the dispersed vehicle pH 1.2, which the pH is lower than the pK_a of succinic acid ($pK_a = 4.21$) at 25°C [212], the particle size of these micelles aggregated to form bigger particles with the size ranging from 1360.33 ± 141.06 to 2595.2 ± 190.34 nm since carboxyl groups of the succinic acid cannot ionize in this solution and remain in an unionized form. The PDI values of nearly 1 indicated a very broad size distribution of the 3A.1-loaded micelles that were dispersed in acidic solution. The zeta potential of the 3A.-loaded micelles had a slightly positive charge ranging from (+) 1.90 ± 0.54 to (+) 5.08 ± 0.51 mV. These low values of electrical repulsion caused particle aggregation of the micelles. The particle size of the micelles was in the range of 122.27 ± 1.91 to 136.30 ± 0.92 nm in the dispersed vehicle pH 6.8 and 121.43 ± 0.49 to 133.67 ± 0.96 nm in the dispersed vehicle pH 7.4. The particles with nanosized diameter were obtained due to the ionization of carboxyl groups of the succinic acid in the vehicle pH 6.8 or 7.4, which was higher than the pK_a value of succinic acid, along with the swelling as a result of deprotonation. The zeta potential of the 3A.1-loaded micelles dispersed in the vehicle pH 6.8 and 7.4 was (-) 17.47 ± 1.60 to (-) 26.60 ± 0.51 mV and (-) 19.43 ± 0.21 to (-) 21.33 ± 0.49 mV, respectively. The higher values of negative surface charge facilitated lessen particle aggregation of micelles with the narrow size distribution. Thus, the insightful results help to understand the function of pH-sensitive polymeric micelles.

4.1.2.2 Micellar morphology

The morphology of the blank and the drug-loaded micelles was examined using a transmission electron microscopy (TEM), and the representative images are illustrated in Figure 20. In comparison with the blank micelles, the TEM images of the 3A.1-loaded micelles (NSC, OSC, and BSC) with 40 wt% initial drug added were spherical, with a smooth surface and uniform size. Their mean sizes were in the nanometer range (approximately 40 to 90 nm in diameter). Notably, the mean particle sizes of the micelles shown in the TEM images were smaller than those from the

DLS technique. This is because the micelles analyzed using TEM were performed in a dry state. On the other hand, those analyzed by DLS were carried out in an aqueous solution [213]. These micelles with a uniform size of not more than 200 nm could penetrate through the leaky vasculature of tumors and accumulate in tumor tissues via passive tumor targeting [91,214].

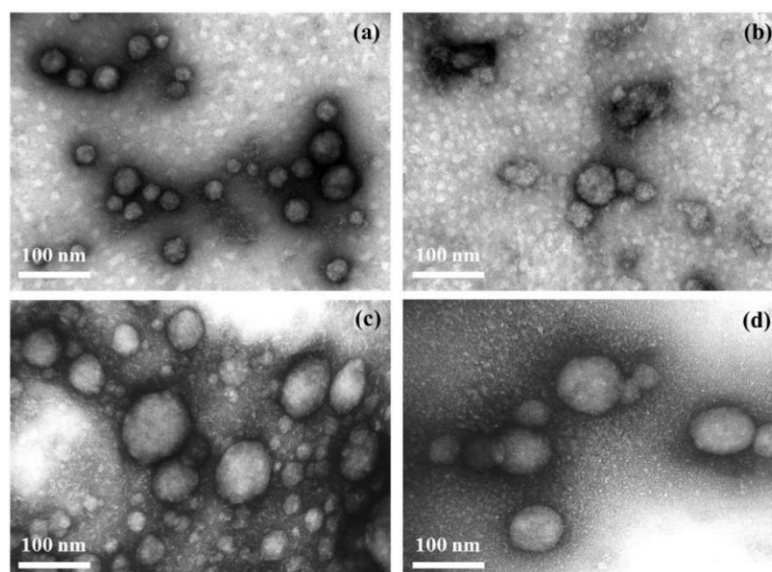


Figure 20 TEM images of polymeric micelles prepared by dropping method: (a) blank NSC PMs, (b) 3A.1-loaded NSC PMs, (c) 3A.1-loaded OSC PMs, and (d) 3A.1-loaded BSC PMs. The scale bars in all images are 100 μm .

4.1.2.3 Entrapment efficiency and loading capacity

A quantitative analysis of the drug content in the hydrophobic core of the micelles was performed using an HPLC. The effects of the initial amount of drug added (5–40 wt% to polymer weight ratio) and the different grafted hydrophobic moieties (naphthyl, octyl, and benzyl groups) on the %EE and LC are presented in Figure 21. The x-axis represents the initial amount of drug added to the micelle formulations, and the y-axis represents the encapsulated drug content in the micelles in terms of %EE (Figure 21a) and LC (Figure 21b). The results revealed that the initial amount of drug added directly correlated with the drug loading content. An increase in the initial amount of drug added resulted in an increase in LC due to the

hydrophobic interactions between the hydrophobic naphthyl, octyl, and benzyl groups with the hydrophobic drug. Moreover, the NSC micelles with 40 wt% initial drug concentration demonstrated the highest value of LC compared with the other micelles. These high levels of the entrapped drug can be explained by the hydrophobic interactions between the hydrophobic moieties of the polymer and the aromatic rings of the drug. These were an important factor when entrapping the drug into the micelles, therefore, the NSC micelles which presented naphthyl groups (double aromatic rings) onto the CS backbone created strong π - π interactions which were greater than the BSC (benzyl group; single aromatic ring) and OSC (octyl group; aliphatic hydrocarbon chain) alternatives. These results were in agreement with the previous study investigated the incorporation behavior of camptothecin by varying the degrees of the hydrophobicity of the inner core of micelles [215]. Overall, these CS graft copolymers are beneficial when designing drug delivery systems due to their highly efficient drug encapsulation and capability of increasing drug solubility.

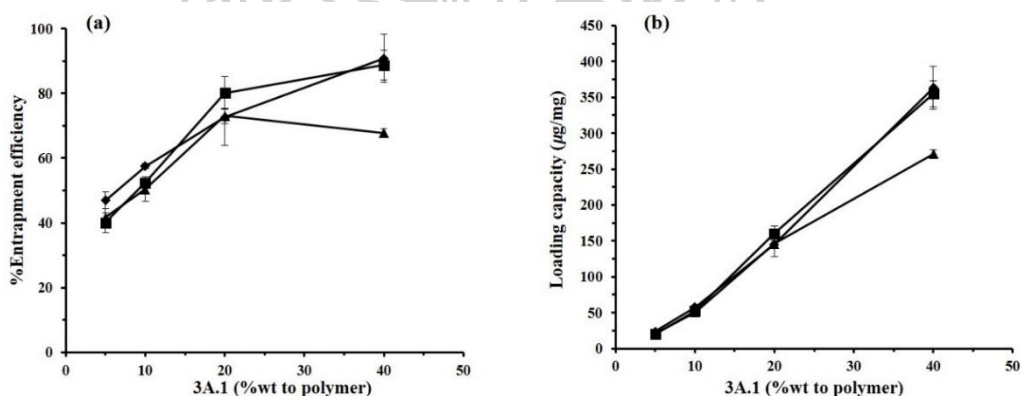


Figure 21 Effects of the initial amount of drug added (5-40 wt% to polymer) on (a) the entrapment efficiency and (b) the loading capacity of 3A.1-loaded NSC PMs (◆), 3A.1-loaded OSC PMs (■), and 3A.1-loaded BSC PMs (▲) prepared by a dropping method. Data are expressed as the mean \pm standard deviation (n= 3).

4.1.3 *In vitro* drug release

The *in vitro* release behaviors of the 3A.1 from the 3A.1-loaded micelles (NSC, OSC, and BSC) with 40 wt% initial drug added were examined at 37°C in three stages with different pH imitated the condition in the GI tract. A plot of the cumulative drug release from free 3A.1 and the 3A.1-loaded micelles as a function of time is shown in Figure 22. In SGF (pH 1.2), there was no apparent amount of drug released from any 3A.1-loaded micelles. However, when the release medium was changed to SIF (pH 6.8) for 6 h, the 3A.1 was considerably released from the 3A.1-loaded micelles, which significant difference in the released amounts was observed from the micelles prepared from different CS derivatives, indicating that the release rate depended on the hydrophobic functionalities of the polymer. The percentages of drug release from these micelles after 4 h were as follows: NSC ($82.10 \pm 2.43\%$) > BSC ($63.41 \pm 2.03\%$) > OSC ($52.03 \pm 3.33\%$). On the other hand, 3A.1 free drug could not be released through the simulated GI tract (SGF, SIF, and SCF). This might be due to the poor aqueous solubility of 3A.1 in all types and pH values of release medium ($<1 \mu\text{g/mL}$ at 37°C).

Generally, the pK_a value of succinic acid is approximately 4.21 at 25°C [212]. In the gastric fluid (pH 1.2), the succinyl groups grafted onto the CS polymer were unionized, resulting in a tight arrangement of the polymer core-shell structure and protection of 3A.1 from the acidic environment. When the micelles were exposed to the alkaline environment in SIF (pH 6.8) and SCF (pH 7.4), the succinyl groups grafted onto the CS polymer showed high ionization and created a negative surface charge, leading to losing compaction of the core-shell structures and promotion of the release of 3A.1 from the inner cores of the micelles. In addition, the different hydrophobic moieties influenced the drug release in SIF and SCF. The extent of drug release was reduced as follows: NSC micelles > BSC micelles > OSC micelles ($p < 0.05$). These results suggested that not only the π - π interactions restrict water penetration but also other factors such as hydrophobicity, mobility/rigidity, hydrogen bonding, and steric factors, influencing the difference in drug release [111]. Hence, many drug release studies inferred that these pH-sensitive micelles could enhance the solubility of 3A.1 in SIF and SCF media, and

different inner cores could influence the degrees of drug release. The OSC could retain 3A.1 within the inner core of the micelles greater than the micelles prepared from NSC and BSC. Therefore, it can be assumed that the 3A.1-loaded micelles (NSC, OSC, and BSC) exhibited delayed release profiles which are useful for improving the bioavailability of 3A.1 for oral intestine/colon drug delivery.

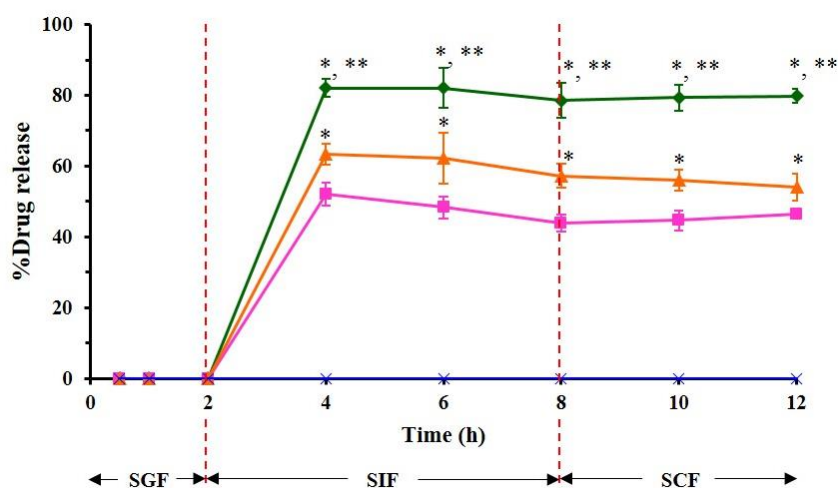


Figure 22 In vitro release profiles of free 3A.1 (×) and 3A.1-loaded polymeric micelles prepared by a dropping method; NSC (◆), OSC (■), and BSC (▲), in simulated gastric fluid (SGF; pH 1.2, 0–2 h), simulated intestinal fluid (SIF; pH 6.8, 2–8 h) followed by simulated colonic fluid (SCF; pH 7.4, 8–12 h). These data are expressed as mean ± standard deviation (n = 3). *Statistically significant difference compared with OSC PMs ($p < 0.05$); **Statistically significant difference compared with BSC PMs ($p < 0.05$).

4.1.4 Short-term stability

One of the main stability concerns regarding polymeric micelles is particle aggregation. The physical stability of the 3A.1-loaded micelles (NSC, OSC, and BSC) was examined under two conditions, an accelerated environment ($25 \pm 2^\circ\text{C}$, $60 \pm 5\% \text{RH}$) and a long-term environment ($5 \pm 3^\circ\text{C}$, $60 \pm 5\% \text{RH}$), for 6 months [208]. The physical stability of the 3A.1-loaded micelles was studied and the data, including particle size, PDI, and percentage of drug remaining, is presented in Figure 23. The results indicated that the particle sizes of the micelles stored at $5 \pm 3^\circ\text{C}$, $60 \pm 5\% \text{RH}$ for 180 days were smaller than those stored at $25 \pm 2^\circ\text{C}$, $60 \pm$

5%RH, the surface charges of the micelles were not altered which had a highly negative zeta potential value of approximately -30 mV. Interestingly, the mean particle size of these micelles in both conditions remained lower than 200 nm without nanoparticle aggregation. These results might suggest that the high negative charge of these micelles helped to stabilize the micelles in the aqueous solution through electrostatic repulsion. After storage at the long-term condition for 6 months, the total contents of 3A.1 in the NSC, OSC, and BSC micelles were 93.65 ± 2.69 , 87.22 ± 2.85 , and $85.67 \pm 3.15\%$, respectively. However, under the accelerated condition the drug content was found to be 81.64 ± 2.87 , 68.27 ± 3.26 , and $53.62 \pm 3.36\%$, respectively. The 3A.1-loaded micelles kept under an accelerated condition exhibited faster degradation than those stored under a long-term condition. The 3A.1-loaded BSC micelles demonstrated poor stability, whereas the NSC micelles showed better stability with the high values of %drug remaining after 6 months when stored under a long-term condition. These results explained that naphthyl groups had stronger hydrophobic interaction between the hydrophobic groups of the polymer and the hydrophobic drug than the benzyl groups, resulting in higher drug protection capability and a decrease in drug leakage from the NSC micelles [216]. Our data suggested that the micelles should be stored in a refrigerator to maintain the particle size, zeta potential, and the amount of drug remaining in the micelles.

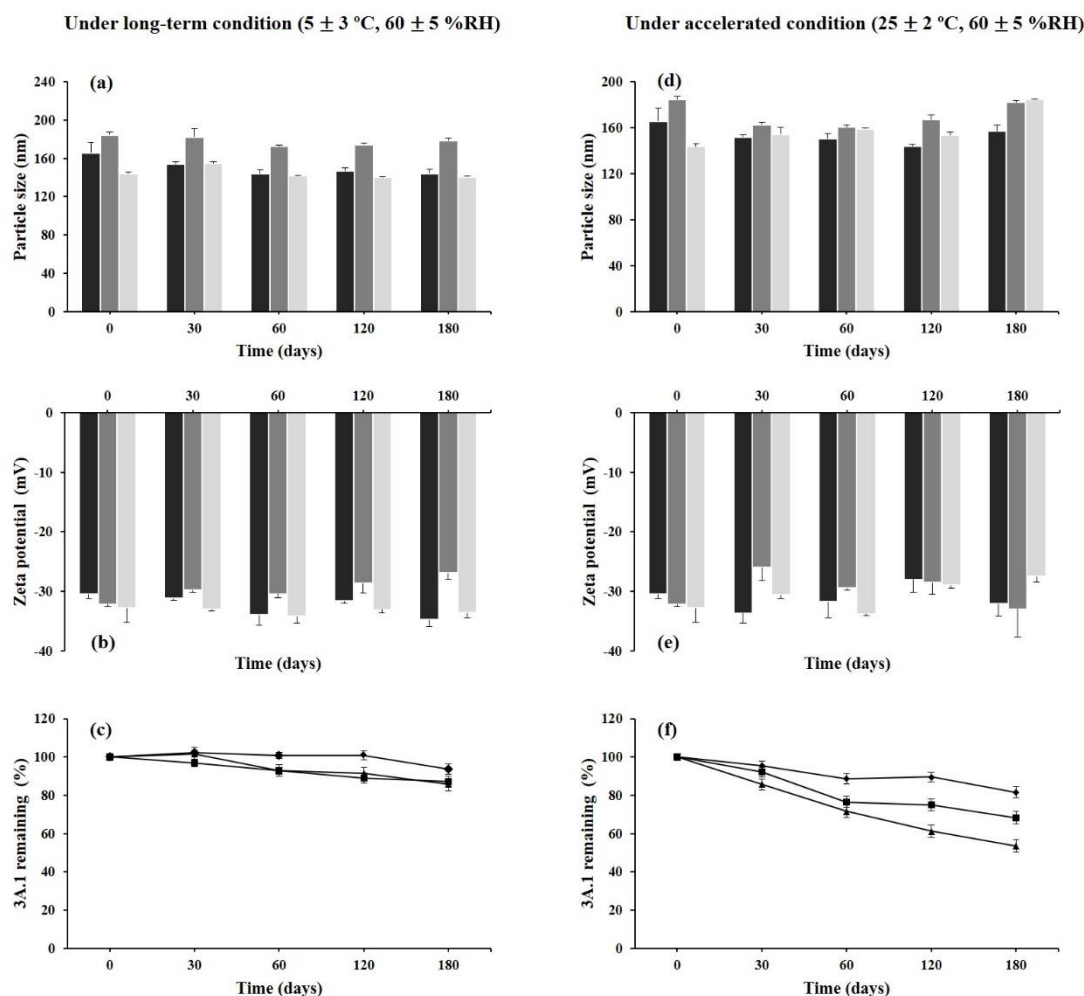


Figure 23 The short-term stability of 3A.1-loaded polymeric micelles stored under long-term condition (left) compared with under accelerated condition (right) for 6 months; (a,d) particle size of NSC PMs (black bar), OSC PMs (dark gray bar), and BSC PMs (light gray bar); (b,e) zeta potential of NSC PMs (black bar), OSC PMs (dark gray bar), and BSC PMs (light gray bar); (c,f) the amount of 3A.1 remaining in NSC PMs (\blacklozenge), OSC PMs (\blacksquare), and BSC PMs (\blacktriangle). All data are presented as the mean \pm standard deviation ($n = 3$).

4.1.5 *In vitro* anticancer activity

The anticancer activity of free 3A.1 and the 3A.1- loaded NSC, OSC, and BSC micelles against human colorectal cancer (HT29) cells was assessed using an MTT colorimetric assay. The finding indicated that the %cell viability was dose-dependent. The half-maximal inhibitory concentration (IC_{50}) was determined from

the %cell viability-drug concentration relationship. The IC_{50} values of the 3A.1-loaded NSC, OSC, and BSC micelles for 36 h-treatment were 1.024 ± 0.071 , 0.693 ± 0.099 , and 0.538 ± 0.025 $\mu\text{g/mL}$, respectively, which were significantly lower than that of the free drug (3.816 ± 0.376 $\mu\text{g/mL}$; $p < 0.05$) (Figure 24). Cell viability of the blank micelles remained more than 80% even at high polymer concentrations up to 500 $\mu\text{g/mL}$. No significant differences in the cytotoxicity were noticed among the blank micelles prepared from different CS derivatives. These results indicated that all blank micelles demonstrated minimal cytotoxicity in HT29 cells, and the cytotoxicity was due to the presence of 3A.1 in the free form and the micelles.

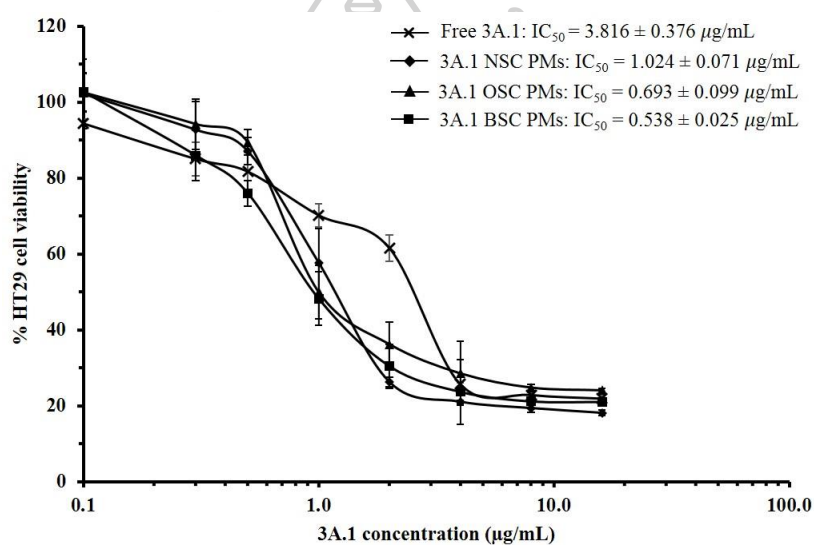


Figure 24 The percentage of cell viability (y-axis) of HT29 cells after being exposed to various concentrations of 3A.1-loaded polymeric micelles or free 3A.1 (x-axis) for 36-h treatment, and the IC_{50} values ($\mu\text{g/mL}$) were included.

4.1.6 Induction of cell apoptosis

To confirm whether this drug can induce apoptosis in HT29 colorectal cancer cells, a co-staining assay (annexin V-FITC and PI) was used to quantitatively analyze the degree of cell death, especially cell apoptosis, by flow cytometry analysis (Figure 25a). In this part, the cell apoptosis rate was calculated by the inclusion of the percentage of early apoptosis (Q4; annexin V-FITC⁺/PI⁻) and the percentage of late apoptosis (Q2; annexin V-FITC⁺/PI⁺) (Figure 25b). After incubation with the free drug and different formulations of 3A.1-loaded micelles

containing equivalent drug concentrations (at IC_{50} of the free drug; $3.8 \mu\text{g/mL}$) for 24 h, the cell apoptosis rates of the drug-loaded NSC, OSC, and BSC micelles were 45.20 ± 3.27 , 41.60 ± 2.45 , and $40.50 \pm 2.04\%$, respectively, which were significantly greater than those of the free drug ($33.10 \pm 2.45\%$) and Triton[®] X-100 ($9.50 \pm 1.63\%$). These degrees of cell apoptosis were in concordance with the results of the *in vitro* anticancer activity. In addition, the percentage of cell necrosis of the cells treated with the drug-loaded micelles were lower than that treated with free drug at this stage. This might be a beneficial property of the micelles for the growth suppression of cancer cells. Thus, 3A.1-loaded NSC, OSC, and BSC micelles induced intense apoptosis in HT29 colorectal cancer cells [20,82].

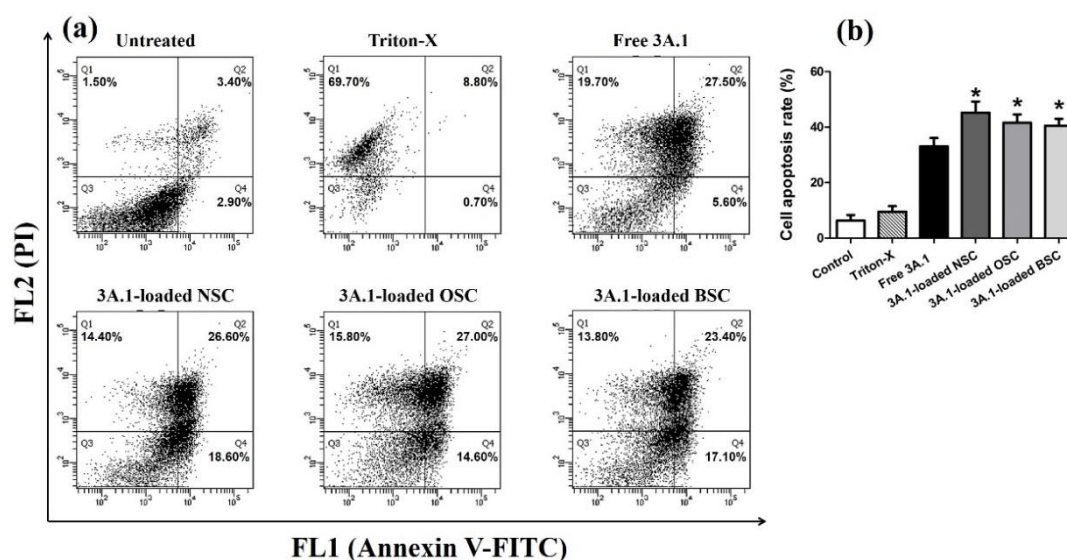


Figure 25 3A.1-loaded PMs induce HT29 cancer cell apoptosis examined by flow cytometry: (a) HT29 cells treated with 3A.1-loaded PMs, free 3A.1 (at the equivalent 3A.1 concentration of $3.8 \mu\text{g/mL}$), and Triton-X[®] for 24 h which are presented in four quadrants (Q) with dot plot. The number of necrosis cells, late apoptosis cells, early apoptosis cells, and living cells are displayed on Q1, Q2, Q4, and Q3, respectively. (b) Percentage of cell apoptosis rate of the cells after being treated with 3A.1-loaded PMs, free drug, and Triton-X[®]. *Statistically significant difference from free 3A.1 group ($p < 0.05$).

4.1.7 *In vitro* anti-migratory activity

The scratch wound migration assay was selected to assess the anti-migratory effect of free 3A.1 and 3A.1-loaded micelles on human oral cancer (HN22) cells because of the simple and cost-effective procedure. The wound gap images of cells treated with the 3A.1-loaded micelles and free drug are shown in Figure 26a. After 24-h treatment, the scratch areas of the untreated cell monolayer were almost fully closed, whereas both free 3A.1 and 3A.1-loaded micelles tended to reduce the cell motility. In addition, the cell migration rate and %wound closure are illustrated in Figure 26b and c. respectively. The results showed that free 3A.1 had a significantly slower cell migration rate than that of the untreated cells, and it also decreased %wound closure compared with the untreated cell, indicating that 3A.1 could suppress cell motility. Moreover, both cell migration rate and %wound closure of 3A.1-loaded micelles were not significantly different from the free drug at the same concentration. From these results, it could be concluded that free 3A.1 might be one of the antimigration compounds, and loading of 3A.1 into the micelles did not affect its anti-migratory activity. Therefore, 3A.1-loaded micelles could be a potential carrier to reduce metastasis of oral cancer.

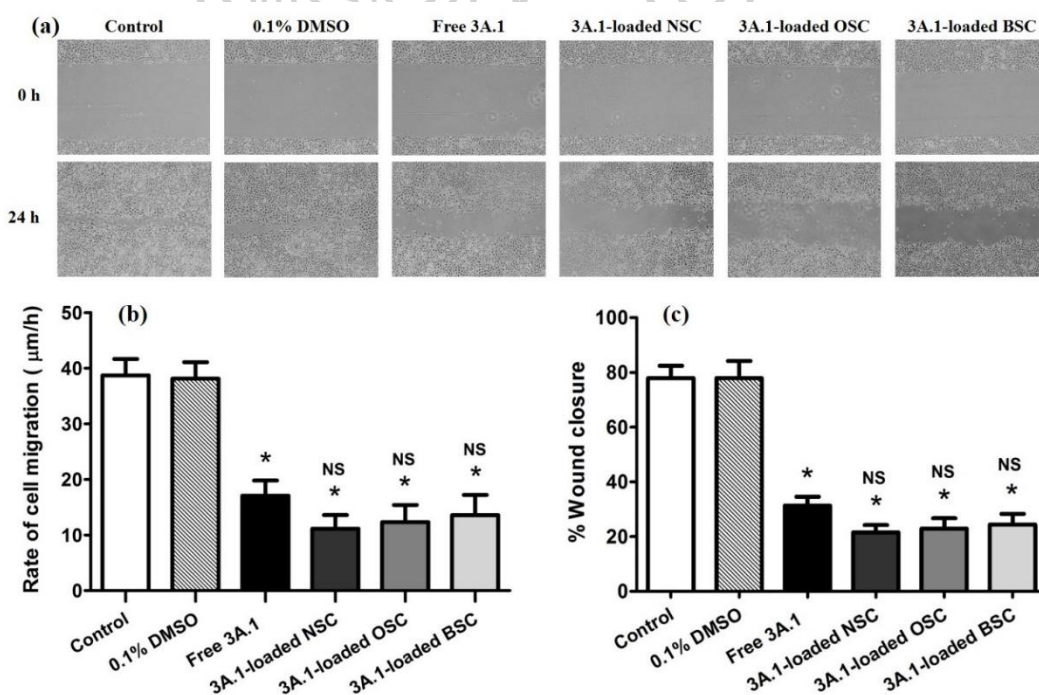


Figure 26 The anti-migratory effect of free 3A.1 and 3A.1-loaded PMs prepared by a dropping method on head and neck (HN22) cancer cells presented as the (a) wound images taken by a microscope (40× magnification) at 0 and 24 h, (b) cell migration rate and (c) % wound closure after 24-h treatment exposure. *Statistically significant difference from the untreated control group ($p<0.05$); NS, no significantly different from free 3A.1 group ($p>0.05$).

4.1.8 *In vitro* cellular uptake

In this experiment, Dox as an anticancer compound with fluorescence property was selected to formulate polymeric micelle using the NSC copolymer. The cellular uptake of free Dox and the 40 wt% Dox-loaded NSC micelles was examined qualitatively using a fluorescence microscopy, as displayed in Figure 27. HT29 cells were exposed to Dox solution and the Dox-loaded micelles for two different periods (12 and 24 h). The results showed that cells incubated with the Dox-loaded micelles emitted higher fluorescent intensity than those incubated with the free drug at both incubation times. To verify this result, the cells were analyzed by flow cytometry for quantitative cellular uptake. From the fluorescent histograms displayed in Figure 28a, the cells incubated with the Dox-loaded micelles emitted a stronger fluorescent intensity than those of the free drug. This result was consistent with the fluorescent image study. As shown in Figure 28b, the MFI of the cells treated with Dox-loaded micelles was significantly higher than ($p<0.05$) those treated with the free drug after 24-h treatment, representing that the Dox-encapsulated micelles were effectively taken up by the cancer cells. The MFI of the cells treated with empty micelles was not different from the control group. Thus, it can be concluded that the Dox-loaded micelles could enhance drug internalization and accumulation into the cancer cells.

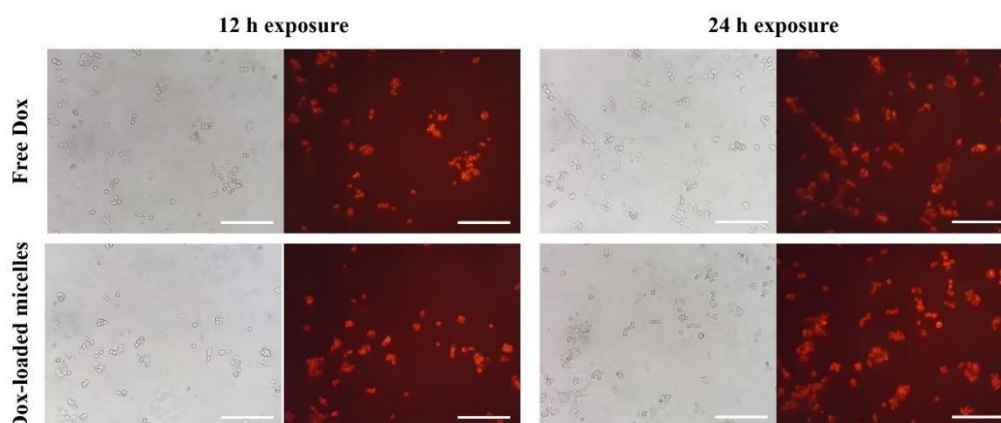


Figure 27 Fluorescent images of HT29 cells that were exposed to 40 wt% Dox-loaded NSC PMs, compared with free Dox for 12-h and 24-h treatment. The scale bars in all images are 200 μm .

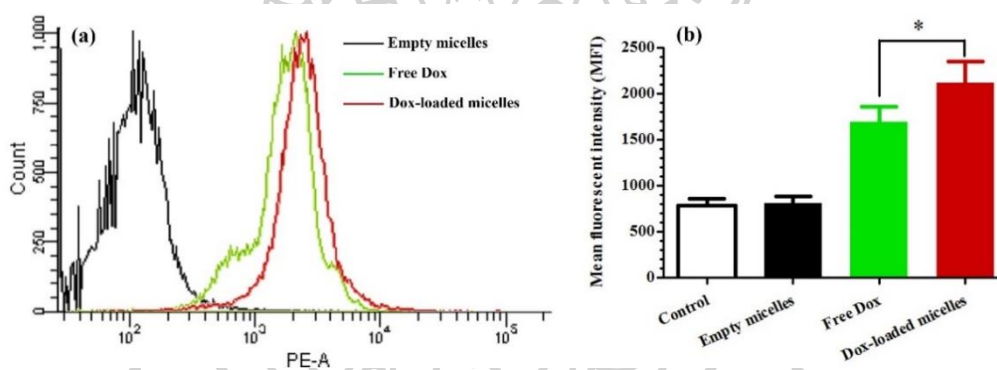


Figure 28 Drug uptake from 40 wt% Dox-loaded NSC PMs and free Dox in HT29 cells determined by flow cytometry; (a) histogram of fluorescent events and (b) mean fluorescent intensity of Dox. *Statistically significant difference compared with free Dox ($p < 0.05$).

4.1.9 Folate-conjugated NSC polymeric micelles as a delivery system of 3A.1 for active tumor targeting

4.1.9.1 Preparation and physicochemical properties of 3A.1-loaded micelles

The blank micelles and the 3A.1-loaded micelles based on the synthesized chitosan derivatives (NSC and folate-conjugated NSC, Fol-NSC) can easily self-aggregate to form micelles in an aqueous solution by dropping method. Based on the results from our previous study [217], 3A.1

(40 %wt to the polymer) was selected to be loaded into both micelles. The morphology of the micelles was determined by TEM, as illustrated in Figure 29. The 3A.1-loaded NSC and Fol-NSC micelles had a spherical shape. Data from the physicochemical evaluation are shown in Table 11. The particle sizes of the 3A.1-loaded NSC and Fol-NSC micelles were less than 200 nm, and the PDI values were less than 0.3. The zeta potential of both 3A.1-loaded micelles was negative due to the dissociation of the succinic groups presented on the micelles. This optimal negative charge could help to prevent particle aggregation. The content of 3A.1 in the micelle formulations is represented in the terms of %EE and LC. The %EE and LC of Fol-NSC micelles were lower than those of NSC micelles, probably because the Fol-NSC might reduce hydrophobic interaction between the hydrophobic compound and hydrophobic cores of micelles.

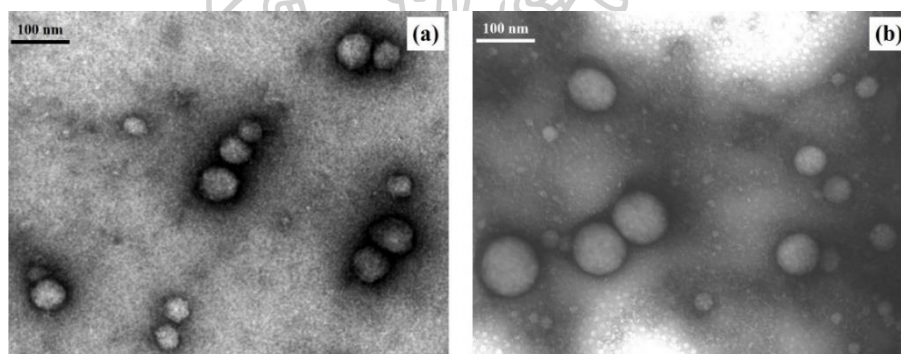


Figure 29 TEM images of (a) 3A.1-loaded NSC PMs and (b) 3A.1-loaded Fol-NSC PMs prepared by a dropping method with drug loading of 40 %wt to polymer. The scale bars in all images are 100 μ m.

4.1.9.2 *In vitro* drug release

The release of 3A.1 from the NSC micelles and the Fol-NSC micelles in the sequential medium pH 1.2, 6.8, and 7.4 at 37°C was studied. The release patterns of the 3A.1 from the 3A.1-loaded micelles compared with that from the 3A.1 suspension are presented in Figure 30. The pH value of the medium was found to affect the release rate of 3A.1, and these micelles also had a pH-sensitive feature. In the SGF (pH 1.2), the 3A.1 was not released from the NSC and the Fol-NSC micelles. After changing the

medium to SIF (pH 6.8), the 3A.1 was extremely released which ~80% and ~50% of the 3A.1 was released from the NSC micelles and the Fol-NSC micelles, respectively, at 8 h. After that, the release remained constant in the SCF (pH 7.4) for 12 h. Overall, the released 3A.1 from the Fol-NSC micelles decreased compared with the NSC micelles because of steric hindrance at the micellar surface. These results indicated that these micelles could be used as a carrier for colon-specific delivery system.

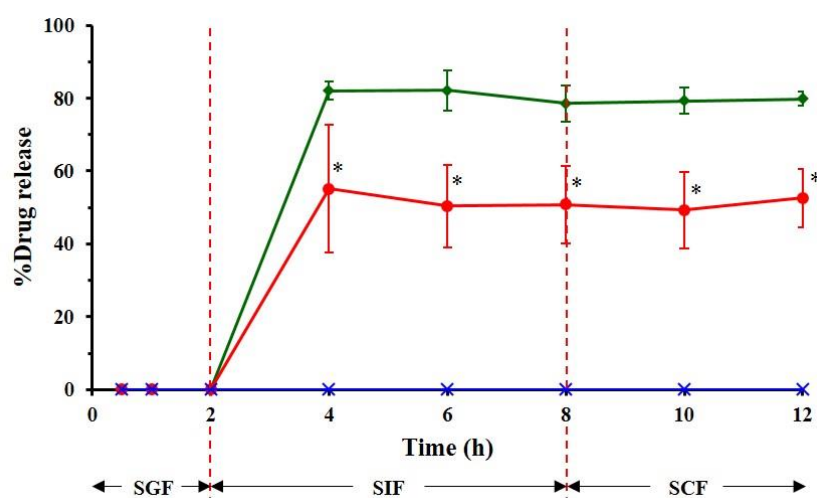


Figure 30 In vitro release patterns of free 3A.1 (X) and 3A.1-loaded polymeric micelles prepared by a dropping method; NSC (◆) vs. Fol-NSC (●), in simulated gastrointestinal fluid. All data are expressed as mean \pm standard deviation (n=3). *Statistically significant difference compared with NSC PMs ($p < 0.05$).

4.1.9.3 *In vitro* anticancer activity

The cytotoxicity after 36-h exposure of the 3A.1-loaded NSC and Fol-NSC micelles against the HT29 cells was assessed using an MTT assay (Figure 31). The results revealed that the growth inhibition of the micelles against the HT29 cells was dose-dependent, and the Fol-NSC micelles had the lowest IC_{50} value ($0.412 \pm 0.056 \mu\text{g/mL}$) which was significantly lower than that of NSC micelles ($1.024 \pm 0.071 \mu\text{g/mL}$) and free 3A.1 ($3.816 \pm 0.376 \mu\text{g/mL}$). The superior anticancer activity of the 3A.1-loaded Fol-NSC micelles was due to the specific binding of folate molecules on micelle surface to the folate receptors overexpressed on HT29 cells together with

the higher amount of 3A.1 taken up into the cancer cells via folate receptor-mediated endocytosis [95,218,219]. In addition, the blank NSC and the Fol-NSC micelles were tested with the same procedure. The results indicated that the amphiphilic copolymers including NSC and Fol-NSC used in this study were less cytotoxicity and they might be used as safe nanomaterials.

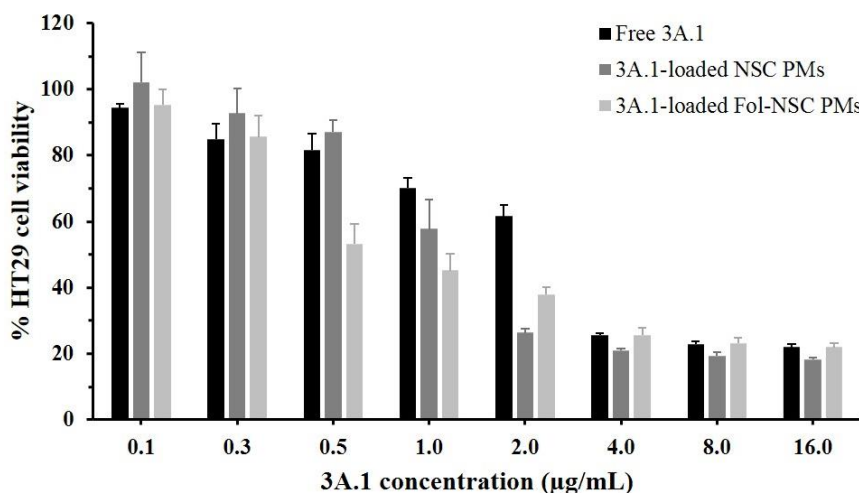


Figure 31 Dose-response curve of the 3A.1-loaded NSC PMs and the 3A.1-loaded Fol-NSC PMs against HT29 cancer cells for 36 h, compared with free 3A.1. Each bar graph is presented as the mean \pm standard deviation ($n = 3$).

4.1.9.4 Induction of cell apoptosis

To confirm the anticancer activity of the 3A.1-loaded micelles, the cell apoptosis of HT29 cells was determined by double staining assay using flow cytometry analysis, and the results are presented in Figure 32. After 24-h incubation with equivalent 3A.1 concentration of 3.8 µg/mL, the cell apoptosis rate of the 3A.1-loaded Fol-NSC micelles ($51.47 \pm 1.76\%$) was higher than that of the NSC micelles ($45.20 \pm 3.27\%$) and both 3A.1-loaded micelles significantly enhanced the levels of cell apoptosis in HT29 cells compared with free 3A.1 ($33.10 \pm 2.45\%$). This result was in agreement with the results from *in vitro* cytotoxicity test. It was clear that the anticancer activity of 3A.1 could be improved when it was encapsulated into micelles, especially Fol-NSC micelles as a targeted nanocarrier.

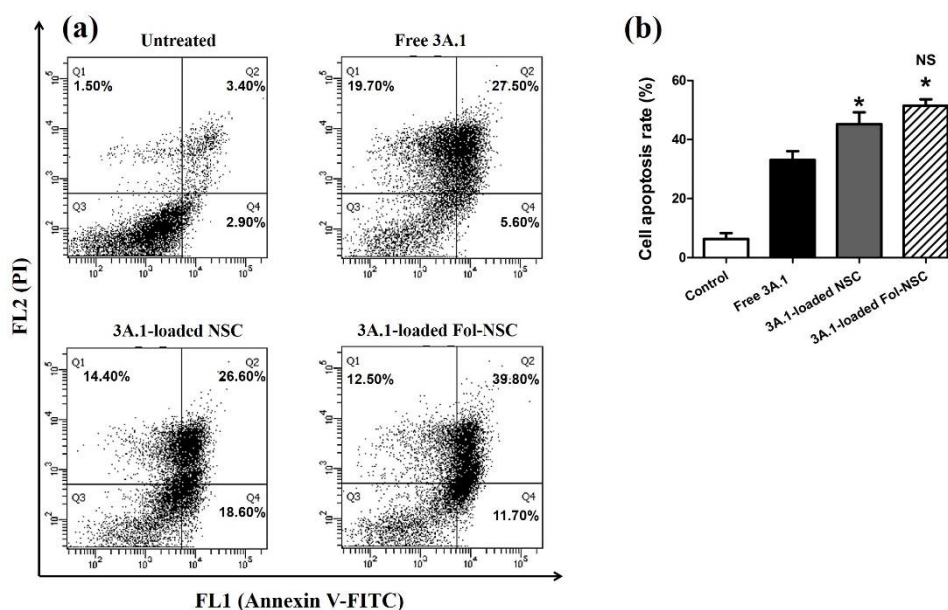


Figure 32 Analysis of HT29 cell apoptosis by flow cytometry after treatment with 3A.1-loaded NSC PMs and Fol-NSC PMs at the equivalent 3A.1 concentration of 3.8 $\mu\text{g}/\text{mL}$ for 24 h. (a) Fluorescent dot-plot and (b) rate of cell apoptosis. Data are presented as mean \pm standard deviation ($n=3$). *, $p<0.05$ vs. free 3A.1 group; NS, no statistically significant difference vs. 3A.1-loaded NSC PMs.

4.2 Formulation screening of liposomes with or without 3A.1 analogue

In our screening experiment, hydrophobic 3A.1 was passively encapsulated into liposomal formulations prepared by a thin-layer hydration followed by probe-type sonication. This method was employed as it provided convenience and a great capability for the encapsulation of various hydrophobic drugs into lipid bilayer [220]. The conventional liposomes (Con LP) were prepared from lipid components including PC and Chol at a fixed molar ratio of 2:1 while the PEGylated liposomes (PEG LP) were formulated as the same lipid ingredients and added DSPE-PEG2000 by varying three different molar ratios (0.125, 0.25, and 0.50). The main reason to use a constant molar ratio of PC: Chol at 2:1 is that this ratio provided appropriate physicochemical properties, as reported in a previous study [221]. We have proposed that the insertion of Chol between the concentric lipid bilayer helps improve the bilayer's rigidity to achieve better physical stability and reduced quick drug release. Both Con LP and PEG LP contained different initial 3A.1 amounts (0-4.0 molar ratio). This experimental

design was to optimize the appropriate 3A.1-loaded Con LP and PEG LP that expressed the highest drug entrapment with desirable physicochemical properties. The physicochemical properties of 3A.1-loaded Con LP and PEG LP are summarized in Table 12. Overall, thin lipid layer hydration was applied to produce multilamellar vesicles (MLVs) having a size of ≥ 500 nm, and vesicle size reduction via probe-ultrasonication method was used to generate unilamellar vesicles (ULVs) having a size of ≤ 100 nm for small ULVs and size of > 100 nm for large ULVs [126].

4.2.1 Effect of initial drug molar ratios

4.2.1.1 Particle size and zeta potential

Concerning the 3A.1-loaded Con LP, the results demonstrated that the initial drug content affected its physicochemical properties. When the molar ratio of drug content was increased from 0.5 to 3.0, the vesicle size was seen to increase from 110.57 ± 0.90 nm to 143.77 ± 4.35 nm while the zeta potential of Con LP was not altered, with only a slightly negative charge of $(-) 7.79 \pm 0.61$ to $(-) 11.10 \pm 0.67$ mV. The negative charge of Con LP arose from the dissociation of the phosphate group in the PC molecule when the pH of the dispersed vehicle was superior to the isoelectric point of PC [222]. As different levels of DSPE-PEG200 were added, the physicochemical characteristics of PEGylated liposomes were altered. An increase in the initial drug molar ratio from 0.5 to 3.0 resulted in an increase in the vesicle size. The insertion of DSPE-PEG2000 tended to slightly increase the negative charge at the liposome's surface since this lipid presented anionic charge at pH 7.4 [223]. At the similar drug molar ratio of 3.0, the vesicle size of PEGylated liposomes was ranked as follows: 0.125 PEG LP (111.77 ± 4.40 nm) $<$ 0.50 PEG LP (113.73 ± 2.91 nm) $<$ 0.25 PEG LP (115.33 ± 3.08 nm). The vesicle size of PEG LP was smaller than that of the Con LP at each drug molar ratio, which is probably due to higher structural condensation between lipids and hydrophobic drugs. Almost all liposome formulations had a PDI value of less than 0.3, indicating that the distribution of vesicle size was narrow.

Table 12 The influence of liposome formulations encapsulated different 3A.1 molar ratios on vesicle size, PDI and zeta potential, %encapsulation efficiency (%EE), and loading capacity (LC). All data represent the mean \pm standard deviation (n=3).

Formulations	PC (mM)	Chol (mM)	DSPE-PEG ₂₀₀₀ (mM)	3A.1 (mM)	Vesicle size (nm)	PDI	ζ (mV)	%EE	LC (μ g/mg of lipids)
Conventional liposomes (Con LP)	10	2	0	0	107.90 \pm 2.25	0.267	(-) 8.86 \pm 0.67	-	-
	10	2	0	0.05	110.57 \pm 0.90	0.258	(-) 8.72 \pm 1.97	57.62 \pm 1.19	20.56 \pm 0.21
	10	2	0	1	108.97 \pm 1.68	0.280	(-) 11.10 \pm 0.67	57.71 \pm 1.83	41.19 \pm 0.28
	10	2	0	2	123.27 \pm 4.41	0.301	(-) 7.79 \pm 0.61	62.28 \pm 0.72	88.91 \pm 2.15
	10	2	0	3	143.77 \pm 4.35	0.193	(-) 8.35 \pm 0.76	48.06 \pm 0.85	102.92 \pm 1.92
PEGylated liposomes (0.125 PEG LP)	10	2	0	4	133.70 \pm 1.98	0.253	(-) 9.11 \pm 0.55	35.62 \pm 0.42	100.63 \pm 2.05
	10	2	0.125	0	109.40 \pm 1.61	0.319	(-) 12.83 \pm 0.66	-	-
	10	2	0.125	0.05	86.47 \pm 0.18	0.241	(-) 12.23 \pm 1.14	73.20 \pm 2.22	26.75 \pm 1.03
	10	2	0.125	1	91.56 \pm 3.33	0.278	(-) 15.33 \pm 0.41	76.03 \pm 1.72	52.11 \pm 1.61
	10	2	0.125	2	100.97 \pm 1.42	0.253	(-) 11.97 \pm 0.38	69.21 \pm 1.42	94.88 \pm 1.98
PEGylated liposomes	10	2	0.125	3	111.77 \pm 4.40	0.216	(-) 11.60 \pm 0.37	57.48 \pm 0.66	118.21 \pm 2.23
	10	2	0.125	4	99.55 \pm 0.64	0.152	(-) 12.80 \pm 0.91	41.18 \pm 0.43	112.90 \pm 2.36
	10	2	0.25	0	84.22 \pm 0.82	0.230	(-) 15.07 \pm 0.88	-	-
	10	2	0.25	0.05	88.45 \pm 0.26	0.227	(-) 15.10 \pm 0.71	78.56 \pm 2.33	25.89 \pm 1.03

(0.25 PEG LP)	10	2	0.25	1	90.23 ± 0.67	0.225	(-) 15.33 ± 0.41	77.73 ± 2.88	51.23 ± 2.84
	10	2	0.25	2	94.95 ± 0.90	0.209	(-) 14.07 ± 1.41	71.80 ± 0.98	94.65 ± 3.28
	10	2	0.25	3	115.33 ± 3.08	0.233	(-) 14.43 ± 0.74	60.24 ± 1.13	119.12 ± 1.68
	10	2	0.25	4	104.80 ± 2.41	0.259	(-) 18.20 ± 0.29	45.52 ± 0.55	118.00 ± 1.12
	10	2	0.50	0	106.80 ± 5.77	0.301	(-) 16.57 ± 1.50	-	-
PEGylated	10	2	0.50	0.05	98.31 ± 4.22	0.371	(-) 15.50 ± 0.42	71.94 ± 0.90	22.02 ± 1.11
liposomes	10	2	0.50	1	102.80 ± 1.63	0.303	(-) 16.53 ± 0.90	70.43 ± 1.48	43.73 ± 2.04
(0.50 PEG LP)	10	2	0.50	2	104.87 ± 1.20	0.27	(-) 16.63 ± 1.06	68.16 ± 1.10	83.45 ± 2.06
	10	2	0.50	3	113.73 ± 2.91	0.205	(-) 16.03 ± 0.75	61.20 ± 2.18	112.41 ± 2.81
	10	2	0.50	4	101.03 ± 0.97	0.234	(-) 16.00 ± 0.65	44.31 ± 2.49	115.85 ± 2.98

4.2.1.2 Drug loading capacity

To determine the drug loading capacity, the effect of initial drug molar ratio on drug encapsulation was analyzed and these values are listed in Table 12. The %encapsulation efficiency (%EE) was calculated by dividing the encapsulated drug amount by the theoretical drug amount. This value implies whether each step of liposome preparation influences drug content. The loading capacity (LC) was computed by dividing the encapsulated drug amount by the total mass lipids. This value provides the capacity of lipids used to reserve an active compound. The LC of the 3A.1-loaded Con LP was directly correlated with the initial drug molar ratio, whereas the %EE was inversely related to the initial drug molar ratio. We found that the Con LP conveying drug molar ratio of 3.0 showed the highest LC (102.92 ± 1.92 $\mu\text{g}/\text{mg}$ of lipid), so this formulation was selected as a representative Con LP for further experimental studies. Likewise, the LC of the 3A.1-loaded PEG LP prepared with the DSPE-PEG2000 molar ratios of 0.125, 0.25, and 0.50 was directly proportional to the initial drug molar ratio. The LC of the PEG LP prepared with the three levels of DSPE-PEG2000 embedded in liposome exhibited the highest LC (118.21 ± 2.23 , 119.12 ± 1.68 , and 112.41 ± 2.81 $\mu\text{g}/\text{mg}$ of lipid with the DSPE-PEG2000 molar ratios of 0.125, 0.25, and 0.50, respectively) at a drug molar ratio of 3.0. In comparison with the Con LP, the higher amount of drug encapsulation into the PEG LP may be explained by the fact that the DSPE-PEG2000 can interact with the hydrophobic 3A.1 molecule via hydrophobic interaction within the lipid bilayer. Despite having similar LC values, PEG LP containing a drug molar ratio of 3.0 was found to have the optimal density of PEG chain at a DSPE-PEG2000 molar ratio of 0.25 and was therefore chosen as typical PEG LP for additional evaluations.

4.2.1.3 Visual appearance

As shown in Figure 33, the visual appearance of liquid liposomes revealed that the empty Con LP (Figure 33a) and the empty PEG LP (Figure 33c) were transparent liquids with white-opalescent, whereas 3A.1-loaded

Con LP (Figure 33b) and 3A.1-loaded PEG LP (Figure 33d) looked more turbid than that of blank liposomes. Moreover, the presence of drug precipitation at the bottom of the container was not found. The liposome formulation is intended for i.v. injection in cancer therapy. We found that the mean pH values of all 3A.1-loaded LP was a mildly acidic solution (pH ~6.0-6.8), which was within an acceptable pH range [224].

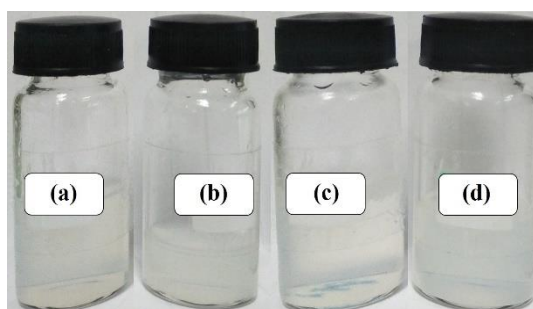


Figure 33 The appearance of liposomal formulations prepared by a thin film hydration and probe-sonication method: (a) blank Con LP, (b) 3A.1-loaded Con LP, (c) blank PEG LP, and (d) 3A.1-loaded PEG LP

4.2.1.4 Morphology

The morphological feature of the liposomes is illustrated in Figure 34. TEM analysis established that closed vesicles in these liposomal formulations had an almost spherical or spherical shape with a regular and smooth surface. The TEM images (Figure 34d) revealed that the particle size of the 3A.1-loaded Con LP (Figure 34b) and the 3A.1-loaded PEG LP was slightly bigger than that of the blank liposomes. Furthermore, the diameter size of the liposomes were measured to be approximately 65 nm to 160 nm, which was smaller than that measured by dynamic light scattering (DLS) techniques. This effect can be explained by the fact that the particle size determined by the DLS method was involved in the analysis of the hydrodynamic diameter, whereas TEM was performed on samples in a dry state [213].

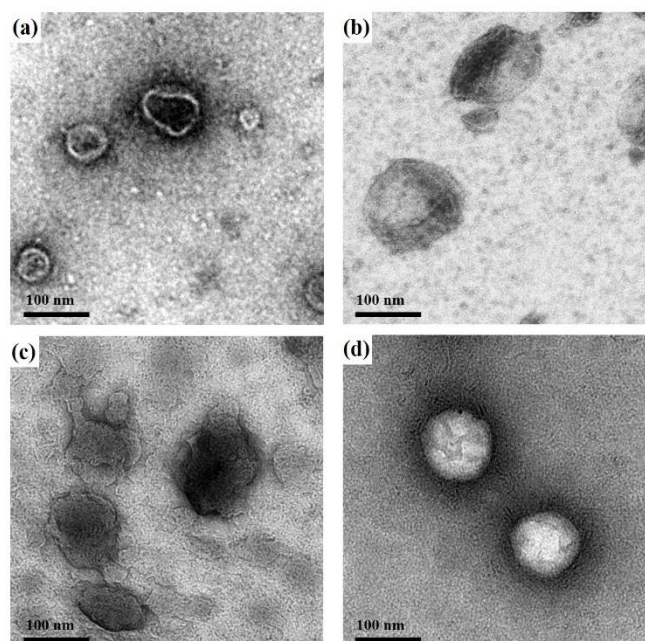


Figure 34 TEM images of liposomal formulations prepared by a thin film hydration and probe-sonication method: (a) blank Con LP, (b) 3A.1-loaded Con LP, (c) blank PEG LP, and (d) 3A.1-loaded PEG LP. The scale bar in each image is equal to 100 nm.

4.2.2 *In vitro* drug release

The release profiles of freshly prepared liposomes including the 3A.1-loaded Con LP and the 3A.1-loaded PEG LP compared to 3A.1 solution were evaluated for 24 h in a PBS buffer (pH 7.4) that mimics an *in vivo* environment, and the results are presented in Figure 35. Theoretically, satisfactory liposomes for effective drug delivery to targeted sites should be able to provide precise drug release from liposomes and deliver sufficient drug concentration, whilst minimizing any drug loss before reaching the diseased tissues [91]. The results demonstrated that free 3A.1 was rapidly released (release rate of > 80%) within the first 30 min followed by a gradual release over 24 h until the release rate was almost 100%. Simultaneously, a burst of drug release from the 3A.1-loaded Con LP was observed in the initial stage with a release rate of > 80% within 2 h. Meanwhile, the 3A.1 showed a continuous release from the liposome into the medium with a final release rate of nearly 100% over the time of the test. In the first 2 h of the release study, the released drug amount was significantly lower than the drug

solution ($p < 0.05$), indicating that the release of drug embedded in the liposome was slightly retarded. However, 3A.1-loaded Con LP released the drug at a relatively similar level in comparison to the drug solution during a period of up to 24 h following the test. Furthermore, the release behavior of the 3A.1-loaded PEG LP showed two-phase release; during the first phase, 3A.1 was immediately released from lipid vesicles whilst in the second phase, liposomes showed a sustained drug release with a release rate of around 67% after 24-h testing. The slow-release pattern was probably due to the diffusion of 3A.1 through the lipid bilayer and shielding of the lipid membrane by steric hindrance of PEG coating at liposome's surface [225].

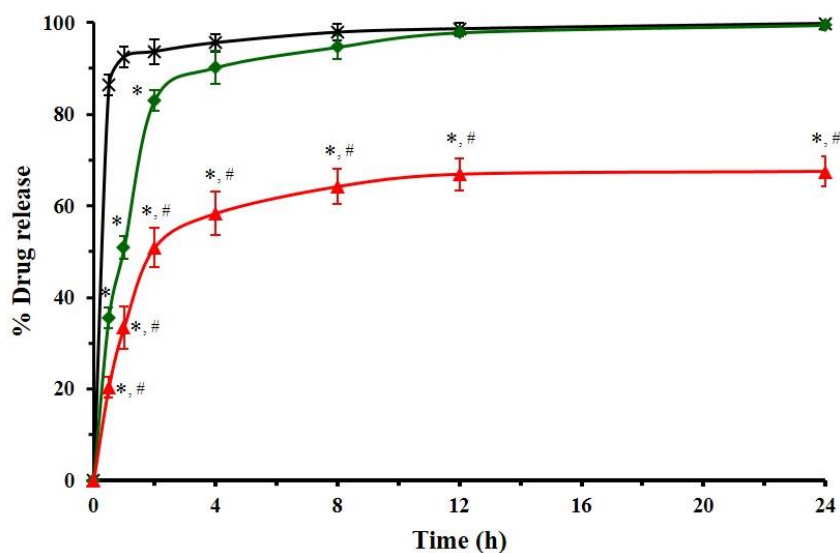


Figure 35 In vitro release profiles of 3A.1 from 3A.1 solution (×), 3A.1-loaded Con LP (◆), and 3A.1-loaded 0.25-PEG LP (▲) in PBS solution (pH 7.4) at 37°C for 24 h. *, $p < 0.05$ compared to free drug; #, $p < 0.05$ compared to Con LP.

4.2.3 Short-term stability

The stability of liposomal formulations is important for the development of lipid-based nanocarriers. The aggregation or agglomeration between nanoparticles usually occurs when liposomes are stored for a long period, especially under very high temperatures. According to the ICH Q1A R2 “Stability study of drug product” contributed by the International Conference on Harmonisation organization [208], the liposomal products in this research were intended to be a group of refrigerated

pharmaceutical products. Parameters including vesicle size, surface charge, and relative drug remaining of 3A.1-encapsulated liposomes were monitored under two different storage conditions to find the optimal storage condition, and the findings are presented in Figure 36. After storage at 4°C for 6 months, there was no irreversible aggregation in either the 3A.1-loaded Con LP or the PEG LP. The vesicle size of the 3A.1-loaded Con LP and PEG LP did not grow significantly ($p < 0.05$) compared to their size on the first day, while the 3A.1-loaded Con LP and PEG LP had a slightly negative zeta potential of approximately -6 to -12 mV which was not different from the original values of -8 to -14 mV. Despite the low zeta potential of these liposomes representing weak electrostatic repulsion, it could confirm that they exhibited good particle dispersibility without particle growth, through dual repulsion of electrical force and steric hindrance of the PEG layer. Furthermore, the total drug remaining of the 3A.1-loaded Con LP and PEG LP was found to be $84.27 \pm 2.77\%$ and $89.13 \pm 1.53\%$, respectively, after 6-month storage. In contrast, white particle aggregation in both liposomes was seen after the liposomes were kept at 25°C for 6 months. The abnormal appearance may be caused by higher temperatures that may lead to the rapid movement of vesicles followed by vesicle's attraction and fusion [226,227]. The change of vesicle size was remarkable, which the size increased from 143.77 nm to 323.54 nm in the 3A.1-loaded Con LP and from 115.33 nm to 179.96 nm in the 3A.1-loaded PEG LP. The zeta potential of both liposomes was still a negative charge (-6 mV to -11 mV), which did not diverge from the first day after storage for 6 months. Unfortunately, the obvious decrease in the remaining drug of both selected liposomes was observed, which probably arose from drug degradation and drug leakage during this period at room temperature. Our findings suggested that storage of the 3A.1-loaded Con LP and PEG LP at a cold temperature could preserve the vesicle size, zeta potential, and amount of drug remaining for at least 6 months. This storage temperature below T_c of phospholipids helps maintain the rigidity of the lipid's bilayer (gel state) which results in a reduction of drug loss and degradation from external environments [149,150].

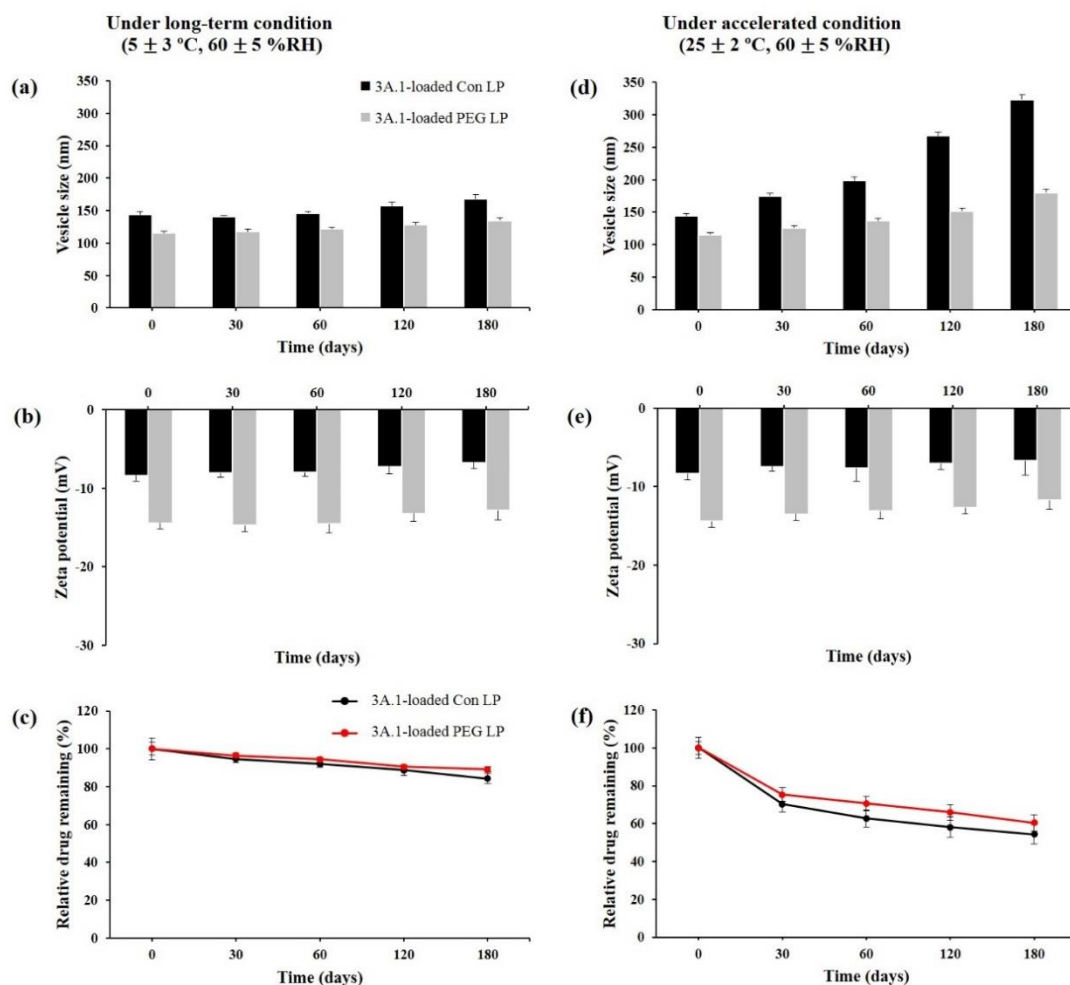


Figure 36 The short-term stability of 3A.1-loaded liposomes stored under long-term condition (left) compared to under accelerated condition (right) for 180 days: (a,d) vesicle size; (b,e) zeta potential of the 3A.1-loaded Con LP (black bar) and the 3A.1-loaded PEG LP (gray bar); (c,f) the relative drug remaining of the 3A.1-loaded Con LP (black line) and the 3A.1-loaded PEG LP (red line). All data are represented as the mean \pm standard deviation ($n=3$).

4.2.4 *In vitro* anticancer activity

The antitumor effect of the 3A.1-encapsulated liposomes on cell viability of HCT116 and HT29 was assessed using an MTT proliferation assay. The survival curves of cancer cells are represented in Figure 37 and half-maximal inhibitory concentration (IC_{50}) values are listed in Table 13. All treatment groups of varying drug concentrations showed a decrease in cell viability of both CRC cells in a dose-

dependent manner. Meanwhile, the cytotoxicity toward cancer cells was studied at two different times (24- and 48-h treatment). Additionally, the time-dependent manner of these treatments was also identified in this experiment. In other words, when cancer cells were exposed to the drug for a longer period, cell proliferation had a lower %cell viability. In detail, the cytotoxicity profiles indicated that both the 3A.1-loaded Con LP and PEG LP provided a stronger suppression of cancer cell growth than the free drug. As seen in Figure 37a and b, the maximum anticancer activity was found in the 3A.1-loaded PEG LP with the IC_{50} values of $1.599 \pm 0.076 \mu\text{g/mL}$ and $1.333 \pm 0.169 \mu\text{g/mL}$ after 24- and 48-h treatment, which was significantly lower than ($p < 0.05$) those of free drug (the IC_{50} values were $3.845 \pm 0.233 \mu\text{g/mL}$ and $2.439 \pm 0.134 \mu\text{g/mL}$ after 24- and 48-h incubation). The 3A.1-loaded Con LP had the IC_{50} values of $3.005 \pm 0.434 \mu\text{g/mL}$ and $1.548 \pm 0.231 \mu\text{g/mL}$, which were significantly lower than ($p < 0.05$) those of the free drug as well, but these values were significantly higher than ($p < 0.05$) that of PEG LP. We observed that the IC_{50} values of the 3A.1-loaded PEG LP after 24- and 48-h treatment were significantly lower than ($p < 0.05$) that of 3A.1-loaded Con LP and free drug (Figure 37c and d), implying that the 3A.1-loaded PEG LP had greater anticancer activity against HT29 cells. Concurrently, the blank Con LP and PEG LP exhibited no apparent sign of cytotoxicity, indicating that lipid content was not harmful to cells. Therefore, the anticancer activity of 3A.1 was well improved after being loaded into the liposomes.

- 1 **Table 13** The IC₅₀ values of free 3A.1, 3A.1-loaded Con LP and 3A.1-loaded 0.25-PEG LP against HCT116 and HT29 after 24- and 48-h
- 2 treatment were determined using GraphPad Prism 5.01 software. Each value was derived from three different experiments in sextuplicate
- 3 wells and reported as mean ± standard error of mean (n=3). *, p<0.05 compared with free 3A.1 group; #, p<0.05 compared with 3A.1-
- 4 loaded Con LP group.

Groups of treatment	IC ₅₀ (µg/mL) in HCT116 cell		IC ₅₀ (µg/mL) in HT29 cell		5
	24-h treatment	48-h treatment	24-h treatment	48-h treatment	
Free 3A.1	3.845 ± 0.233	2.439 ± 0.134	4.201 ± 0.185	2.207 ± 0.146	
3A.1-loaded Con LP	3.005 ± 0.434 *	1.548 ± 0.231 *	4.184 ± 0.474	2.096 ± 0.100	7
3A.1-loaded PEG LP	1.599 ± 0.076 *#	1.333 ± 0.169 *	1.610 ± 0.282 *#	1.362 ± 0.062 *#	

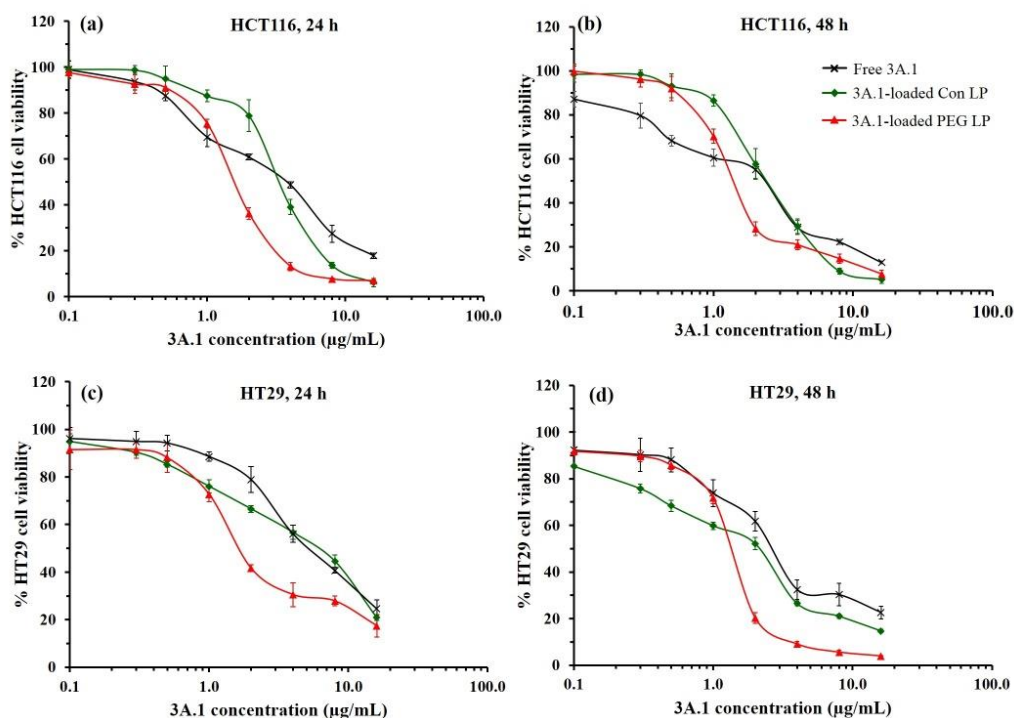


Figure 37 In vitro anticancer activity of 3A.1 solution (×), 3A.1-loaded Con LP (◆), and 3A.1-loaded PEG LP (▲) against HCT116 cell line for (a) 24 h and (b) 48 h and HT29 cell line for (c) 24 h and (d) 48 h. The data are shown as the mean ± standard deviation of three independent replicates.

4.2.5 Induction of cell apoptosis

To further explore whether the 3A.1 entrapped in liposomes could enhance the anticancer activity against HCT116 cells, the percentage of total apoptotic cell death was quantitatively detected by the double staining of Annexin V-FITC/PI followed by a flow cytometry analysis. Annexin V was used to specifically bind to phosphatidylserine (PS) as an apoptosis marker, which was translocated from the inner cell membrane to the surface's cell membrane at apoptotic phase, whereas PI was employed as a necrosis indicator penetrated the membrane of dead and damaged cell and bound double-stranded DNA in the nucleus. Thus, the result of dot-plot analysis provided 4 types of the cell including viable cells (lower left quarter, Annexin V⁻/PI⁻), early apoptotic cells (lower right quarter, Annexin V⁺/PI⁻), late apoptotic cells (upper right quarter, Annexin V⁺/PI⁺), and necrotic cells (upper left quarter, Annexin V⁻/PI⁺). Figure 38 shows that the living cells of the

control group accounted for at least 96%. Overall, the exposure of HCT116 cell to 3A.1 solution and the 3A.1-loaded liposomal formulations intensively induced cell death by both early and late apoptosis. The necrotic cell death found in each treatment was observed at a very low value (<2%), indicating that 3A.1 killed cancer cells without inflammable effect. The 3A.1-loaded Con LP displayed a higher level of cell apoptosis rate than the free 3A.1 ($11.61 \pm 1.92\%$) ($p>0.05$). Moreover, 3A.1-loaded PEG LP exhibited the highest percentage of cell apoptosis (20.95 ± 1.85%), especially late apoptosis, in HCT116 cell, which was significantly greater than that of the free 3A.1 as well ($p<0.05$). The possible explanation of this result was related to the artificial lipid membranes of liposomes having more biocompatibility, and easy to penetrate and uptake into cancer cells [21,228]. These results were consistent with the results of the *in vitro* cytotoxicity tests in section 4.2.4.

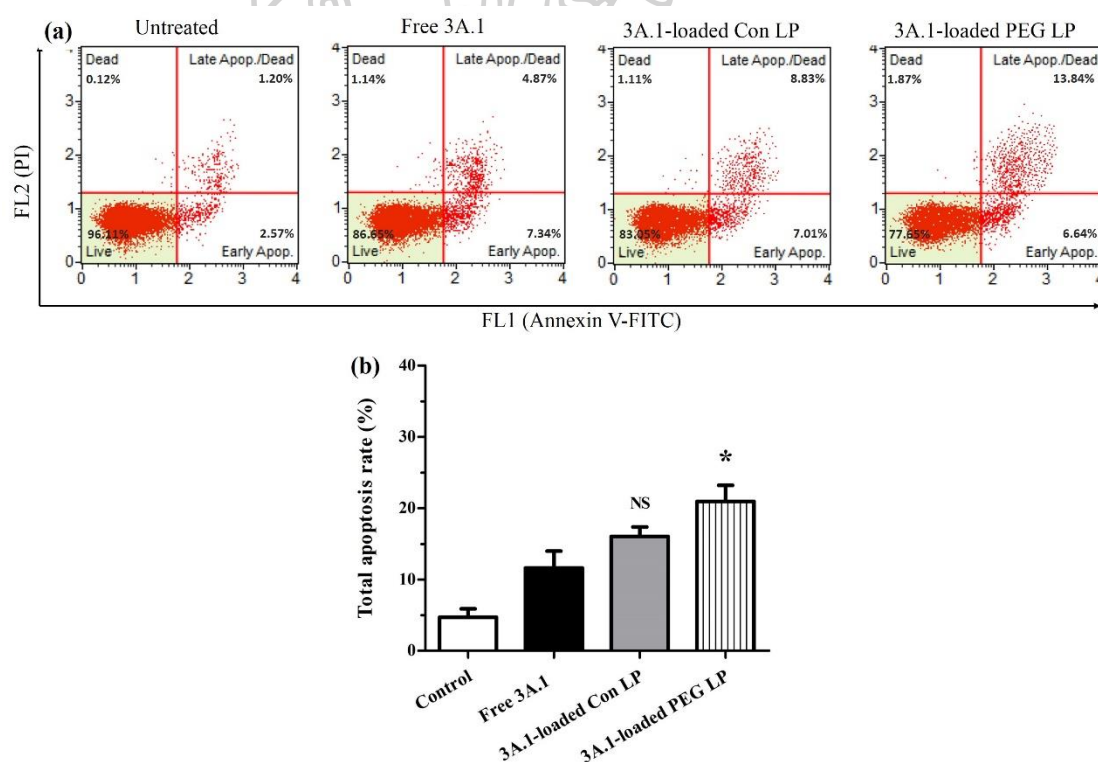


Figure 38 Apoptosis inductive effect of HCT116 cancer cells after treatment with free 3A.1 and 3A.1-loaded liposomes (at the equivalent 3A.1 concentration of 3.8 $\mu\text{g/mL}$) *in vitro*. (a) Flow cytometry analysis of dot plot in groups of control, free 3A.1, and 3A.1- encapsulated liposomes. (b) Percentage of cell apoptosis rate of

HCT116 cells after being exposed to free 3A.1 and 3A.1-loaded liposomes for 24-h treatment. *, $p < 0.05$ compared to free drug; NS, no statistically significant difference compared to free drug.

4.2.6 *In vitro* anti-migratory effect

4.2.6.1 Wound-healing assay

The anti-migratory activity of 3A.1 against HN22 as model cancer cells was examined using a wound-healing assay because of simple and convenient method without complicated instruments [229]. After 18-h observation, the cell-free zones of the HN22 monolayer were nearly fully closed (Figure 39a). As seen in the photographs of the wound gap, we observed that the wound areas of free drug and both 3A.1-loaded Con LP and PEG LP seemed to be larger than that of the control group after 18-h incubation, implying that this compound was inclined to reduce the cell motility. In this experiment, two parameters, cell migration rate and %wound closure, were quantitatively analyzed and reported in Figure 39b and c, respectively. The cells exposed to drug solution in 0.1% DMSO had a migration rate of $22.49 \pm 0.33 \mu\text{m/h}$ and a %wound closure of $83.37 \pm 2.15\%$, which did not augment the suppression of cell motility, compared to the control group showing a migration rate of $23.74 \pm 0.19 \mu\text{m/h}$ and a %wound closure of $85.52 \pm 0.92\%$ ($p > 0.05$). In comparison to free 3A.1, both 3A.1-entrapped liposomes significantly reduced the cell migration rate of HN22 cells and also decreased %wound closure ($p < 0.05$). Although free 3A.1 showed a mild capability in slowing down of cell motility, loading 3A.1 into the Con LP and PEG LP enhanced inhibition of cell movement in a horizontal direction, indicating that these 3A.1-loaded liposomes could be potentially used to reduce metastasis of oral cancer cells.

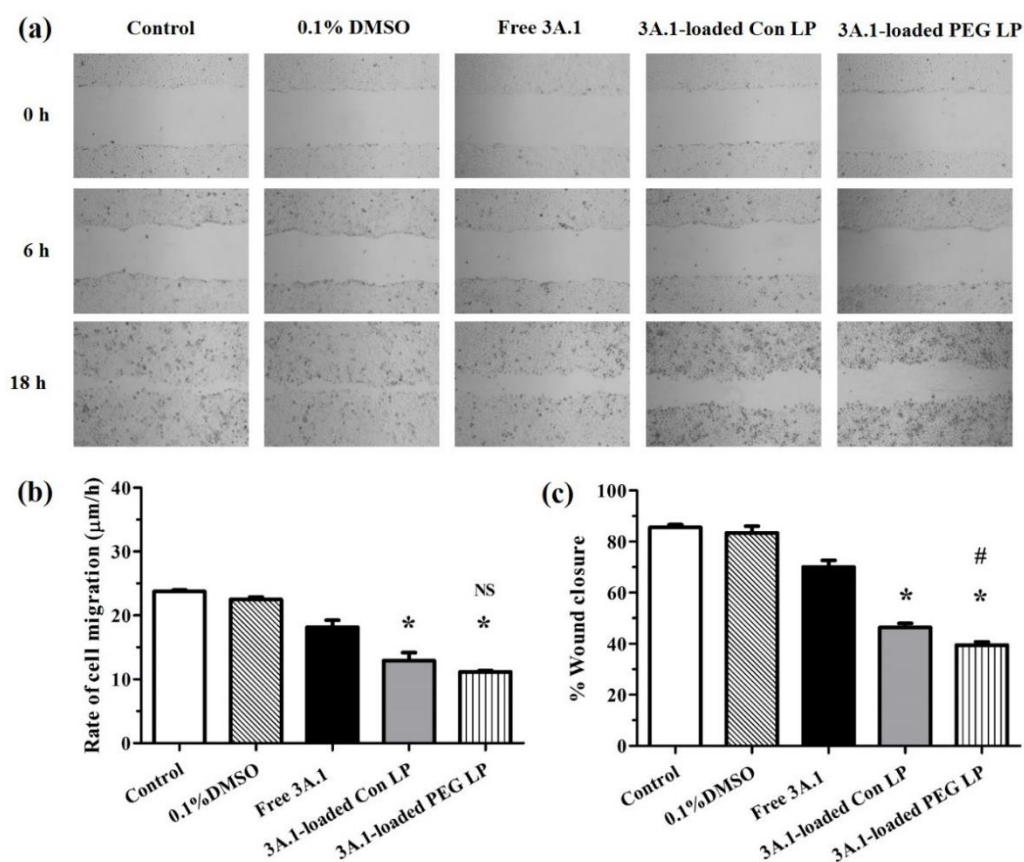


Figure 39 Inhibition effect of free 3A.1 and 3A.1-loaded liposomes on cell migration of HN22 cancer cells was measured by scratch assay. (a) Photographs of wound area captured by an inverted microscope (40 \times magnification) at 0, 6, and 18 h. (b) Cell migration rate and (c) %wound closure after 18-h treatment in each experimental group. *, $p < 0.05$ compared to free drug; #, $p < 0.05$ compared to Con LP; NS, no statistically significant difference, compared to Con LP.

4.2.6.2 Transwell migration assay

The cell migration of colorectal cancer (HCT116) in a vertical direction was further assessed using a transwell chamber migration [230]. The effect of 3A.1 in each treatment on the cell movement is illustrated in Figure 40. As seen in representative photographs of migrated cells under an inverted microscope (Figure 40a), it can be observed that the number of cancer cells penetrated through the membrane in the group of 3A.1 treatment (free drug and drug-loaded LP) was lower than that of the control which had more cell density. 0.1% w/v DMSO as a vehicle control showed

96.26 ± 3.36% of cell migration, compared with 100% of cell migration in the untreated group; thus, the use of this solvent to solubilize the drug did not affect the migration capacity. After quantitative data analysis (Figure 40b), the results demonstrated that relative %cell migration of the cell treated with the 3A.1-loaded Con LP and PEG LP was calculated to be 53.12 ± 1.22%, and 51.62 ± 1.62%, respectively, in which both liposome formulations could significantly suppress HCT116 cell motility greater than that suppressed by free 3A.1 ($p < 0.05$). Despite the inhibition of cell motility detected in different cancer cell lines, the results of transwell migration assay were in accordance with those of scratch assay, as mentioned above. These findings revealed that 3A.1 inhibited the migration capacity of cancer cells and this compound might be a potential anti-metastatic agent.

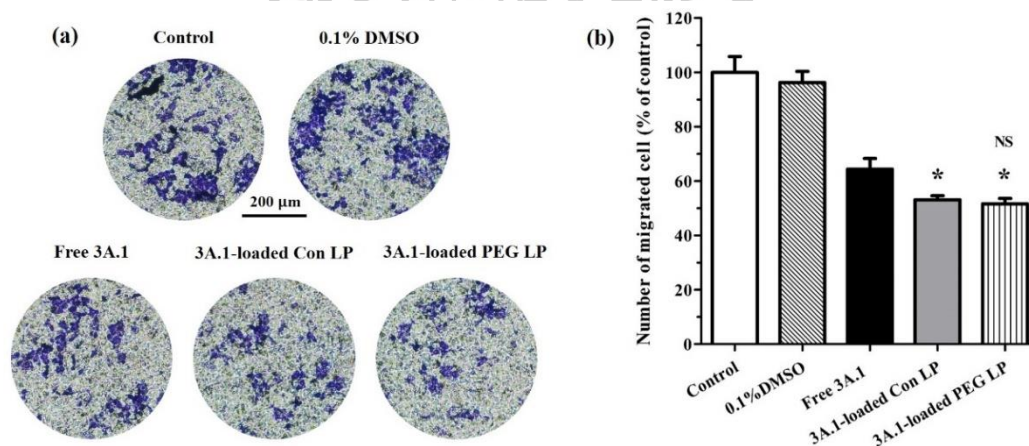


Figure 40 Anti-migratory effect of free 3A.1 and 3A.1-loaded liposomes on HCT116 cancer cells after 24-h incubation was investigated using a transwell migration assay. (a) Photographs of migrated cancer cells stained with the purple color of crystal violet in each treatment group under an inverted microscope. (b) The number of migrated cancer cells was counted and reported as the percentage of control. *Statistically significant difference ($p < 0.05$) compared to free drug; NS, no statistically significant difference compared to the Con LP.

4.3 Nanosuspensions with or without 3A.1 analogue

In this work, 3A.1 NS was successfully prepared by an anti-solvent precipitation method. When the drug solution in DMSO as a miscible organic solvent was dropped

into distilled water as an anti-solvent, the state of the drug changed from molecules to nanoparticles dispersed in an aqueous medium with the formation of drug nucleation. In the first trial test, we used amphiphilic chitosan (CS) derivatives - NSC, OSC, and BSC, as stabilizers to prepare drug NSs, compared with three stabilizers i.e. SDS, Tween[®] 80, and Poloxamer 188.

4.3.1 Effect of drug to polymer ratios and the hydrophobic parts of their polymers

The ratio of the drug to polymer needs to be optimized to find the appropriate NS formulations so that the specific drug molecule can be physically compatible with its stabilizer. The major problem of liquid NS is flocculation or crystal growth. This issue is relevant due to insufficient amounts or inappropriate types of stabilizers. It cannot completely cover the surface of drug nanoparticles, which is required to maintain repulsion between the particles in NSs. To prevent this undesirable problem, the stabilizers, which have a principal role, are divided into 2 main groups (polymers and surfactants). The addition of non-ionic stabilizers creates a steric barrier while the addition of ionic stabilizers into NSs causes an electrostatic repulsion. These barriers are responsible for the protection of particle aggregation and maintaining low PDI in formulations [41,175,184]. Our research investigated the effect of different stabilizers, based on amphiphilic chitosan derivatives and their stabilizer concentrations, relevant to the drug quantity on the physicochemical properties, including particle size, zeta potential, and drug content, with results shown in Table 14.

4.3.1.1 Particle size and zeta potential

The results revealed that the 3A.1 coarse suspension, without any stabilizers prepared by an anti-solvent precipitation method, had a mean particle size larger than 1 μm and a PDI value of approximately 1.0, whereas three 3A.1 NS stabilized by NSC, OSC, and BSC, at a various drug to polymer ratios, presented a mean particle size smaller than 500 nm, indicating that these CS copolymers had an important role in reducing drug particles into a nanometer-scale during the formulation process. Among these copolymers, it was found that NSC, which was used as a stabilizer in 3A.1 NS, provided

the smallest particle size (153.37 ± 1.11 to 188.23 ± 1.47 nm) and the narrowest size distribution (0.085-0.173) when compared with other copolymers at the same drug to polymer ratio. Meanwhile, the particle size and PDI values of 3A.1 NS-BSC and NS-OSC were found to be 221.77 ± 3.31 to 289.10 ± 4.10 nm, 0.187 to 0.232, and 226.37 ± 3.63 to 400.80 ± 50.23 nm, 0.221 to 0.520, respectively. Generally, NSs with suitable electric stability should have a minimum zeta potential of 30 mV [231,232]. In this experiment, the zeta potentials of all 3A.1 NS were found to be a negative surface charge of at least -30 mV. The negative charge of nanoparticles has arisen from CS derivatives grafted with succinic acid adsorbed on the 3A.1, leading to repulsion between each other and creating an electrostatic force. When succinic moieties, which have a pK_a value of approximately 4.21 and 5.64 at 25°C [212], were ionized in the aqueous solvent that has a pH value of 6-7, this resulted in numerous anions from $-\text{COOH}$ being adsorbed on surface nanoparticles. Moreover, amphiphilic CS polymers provided a steric effect from different grafted hydrophobic groups on the CS polymer as follows: naphthyl (double aromatic ring) in NSC, octyl group (linear chain) in OSC, and benzyl (single aromatic ring) in BSC. The dual stabilizer action, including the electrostatic and steric repelling force, resulted in the reduction and prevention of particle aggregation. It should be noted that not only the type of amphiphilic CS derivatives but also the drug to polymer ratio could affect the formulation's physicochemical properties. Therefore, we have preferred NS formulations with the drug to polymer ratio at 1.5:1 (w/w) and optimal physicochemical properties for additional tests.

Table 14 The influence of drug to stabilizers ratios on the particle size, PDI, and zeta potential of 3A.1 nanosuspensions prepared by a nanoprecipitation method. All data represent the mean \pm standard deviation (n=3).

3A.1 to stabilizer	NSC			OSC			BSC		
	Size (nm)	PDI	ζ (mV)	Size (nm)	PDI	ζ (mV)	Size (nm)	PDI	ζ (mV)
0.8 : 1	153.37 \pm	0.091	(-) 30.77 \pm	400.80 \pm	0.520	(-) 25.13 \pm	221.77 \pm	0.220	(-) 32.27 \pm
	1.11		0.98	50.23		0.69	3.31		1.18
1 : 1	177.33 \pm	0.173	(-) 32.83 \pm	226.37 \pm	0.320	(-) 39.40 \pm	289.10 \pm	0.232	(-) 33.23 \pm
	1.35		0.54	3.63		0.33	4.10		0.37
1.5 : 1	185.80 \pm	0.098	(-) 32.00 \pm	232.77 \pm	0.221	(-) 38.77 \pm	278.37 \pm	0.187	(-) 33.43 \pm
	1.14		0.08	2.83		1.01	2.13		0.52
2 : 1	188.23 \pm	0.085	(-) 32.17 \pm	342.77 \pm	0.471	(-) 32.17 \pm	266.80 \pm	0.205	(-) 31.70 \pm
	1.47		0.90	31.37		0.75	4.93		0.50
No polymer	~ 2000 nm	0.980	(-) 21.60 \pm						
			2.52						

3

4

4.3.1.2 Drug content

Furthermore, we studied the effect of the drug to polymer ratios and hydrophobic parts of polymer (naphthyl, octyl, and benzyl groups) on drug content in terms of the 3A.1 concentration and percentage of the 3A.1 yield as presented in Figure 41a and b. The results displayed that the drug to polymer ratio seemed to be directly correlated to the drug content. An increase in the drug to polymer ratio led to an increase in the 3A.1 concentration and %yield, except in 3A.1 NS-OSC that had a lower drug content at the maximum ratio. This result can be explained that the hydrophobic naphthyl, benzyl, and octyl groups that were adsorbed on the drug's surface could interact with the hydrophobic drug through the hydrophobic interaction at different force levels. Overall, the rank of the drug content was 3A.1 NS-NSC > NS-BSC > NS-OSC. The 3A.1 NS-NSC prepared at the drug to polymer ratio of 1.5:1 expressed the highest value of %yield ($82.21 \pm 5.87\%$), compared to other NS formulations. This finding suggested that the NSC polymer containing the double aromatic ring of naphthyl groups was the appropriate stabilizer for the production of 3A.1 NS at the ratio of 1.5:1 (w/w).

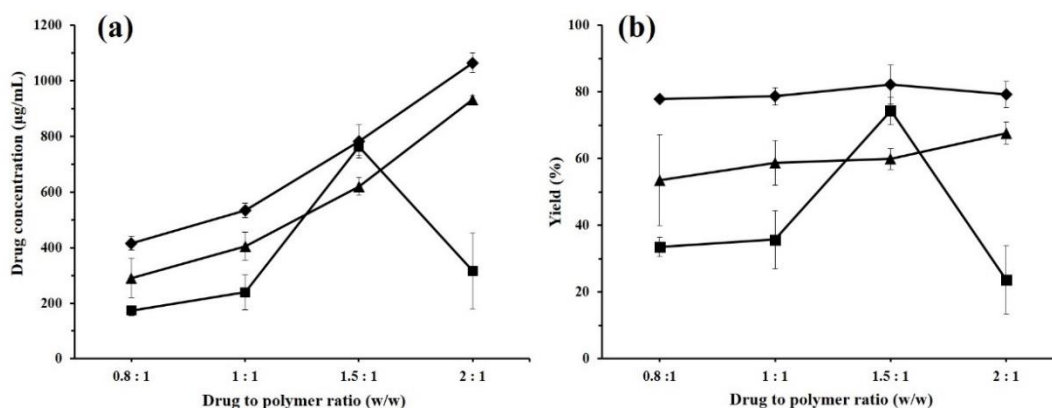


Figure 41 Effects of the drug to stabilizer weight ratios on (a) 3A.1 concentration and (b) percentage yield of 3A.1 NSs stabilized by NSC (◆), OSC (■), and BSC (▲). Data are represented as the mean \pm standard deviation (n=3).

4.3.1.3 Visual appearance

During a visual inspection, it was found that the 3A.1 NS with a slightly turbid liquid was homogeneously suspended into the water without any drug crystals formation (Figure 42b-d). Meanwhile, the coarse 3A.1 suspension containing an equivalent drug amount was completely insoluble in water and precipitated at the bottom of the bottle (Figure 42a). Overall, the pH of these 3A.1 NS was in the ranges of 5.3-5.6, representing slightly acidic solution.

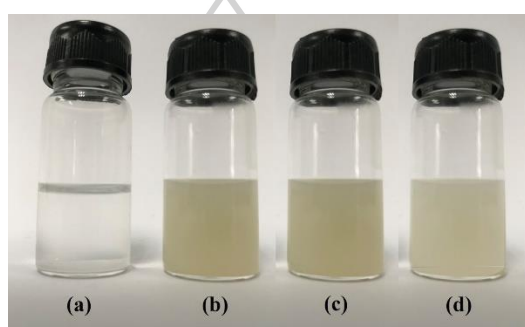


Figure 42 The appearance of (a) 3A.1 coarse suspension without stabilizer and 3A.1 nanosuspensions stabilized by CS derivatives; (b) NSC, (c) OSC, and (d) BSC at a drug to polymer ratio of 1.5:1 (w/w)

4.3.2 Comparison of the use of chitosan derivatives and surfactants

In this study, three surfactants, including SDS (anionic surfactant), Tween[®] 80 (non-ionic surfactant), and Poloxamer 188 (amphiphilic surfactant), were chosen to prepare NS formulations because of their low cost and widespread use in marketed nanosuspension products, compared with new CS derivative stabilizers with the same drug to stabilizer ratio of 1.5:1 (w/w). In comparison with the 3A.1 NS stabilized by CS derivatives, the particle size of 3A.1 NS stabilized by SDS, Tween[®] 80, and Poloxamer 188 was found to be 227.23 ± 2.24 , 1059.73 ± 152.36 , and 510.10 ± 152.52 nm with PDI values of 0.512, 0.902, and 0.527, respectively. Although the particle size of 3A.1 NS stabilized by SDS and Poloxamer 188 seemed to be in the nanometer scale, their sizes were quite broad distribution. The zeta potential of the 3A.1 NS stabilized by surfactants was ranked as the 3A.1 NS-Poloxamer 188 (-3.0 ± 0.87 mV) > 3A.1 NS-SDS (-23.33 ± 0.99

mV) > 3A.1 NS-Tween[®] 80 (-24.57 ± 0.70 mV). These surface charge values would not be enough to protect particle growth. In addition, the drug content, in terms of %yield of 3A.1 NS stabilized by SDS, Tween[®] 80, and Poloxamer 188 was $43.63 \pm 2.71\%$, $46.15 \pm 1.49\%$, and $5.43 \pm 0.33\%$, respectively. The low drug content revealed that the three surfactants were not good stabilizers for the preparation of the 3A.1 NS. In other words, the CS derivative stabilizers, especially NSC copolymer, could make the 3A.1 NS to produce suitable physicochemical properties.

4.3.3 Reconstitution test

Lyophilization is a well-known process that does not depend on high temperatures to transform a liquid sample into a dried solid sample. The main reason for the addition of cryoprotectant, especially a polyalcohol sugar, into the freshly prepared NS is to shield the particle agglomeration or crystal growth and provide the particle size in nanoscale during the drying process. Mannitol with the concentration at 5% w/v was selected as a cryoprotectant for drug NSs. The characteristics of the lyophilized 3A.1 NS with and without mannitol are summarized in Table 15. Overall, the feature of all the 3A.1 NS was completely dried powder and the 3A.1 NS with mannitol was fine and white powder, which is similar to mannitol, while the 3A.1 NS without mannitol was bulky and yellow-brown. After redispersion in aqueous to make the original liquid form, it was found that all lyophilized powder could be reconstituted within a few minutes. The mean particle size of the lyophilized 3A.1 NS with mannitol was smaller than and a PDI value of 3A.1 NS with mannitol was also lower than those without mannitol. This indicated that the mannitol had an important function in maintaining the particle size in the nanometer scale with narrow size distribution and kept the original size, compared to that of freshly prepared NSs. The zeta potential of the redispersed 3A.1 NS with mannitol was a negative surface charge with a range of (-) 30.17 ± 1.24 to (-) 32.40 ± 1.40 mV. Meanwhile, the zeta potential of the redispersed 3A.1 NS without mannitol was not different from formulations that added mannitol. This result revealed that this value provided an optimal electrostatic force for the

stability of 3A.1 NS and this cryoprotectant did not affect the charge on surface nanoparticles.

4.3.4 Morphological analysis

The morphologies of the liquid 3A.1 NS stabilized by CS copolymers were observed by a transmission electron microscope (TEM). As illustrated in Figure 43a–c, all NS samples had a round shape and a smooth surface. The particle size of 3A.1 NS measured by the TEM was in the range of 180–300 nm, which conformed to the results determined by a dynamic light scattering (DLS) technique. The SEM photographs of the 3A.1 coarse powder and freeze-dried 3A.1 NS are shown in Figure 43d and e. There were differences in the particle size and shape, the coarse drug had an angular shape with flake and flat sheet and its size was larger than 100 μm ; whereas, the size of the freeze-dried 3A.1 NS was smaller than the bulk drug and looked like fine particles with a regular shape. The drug nanoparticles with size < 200 nm were valuable to highly efficient reach and accumulate drug in tumor tissue through enhanced permeability and retention effect (EPR) [214,233].

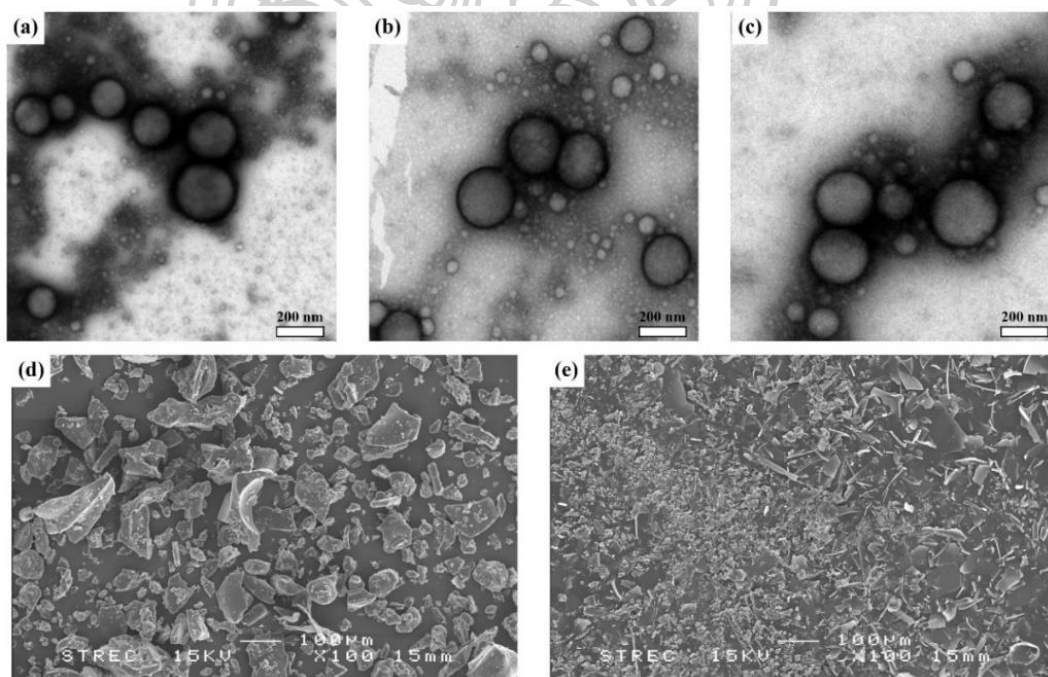


Figure 43 TEM images of nanosuspensions with a drug to polymer ratio of 1.5: 1 (w/w) prepared by a nanoprecipitation method: (a) 3A.1 NS-NSC, (b) 3A.1 NS-

OSC and (c) 3A.1 NS-BSC. SEM images of (d) 3A.1 coarse powder and (e) freeze-dried 3A.1 NS-NSC powder.

4.3.5 DSC

DSC was performed to analyze any changes in the physical state of solid samples. According to the DSC thermograms in Figure 44a, surprisingly, the 3A.1 coarse powder presented no sharp endothermic peak throughout the observed temperature, indicating that this drug had a naturally arranged structure in the amorphous state. In the pure CS copolymers, their thermograms did not appear at any peak. The lack of endothermic drug peaks in the physical mixture and the freeze-dried 3A.1 NS revealed that there were not any drug crystals or materials. These patterns of thermograms could not determine the endothermic melting point of the drug powder and the drug NSs.

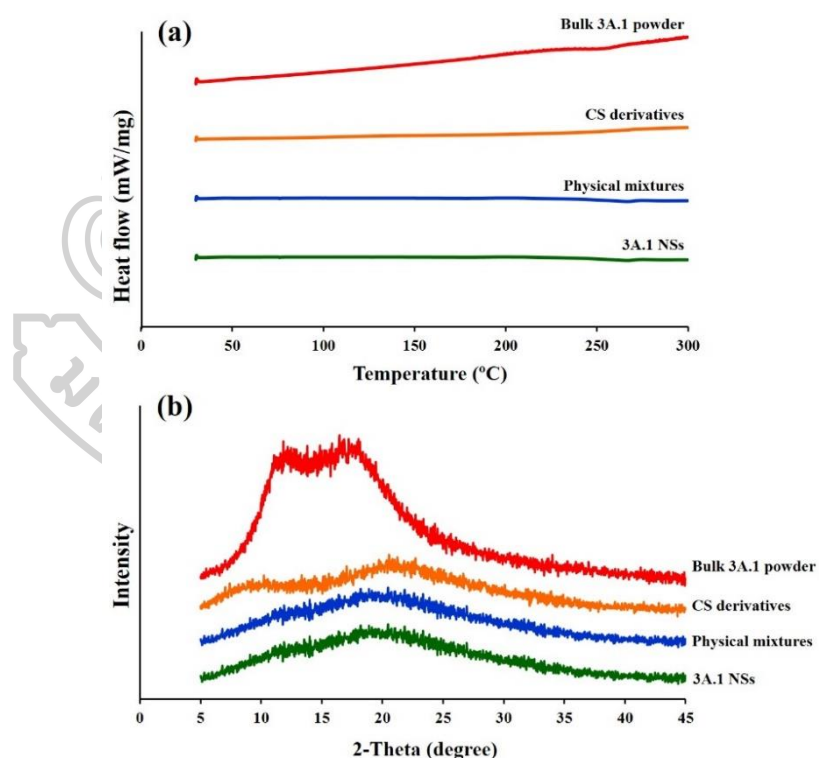








Figure 44 (a) Differential scanning calorimetry (DSC) patterns and (b) X-ray diffraction (XRD) patterns of bulk 3A.1 powder, excipient of CS derivatives, physical mixtures of 3A.1/CS derivatives, and lyophilized 3A.1 NSs (1.5:1, w/w)

1 **Table 15** The properties of 3A.1 nanosuspensions with and without cryoprotectant after the process of lyophilization.

3A.1 to stabilizer weight ratio	NS-NSC		NS-OSC		NS-BSC	
	with mannitol	without mannitol	with mannitol	without mannitol	with mannitol	without mannitol
Appearance						
Particle size (nm)	188.20 ± 2.48	279.80 ± 6.02	338.50 ± 6.23	463.90 ± 96.61	323.60 ± 1.99	786.93 ± 90.61
PDI	0.181	0.318	0.511	0.630	0.332	0.893
Zeta potential (mV)	(-) 30.43 ± 1.83	(-) 30.47 ± 0.17	(-) 30.17 ± 1.24	(-) 28.47 ± 1.13	(-) 32.40 ± 1.40	(-) 31.93 ± 1.32

2

3

4

5

6

4.3.6 PXRD

To confirm the crystallinity of the 3A.1 coarse powder and the freeze-dried 3A.1 NS, XRD spectra are shown in Figure 44b. The XRD curve of the 3A.1 powder did not have the characteristic, high-intensity peaks, which implied that this drug was molecularly organized in an amorphous structure. In comparison to drug powder's XRD spectrum, the CS copolymers, physical mixtures, and freeze-dried 3A.1 NS showed the same pattern without high-intensity peaks, indicating that they were all of a non-crystal substance. Therefore, the DSC and XRD results confirmed that the freeze-dried 3A.1 NS presented an inner structure in an amorphous status. This might be suitable to enhance aqueous stability [234].

4.3.7 FT-IR

As shown in Figure 45, the FTIR spectra of the coarse 3A.1 and the 3A.1 NS were analyzed as to the interaction between drug and excipients. As per comparable literature, the main structure of andrographolide had characteristic absorption peaks at 3423 cm^{-1} (O-H stretching), 2932 & 2857 cm^{-1} (C-H stretching), 1757 cm^{-1} (C=O stretching of lactone ring), 1472 & 1428 cm^{-1} (C=C stretching), 1185 cm^{-1} (C-O-C of lactone ring), and 1049 cm^{-1} (C-O stretching of alcohol) [235]. In addition, diphenylsilyl that was attached to the 3A.1 structure showed corresponding peaks of its chemical group at 742 & 703 cm^{-1} [236]. The FTIR spectra of the physical mixtures and the 3A.1 NS still presented absorption peaks similar to the 3A.1, indicating that the chemical structure of the drug compound did not change. Moreover, there was not any new peak presenting in the FTIR spectrum of the 3A.1 NS; therefore, the 3A.1 was compatible with these stabilizers.

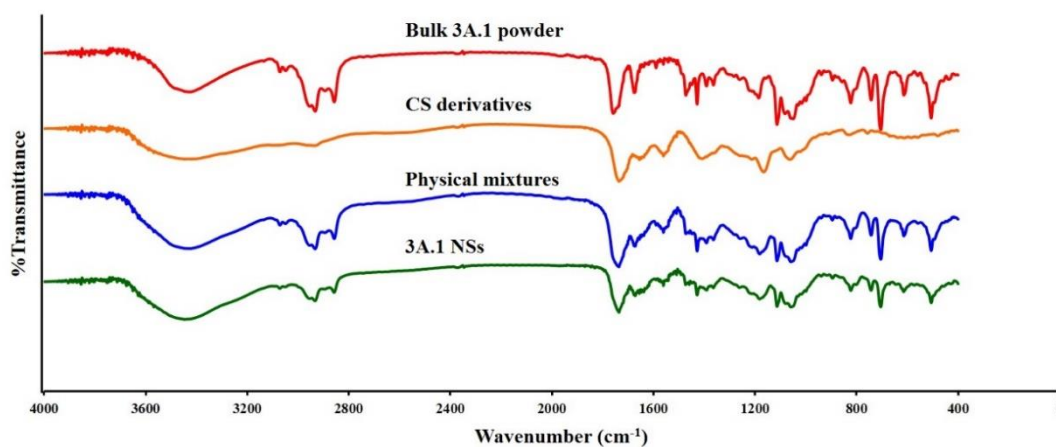


Figure 45 Fourier transform infrared spectra of bulk 3A.1 powder, excipient of CS derivatives, physical mixtures of 3A.1/CS derivatives, and lyophilized 3A.1 NSs (1.5:1, w/w)

4.3.8 Solubility

The parent andrographolide has been reported that it has poor water solubility ($\sim 46 \mu\text{g/mL}$ in water at 25°C) [237,238]. Meanwhile, the results of the solubility test of the coarse 3A.1 and 3A.1 NSs are presented in Figure 46. The results showed that bulk 3A.1 as a poorly water-soluble compound, cannot solubilize in many types of aqueous medium with a solubility of less than $1.0 \mu\text{g/mL}$ at 37°C and it could not any detect the amount of 3A.1 by an HPLC analysis. After preparing 3A.1 into nanosuspension formulations, we found that three 3A.1 NSs (NS-NSC, NS-OSC, and NS-BSC) had improved aqueous solubility in distilled water and buffer solution in the range of 17.34 to $30.49 \mu\text{g/mL}$ at 37°C . This study revealed that the preparation of 3A.1 NSs stabilized by CS derivatives led to an increase in 3A.1 aqueous solubility, probably due to the reduced diameter of the particle in the nanometer scale with high surface area and high wetting ability [177].

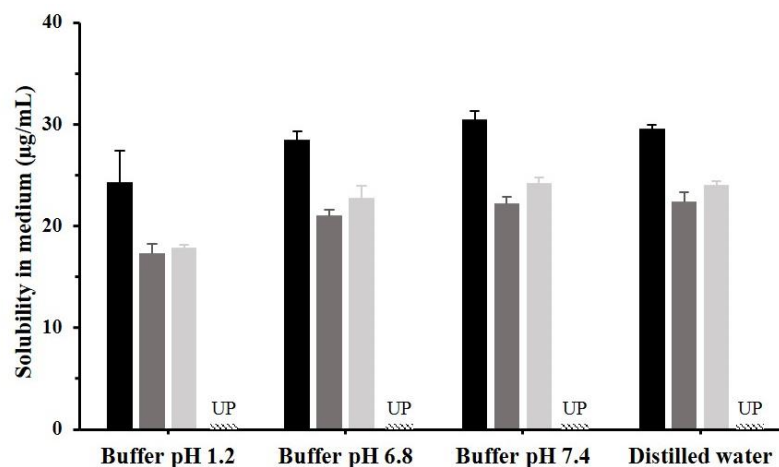


Figure 46 Solubility data of bulk 3A.1 (striped bar) and 3A.1 NSs stabilized by NSC (black bar), OSC (dark gray bar), and BSC (light gray bar) in various types of solvent. All bar graphs are presented as the mean \pm standard deviation ($n=3$). UP, undetectable peak of 3A.1 in HPLC chromatogram.

4.3.9 Short-term stability

It is well-known that the main instability issue of NS formulations is associated with particle growth and flocculation [184-186]. The particle size, PDI, and zeta potential of the 3A.1 NS (NSC, OSC, and BSC) were used as optimal indicators to evaluate the physical stability of liquid NS (Figure 47). The stability of the 3A.1 NS was detected under two conditions as described in the ICH guideline Q1A R2, an accelerated storage testing at $25 \pm 2^\circ\text{C}/ 60 \pm 5\% \text{RH}$ and a long-term storage testing at $5 \pm 3^\circ\text{C}/ 60 \pm 5\% \text{RH}$, for 6 months [208]. During the storage period, the appearance of liquid 3A.1 NS did not change and was not tightly aggregated. The drug nanoparticles were well suspended in the aqueous medium in each formulation. Overall, the particle size of three 3A.1 NS formulations was not higher than $1 \mu\text{m}$ after 6 months of being stored in a refrigerator and room temperature. The particle size of the 3A.1 NS, which was kept in the refrigerator, did not change from the original value for 6 months, suggesting that the three 3A.1 NS were physically stable for at least 6 months. In contrast, the particle size of the 3A.1 NS, which was stored at room temperature, significantly increased compared with its starting date. The highest change in particle size was the 3A.1 NS-OSC formulation which increased from 232.77 ± 2.83 to 544.23 ± 55.50 nm with wider

size distribution. The zeta potential of the 3A.1 NS, which was kept in the refrigerator, slightly decreased and its negative charge values were approximately -30 mV, which was adequate to stabilize each nanoparticle in the formulation. However, the zeta potential of the 3A.1 NS, which was stored at room temperature, decreased when values were lower than -30 mV; especially, in the 3A.1 NS-OSC which had the lowest zeta potential at -26 mV. As previously stated, the different storage temperatures for NS greatly affected the particle size and surface charge of NS formulations. This particle growth phenomenon was mainly caused by Oswald ripening, which explains that NS are thermodynamically unstable colloidal systems, and high surface area of nanoparticles with high surface energy would try to aggregate for reducing the Gibbs free energy during storage. The higher temperature of the NS system increased the rate of particle aggregation [239,240]. After 6 months of storage, the remaining content of 3A.1 in NS-NSC, NS-OSC, and NS-BSC kept at refrigerator was 75.29 ± 0.77 , 62.84 ± 6.20 , and $54.34 \pm 6.95\%$, respectively; whereas, these NS formulations stored at room temperature were 69.92 ± 1.46 , 59.56 ± 4.49 , and $51.68 \pm 4.22\%$, respectively. This result showed that storage 3A.1 NS in the refrigerator resulted in higher chemical stability than those at room temperature. The 3A.1 NS-NSC had the highest percentage of remaining content most likely because the naphthyl groups could be adsorbed on drug surfaces through hydrophobic interaction, resulting in the stabilization of drug nanoparticles in NS. Therefore, 3A.1 NS should be stored in the refrigerator to keep physical properties and drug content. In this experiment, the 3A.1 NS-NSC had the best formulation that provided physical and chemical stability with a shelf-life of at least 6 months in the refrigerator.

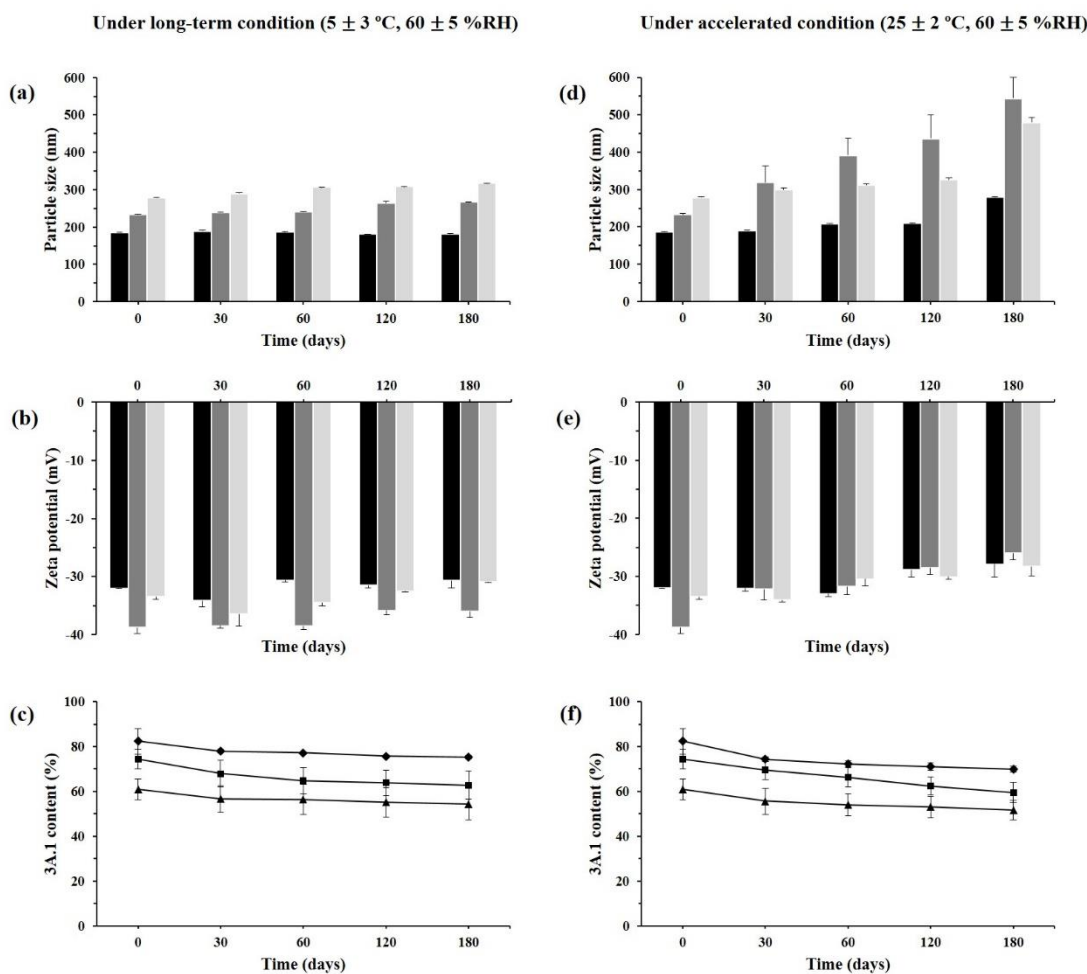


Figure 47 The short-term stability of 3A.1 nanosuspensions stored under long-term condition (left) compared to under-accelerated condition (right) for 6 months; (a,d) particle size; (b,e) zeta potential of 3A.1 NS-NSC (black bar), NS-OSC (gray bar) and NS-BSC (light gray bar); (c,f) the drug remaining of 3A.1 NS-NSC (◆), NS-OSC (■) and NS-BSC (▲). All data are expressed as the mean \pm standard deviation (n=3).

4.3.10 *In vitro* anticancer activity

The cytotoxicity of the 3A.1 NS was compared to the drug solution and evaluated using an MTT colorimetric method. HCT116 (human colorectal cancer cells) were exposed with various 3A.1 concentrations and the results of the cell viability curves are presented in Figure 48. The 3A.1 solution and three formulations of 3A.1 NS were found to efficiently inhibit the growth of tumor cells in a dose-dependent pattern. According to the IC_{50} values for 24-h treatment, the

IC₅₀ value of the 3A.1 NS-NSC, NS-OSC, and NS-BSC were 0.676 ± 0.022 , 1.013 ± 0.020 , and 1.143 ± 0.011 $\mu\text{g/mL}$, respectively. It was found that the 3A.1 NS-NSC had the strongest anticancer effect, compared to the 3A.1 solution (3.845 ± 0.233 $\mu\text{g/mL}$; $p < 0.05$). When the incubation time of both free 3A.1 and 3A.1 NS was extended from 24 h to 48 h, the IC₅₀ values had lower, indicating the time-dependent manner of these treatments (Table 16). The much higher cytotoxicity of the 3A.1 NS might be attributed to the presence of the small diameter and the large surface area of the nanoparticles that were nonspecifically adsorbed on the cell surface and highly internalized into tumor cells via endocytosis pathway [241]. Meanwhile, the cytotoxicity of polymers alone (NSC, OSC, and BSC; negative control) was also tested with the same procedure. It was shown that all of the cells had cell viability of over 95% after 24-h incubation period with an equal concentration of polymer used in NS formulations. This meant that these chitosan derivatives, acting as a stabilizer and used in formulation, had little influence on cell growth inhibition. Therefore, they can be safe and compatible excipient.

Table 16 The IC₅₀ values of free 3A.1 and 3A.1 nanosuspensions against HCT116 after 24- and 48-h treatment were determined using GraphPad Prism 5.01 software. Each value was derived from three different experiments in sextuplicate wells and reported as mean \pm standard error of mean (n=3). *, $p < 0.05$ compared with free 3A.1 group.

Groups of treatment	IC ₅₀ ($\mu\text{g/mL}$) in HCT116 cell	
	24-h treatment	48-h treatment
Free 3A.1	3.845 ± 0.233	2.439 ± 0.134
3A.1 NS-NSC	0.676 ± 0.022 *	0.567 ± 0.013 *
3A.1 NS-OSC	1.013 ± 0.020 *	0.653 ± 0.010 *
3A.1 NS-BSC	1.143 ± 0.011 *	0.615 ± 0.009 *

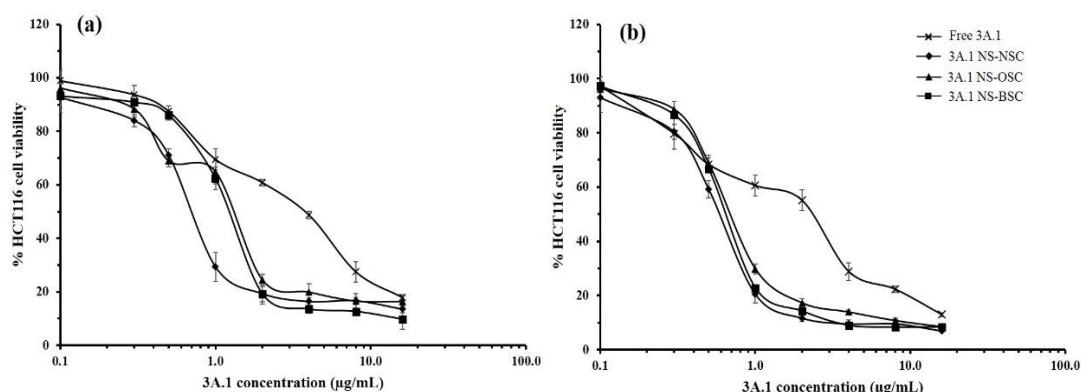


Figure 48 In vitro anticancer activity of 3A.1 solution (×) and 3A.1 NS-NSC (◆), NS-OSC (■), and NS-BSC (▲) against HCT116 cell line for (a) 24 h and (b) 48 h. The data are shown as the mean \pm standard deviation of three independent replicates.

4.3.11 *In vivo* anticancer efficacy

4.3.11.1 Establishment of HCT116 tumor-bearing nude mice

In the first step, we attempted to inoculate the HCT116 cancer cells into athymic nude mice by s.c. injection of different cell densities. As shown in Figure 49, the tumor growth curves revealed that the cell density of 5×10^6 cells/mouse expressed an optimal tumor volume against the observation time. Meanwhile, the cell density of 1×10^6 cells/mouse cannot induce the tumor mass on the lower back's mice and the cell density of 10×10^6 cells/mouse showed very rapid tumor growth within 4 weeks. No significant loss of body weight was found in all nude mice. Therefore, we selected the HCT116 cell density of 5×10^6 cells/mouse for generating the tumor mass in all xenograft nude mice to assess *in vivo* antitumor efficacy [242].

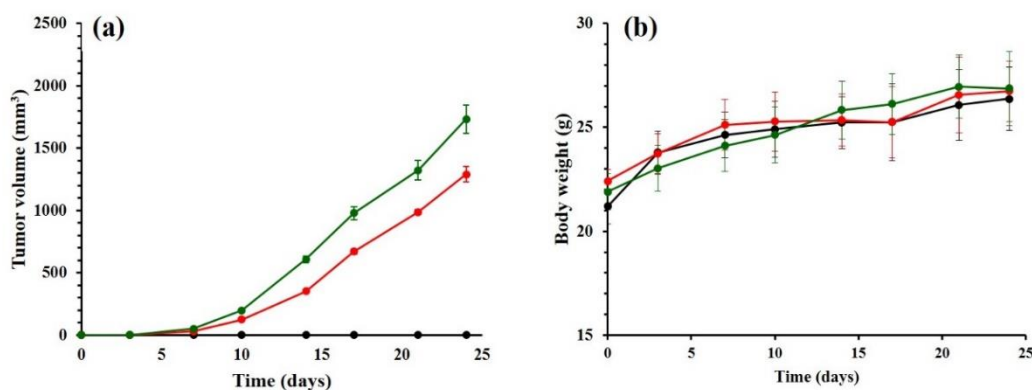


Figure 49 Establishment of CRC xenograft nude mice. (a) Tumor growth curves of the subcutaneous HCT116 tumor-bearing mice with initial cell density of 1 million (black line), 5 million (red line), and 10 million (green line). (b) Body weight of mice over observation time. The data are represented mean \pm standard deviation ($n = 2$).

4.3.11.2 *In vivo* antitumor efficacy of drug NSs

After verifying *in vitro* antitumor activity of the free 3A.1 and 3A.1 NS, we consecutively investigated whether the anticancer activity of this compound could inhibit tumor growth *in vivo*. The *in vivo* antitumor efficacy of the 3A.1 solution and 3A.1 NS was tested on an animal model. Xenograft nude mice were subcutaneously inoculated on the right flank of mice by injection of HCT116 cancer cells. After the tumor volume reached 100-150 mm³, all groups of HCT116 tumor-bearing mice were administered via i.p. with 3A.1 solution and 3A.1 NS for almost 3 weeks with a total of six doses (Figure 19). The positive control group received 30 mg/kg of 5-FU solution intraperitoneally as standard chemotherapy [243]. The tumor growth profiles and body mice weight in each treatment are displayed in Figure 50. The tumor volume in the groups of vehicle and blank NS were similar, rapidly grew to ~ 2000 mm³ within 28 days post-tumor cell inoculation. This implied that the used polymer as a stabilizer in nanosuspension formulation did not affect the tumor growth rate of HCT116 in mice throughout the observation time. In this study, dosing of 3A.1 was performed at 2 levels (low dose at 20 mg/kg and high dose at 40

mg/kg of body weight). It was observed that the low dose of 3A.1 solution cannot inhibit tumor growth of HCT116 in nude mice. Although the 3A.1 was prepared into 3A.1 NS, it still had no effect on tumor growth suppression. In comparison to the low dose of 3A.1 solution, the high dose of 3A.1 solution tends to inhibit tumor growth of HCT116 in nude mice. When the 3A.1 was transformed into 3A.1 NS, it showed higher anticancer efficacy with lower mean tumor volume. This indicated that the high dose of 3A.1 at 40 mg/kg could provide the effective inhibition of tumor growth in HCT116 xenograft nude mice. The mean tumor volume on the end of treatment of 3A.1 solution at the high dose and 5-FU solution were $1219.34 \pm 107.85 \text{ mm}^3$ and $1367.28 \pm 100.04 \text{ mm}^3$, respectively, which were significantly smaller ($p < 0.05$) as compared to the vehicle group ($2045.24 \pm 151.66 \text{ mm}^3$) and blank NS ($2021.38 \pm 153.01 \text{ mm}^3$). There is no significant difference in mean tumor volume between a high dose of 3A.1 solution and 3A.1 NS, indicating that the 3A.1 NS remains its anticancer efficacy against the growth of HCT116 tumor. Based on the percentage of tumor growth inhibition (%TGI), the high dose of 3A.1 NS had the highest growth inhibitory capacity (46.64%), followed by high dose of 3A.1 solution (40.38%) and 5-FU solution (33.15%). On the other hand, the %TGI of low dose of 3A.1 solution and low dose of 3A.1 NS was less than 15%, which slightly higher than the vehicle group. The representative tumor mass in each group is presented in Figure 50c. We can observe that the tumor size in the group treated with the high dose of 3A.1 NS was the smallest but did not differ from high dose of 3A.1 solution and 5-FU solution. The tumor mass of both low doses of 3A.1 solution and 3A.1 NS was as big as the group of the vehicle and blank NS. Overall, the high dose of 3A.1 NS can inhibit tumor growth rate slightly better than high dose of 3A.1 solution. Furthermore, there was no significant body weight loss observed in the group of 3A.1 NS and 3A.1 solution, indicating that i.p injection of 3A.1 formulation might not be harmful in nude mice. The *in vivo* study indicated that the i.p injection of 3A.1 NS at high dose inhibited CRC tumor growth in HCT116 xenograft nude mice.

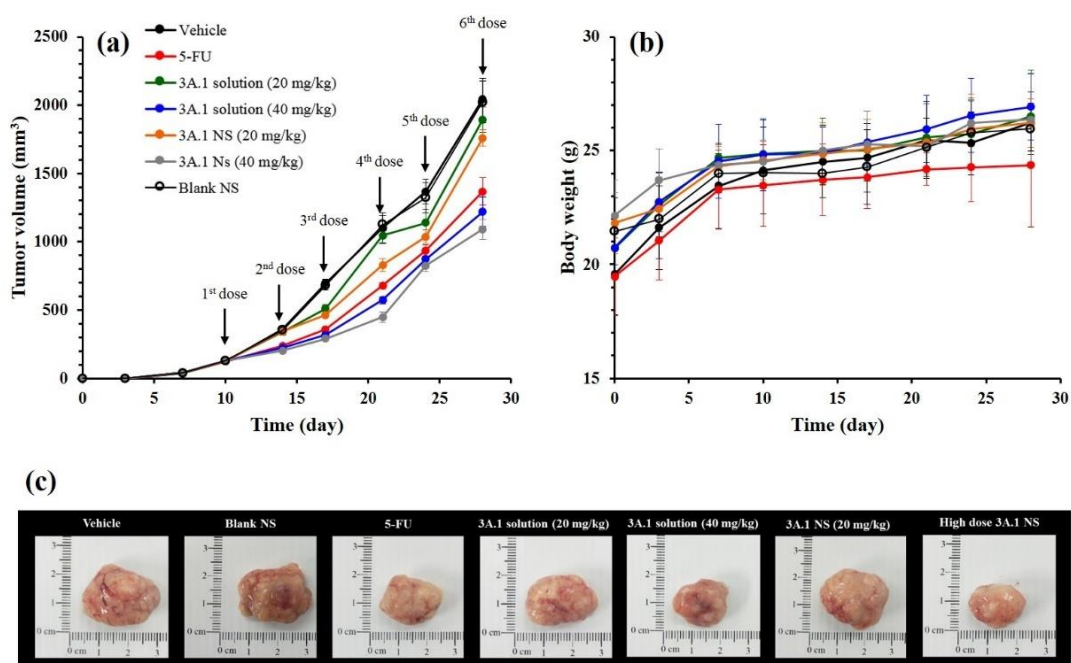


Figure 50 In vivo antitumor efficacy of 3A.1 NSs compared to free 3A.1 solution against HCT116 tumor xenograft-induced nude mice. (a) The tumor growth curves of each group in tumor-bearing mice; (b) The body weight of mice in each group; (c) Representative photographs of subcutaneous tumor mass in each group.

CHAPTER 5

CONCLUSION

In this study, semi-synthetic andrographolide (3A.1) was developed and prepared in the three DDSs including 3A.1-loaded PMs, 3A.1-loaded LPs, and 3A.1-NSs for delivery of 3A.1 into cancer cells and improving anticancer efficacy. The amphiphilic chitosan derivatives (NSC, OSC, and BSC) was used to formulate 3A.1-loaded PMs and as stabilizer for 3A.1-NSs. The results could be summarized as follows:

5.1 Development of 3A.1-loaded polymeric micelles (PMs)

The PMs were formed by self-assembly in an aqueous solution and their hydrophobic moieties that grafted onto CS backbone facilitated to solubilize the hydrophobic compound within the micelle's core. The 3A.1-loaded NSC PMs with 40%wt drug to polymer prepared by a dropping method showed the highest drug loading capacity, desirable properties (spherical shape, size in nanometer-range, negative surface charge), and good stability in a refrigerator at 4°C for at least 6 months. The release patterns of the 3A.1 from micelles depended on the pH of medium and high amounts of drug were specifically released at intestinal/colon sites. The 3A.1-loaded PMs clearly showed better anticancer activity against HT29 cell and promotion of cell apoptosis, compared with free 3A.1. In addition, the 3A.1-loaded PMs also inhibited cell migration of HN22 cell. The *in vitro* cellular uptake was found that the fluorescent intensity of doxorubicin-loaded NSC PMs was higher than that of free Dox, representing the augmented drug accumulation in cancer cells. In comparison with unconjugated PMs, the Fol-NSC PMs loaded 3A.1 at 40%wt drug to polymer had greater cytotoxic activity against HT29 due to enhancing cellular uptake via receptor-mediated endocytosis.

5.2 Development of 3A.1-loaded liposomes (LPs)

The two types of liposome including conventional LPs and PEGylated LPs were prepared through a thin-film hydration and probe-sonication method. Overall, the initial drug molar ratio and lipid components affected the physicochemical properties of these LPs. The screening of liposomal formulation revealed that conventional LPs containing PC:Chol at 10:2 molar ratio and PEGylated LPs containing PC:Chol:DSPE-PEG2000

at 10:2:0.25 molar ratio had the maximum values of %EE and LC at the initial drug content of 3.0 mmol. Both conventional LPs and PEGylated LPs had nanometer size, mildly negative surface charge, and spherical shape. The PEGylated LPs exhibited a prolonged release profile and these formulations were stable at 4°C for at least 6 months. In addition, the delivery of 3A.1 using PEGylated LPs improved anticancer activity against HCT116 and HT29 cells caused by induction of cell apoptosis. Moreover, the 3A.1-loaded LPs were also stronger inhibition of cancer cell migration than that of free 3A.1.

5.3 Development of 3A.1 nanosuspensions (NSs)

The 3A.1-NSs were produced by an anti-solvent method and these 3A.1-NSs were stabilized by amphiphilic chitosan copolymers (NSC, OSC, and BSC). The 3A.1-NSs with drug to polymer ratio of 1.5:1 (w/w) represented favourable properties such as nanometer range size, narrow size distribution, negative surface charge, spherical morphology and maximum drug content. Subsequently, the 3A.1-NSs were freeze-dried using 5%w/v mannitol as a cryoprotectant to transform into powder and well dispersed in aqueous medium. The reconstitution of freeze-dried powder of 3A.1-NS with mannitol in water showed no significant change of particle size and zeta potential, compared to freshly prepared liquid NSs. The 3A.1 and chitosan copolymers were good compatible without any degradation of substances. The 3A.1-NSs were physical and chemical stability in refrigerator for at least 6 months. Furthermore, the 3A.1-NSs had better anticancer activity against HCT116 than free 3A.1. For *in vivo* antitumor study, the intraperitoneal injection of 3A.1-NSs at high dose of 40 mg/kg/day had greater suppression of CRC tumor growth and smaller tumor mass than free drug solution and blank NS. No significant body weight loss was observed in group of 3A.1-NSs at high dose.

Based on all of data, the 3A.1 compound possesses potential anticancer activity and anti-migratory effect. By using nanotechnology, our study suggested that these nanocarriers (pH-sensitive micelles, PEGylated liposomes) and nanosuspensions could be a great promising drug delivery of 3A.1 for cancer treatment.

REFERENCES

1. Torre, L.A., et al., *Global cancer statistics, 2012*. CA Cancer J Clin, 2015. **65(2)**: 87-108.
2. World Health Organization. *Cancer fact sheet 2018* [Available from: <https://www.who.int/news-room/fact-sheets/detail/cancer>. [last accessed 15 Jan 2020].
3. Siegel, R.L., Miller, K.D. and Jemal, A., *Cancer Statistics, 2017*. CA Cancer J Clin, 2017. **67(1)**: 7-30.
4. Borders, E.B. and Medina, P.J. *Colorectal Cancer*. In: Chisholm-Burns, M.A., et al., Editors. *Pharmacotherapy Principles & Practice*, 4ed. New York: McGraw-Hill Education; 2016, p. 1310-1316.
5. Manchun, S., et al., *Enhanced anti-tumor effect of pH-responsive dextran nanogels delivering doxorubicin on colorectal cancer*. Carbohydr Polym, 2015. **126**: 222-230.
6. Tiwari, G., et al., *Drug delivery systems: An updated review*. Int J Pharm Investig, 2012. **2(1)**: 2-11.
7. Cho, K., et al., *Therapeutic nanoparticles for drug delivery in cancer*. Clin Cancer Res, 2008. **14(5)**: 1310-1316.
8. Davis, M.E., Chen, Z.G. and Shin, D.M., *Nanoparticle therapeutics: an emerging treatment modality for cancer*. Nat Rev Drug Discov, 2008. **7(9)**: 771-782.
9. Faraji, A.H. and Wipf, P., *Nanoparticles in cellular drug delivery*. Bioorg Med Chem, 2009. **17(8)**: 2950-2962.
10. Haley, B. and Frenkel, E., *Nanoparticles for drug delivery in cancer treatment*. Urol Oncol, 2008. **26(1)**: 57-64.
11. Suk, J.S., et al., *PEGylation as a strategy for improving nanoparticle-based drug and gene delivery*. Adv Drug Deliv Rev, 2016. **99(Pt A)**: 28-51.
12. Brigger, I., Dubernet, C. and Couvreur, P., *Nanoparticles in cancer therapy and diagnosis*. Adv Drug Deliv Rev, 2002. **54(5)**: 631-651.
13. Brannon-Peppas, L. and Blanchette, J.O., *Nanoparticle and targeted systems for cancer therapy*. Adv Drug Deliv Rev, 2004. **56(11)**: 1649-1659.
14. Lee, K.S., et al., *Multicenter phase II trial of Genexol-PM, a Cremophor-free, polymeric micelle formulation of paclitaxel, in patients with metastatic breast cancer*. Breast Cancer Res Treat, 2008. **108(2)**: 241-250.
15. Wang, A.Z., Langer, R. and Farokhzad, O.C., *Nanoparticle delivery of cancer drugs*. Annu Rev Med, 2012. **63**: 185-198.
16. Demain, A.L. and Vaishnav, P., *Natural products for cancer chemotherapy*. Microb Biotechnol, 2011. **4(6)**: 687-699.
17. Hossain, M.S., et al., *Andrographis paniculata (Burm. f.) Wall. ex Nees: a review of ethnobotany, phytochemistry, and pharmacology*. Sci World J, 2014. **2014**: 1-28.
18. Jada, S.R., et al., *Semisynthesis and cytotoxic activities of andrographolide analogues*. J Enzyme Inhib Med Chem, 2006. **21(2)**: 145-155.
19. Sirion, U., et al., *New substituted C-19-andrographolide analogues with potent cytotoxic activities*. Bioorg Med Chem Lett, 2012. **22(1)**: 49-52.

20. Nateewattana, J., et al., *Inhibition of topoisomerase II alpha activity and induction of apoptosis in mammalian cells by semi-synthetic andrographolide analogues*. Invest New Drugs, 2013. **31(2)**: 320-332.
21. Deshpande, P.P., Biswas, S. and Torchilin, V.P., *Current trends in the use of liposomes for tumor targeting*. Nanomedicine (Lond), 2013. **8(9)**: 1509-1528.
22. Lee, S.E., et al., *Paclitaxel nanosuspensions for targeted chemotherapy - nanosuspension preparation, characterization, and use*. Pharm Dev Technol, 2014. **19(4)**: 438-453.
23. Biswas, S., et al., *Recent advances in polymeric micelles for anti-cancer drug delivery*. Eur J Pharm Sci, 2016. **83**: 184-202.
24. Deshmukh, A.S., et al., *Polymeric micelles: Basic research to clinical practice*. Int J Pharm, 2017. **532(1)**: 249-268.
25. Xin, Y., et al., *Nanoscale drug delivery for targeted chemotherapy*. Cancer Lett, 2016. **379(1)**: 24-31.
26. Sajomsang, W., et al., *Synthesis and anticervical cancer activity of novel pH responsive micelles for oral curcumin delivery*. Int J Pharm, 2014. **477(1-2)**: 261-272.
27. Woraphatphadung, T., et al., *Synthesis and characterization of pH-responsive N-naphthyl-N,O-succinyl chitosan micelles for oral meloxicam delivery*. Carbohydr Polym, 2015. **121(5)**: 99-106.
28. Woraphatphadung, T., et al., *pH-responsive polymeric micelles based on amphiphilic chitosan derivatives: Effect of hydrophobic cores on oral meloxicam delivery*. Int J Pharm, 2016. **497(1-2)**: 150-160.
29. Soodvilai, S., et al., *Effects of silymarin-loaded amphiphilic chitosan polymeric micelles on the renal toxicity and anticancer activity of cisplatin*. Pharm Dev Technol, 2019. **24(8)**: 927-934.
30. Allen, T.M. and Cullis, P.R., *Liposomal drug delivery systems: from concept to clinical applications*. Adv Drug Deliv Rev, 2013. **65(1)**: 36-48.
31. Patil, Y.P. and Jadhav, S., *Novel methods for liposome preparation*. Chem Phys Lipids, 2014. **177**: 8-18.
32. Rangsimawong, W., et al., *Skin transport of hydrophilic compound-loaded PEGylated lipid nanocarriers: Comparative study of liposomes, niosomes, and solid lipid nanoparticles*. Biol Pharm Bull, 2016. **39(8)**: 1254-1262.
33. Mishra, P., Nayak, B. and Dey, R.K., *PEGylation in anti-cancer therapy: An overview*. Asian J Pharm Sci, 2016. **11(3)**: 337-348.
34. Verhoef, J.J. and Anchordoquy, T.J., *Questioning the Use of PEGylation for Drug Delivery*. Drug Deliv Transl Res, 2013. **3(6)**: 499-503.
35. Hossen, S., et al., *Smart nanocarrier-based drug delivery systems for cancer therapy and toxicity studies: A review*. J Adv Res, 2019. **15**: 1-18.
36. Perche, F. and Torchilin, V.P., *Recent trends in multifunctional liposomal nanocarriers for enhanced tumor targeting*. J Drug Deliv, 2013. **2013**: 705265.
37. Riaz, M.K., et al., *Surface functionalization and targeting strategies of liposomes in solid tumor therapy: A review*. Int J Mol Sci, 2018. **19(1)**: 195.
38. Bulbake, U., et al., *Liposomal formulations in clinical use: An updated review*. Pharmaceutics, 2017. **9(2)**: 1-33.
39. Olusanya, T.O.B., et al., *Liposomal drug delivery systems and anticancer drugs*. Molecules, 2018. **23(4)**: 1-27.

40. Chang, T.-L., et al., *Nanocrystal technology for drug formulation and delivery*. Front Chem Sci Eng, 2015. **9(1)**: 1-14.
41. Hollis, C.P. and Li, T. *Nanocrystals production, characterization, and application for cancer therapy*. In: Yeo, Y., Editor. Nanoparticulate drug delivery systems: strategies, technologies, and applications 1st ed. New Jersey: Wiley&Sons Inc; 2013, p. 183-200.
42. Junghanns, J.U. and Müller, R.H., *Nanocrystal technology, drug delivery and clinical applications*. Int J Nanomedicine, 2008. **3(3)**: 295-309.
43. Müller, R.H., Gohla, S. and Keck, C.M., *State of the art of nanocrystals-special features, production, nanotoxicology aspects and intracellular delivery*. Eur J Pharm Biopharm, 2011. **78(1)**: 1-9.
44. Ahire, E., et al., *Parenteral nanosuspensions: a brief review from solubility enhancement to more novel and specific applications*. Acta Pharm Sin B, 2018. **8(5)**: 733-755.
45. Lu, Y., Li, Y. and Wu, W., *Injected nanocrystals for targeted drug delivery*. Acta Pharm Sin B, 2016. **6(2)**: 106-113.
46. World Health Organization. *Cancer Key Statistics 2018* [Available from: <https://www.who.int/cancer/resources/keyfacts/en/>. [last accessed 15 Jan 2020].
47. Wu, S., et al., *Evaluating intrinsic and non-intrinsic cancer risk factors*. Nat Commun, 2018. **9(1)**: 3490.
48. Schirmacher, V., *From chemotherapy to biological therapy: A review of novel concepts to reduce the side effects of systemic cancer treatment (Review)*. Int J Oncol, 2019. **54(2)**: 407-419.
49. Harrington, S.E. and Smith, T.J., *The role of chemotherapy at the end of life: "when is enough, enough?"*. Jama, 2008. **299(22)**: 2667-2678.
50. Steeg, P.S., *Targeting metastasis*. Nat Rev Cancer, 2016. **16(4)**: 201-218.
51. Fleming, M., et al., *Colorectal carcinoma: Pathologic aspects*. J Gastrointest Oncol, 2012. **3(3)**: 153-173.
52. Siegel, R.L., et al., *Colorectal cancer statistics, 2020*. CA Cancer J Clin, 2020. **70(3)**: 145-164.
53. Siegel, R.L., Miller, K.D. and Jemal, A., *Cancer statistics, 2020*. CA Cancer J Clin, 2020. **70(1)**: 7-30.
54. National Cancer Institute Thailand. *Hospital-based cancer therapy 2018*. Bangkok: New Thammada Press; 2019.
55. World Health Organization. *Thailand Globocan 2018 2018* [Available from: <https://gco.iarc.fr/today/data/factsheets/populations/764-thailand-fact-sheets.pdf>. [last accessed 15 Feb 2020].
56. Marley, A.R. and Nan, H., *Epidemiology of colorectal cancer*. Int J Mol Epidemiol Genet, 2016. **7(3)**: 105-114.
57. Centers for Disease Control and Prevention. *Colorectal cancer screening tests 2020* [Available from: https://www.cdc.gov/cancer/colorectal/basic_info/screening/tests.htm. [last accessed 1 Mar 2020].
58. Brown, K.G.M., et al., *Management of colorectal cancer*. BMJ, 2019. **366**: 14561.
59. National Cancer Institute. *Drugs approved for colon and rectal cancer 2020* [Available from: <https://www.cancer.gov/about-cancer/treatment/drugs/colorectal>. [last accessed 20 Sep 2020].

60. Gustavsson, B., et al., *A review of the evolution of systemic chemotherapy in the management of colorectal cancer*. Clin Colorectal Cancer, 2015. **14(1)**: 1-10.
61. Lichota, A. and Gwozdziński, K., *Anticancer Activity of Natural Compounds from Plant and Marine Environment*. Int J Mol Sci, 2018. **19(11)**: 3533.
62. Xiao, Z., Morris-Natschke, S.L. and Lee, K.H., *Strategies for the optimization of natural leads to anticancer drugs or drug candidates*. Med Res Rev, 2016. **36(1)**: 32-91.
63. Seca, A.M.L. and Pinto, D., *Plant secondary metabolites as anticancer agents: Successes in clinical trials and therapeutic application*. Int J Mol Sci, 2018. **19(1)**: 263.
64. Pawar, A., et al., *Strategies for formulation development of andrographolide*. RSC Adv, 2016. **6(73)**: 69282-69300.
65. Varma, A., Padh, H. and Shrivastava, N., *Andrographolide: a new plant-derived antineoplastic entity on horizon*. Evid Based Complement Alternat Med, 2011. **2011**: 815390.
66. Department of Medical Sciences, Ministry of Public Health. *Thai herbal pharmacopoeia 2019*. Nonthaburi: Department of Medical Sciences; 2019.
67. Mishra, S.K., et al., *Andrographolide and analogues in cancer prevention*. Front Biosci (Elite Ed), 2015. **7**: 255-266.
68. Jayakumar, T., et al., *Experimental and clinical pharmacology of Andrographis paniculata and its major bioactive phytoconstituent andrographolide*. Evid Based Complement Alternat Med, 2013. **2013**: 846740.
69. Dai, Y., et al., *Overview of pharmacological activities of Andrographis paniculata and its major compound andrographolide*. Crit Rev Food Sci Nutr, 2019. **59(sup1)**: S17-S29.
70. Banerjee, M., et al., *Cytotoxicity and cell cycle arrest induced by andrographolide lead to programmed cell death of MDA-MB-231 breast cancer cell line*. J Biomed Sci, 2016. **23(1)**: 40.
71. Islam, M.T., et al., *Andrographolide, a diterpene lactone from Andrographis paniculata and its therapeutic promises in cancer*. Cancer Lett, 2018. **420**: 129-145.
72. Choudhari, A.S., et al., *Phytochemicals in cancer treatment: From preclinical studies to clinical practice*. Front Pharmacol, 2019. **10**: 1614.
73. Jada, S.R., et al., *Semisynthesis and in vitro anticancer activities of andrographolide analogues*. Phytochemistry, 2007. **68(6)**: 904-912.
74. Nanduri, S., et al., *Synthesis and structure-activity relationships of andrographolide analogues as novel cytotoxic agents*. Bioorg Med Chem Lett, 2004. **14(18)**: 4711-4717.
75. Aromdee, C., *Modifications of andrographolide to increase some biological activities: a patent review (2006 - 2011)*. Expert Opin Ther Pat, 2012. **22(2)**: 169-180.
76. Das, B., et al., *Synthesis, cytotoxicity, and structure-activity relationship (SAR) studies of andrographolide analogues as anti-cancer agent*. Bioorg Med Chem Lett, 2010. **20(23)**: 6947-6950.
77. Lim, J.C., et al., *Andrographolide and its analogues: versatile bioactive molecules for combating inflammation and cancer*. Clin Exp Pharmacol Physiol, 2012. **39(3)**: 300-310.

78. Preet, R., et al., *Synthesis and biological evaluation of andrographolide analogues as anti-cancer agents*. Eur J Med Chem, 2014. **85**: 95-106.
79. Jada, S.R., et al., *Benzylidene derivatives of andrographolide inhibit growth of breast and colon cancer cells in vitro by inducing G(1) arrest and apoptosis*. Br J Pharmacol, 2008. **155(5)**: 641-654.
80. Peng, Y., et al., *SAR studies of 3,14,19-derivatives of andrographolide on anti-proliferative activity to cancer cells and toxicity to zebrafish: an in vitro and in vivo study*. RSC Adv, 2015. **5(29)**: 22510-22526.
81. Nateewattana, J., et al., *Induction of apoptosis in cholangiocarcinoma by an andrographolide analogue is mediated through topoisomerase II alpha inhibition*. Eur J Pharmacol, 2014. **723**: 148-155.
82. Reabroi, S., et al., *A silyl andrographolide analogue suppresses Wnt/beta-catenin signaling pathway in colon cancer*. Biomed Pharmacother, 2018. **101**: 414-421.
83. Wicki, A., et al., *Nanomedicine in cancer therapy: challenges, opportunities, and clinical applications*. J Control Release, 2015. **200**: 138-157.
84. Din, F.U., et al., *Effective use of nanocarriers as drug delivery systems for the treatment of selected tumors*. Int J Nanomedicine, 2017. **12**: 7291-7309.
85. Jeong, K., et al., *Development of highly efficient nanocarrier-mediated delivery approaches for cancer therapy*. Cancer Lett, 2016. **374(1)**: 31-43.
86. Ali, I., et al., *Advances in nanocarriers for anticancer drugs delivery*. Curr Med Chem, 2016. **23(20)**: 2159-2187.
87. Akhter, M.H., et al., *Nanocarriers in advanced drug targeting: setting novel paradigm in cancer therapeutics*. Artif Cells Nanomed Biotechnol, 2018. **46(5)**: 873-884.
88. Attia, M.F., et al., *An overview of active and passive targeting strategies to improve the nanocarriers efficiency to tumour sites*. J Pharm Pharmacol, 2019. **71(8)**: 1185-1198.
89. Miao, L. and Huang, L., *Exploring the tumor microenvironment with nanoparticles*. Cancer Treat Res, 2015. **166**: 193-226.
90. National Cancer Institute. *Benefits of nanotechnology for cancer 2017* [Available from: <https://www.cancer.gov/nano/cancer-nanotechnology/benefits>]. [last accessed 1 Aug 2020].
91. Kumari, P., Ghosh, B. and Biswas, S., *Nanocarriers for cancer-targeted drug delivery*. J Drug Target, 2016. **24(3)**: 179-191.
92. Jani, R.K. and Krupa, G., *Active targeting of nanoparticles: An innovative technology for drug delivery in cancer therapeutics*. J Drug Deliv Ther, 2019. **9(1-s)**: 408-415.
93. Salahpour Anarjan, F., *Active targeting drug delivery nanocarriers: Ligands*. Nano-Struct Nano-Objects, 2019. **19**: 100370.
94. Kutova, O.M., et al., *Targeted delivery to tumors: Multidirectional strategies to improve treatment efficiency*. Cancers (Basel), 2019. **11(1)**: 68.
95. Xu, S., et al., *Targeting receptor-mediated endocytotic pathways with nanoparticles: rationale and advances*. Adv Drug Deliv Rev, 2013. **65(1)**: 121-138.
96. Danhier, F., Feron, O. and Préat, V., *To exploit the tumor microenvironment: Passive and active tumor targeting of nanocarriers for anti-cancer drug delivery*. J Control Release, 2010. **148(2)**: 135-146.

97. Yoo, J., et al., *Active targeting strategies using biological ligands for nanoparticle drug delivery systems*. *Cancers* (Basel), 2019. **11(5)**: 640.
98. Qiao, W., et al., *Cancer therapy based on nanomaterials and nanocarrier systems*. *J Nanometer*, 2010. **2010**: 796303.
99. Croy, S.R. and Kwon, G.S., *Polymeric micelles for drug delivery*. *Curr Pharm Des*, 2006. **12(36)**: 4669-4684.
100. Ahmad, Z., et al., *Polymeric micelles as drug delivery vehicles*. *RSC Adv*, 2014. **4(33)**: 17028-17038.
101. Xu, W., Ling, P. and Zhang, T., *Polymeric micelles, a promising drug delivery system to enhance bioavailability of poorly water-soluble drugs*. *J Drug Deliv*, 2013. **2013**: 340315.
102. Tai, W. and Cheng, K. *Advanced drug delivery in cancer therapy*. In: Mitra, A.K., Editor. New Jersey: John Wiley&Sons Inc; 2014, p. 323-326.
103. Ma, P. and Mumper, R.J., *Paclitaxel nano-delivery systems: A comprehensive review*. *J Nanomed Nanotechnol*, 2013. **4(2)**: 1000164.
104. Oerlemans, C., et al., *Polymeric micelles in anticancer therapy: Targeting, imaging and triggered release*. *Pharm Res*, 2010. **27(12)**: 2569-2589.
105. Kedar, U., et al., *Advances in polymeric micelles for drug delivery and tumor targeting*. *Nanomedicine*, 2010. **6(6)**: 714-729.
106. Hussein, Y.H.A. and Youssry, M., *Polymeric micelles of biodegradable diblock copolymers: Enhanced encapsulation of hydrophobic drugs*. *Materials* (Basel), 2018. **11(5)**: 688.
107. Gothwal, A., Khan, I. and Gupta, U., *Polymeric micelles: Recent advancements in the delivery of anticancer drugs*. *Pharm Res*, 2016. **33(1)**: 18-39.
108. Lu, Y. and Park, K., *Polymeric micelles and alternative nanonized delivery vehicles for poorly soluble drugs*. *Int J Pharm*, 2013. **453(1)**: 198-214.
109. Kulthe, S.S., et al., *Polymeric micelles: authoritative aspects for drug delivery*. *Des Monomers Polym*, 2012. **15(5)**: 465-521.
110. Tian, Y. and Mao, S., *Amphiphilic polymeric micelles as the nanocarrier for peroral delivery of poorly soluble anticancer drugs*. *Expert Opin Drug Deliv*, 2012. **9(6)**: 687-700.
111. Yokoyama, M., *Polymeric micelles as drug carriers: their lights and shadows*. *J Drug Target*, 2014. **22(7)**: 576-583.
112. Nagaich, D.U., et al., *Polymeric micelles: potential drug delivery devices*. *Indonesian J Pharm*, 2013. **24(4)**: 223-238.
113. Yokoyama, M., et al., *Characterization of physical entrapment and chemical conjugation of adriamycin in polymeric micelles and their design for in vivo delivery to a solid tumor*. *J Control Release*, 1998. **50(1-3)**: 79-92.
114. Ding, J., et al., *Noncovalent interaction-assisted polymeric micelles for controlled drug delivery*. *Chem Commun*, 2014. **50(77)**: 11274-11290.
115. Ohno, S., Ishihara, K. and Yusa, S., *Formation of polyion complex (PIC) micelles and vesicles with anionic pH-responsive unimer micelles and cationic diblock copolymers in water*. *Langmuir*, 2016. **32(16)**: 3945-3953.
116. Zhou, W., et al., *Factors affecting the stability of drug-loaded polymeric micelles and strategies for improvement*. *J Nanopart Res*, 2016. **18(9)**: 275.

117. Chakraborty, T., Chakraborty, I. and Ghosh, S., *The methods of determination of critical micellar concentrations of the amphiphilic systems in aqueous medium*. Arab J Chem, 2011. **4(3)**: 265-270.
118. Owen, S.C., Chan, D.P.Y. and Shoichet, M.S., *Polymeric micelle stability*. Nano Today, 2012. **7(1)**: 53-65.
119. Zhang, Y., Huang, Y. and Li, S., *Polymeric micelles: nanocarriers for cancer-targeted drug delivery*. AAPS PharmSciTech, 2014. **15(4)**: 862-871.
120. Zhou, Q., et al., *Stimuli-responsive polymeric micelles for drug delivery and cancer therapy*. Int J Nanomedicine, 2018. **13**: 2921-2942.
121. Wang, C., et al., *Bicomponent polymeric micelles for pH-controlled delivery of doxorubicin*. Drug Deliv, 2020. **27(1)**: 344-357.
122. Pandey, H., Rani, R. and Agarwal, V., *Liposome and their applications in cancer therapy*. Braz Arch Biol Technol, 2016. **59**: e16150477.
123. García-Pinel, B., et al., *Lipid-based nanoparticles: Application and recent advances in cancer treatment*. Nanomaterials (Basel), 2019. **9(4)**: 638.
124. Samad, A., Sultana, Y. and Aqil, M., *Liposomal drug delivery systems: an update review*. Curr Drug Deliv, 2007. **4(4)**: 297-305.
125. Alavi, M., Karimi, N. and Safaei, M., *Application of various types of liposomes in drug delivery systems*. Adv Pharm Bull, 2017. **7(1)**: 3-9.
126. Akbarzadeh, A., et al., *Liposome: classification, preparation, and applications*. Nanoscale Res Lett, 2013. **8(1)**: 102.
127. Malam, Y., Loizidou, M. and Seifalian, A.M., *Liposomes and nanoparticles: nanosized vehicles for drug delivery in cancer*. Trends Pharmacol Sci, 2009. **30(11)**: 592-599.
128. Li, J., et al., *A review on phospholipids and their main applications in drug delivery systems*. Asian J Pharm Sci, 2015. **10(2)**: 81-98.
129. Briuglia, M.L., et al., *Influence of cholesterol on liposome stability and on in vitro drug release*. Drug Deliv Transl Res, 2015. **5(3)**: 231-242.
130. Lee, S.-C., et al., *The effect of cholesterol in the liposome bilayer on the stabilization of incorporated retinol*. J Liposome Res, 2005. **15(3-4)**: 157-166.
131. Wu, H., et al., *Cholesterol-tuned liposomal membrane rigidity directs tumor penetration and anti-tumor effect*. Acta Pharm Sin B, 2019. **9(4)**: 858-870.
132. Cagdas, M., Sezer, A.D. and Bucak, S. *Liposomes as potential drug carrier systems for drug delivery*. In: Sezer, A.D., Editor. Application of nanotechnology in drug delivery. London: IntechOpen; 2014.
133. Zhang, J., et al., *The influence of different long-circulating materials on the pharmacokinetics of liposomal vincristine sulfate*. Int J Nanomedicine, 2016. **11**: 4187-4197.
134. Immordino, M.L., Dosio, F. and Cattell, L., *Stealth liposomes: Review of the basic science, rationale, and clinical applications, existing and potential*. Int J Nanomedicine, 2006. **1(3)**: 297-315.
135. Wang, R., et al., *Application of poly(ethylene glycol)-distearoylphosphatidylethanolamine (PEG-DSPE) block copolymers and their derivatives as nanomaterials in drug delivery*. Int J Nanomedicine, 2012. **7**: 4185-4198.

136. Lee, J.S., et al., *Circulation kinetics and biodistribution of dual-labeled polymersomes with modulated surface charge in tumor-bearing mice: Comparison with stealth liposomes*. J Control Release, 2011. **155(2)**: 282-288.
137. McSweeney, M.D., et al., *Overcoming anti-PEG antibody mediated accelerated blood clearance of PEGylated liposomes by pre-infusion with high molecular weight free PEG*. J Control Release, 2019. **311-312**: 138-146.
138. Suzuki, T., et al., *Accelerated blood clearance of PEGylated liposomes containing doxorubicin upon repeated administration to dogs*. Int J Pharm, 2012. **436(1-2)**: 636-643.
139. Balazs, D.A. and Godbey, W., *Liposomes for use in gene delivery*. J Drug Deliv, 2011. **2011**: 326497.
140. An, X. and Gui, R. *Stimuli-responsive liposome and control release drug*. In: Andronescu, E. and Grumezescu, A., Editors. Nanostructures for drug delivery. Amsterdam: Elsevier; 2017, p. 887-917.
141. Ganta, S., et al., *A review of stimuli-responsive nanocarriers for drug and gene delivery*. J Control Release, 2008. **126(3)**: 187-204.
142. Lee, Y. and Thompson, D.H., *Stimuli-responsive liposomes for drug delivery*. Wiley Interdiscip Rev Nanomed Nanobiotechnol, 2017. **9(5)**: 1-40.
143. Heidarli, E., Dadashzadeh, S. and Haeri, A., *State of the art of stimuli-responsive liposomes for cancer therapy*. Iran J Pharm Res, 2017. **16(4)**: 1273-1304.
144. Jain, A. and Jain, S.K., *Stimuli-responsive smart liposomes in cancer targeting*. Curr Drug Targets, 2018. **19(3)**: 259-270.
145. Lopes, S.C.d.A., et al. *Liposomes as carriers of anticancer drugs*. In: Rangel, L., Editor. Cancer treatment-conventional and innovative approaches. Rijeka: IntechOpen; 2013, p. 85-124.
146. Zhang, H., *Thin-film hydration followed by extrusion method for liposome preparation*. Methods Mol Biol, 2017. **1522**: 17-22.
147. Huang, Z., et al., *Progress involving new techniques for liposome preparation*. Asian J Pharm Sci, 2014. **9(4)**: 176-182.
148. Rahman, A., Uahengo, V. and Likius, D., *Mini review on emerging methods of preparation of liposome and its application as liposome drug delivery systems*. Open J Pharmacol Pharmacother, 2018. **3(1)**: 5-21.
149. Koynova, R. and Tenchov, B., *Lipids: Phase transitions*. Wiley Encycl Chem Biol, 2008. 1-15.
150. Lee, K.-E., et al., *Effect of phase transition temperature of phospholipid on the stability of retinol incorporated into liposomes*. Prev Nutr Food Sci, 2003. **8(3)**: 235-238.
151. Zylberberg, C. and Matosevic, S., *Pharmaceutical liposomal drug delivery: a review of new delivery systems and a look at the regulatory landscape*. Drug Deliv, 2016. **23(9)**: 3319-3329.
152. Ahmed, K.S., et al., *Liposome: composition, characterisation, preparation, and recent innovation in clinical applications*. J Drug Target, 2019. **27(7)**: 742-761.
153. Simão, A.M.S., et al., *Liposomal systems as carriers for bioactive compounds*. Biophys Rev, 2015. **7(4)**: 391-397.
154. Abu Lila, A.S. and Ishida, T., *Liposomal delivery systems: Design optimization and current applications*. Biol Pharm Bull, 2017. **40(1)**: 1-10.

155. Saraf, S., et al., *Advances in liposomal drug delivery to cancer: An overview*. J Drug Deliv Sci Technol, 2020. **56(A)**: 101549.
156. Kawabata, Y., et al., *Formulation design for poorly water-soluble drugs based on biopharmaceutics classification system: basic approaches and practical applications*. Int J Pharm, 2011. **420(1)**: 1-10.
157. Bhakay, A., et al., *Bioavailability enhancement of poorly water-soluble drugs via nanocomposites: Formulation-processing aspects and challenges*. Pharmaceutics, 2018. **10(3)**: 86.
158. Joshi, K., et al., *Nanocrystallization: An emerging technology to enhance the bioavailability of poorly soluble drugs*. Pharm Nanotechnol, 2019. **7(4)**: 259-278.
159. Kumar, A., et al., *Review on solubility enhancement techniques for hydrophobic drugs*. Pharmacie Globale (IJCP), 2011. **2(3)**: 1-7.
160. Savjani, K.T., Gajjar, A.K. and Savjani, J.K., *Drug solubility: Importance and enhancement techniques*. ISRN Pharm, 2012. **2012**: 195727.
161. Serajuddin, A.T., *Salt formation to improve drug solubility*. Adv Drug Deliv Rev, 2007. **59(7)**: 603-616.
162. Rangel-Yagui, C., Pessoa, A. and Tavares, L., *Micellar solubilization of drugs*. J Pharm Pharmaceut Sci, 2005. **8(2)**: 147-165.
163. Saokham, P., et al., *Solubility of cyclodextrins and drug/cyclodextrin complexes*. Molecules, 2018. **23(5)**: 1161.
164. Deshmukh, A.S., Tiwari, K.J. and Mahajan, V.R., *Solubility enhancement techniques for poorly water-soluble drugs*. Int J Pharm Sci Nanotech, 2017. **10(3)**: 3701-3708.
165. Narvekar, M., et al., *Nanocarrier for poorly water-soluble anticancer drugs barriers of translation and solutions*. AAPS PharmSciTech, 2014. **15(4)**: 822-833.
166. Gigliobianco, M.R., et al., *Nanocrystals of poorly soluble drugs: Drug bioavailability and physicochemical stability*. Pharmaceutics, 2018. **10(3)**: 134.
167. Junyaprasert, V.B. and Morakul, B., *Nanocrystals for enhancement of oral bioavailability of poorly water-soluble drugs*. Asian J Pharm Sci, 2015. **10(1)**: 13-23.
168. Buckton, G. and Beezer, A.E., *The relationship between particle size and solubility*. Int J Pharm, 1992. **82(3)**: R7-R10.
169. Sun, J., et al., *Effect of particle size on solubility, dissolution rate, and oral bioavailability: evaluation using coenzyme Q₁₀ as naked nanocrystals*. Int J Nanomedicine, 2012. **7**: 5733-5744.
170. Lu, Y., et al., *Developing nanocrystals for cancer treatment*. Nanomedicine (Lond), 2015. **10(16)**: 2537-2552.
171. Möschwitzer, J.P., *Drug nanocrystals in the commercial pharmaceutical development process*. Int J Pharm, 2013. **453(1)**: 142-156.
172. Wu, L., Zhang, J. and Watanabe, W., *Physical and chemical stability of drug nanoparticles*. Adv Drug Deliv Rev, 2011. **63(6)**: 456-469.
173. Sinha, B., Müller, R.H. and Möschwitzer, J.P., *Bottom-up approaches for preparing drug nanocrystals: formulations and factors affecting particle size*. Int J Pharm, 2013. **453(1)**: 126-141.
174. Guo, S. and Huang, L., *Nanoparticles containing insoluble drug for cancer therapy*. Biotechnol Adv, 2014. **32(4)**: 778-788.

175. Tuomela, A., Hirvonen, J. and Peltonen, L., *Stabilizing agents for drug nanocrystals: Effect on bioavailability*. *Pharmaceutics*, 2016. **8(2)**: 16.
176. Yang, C., et al., *Recent advances in the application of vitamin E TPGS for drug delivery*. *Theranostics*, 2018. **8(2)**: 464-485.
177. Jacob, S., Nair, A.B. and Shah, J., *Emerging role of nanosuspensions in drug delivery systems*. *Biomater Res*, 2020. **24**: 3.
178. Sun, B. and Yeo, Y., *Nanocrystals for the parenteral delivery of poorly water-soluble drugs*. *Curr Opin Solid State Mater Sci*, 2012. **16(6)**: 295-301.
179. Danaei, M., et al., *Impact of particle size and polydispersity index on the clinical applications of lipidic nanocarrier systems*. *Pharmaceutics*, 2018. **10(2)**: 57.
180. Shah, M.R., Imran, M. and Ullah, S. *Nanosuspensions*. In: Shah, M.R., Editor. *Lipid-based nanocarriers for drug delivery and diagnosis* 1st ed. Oxford: Elsevier Science; 2017, p. 139-172.
181. Patel, V.R. and Agrawal, Y.K., *Nanosuspension: An approach to enhance solubility of drugs*. *J Adv Pharm Technol Res*, 2011. **2(2)**: 81-87.
182. Liu, P., et al., *Dissolution studies of poorly soluble drug nanosuspensions in non-sink conditions*. *AAPS PharmSciTech*, 2013. **14(2)**: 748-756.
183. Rabinow, B.E., *Nanosuspensions in drug delivery*. *Nat Rev Drug Discov*, 2004. **3(9)**: 785-796.
184. Wang, Y., et al., *Stability of nanosuspensions in drug delivery*. *J Control Release*, 2013. **172(3)**: 1126-1141.
185. Verma, S., et al., *Physical stability of nanosuspensions: Investigation of the role of stabilizers on Ostwald ripening*. *Int J Pharm*, 2011. **406(1-2)**: 145-152.
186. Agarwal, V. and Bajpai, M., *Stability issues related to nanosuspensions: A review*. *Pharm Nanotechol*, 2013. **1**: 85-92.
187. Yadollahi, R., Vasilev, K. and Simovic, S., *Nanosuspension technologies for delivery of poorly soluble drugs*. *J Nanometer*, 2015. **2015**: 216375.
188. Wang, L., et al., *Cryoprotectant choice and analyses of freeze-drying drug suspension of nanoparticles with functional stabilisers*. *J Microencapsul*, 2018. **35(3)**: 241-248.
189. Behzadi, S., et al., *Cellular uptake of nanoparticles: Journey inside the cell*. *Chem Soc Rev*, 2017. **46(14)**: 4218-4244.
190. Miao, X., et al., *Drug nanocrystals for cancer therapy*. *Wiley Interdiscip Rev Nanomed Nanobiotechnol*, 2018. **10(3)**: e1499.
191. Gao, L., et al., *Drug nanocrystals: In vivo performances*. *J Control Release*, 2012. **160(3)**: 418-430.
192. Pawar, V.K., et al., *Engineered nanocrystal technology: in-vivo fate, targeting and applications in drug delivery*. *J Control Release*, 2014. **183**: 51-66.
193. Dutta, P.K., Dutta, J. and Tripathi, V.S., *Chitin and chitosan: Chemistry, properties and applications*. *J Sci Indus Res*, 2003. **63(1)**: 20-31.
194. United States Pharmacopeia and National Formulary (USP 43-NF 38). Rockville, MD: United States Pharmacopeial Convention 2020. Available from: https://online.uspnf.com/uspnf/document/1_GUID-30832BBE-AFC1-463B-9695-AB4EF0A14413_6_en-US.
195. Kumar, R. and Majeti, N.V., *A review of chitin and chitosan applications*. *React Funct Polym*, 2000. **46(1)**: 1-27.

196. Kumirska, J., et al., *Biomedical activity of chitin/chitosan based materials- Influence of physicochemical properties apart from molecular weight and degree of N-acetylation*. *Polymers*, 2011. **3(4)**: 1875-1901.
197. Shariatinia, Z., *Carboxymethyl chitosan: Properties and biomedical applications*. *Int J Biol Macromol*, 2018. **120(B)**: 1406-1419.
198. Zargar, V., Asghari, M. and Dashti, A., *A review on chitin and chitosan polymers: Structure, chemistry, solubility, derivatives, and applications*. *Chem Bio Eng Reviews*, 2015. **2(3)**: 204-226.
199. Prabakaran, M., *Chitosan-based nanoparticles for tumor-targeted drug delivery*. *Int J Biol Macromol*, 2015. **72**: 1313-1322.
200. Mateescu, M.A., Ispas-Szabo, P. and Assaad, E. *Chitosan and its derivatives as self-assembled systems for drug delivery*. In: Mateescu, M.A., Ispas-Szabo, P. and Assaad, E., Editors. *Controlled drug delivery*. Kidlington: Woodhead Publishing; 2015, p. 85-125.
201. Miwa, A., et al., *Development of novel chitosan derivatives as micellar carriers of taxol*. *Pharm Res*, 1998. **15(12)**: 1844-1850.
202. Jin, X., et al., *Paclitaxel-loaded N-octyl-O-sulfate chitosan micelles for superior cancer therapeutic efficacy and overcoming drug resistance*. *Mol Pharm*, 2014. **11(1)**: 145-157.
203. Qu, G., et al., *PEG conjugated N-octyl-O-sulfate chitosan micelles for delivery of paclitaxel: in vitro characterization and in vivo evaluation*. *Eur J Pharm Sci*, 2009. **37(2)**: 98-105.
204. Huo, M., et al., *Synthesis and characterization of low-toxic amphiphilic chitosan derivatives and their application as micelle carrier for antitumor drug*. *Int J Pharm*, 2010. **394(1-2)**: 162-173.
205. Yuan, H., et al., *Stearic acid-g-chitosan polymeric micelle for oral drug delivery: in vitro transport and in vivo absorption*. *Mol Pharm*, 2011. **8(1)**: 225-238.
206. Tahvilian, R., et al., *Preparation and characterization of pH-sensitive camptothecin-cis-aconityl grafted chitosan oligosaccharide nanomicelles*. *Int J Biol Macromol*, 2016. **92**: 795-802.
207. Dai, Y., et al., *pH-responsive carboxymethyl chitosan-derived micelles as apatinib carriers for effective anti-angiogenesis activity: Preparation and in vitro evaluation*. *Carbohydr Polym*, 2017. **176**: 107-116.
208. International Conference on Harmonisation (ICH). *Stability testing of new drug substances and products, ICH Q1A (R2)2003*.
209. Borner, M.M., et al., *The detergent Triton X-100 induces a death pattern in human carcinoma cell lines that resembles cytotoxic lymphocyte-induced apoptosis*. *FEBS Letters*, 1994. **353(2)**: 129-132.
210. Cummings, B.S., Wills, L.P. and Schnellmann, R.G., *Measurement of cell death in mammalian cells*. *Curr Protoc Pharmacol*, 2004. **Chapter 12**: Unit 12.18.
211. Central Animal Facility (CAF), Faculty of Science Mahidol University. *Policies and guidelines in animal care 2020* [Available from: <https://science.mahidol.ac.th/caf/policies-and-guidelines/>]. [last accessed 1 Sep 2020].
212. Nghiem, N., Kleff, S. and Schwegmann, S., *Succinic acid: Technology development and commercialization*. *Fermentation*, 2017. **3(2)**: 26.

213. Jain, A.K. and Thareja, S., *In vitro and in vivo characterization of pharmaceutical nanocarriers used for drug delivery*. *Artif Cells Nanomed Biotechnol*, 2019. **47(1)**: 524-539.
214. You, X., et al., *Polymeric nanoparticles for colon cancer therapy: Overview and perspectives*. *J Mater Chem B*, 2016. **4(48)**: 7779-7792.
215. Opanasopit, P., et al., *Block copolymer design for camptothecin incorporation into polymeric micelles for passive tumor targeting*. *Pharm Res*, 2004. **21(11)**: 2001-2008.
216. Lu, Y., et al., *Strategies to improve micelle stability for drug delivery*. *Nano Res*, 2018. **11(10)**: 4985-4998.
217. Kansom, T., et al., *Apoptosis induction and antimigratory activity of andrographolide analog (3A.1)-incorporated self-assembled nanoparticles in cancer cells*. *AAPS PharmSciTech*, 2018. **19(7)**: 3123-3133.
218. Wang, Y., et al., *Targeted delivery of 5-fluorouracil to HT-29 cells using high efficient folic acid-conjugated nanoparticles*. *Drug Deliv*, 2015. **22(2)**: 191-198.
219. Wei, L., et al., *Folate-conjugated pH-responsive nanocarrier designed for active tumor targeting and controlled release of doxorubicin*. *Font Mater Sci*, 2017. **11(4)**: 328-343.
220. Karami, N., Moghimipour, E. and Salimi, A., *Liposomes as a novel drug delivery system: Fundamental and pharmaceutical application*. *Asian J Pharm*, 2018. **12**: S31.
221. Rangsimawong, W., et al., *Terpene-containing PEGylated liposomes as transdermal carriers of a hydrophilic compound*. *Biol Pharm Bull*, 2014. **37(12)**: 1936-1943.
222. Chain, E. and Kemp, I., *The isoelectric points of lecithin and sphingomyelin*. *Biochem J*, 1934. **28(6)**: 2052-2055.
223. Mare, R., et al., *Anchoring property of a novel hydrophilic lipopolymer, HDAS-SHP, post-inserted in preformed liposomes*. *Nanomaterials (Basel)*, 2019. **9(9)**: 1185.
224. Turner, P.V., et al., *Administration of substances to laboratory animals: equipment considerations, vehicle selection, and solute preparation*. *J Am Assoc Lab Anim Sci*, 2011. **50(5)**: 614-627.
225. Fam, S.Y., et al., *Stealth coating of nanoparticles in drug delivery systems*. *Nanomaterials (Basel)*, 2020. **10(4)**: 787.
226. Maurya, S., *Effects of pH, salt, temperature on conventional liposomes size enlargement analyzed by optical microscope*. *Int J Drug Regul Aff*, 2018. **1(1)**: 10-15.
227. Yadav, A.V., et al., *Stability aspects of liposome*. *Indian J Pharm Educ*, 2011. **45**: 402-413.
228. Siontorou, C.G., et al., *Artificial lipid membranes: Past, present, and future*. *Membranes (Basel)*, 2017. **7(3)**: 38.
229. Liang, C.-C., Park, A.Y. and Guan, J.-L., *In vitro scratch assay: a convenient and inexpensive method for analysis of cell migration in vitro*. *Nat Protoc*, 2007. **2(2)**: 329-333.
230. Justus, C.R., et al., *In vitro cell migration and invasion assays*. *J Vis Exp*, 2014. **(88)**: e51046.

231. Wang, L., et al., *Safety of nanosuspensions in drug delivery*. Nanomedicine, 2017. **13(2)**: 455-469.
232. Yang, H., et al., *Pharmaceutical strategies for stabilizing drug nanocrystals*. Curr Pharm Des, 2018. **24(21)**: 2362-2374.
233. Wang, Y., et al., *In vitro and in vivo anticancer activity of a novel puerarin nanosuspension against colon cancer, with high efficacy and low toxicity*. Int J Pharm, 2013. **441(1-2)**: 728-735.
234. Sari, R., et al., *Development of andrographolide-chitosan solid dispersion system: Physical characterization, solubility, and dissolution testing*. Asian J Pharm, 2019. **13(1)**: 5-9.
235. Guo, L., et al., *A novel nanosuspension of andrographolide: Preparation, characterization and passive liver target evaluation in rats*. Eur J Pharm Sci, 2017. **104**: 13-22.
236. Launer, P.J. and Arkles, B. *Infrared analysis of organosilicon compounds*. In: Arkles, B. and, Larson, G.L., Editors. Silicon compounds: Silanes & silicones, 3rd ed. Pennsylvania: Gelest Inc; 2013, p. 175-178.
237. Chen, M., Xie, C. and Liu, L., *Solubility of andrographolide in various solvents from (288.2 to 323.2) K*. J Chem Eng Data, 2010. **55(11)**: 5297-5298.
238. Yan, Y., Fang, L.-H. and Du, G.-H. *Andrographolide*. In: Du, G.-H., Editor. Natural small molecule drugs from plants. Shanghai: Springer; 2018, p. 357-362.
239. Teeranachaideekul, V., et al., *Development of ascorbyl palmitate nanocrystals applying the nanosuspension technology*. Int J Pharm, 2008. **354(1-2)**: 227-234.
240. Westen, T.V. and Groot, R.D., *Effect of temperature cycling on Ostwald ripening*. Cryst Growth Des, 2018. **18(9)**: 4952-4962.
241. Hong, J., et al., *High drug payload curcumin nanosuspensions stabilized by mPEG-DSPE and SPC: in vitro and in vivo evaluation*. Drug Deliv, 2017. **24(1)**: 109-120.
242. Kim, H.Y., et al., *Paclitaxel-incorporated nanoparticles using block copolymers composed of poly(ethylene glycol)/poly(3-hydroxyoctanoate)*. Nanoscale Res Lett, 2014. **9(1)**: 525.
243. Wang, J., et al., *Bufalin inhibits HCT116 colon cancer cells and its orthotopic xenograft tumor in mice model through genes related to apoptotic and PTEN/AKT pathways*. Gastroenterol Res Pract, 2015. **2015**: 457193.



APPENDIX

APPENDIX A

1. Standard curve for determination of 3A.1 concentration

Method : HPLC analysis
 Analytical column : Phenomenex[®] C18 column; 5 μ m particle size; 250 \times 4.6 mm
 Mobile phase : Methanol:water (80:20, v/v)
 Flow rate : 1.0 mL/min
 UV-Visible detector : 219 nm

Table A.1 Peak area and retention of 3A.1

3A.1 concentration (μ g/mL)	Retention time (min)	Peak area (mAu)
10	25.4370	472.8529
50	25.2940	2295.1702
100	25.1160	4678.8403
150	25.1860	7112.4546
200	25.0090	9444.8203

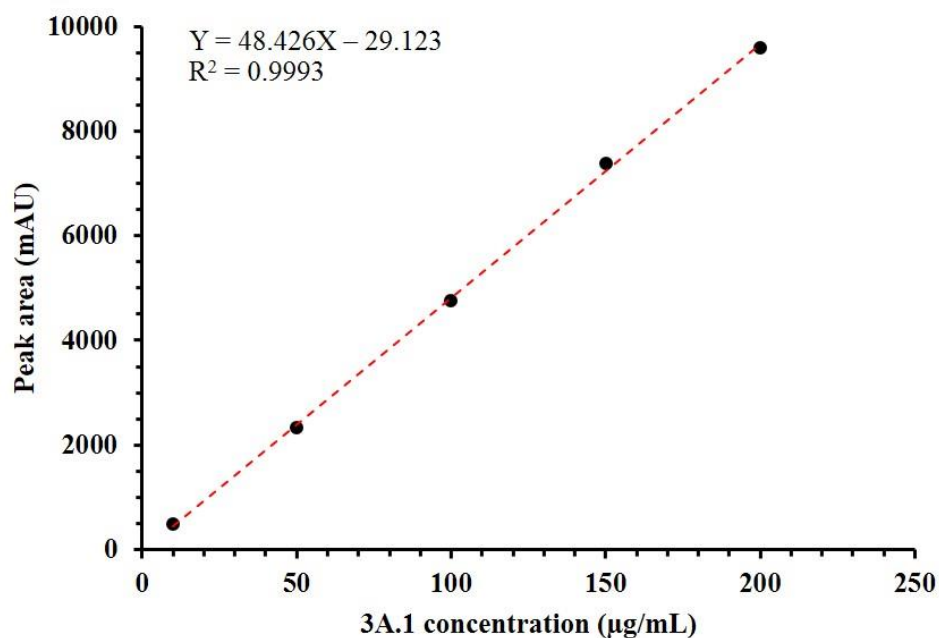


Figure A.1 Standard curve of 3A.1 analogue, when X and Y refer to 3A.1 concentration and peak area, respectively.

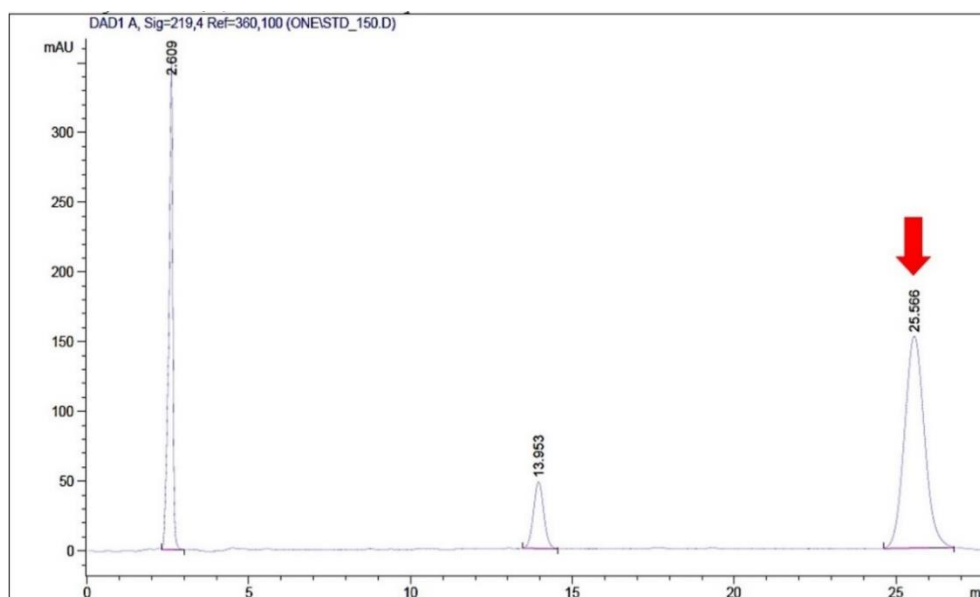


Figure A.2 HPLC chromatogram of 3A.1. Its retention time was around 25-26 min.

2. Standard curve for determination of doxorubicin concentration

Method : Fluorescence spectrophotometry

Excitation/emission wavelength : 470/550 nm

Table A.2 Fluorescent intensity of 3A.1

DOX concentration ($\mu\text{g/mL}$)	Fluorescent intensity
0.50	201.11
1.00	376.52
1.50	556.03
2.00	731.87
2.50	931.64

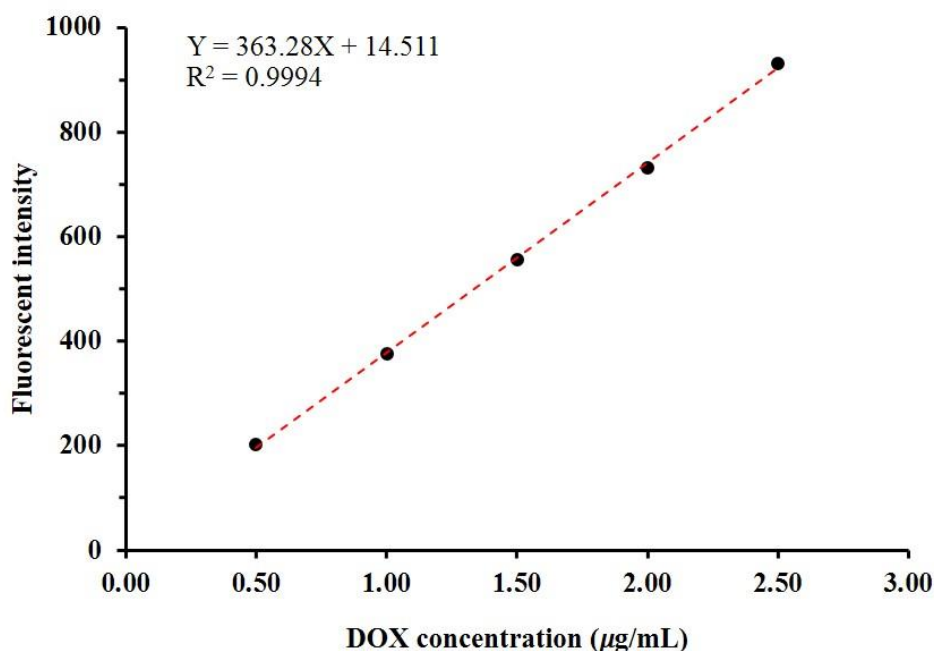


Figure A.3 Standard curve of doxorubicin, when X and Y refer to doxorubicin concentration and fluorescent intensity, respectively.

3. Preparation of solutions

Phosphate-buffered saline (1x PBS, pH 7.4)

For preparation of 1000 mL of PBS (1x), add these chemicals into approximately 800 mL of ultra-purified water under vigorous stirring;

Ingredient	Final concentration (mM)	Amount (g/L)
NaCl (58.44 g/mol)	137.00	8.00
KCl (74.55 g/mol)	2.68	0.20
Na ₂ HPO ₄ (141.96 g/mol)	10.14	1.44
KH ₂ PO ₄ (136.09 g/mol)	1.47	0.24

The pH of buffer solution was adjusted to 7.4 with diluted HCl or NaOH. Then, added water to a total volume of 1000 mL in a beaker, dispensed the solution into a glass bottle and was sterilized by autoclaving (20 min, 121°C, 15 pound per square inch on liquid cycle). The PBS (pH 7.4) is stored at room temperature.

10% Neutral buffered formalin (NBF)

The NBF as a histological fixation solution, was used to fix the animal tissues. First, the formalin was poured into a beaker to mix with 800 mL of ultra-purified water, then dissolved salts to obtain clear solution and made the total volume of buffer to 1000 mL with water. The NBF solution is stored at room temperature.

Ingredient	Amount (unit/L)
Formalin (38 % w/w CH ₂ O in water)	100.0 mL
NaH ₂ PO ₄ (monobasic)	6.5 g
KH ₂ PO ₄ (dibasic)	4.0 g

Preparation of cell culture media

DMEM medium powder and 2.2 g of NaHCO₃ was dissolved in 1000 mL of sterile water for irrigation in a 1000 mL glass beaker and was then adjusted pH solution to pH 7.4 by NaOH or HCl solution. The solution was filtered through 0.22 µm membrane filter set. The medium was supplemented with fetal bovine serum (FBS) and penicillin-streptomycin antibiotics.

Preparation of MTT solution

For preparation of 50 mL of 5 mg/mL of MTT solution, weighed 250 mg (0.25 g) of MTT powder into a plastic tube, added PBS pH 7.4 solution until the final volume reach 50 mL, mixed by vortexing or sonication until completely dissolved and obtained yellow solution. Finally, the solution was filtered through 0.22 µm membrane filter into an amber glass container. Once prepared, the MTT solution can be stored for 4 weeks at 4°C protected from light while the MTT solution will be stable at -20°C for at least 6 months.

APPENDIX B

Table B.1 Entrapment efficiency of 3A.1 into polymeric micelles based on different amphiphilic chitosan derivatives with initial drug to polymer (5-40%) prepared by a dropping method.

Amphiphilic CS derivatives	3A.1 to polymer (%)	%Entrapment efficiency			Average	SD
		n1	n2	n3		
NSC	0	-	-	-	-	-
	5	50.24	46.76	43.84	46.95	2.62
	10	56.45	57.60	58.41	57.49	0.80
	20	60.84	75.70	81.22	72.59	8.61
	40	97.34	80.43	94.74	90.84	7.43
OSC	0	-	-	-	-	-
	5	43.45	36.20	40.56	40.07	2.98
	10	53.32	50.65	53.32	52.43	1.26
	20	86.58	79.47	74.35	80.13	5.01
	40	93.01	90.96	82.43	88.80	4.58
BSC	0	-	-	-	-	-
	5	45.36	40.85	38.65	41.62	2.79
	10	55.67	46.76	48.90	50.44	3.80
	20	76.33	72.14	70.72	73.06	2.38
	40	68.76	68.82	65.80	67.79	1.41

Table B.2 Loading capacity of 3A.1 into polymeric micelles based on different amphiphilic chitosan derivatives with initial drug to polymer (5-40%) prepared by a dropping method.

Amphiphilic CS derivatives	3A.1 to polymer (%)	Loading capacity ($\mu\text{g}/\text{mg}$)			Average	SD
		n1	n2	n3		
NSC	0	-	-	-	-	-
	5	25.12	23.38	21.92	23.47	1.31
	10	56.45	57.60	58.41	57.49	0.80
	20	121.68	151.40	162.44	145.17	17.21
	40	389.36	321.72	378.96	363.35	29.74
OSC	0	-	-	-	-	-
	5	21.73	18.10	20.28	20.04	1.49
	10	53.32	50.65	53.32	52.43	1.26
	20	173.16	158.94	148.70	160.27	10.03
	40	372.04	363.84	329.72	355.20	18.33

	0	-	-	-	-	-
	5	22.68	20.43	19.33	20.81	1.40
BSC	10	55.67	46.76	48.90	50.44	3.80
	20	152.66	144.28	141.44	146.13	4.76
	40	275.04	275.28	263.20	271.17	5.64

Table B.3 The percentage of 3A.1 release from 3A.1-loaded polymeric micelles in SGF (pH 1.2) for 2 h and then changed to SIF (pH 6.8) to 6 h followed by in SCF (pH 7.4) for 4 h.

Formulations	Time (h)	pH	%Drug release			Average	SD
			n1	n2	n3		
Free 3A.1	0.5	1.2	0.00	0.00	0.00	0.00	0.00
	1	1.2	0.00	0.00	0.00	0.00	0.00
	2	1.2	0.00	0.00	0.00	0.00	0.00
	4	6.8	0.00	0.00	0.00	0.00	0.00
	6	6.8	0.00	0.00	0.00	0.00	0.00
	8	6.8	0.00	0.00	0.00	0.00	0.00
	10	7.4	0.00	0.00	0.00	0.00	0.00
	12	7.4	0.00	0.00	0.00	0.00	0.00
	3A.1 NSC PMs	0.5	1.2	0.00	0.00	0.00	0.00
1		1.2	0.00	0.00	0.00	0.00	0.00
2		1.2	0.00	0.00	0.00	0.00	0.00
4		6.8	78.66	83.76	83.88	82.10	2.43
6		6.8	74.39	87.69	84.21	82.10	5.63
8		6.8	71.60	83.23	80.78	78.54	5.01
10		7.4	74.18	82.12	81.61	79.30	3.63
12		7.4	77.16	80.80	81.55	79.84	1.92
3A.1 OSC PMs		0.5	1.2	0.00	0.00	0.00	0.00
	1	1.2	0.00	0.00	0.00	0.00	0.00
	2	1.2	0.00	0.00	0.00	0.00	0.00
	4	6.8	51.84	48.04	56.19	52.03	3.33
	6	6.8	46.13	46.11	52.72	48.32	3.11
	8	6.8	40.93	44.21	46.73	43.96	2.37
	10	7.4	46.01	40.66	47.19	44.62	2.84
	12	7.4	46.35	45.30	48.00	46.55	1.11
	3A.1 BSC PMs	0.5	1.2	0.00	0.00	0.00	0.00
1		1.2	0.00	0.00	0.00	0.00	0.00
2		1.2	0.00	0.00	0.00	0.00	0.00
4		6.8	66.23	62.47	61.53	63.41	2.03

	6	6.8	67.82	60.02	59.15	62.33	3.90
	8	6.8	64.19	57.26	55.39	58.95	3.79
	10	7.4	63.51	55.72	51.07	56.77	5.13
	12	7.4	60.60	53.38	49.81	54.60	4.49
3A.1 Fol-NSC PMs	0.5	1.2	0.00	0.00	0.00	0.00	0.00
	1	1.2	0.00	0.00	0.00	0.00	0.00
	2	1.2	0.00	0.00	0.00	0.00	0.00
	4	6.8	78.15	51.70	35.51	55.12	17.57
	6	6.8	66.47	43.46	41.12	50.35	11.44
	8	6.8	65.83	44.88	41.83	50.85	10.67
	10	7.4	64.07	40.41	43.22	49.23	10.55
	12	7.4	63.75	46.99	46.89	52.55	7.92

Table B.4 The particle size, zeta potential, and relative %drug remaining of 3A.1-loaded polymeric micelles stored at a $5 \pm 3^\circ\text{C}$, $60 \pm 5\% \text{RH}$ (long-term condition) for 6 months.

Formulations	Period time (month)	Particle size (nm)	Zeta potential (mV)	%Drug remaining
3A.1 NSC PMs	0	167.77 ± 11.29	$(-) 30.43 \pm 0.76$	100.00 ± 1.20
	1	154.00 ± 2.36	$(-) 31.13 \pm 0.42$	102.25 ± 1.45
	2	144.10 ± 3.72	$(-) 33.93 \pm 1.73$	100.81 ± 1.56
	4	146.67 ± 3.38	$(-) 31.60 \pm 0.38$	100.91 ± 2.30
	6	144.30 ± 4.50	$(-) 34.73 \pm 1.17$	93.65 ± 2.69
	3A.1 OSC PMs	0	184.50 ± 2.91	$(-) 32.13 \pm 0.41$
1		182.33 ± 8.83	$(-) 29.80 \pm 0.37$	96.91 ± 2.12
2		172.50 ± 1.23	$(-) 30.40 \pm 0.71$	92.84 ± 1.76
4		174.30 ± 1.65	$(-) 28.60 \pm 1.65$	89.12 ± 2.65
6		178.23 ± 3.22	$(-) 26.90 \pm 1.06$	87.22 ± 2.85
3A.1 BSC PMs		0	143.73 ± 2.26	$(-) 32.80 \pm 2.41$
	1	154.80 ± 1.61	$(-) 33.00 \pm 0.22$	101.73 ± 3.09
	2	141.60 ± 1.00	$(-) 34.13 \pm 1.14$	92.95 ± 2.89
	4	140.47 ± 0.58	$(-) 33.07 \pm 0.58$	91.52 ± 2.88
	6	140.60 ± 1.18	$(-) 33.57 \pm 0.83$	85.67 ± 3.15

Table B.5 The particle size, zeta potential, and relative %drug remaining of 3A.1-loaded polymeric micelles stored at $25 \pm 2^\circ\text{C}$, $60 \pm 5\% \text{RH}$ (accelerated condition) for 6 months.

Formulations	Period time (month)	Particle size (nm)	Zeta potential (mV)	%Drug remaining
3A.1 NSC PMs	0	165.77 ± 11.29	(-) 30.43 ± 0.76	100.00 ± 1.30
	1	151.93 ± 1.73	(-) 33.63 ± 1.64	95.58 ± 2.30
	2	150.50 ± 4.69	(-) 31.70 ± 2.71	88.70 ± 2.56
	4	144.00 ± 1.59	(-) 27.97 ± 2.19	89.53 ± 2.64
	6	157.17 ± 5.03	(-) 32.10 ± 2.07	81.64 ± 2.87
3A.1 OSC PMs	0	184.50 ± 2.91	(-) 32.13 ± 0.41	100.00 ± 1.50
	1	162.77 ± 1.99	(-) 26.00 ± 2.19	92.15 ± 2.50
	2	160.50 ± 1.63	(-) 29.40 ± 0.36	76.47 ± 2.87
	4	167.17 ± 4.11	(-) 28.53 ± 1.91	75.02 ± 3.02
	6	182.20 ± 1.69	(-) 32.93 ± 4.72	68.27 ± 3.26
3A.1 BSC PMs	0	143.73 ± 2.26	(-) 32.80 ± 2.41	100.00 ± 1.75
	1	154.30 ± 5.95	(-) 30.60 ± 0.59	85.67 ± 2.80
	2	159.13 ± 0.47	(-) 33.73 ± 0.38	71.61 ± 3.10
	4	153.40 ± 2.65	(-) 28.97 ± 0.52	61.17 ± 3.22
	6	184.60 ± 0.53	(-) 27.47 ± 0.94	53.62 ± 3.36

***In vitro* cytotoxicity of 3A.1-loaded polymeric micelles**

Table B.6 The %cell viability of HT29 exposed by free 3A.1 for 36 h.

Concentration ($\mu\text{g/mL}$)	%Cell viability					Average	SD
	n1	n2	n3	n4	n5		
Control	103.5 4	96.02	97.86	97.80	104.78	100.00	3.48
0.1	95.12	94.28	96.21	93.29	92.64	94.31	1.27
0.3	91.41	84.37	86.03	85.73	77.45	85.00	4.47
0.5	85.79	85.49	85.97	76.20	74.90	81.67	5.01
1	66.50	74.19	72.12	71.06	67.03	70.18	2.97
2	63.78	55.91	58.93	64.84	64.25	61.54	3.52
4	25.14	26.03	26.33	25.44	25.68	25.72	0.42
8	21.89	23.49	22.54	22.54	23.96	22.88	0.74
16	20.89	22.01	21.12	21.71	23.96	21.94	1.09

Table B.7 The %cell viability of HT29 exposed by 3A.1 NSC PMs for 36 h.

Conc. ($\mu\text{g/mL}$)	%Cell viability					Average	SD
	n1	n2	n3	n4	n5		
Control	95.61	105.05	95.85	103.31	100.18	100.00	3.82
0.1	96.75	89.48	79.98	87.49	106.86	92.11	9.10
0.3	92.96	87.91	81.42	99.04	102.16	92.70	7.48
0.5	85.09	89.06	84.13	93.27	83.76	87.06	3.63
1	56.64	58.03	45.76	73.54	54.72	57.74	8.98
2	27.24	27.60	24.41	25.32	26.88	26.29	1.22
4	21.47	21.41	20.20	21.35	21.05	21.09	0.47
8	17.62	20.08	20.32	18.76	20.26	19.41	1.06
16	18.28	18.94	17.20	17.44	18.94	18.16	0.73

Table B.8 The %cell viability of HT29 exposed by 3A.1 OSC PMs for 36 h.

Conc. ($\mu\text{g/mL}$)	%Cell viability					Average	SD
	n1	n2	n3	n4	n5		
Control	106.00	100.31	95.35	98.41	99.94	100.00	3.47
0.1	100.98	93.82	95.65	100.24	121.79	102.50	10.02
0.3	98.04	91.25	85.37	99.63	96.57	94.17	5.23
0.5	100.55	87.39	85.19	82.25	91.49	89.38	6.35
1	50.06	51.04	46.45	47.80	54.65	50.00	2.83
2	47.43	33.72	31.64	33.48	34.94	36.24	5.69
4	30.91	28.03	26.38	30.17	27.42	28.58	1.70
8	24.30	25.95	23.87	23.99	26.07	24.83	0.97
16	24.48	22.89	24.85	25.09	23.26	24.11	0.88

Table B.9 The %cell viability of HT29 exposed by 3A.1 BSC PMs for 36 h.

Conc. ($\mu\text{g/mL}$)	%Cell viability					Average	SD
	n1	n2	n3	n4	n5		
Control	104.70	93.31	105.64	99.78	96.57	100.00	4.70
0.1	103.93	97.57	103.26	97.40	111.17	102.67	5.06
0.3	81.80	86.62	76.77	87.83	96.63	85.93	6.62
0.5	76.33	70.96	73.56	78.48	80.42	75.95	3.38
1	49.45	35.34	55.25	47.35	53.82	48.24	7.06
2	40.60	27.65	32.74	24.06	27.10	30.43	5.80
4	40.60	20.30	19.75	19.03	18.75	23.68	8.47
8	21.85	21.96	20.80	19.75	21.46	21.16	0.82

16	20.74	22.01	20.80	20.35	21.18	21.02	0.56
----	-------	-------	-------	-------	-------	-------	------

Table B.10 The %cell viability of HT29 exposed by 3A.1 Fol-NSC PMs for 36 h.

Conc. ($\mu\text{g/mL}$)	%Cell viability					Average	SD
	n1	n2	n3	n4	n5		
Control	108.59	105.48	101.98	88.38	95.57	100.00	7.24
0.1	99.54	97.29	99.21	93.46	86.99	95.30	4.68
0.3	79.11	88.90	83.75	79.99	96.17	85.59	6.32
0.5	51.25	53.63	53.17	44.58	63.47	53.22	6.06
1	38.90	48.22	44.85	40.95	52.77	45.14	4.99
2	37.85	36.39	34.87	39.96	40.49	37.91	2.12
4	29.59	25.23	25.56	22.79	25.17	25.67	2.20
8	25.43	24.24	23.18	21.14	21.40	23.08	1.64
16	24.17	22.13	21.07	21.73	20.74	21.97	1.21

Table B.11 The half-maximal inhibitory drug concentration (IC_{50}) of free 3A.1 and 3A.1-loaded polymeric micelles against HT29 for 36 h.

Treatments	IC_{50} value ($\mu\text{g/mL}$)			Average	SD
	n1	n2	n3		
Free 3A.1	4.253	3.336	3.860	3.816	0.376
3A.1 NSC PMs	0.986	0.963	1.123	1.024	0.071
3A.1 OSC PMs	0.568	0.700	0.811	0.693	0.099
3A.1 BSC PMs	0.539	0.507	0.568	0.538	0.025
3A.1 Fol-NSC PMs	0.490	0.369	0.376	0.412	0.056

Inhibition of cell migration of 3A.1-loaded polymeric micelles

Table B.12 The rate of HN22 cell migration calculated from scratch assay.

Treatments	Cell migration rate ($\mu\text{m/h}$)			Average	SD
	n1	n2	n3		
Control	38.21	36.28	41.64	38.71	2.22
0.1% DMSO	38.31	35.03	41.08	38.14	2.47
Free 3A.1	17.71	13.68	19.82	17.07	2.55
3A.1 NSC PMs	12.07	8.75	12.60	11.14	1.70
3A.1 OSC PMs	12.16	10.36	14.41	12.31	1.66
3A.1 BSC PMs	13.42	10.89	16.46	13.59	2.28

Table B.13 The percentage of wound closure in HN22 cell calculated from scratch assay.

Treatments	% Wound closure			Average	SD
	n1	n2	n3		
Control	76.56	74.83	82.43	77.94	3.25
0.1% DMSO	76.81	72.76	84.16	77.91	4.72
Free 3A.1	30.25	30.06	33.56	31.29	1.61
3A.1 NSC PMs	20.28	20.07	24.24	21.53	1.92
3A.1 OSC PMs	21.62	20.33	26.75	22.90	2.77
3A.1 BSC PMs	23.74	21.24	28.31	24.43	2.93

Table B.14 The mean fluorescent intensity (MFI) of free Dox and Dox-loaded polymeric micelles in HT29 for 24 h. These values were detected by flow cytometry analysis.

Treatments	Mean fluorescent intensity			Average	SD
	n1	n2	n3		
Control	835	819	705	786.33	57.88
Empty NSC PMs	821	877	733	810.33	59.27
Free Dox	1797	1502	1782	1693.67	135.67
Dox-loaded NSC PMs	1923	2043	2375	2113.67	191.17

APPENDIX C

Table C.1 The percentage of encapsulation efficiency of 3A.1 into liposomes with initial drug molar ratios (0-4.0) prepared by thin-film hydration and sonication method.

Formulations	3A.1 (mM)	% EE			Average	SD
		n1	n2	n3		
Con LPs (PC : Chol : DSPE- PEG2000, 10:2:0)	0	-	-	-	-	-
	0.05	57.05	59.28	56.53	57.62	1.19
	1	57.56	60.02	55.55	57.71	1.83
	2	63.24	62.11	61.49	62.28	0.72
	3	48.68	46.86	48.64	48.06	0.85
	4	36.20	35.21	35.45	35.62	0.42
0.125-PEG LPs (PC : Chol : DSPE- PEG2000, 10:2:0.125)	0	-	-	-	-	-
	0.05	71.35	76.32	71.93	73.20	2.22
	1	74.86	78.46	74.77	76.03	1.72
	2	71.17	68.63	67.83	69.21	1.42
	3	57.61	58.21	56.62	57.48	0.66
	4	41.77	41.02	40.75	41.18	0.43
0.25 PEG LPs (PC : Chol : DSPE- PEG2000, 10:2:0.25)	0	-	-	-	-	-
	0.05	80.87	75.37	79.44	78.56	2.33
	1	80.58	73.78	78.83	77.73	2.88
	2	72.56	70.42	72.42	71.80	0.98
	3	61.03	58.64	61.05	60.24	1.13
	4	44.75	45.80	46.01	45.52	0.55
0.50 PEG LPs (PC : Chol : DSPE- PEG2000, 10:2:0.50)	0	-	-	-	-	-
	0.05	70.67	72.65	72.50	71.94	0.90
	1	68.42	71.96	70.91	70.43	1.48
	2	66.64	68.62	69.22	68.16	1.10
	3	59.04	60.37	64.19	61.20	2.18
	4	45.83	46.30	40.80	44.31	2.49

Table C.2 The loading capacity of 3A.1 into liposomes with initial drug molar ratios (0-4.0) prepared by thin-film hydration and sonication method.

Formulations	3A.1 (mM)	% EE			Average	SD
		n1	n2	n3		
Con LPs (PC : Chol : DSPE- PEG2000, 10:2:0)	0	-	-	-	-	-
	0.05	20.36	20.85	20.47	20.56	0.21
	1	41.08	41.57	40.92	41.19	0.28
	2	90.29	90.56	85.88	88.91	2.15
	3	104.24	104.31	100.21	102.92	1.92
	4	103.37	100.07	98.45	100.63	2.05
0.125-PEG LPs (PC : Chol : DSPE- PEG2000, 10:2:0.125)	0	-	-	-	-	-
	0.05	26.07	28.21	25.97	26.75	1.03
	1	51.31	54.35	50.67	52.11	1.61
	2	97.56	94.23	92.85	94.88	1.98
	3	120.80	115.36	118.47	118.21	2.23
	4	114.51	109.57	114.62	112.90	2.36
0.25 PEG LPs (PC : Chol : DSPE- PEG2000, 10:2:0.25)	0	-	-	-	-	-
	0.05	26.65	24.43	26.59	25.89	1.03
	1	53.11	47.21	53.37	51.23	2.84
	2	95.65	90.23	98.07	94.65	3.28
	3	120.68	116.79	119.89	119.12	1.68
	4	117.99	119.38	116.63	118.00	1.12
0.50 PEG LPs (PC : Chol : DSPE- PEG2000, 10:2 0.50)	0	-	-	-	-	-
	0.05	21.63	23.53	20.90	22.02	1.11
	1	41.88	46.58	42.73	43.73	2.04
	2	81.59	86.32	82.44	83.45	2.06
	3	108.45	114.64	114.14	112.41	2.81
	4	112.22	119.53	115.80	115.85	2.98

Table C.3 The percentage of 3A.1 release from 3A.1-loaded liposomes in PBS (pH 7.4) for 24 h.

Formulations	Time (h)	%Drug release			Average	SD
		n1	n2	n3		
Free 3A.1	0.5	84.31	85.56	89.39	86.42	2.16
	1	90.00	92.33	95.32	92.55	2.18
	2	90.05	94.58	96.51	93.71	2.71
	4	92.98	96.62	97.26	95.62	1.88

	8	96.12	97.25	100.37	97.91	1.80
	12	97.26	98.24	100.50	98.67	1.36
	24	99.59	99.01	100.90	99.83	0.79
	0.5	37.04	33.32	36.26	35.54	1.60
	1	54.21	47.53	53.24	51.66	2.95
	2	84.76	79.85	84.63	83.08	2.28
3A.1-Con LPs	4	86.84	95.17	88.65	90.22	3.58
	8	91.38	96.74	95.01	94.38	2.23
	12	94.40	98.43	97.85	96.89	1.78
	24	100.42	98.05	100.05	99.51	1.04
	0.5	31.24	33.21	27.68	30.71	2.29
	1	41.56	44.13	38.05	41.25	2.49
	2	55.47	60.02	52.19	55.89	3.21
3A.1-0.125 PEG LPs	4	65.72	72.12	62.13	66.66	4.13
	8	71.01	74.41	67.19	70.87	2.95
	12	74.41	77.11	69.21	73.58	3.28
	24	76.18	80.91	72.52	76.54	3.43
	0.5	24.21	18.42	19.18	20.60	2.57
	1	36.54	31.35	32.14	33.34	2.28
	2	54.55	47.53	49.67	50.58	2.94
3A.1-0.25 PEG LPs	4	60.85	56.25	58.44	58.51	1.88
	8	67.72	61.67	64.04	64.48	2.49
	12	69.22	64.51	65.91	66.55	1.97
	24	71.53	65.04	66.42	67.66	2.79
	0.5	28.21	26.18	22.21	25.53	2.49
	1	41.54	38.71	36.35	38.87	2.12
	2	55.33	53.22	50.12	52.89	2.14
3A.1-0.50 PEG LPs	4	63.52	61.91	57.25	60.89	2.66
	8	70.62	68.21	66.38	68.40	1.74
	12	73.57	71.76	67.25	70.86	2.66
	24	75.68	73.28	70.35	73.10	2.18

Table C.4 The vesicle size, zeta potential, and relative %drug remaining of 3A.1-loaded liposomes stored at a $5 \pm 3^\circ\text{C}$, $60 \pm 5\% \text{RH}$ (long-term condition) for 6 months.

Formulations	Period time (month)	Vesicle size (nm)	Zeta potential (mV)	%Drug remaining
3A.1-Con LPs	0	143.77 ± 4.35	(-) 8.35 ± 0.76	100.00 ± 5.71
	1	140.97 ± 1.38	(-) 8.08 ± 0.49	94.62 ± 1.81
	2	146.10 ± 2.65	(-) 7.96 ± 0.58	91.88 ± 1.45
	4	157.40 ± 5.35	(-) 7.23 ± 0.98	88.62 ± 2.74
	6	167.87 ± 6.75	(-) 6.74 ± 0.72	84.27 ± 2.77
3A.1-0.25PEG LPs	0	115.33 ± 3.08	(-) 14.43 ± 0.74	100.00 ± 3.43
	1	117.65 ± 3.83	(-) 14.73 ± 0.80	96.43 ± 1.32
	2	121.53 ± 2.71	(-) 14.57 ± 1.08	94.36 ± 1.46
	4	127.79 ± 4.12	(-) 13.22 ± 0.98	90.42 ± 1.42
	6	134.45 ± 4.53	(-) 12.83 ± 1.21	89.13 ± 1.53

Table C.5 The vesicle size, zeta potential, and relative %drug remaining of 3A.1-loaded liposomes stored at $25 \pm 2^\circ\text{C}$, $60 \pm 5\% \text{RH}$ (accelerated condition) for 6 months.

Formulations	Period time (month)	Vesicle size (nm)	Zeta potential (mV)	%Drug remaining
3A.1-Con LPs	0	143.77 ± 4.35	(-) 8.35 ± 0.76	100.00 ± 5.71
	1	174.86 ± 4.86	(-) 7.44 ± 0.56	70.24 ± 4.33
	2	198.53 ± 5.73	(-) 7.65 ± 1.67	62.63 ± 4.62
	4	267.73 ± 5.84	(-) 7.04 ± 0.85	58.04 ± 5.41
	6	323.54 ± 7.57	(-) 6.73 ± 1.80	54.37 ± 5.27
3A.1-0.25PEG LPs	0	115.33 ± 3.08	(-) 14.43 ± 0.74	100.00 ± 3.43
	1	125.46 ± 4.05	(-) 13.51 ± 0.85	75.38 ± 3.72
	2	136.58 ± 4.39	(-) 13.10 ± 0.94	70.53 ± 3.64
	4	151.83 ± 4.91	(-) 12.68 ± 0.83	65.85 ± 4.11
	6	179.96 ± 5.12	(-) 11.72 ± 1.11	60.38 ± 4.28

In vitro* cytotoxicity of 3A.1-loaded liposomes against HCT116*Table C.6** The %cell viability of HCT116 exposed by free 3A.1 for 24 h.

Conc. ($\mu\text{g/mL}$)	%Cell viability					Average	SD
	n1	n2	n3	n4	n5		
Control	95.10	99.88	103.61	104.78	96.62	100.00	3.78
0.1	98.48	104.55	93.12	100.47	97.90	98.90	3.71
0.3	97.09	95.22	87.18	92.89	96.04	93.68	3.53
0.5	88.00	90.09	83.80	88.34	87.06	87.46	2.08
1	63.87	73.19	69.00	74.83	66.67	69.51	4.05
2	58.62	61.31	60.37	62.24	61.66	60.84	1.26
4	48.48	49.18	49.30	50.35	46.04	48.67	1.45
8	34.73	24.24	25.17	26.69	26.46	27.46	3.74
16	16.90	18.76	19.58	17.37	16.55	17.83	1.15

Table C.7 The %cell viability of HCT116 exposed by 3A.1-Con LPs for 24 h.

Conc. ($\mu\text{g/mL}$)	%Cell viability					Average	SD
	n1	n2	n3	n4	n5		
Control	101.80	95.79	102.78	99.83	99.80	100.00	2.40
0.1	104.11	105.80	95.01	90.23	100.31	99.09	5.78
0.3	97.59	101.73	93.25	101.36	99.56	98.70	3.10
0.5	93.89	95.79	95.18	94.57	95.08	94.90	0.64
1	87.85	87.82	84.90	93.82	82.83	87.44	3.71
2	74.41	76.45	78.55	84.63	80.32	78.87	3.49
4	36.21	38.62	42.35	39.12	38.95	39.05	1.96
8	18.60	13.91	13.13	12.01	10.35	13.60	2.77
16	5.87	6.18	6.04	6.18	6.24	6.10	0.13

Table C.8 The %cell viability of HCT116 exposed by 3A.1-0.25 PEG LPs for 24 h.

Conc. ($\mu\text{g/mL}$)	%Cell viability					Average	SD
	n1	n2	n3	n4	n5		
Control	100.38	97.84	101.17	103.08	97.53	100.00	2.09
0.1	98.40	101.89	93.48	97.45	96.89	97.62	2.70
0.3	91.98	95.39	97.84	92.06	85.95	92.64	4.00
0.5	91.18	96.89	91.34	92.53	83.33	91.06	4.38
1	74.45	76.20	78.81	73.26	74.61	75.47	1.92
2	31.80	35.68	39.25	36.08	38.46	36.25	2.61

4	11.58	10.94	15.78	13.00	14.51	13.16	1.80
8	7.29	7.77	7.45	8.33	7.69	7.71	0.35
16	7.22	7.37	6.82	6.74	6.74	6.98	0.27

Table C.9 The %cell viability of HCT116 exposed by free 3A.1 for 48 h.

Conc. ($\mu\text{g/mL}$)	%Cell viability					Average	SD
	n1	n2	n3	n4	n5		
Control	99.07	91.51	106.86	98.90	103.65	100.00	5.19
0.1	85.58	85.07	90.78	82.31	91.85	87.12	3.62
0.3	78.13	74.40	81.91	74.18	89.48	79.62	5.68
0.5	67.63	65.26	71.30	66.22	70.96	68.27	2.45
1	56.28	55.66	62.21	65.48	63.06	60.54	3.89
2	52.61	51.65	51.54	59.95	59.56	55.06	3.85
4	24.44	25.69	29.98	32.07	32.01	28.84	3.19
8	20.15	22.13	22.92	23.48	22.81	22.30	1.16
16	12.59	13.72	11.91	13.83	12.48	12.91	0.75

Table C.10 The %cell viability of HCT116 exposed by 3A.1-Con LPs for 48 h.

Conc. ($\mu\text{g/mL}$)	%Cell viability					Average	SD
	n1	n2	n3	n4	n5		
Control	102.47	99.78	102.05	93.72	101.99	100.00	3.28
0.1	97.14	100.04	94.82	104.89	95.46	98.47	3.68
0.3	96.30	99.78	100.31	95.56	99.78	98.34	1.99
0.5	84.65	100.57	91.40	91.71	97.51	93.17	5.50
1	82.12	89.66	86.92	88.08	85.55	86.46	2.56
2	68.52	54.40	56.66	47.60	60.98	57.63	6.96
4	32.52	31.36	25.99	32.05	24.67	29.32	3.31
8	9.96	10.75	8.64	7.75	7.48	8.92	1.26
16	4.74	4.69	8.54	4.01	3.64	5.12	1.76

Table C.11 The %cell viability of HCT116 exposed by 3A.1-0.25 PEG LPs for 48 h.

Conc. ($\mu\text{g/mL}$)	%Cell viability					Average	SD
	n1	n2	n3	n4	n5		
Control	101.72	94.01	100.67	102.36	101.25	100.00	3.05
0.1	100.43	96.52	99.44	105.63	97.10	99.82	3.24
0.3	92.61	97.40	99.21	99.96	91.50	96.14	3.45

0.5	84.02	89.98	98.39	98.04	89.10	91.91	5.54
1	68.78	68.20	76.08	66.86	71.59	70.30	3.27
2	27.39	28.90	33.40	28.26	23.65	28.32	3.12
4	20.32	20.09	24.41	21.72	17.98	20.90	2.12
8	13.90	17.05	17.23	12.03	12.79	14.60	2.16
16	6.54	5.61	8.64	7.12	10.28	7.64	1.65

Table C.12 The half-maximal inhibitory drug concentration (IC_{50}) of free 3A.1 and 3A.1-loaded liposomes against HCT116 for 24 h.

Treatments	IC_{50} value ($\mu\text{g/mL}$)			Average	SD
	n1	n2	n3		
Free 3A.1	3.539	3.894	4.103	3.845	0.233
3A.1-Con LPs	2.391	3.325	3.298	3.005	0.434
3A.1-0.25 PEG LPs	1.538	1.553	1.706	1.599	0.076

Table C.13 The half-maximal inhibitory drug concentration (IC_{50}) of free 3A.1 and 3A.1-loaded liposomes against HCT116 for 48 h.

Treatments	IC_{50} value ($\mu\text{g/mL}$)			Average	SD
	n1	n2	n3		
Free 3A.1	2.468	2.262	2.587	2.439	0.134
3A.1-Con LPs	1.256	1.820	1.567	1.548	0.231
3A.1-0.25PEG LPs	1.572	1.221	1.207	1.333	0.169

***In vitro* cytotoxicity of 3A.1-loaded liposomes against HT29**

Table C.14 The %cell viability of HCT116 exposed by free 3A.1 for 24 h.

Conc. ($\mu\text{g/mL}$)	%Cell viability					Average	SD
	n1	n2	n3	n4	n5		
Control	97.53	107.45	98.05	100.31	96.66	100.00	3.92
0.1	97.53	98.75	89.86	95.26	92.82	94.85	3.21
0.3	90.34	92.46	89.35	88.84	90.23	90.24	1.24
0.5	85.39	86.43	83.19	86.34	84.95	85.26	1.18
1	75.93	78.89	79.43	72.10	73.84	76.04	2.83
2	65.43	68.73	65.43	65.43	67.90	66.58	1.44
4	56.32	59.87	54.57	60.34	52.57	56.73	3.00
8	45.11	46.67	42.84	40.58	47.89	44.62	2.63

16	21.94	20.72	20.90	21.94	18.81	20.86	1.15
----	-------	-------	-------	-------	-------	-------	------

Table C.15 The %cell viability of HCT116 exposed by 3A.1-Con LPs for 24 h.

Conc. ($\mu\text{g/mL}$)	%Cell viability					Average	SD
	n1	n2	n3	n4	n5		
Control	94.83	107.20	95.46	100.31	102.19	100.00	4.56
0.1	95.61	92.40	100.00	89.82	102.74	96.12	4.75
0.3	87.24	99.77	94.13	96.08	97.26	94.89	4.24
0.5	91.93	95.22	95.14	89.66	99.14	94.22	3.23
1	90.84	87.47	89.98	85.43	88.96	88.54	1.91
2	77.37	82.93	86.69	76.27	71.18	78.89	5.40
4	51.29	57.40	52.39	58.89	60.38	56.07	3.60
8	40.02	40.41	39.15	41.19	42.52	40.66	1.14
16	19.81	21.06	26.78	30.23	24.90	24.56	3.79

Table C.16 The %cell viability of HCT116 exposed by 3A.1-0.25 PEG LPs for 24 h.

Conc. ($\mu\text{g/mL}$)	%Cell viability					Average	SD
	n1	n2	n3	n4	n5		
Control	105.22	103.58	86.34	111.95	92.91	100.00	9.16
0.1	86.18	90.77	103.82	79.94	96.77	91.50	8.27
0.3	86.67	96.77	93.65	92.17	88.31	91.51	3.64
0.5	88.72	93.40	96.27	80.19	82.24	88.16	6.20
1	75.76	67.22	75.43	70.83	74.61	72.77	3.28
2	43.42	40.13	42.84	42.02	39.72	41.63	1.46
4	39.40	25.11	29.63	31.93	26.67	30.55	5.01
8	29.30	30.94	28.07	25.11	26.02	27.89	2.12
16	14.53	21.26	11.49	15.59	24.54	17.48	4.74

Table C.17 The %cell viability of HCT116 exposed by free 3A.1 for 48 h.

Conc. ($\mu\text{g/mL}$)	%Cell viability					Average	SD
	n1	n2	n3	n4	n5		
Control	95.27	101.30	97.44	99.60	106.39	100.00	3.78
0.1	86.32	84.72	85.38	86.02	84.22	85.33	0.78
0.3	75.20	79.52	74.23	75.51	74.27	75.75	1.95
0.5	66.86	69.80	67.33	65.47	72.42	68.38	2.46
1	59.34	62.80	59.35	58.34	59.25	59.82	1.54

2	50.98	51.73	49.34	57.13	51.73	52.18	2.63
4	27.46	26.34	27.86	25.31	25.37	26.47	1.05
8	19.78	21.48	22.57	20.21	21.02	21.01	0.98
16	14.56	13.67	15.92	14.82	14.56	14.71	0.72

Table C.18 The %cell viability of HCT116 exposed by 3A.1-Con LPs for 48 h.

Conc. ($\mu\text{g/mL}$)	%Cell viability					Average	SD
	n1	n2	n3	n4	n5		
Control	98.23	98.23	100.49	99.98	103.06	100.00	1.78
0.1	91.81	85.76	81.85	103.69	98.02	92.23	7.93
0.3	91.51	77.48	90.90	92.20	99.48	90.31	7.13
0.5	83.54	80.70	90.28	91.89	94.19	88.12	5.13
1	76.87	72.65	72.88	82.00	64.68	73.82	5.69
2	66.29	65.30	58.17	55.56	63.38	61.74	4.17
4	26.52	36.48	37.94	30.73	30.50	32.43	4.20
8	23.68	32.57	29.51	38.01	27.51	30.26	4.83
16	18.78	21.92	21.31	26.75	24.22	22.60	2.70

Table C.19 The %cell viability of HCT116 exposed by 3A.1-0.25 PEG LPs for 48 h.

Conc. ($\mu\text{g/mL}$)	%Cell viability					Average	SD
	n1	n2	n3	n4	n5		
Control	96.31	99.05	98.74	101.86	104.03	100.00	2.68
0.1	89.77	92.73	89.73	92.89	93.84	91.79	1.71
0.3	91.97	93.50	88.89	89.08	94.94	91.68	2.39
0.5	87.18	86.61	85.13	82.35	87.56	85.77	1.90
1	71.81	67.78	72.61	75.28	71.36	71.77	2.41
2	24.08	21.64	20.01	18.11	17.73	20.31	2.35
4	10.23	9.93	8.10	7.68	9.51	9.09	1.01
8	6.73	5.71	4.56	6.28	4.75	5.61	0.84
16	4.34	3.88	3.88	3.96	3.84	3.98	0.18

Table C.20 The half-maximal inhibitory drug concentration (IC_{50}) of free 3A.1 and 3A.1-loaded liposomes against HT29 for 24 h.

Treatments	IC_{50} value ($\mu\text{g/mL}$)			Average	SD
	n1	n2	n3		
Free 3A.1	3.967	4.217	4.419	4.201	0.185
3A.1-Con LPs	4.322	4.684	3.547	4.184	0.474
3A.1-0.25PEG LPs	1.419	2.009	1.402	1.610	0.282

Table C.21 The half-maximal inhibitory drug concentration (IC_{50}) of free 3A.1 and 3A.1-loaded liposomes against HT29 for 48 h.

Treatments	IC_{50} value ($\mu\text{g/mL}$)			Average	SD
	n1	n2	n3		
Free 3A.1	2.015	2.368	2.238	2.207	0.146
3A.1-Con LPs	1.994	2.231	2.062	2.096	0.100
3A.1-0.25PEG LPs	1.386	1.423	1.277	1.362	0.062

Inhibition of cell migration of 3A.1-loaded liposomes

Table C.22 The rate of HN22 cell migration calculated from scratch assay.

Treatments	Cell migration rate ($\mu\text{m/h}$)			Average	SD
	n1	n2	n3		
Control	23.80	23.94	23.49	23.74	0.19
0.1% DMSO	22.60	22.05	22.83	22.49	0.33
Free 3A.1	18.21	19.21	17.00	18.14	0.90
3A.1-Con LPs	13.21	14.00	11.55	12.92	1.02
3A.1-0.25PEG LPs	11.07	10.95	11.39	11.14	0.19

Table C.23 The percentage of wound closure in HN22 cell calculated from scratch assay.

Treatments	% Wound closure			Average	SD
	n1	n2	n3		
Control	85.98	86.35	84.24	85.52	0.92
0.1% DMSO	84.31	85.41	80.40	83.37	2.15
Free 3A.1	69.89	67.55	72.74	70.06	2.12
3A.1-Con LPs	46.88	47.62	44.62	46.37	1.28
3A.1-0.25PEG LPs	39.57	38.13	40.65	39.45	1.03

Table C.24 The percentage of cell migration in HCT116 calculated from transwell migration assay.

Treatments	No. of cell migration (% of control)			Average	SD
	n1	n2	n3		
Control	104.74	93.52	101.75	100.00	4.74
0.1% DMSO	100.25	96.51	92.02	96.26	3.36
Free 3A.1	65.84	67.33	59.85	64.34	3.23
3A.1-Con LPs	53.12	54.61	51.62	53.12	1.22
3A.1-0.25PEG LPs	50.12	53.87	50.87	51.62	1.62



APPENDIX D

Table D.1 Concentration of 3A.1 into nanosuspensions stabilized by different amphiphilic chitosan derivatives and three surfactants with drug to polymer ratios prepared by a nanoprecipitation method.

CS derivatives	3A.1 to polymer	Drug concentration ($\mu\text{g/mL}$)			Average	SD
		n1	n2	n3		
	0	-	-	-	-	-
NSC	0.8 : 1	439.96	380.09	428.51	416.19	25.95
	1 : 1	545.59	497.01	559.70	534.10	26.85
	1.5 : 1	753.55	728.79	864.11	782.15	58.83
	2 : 1	1018.43	1072.69	1103.46	1064.86	35.15
	0	-	-	-	-	-
OSC	0.8 : 1	184.65	163.83	171.27	173.25	8.61
	1 : 1	289.68	201.79	225.77	239.08	37.09
	1.5 : 1	706.77	812.43	768.93	762.71	43.36
	2 : 1	363.91	285.48	298.64	316.01	34.29
	0	-	-	-	-	-
BSC	0.8 : 1	364.17	194.70	312.10	290.33	70.88
	1 : 1	447.50	432.37	332.98	404.28	50.80
	1.5 : 1	581.00	658.66	621.35	620.33	31.71
	2 : 1	931.58	913.82	951.71	932.37	15.48
Surfactants						
SDS	1.5 : 1	470.99	430.27	501.09	467.45	29.02
Tween [®] 80	1.5 : 1	516.95	485.13	481.27	494.45	15.99
Poloxamer 188	1.5 : 1	55.93	63.11	55.50	58.18	3.49

Table D.2 The percentage of 3A.1 yield into nanosuspensions stabilized by different amphiphilic chitosan derivatives and three surfactants with drug to polymer ratios prepared by a nanoprecipitation method.

CS derivatives	3A.1 to polymer	Drug concentration ($\mu\text{g/mL}$)			Average	SD
		n1	n2	n3		
	0	-	-	-	-	-
NSC	0.8 : 1	79.32	76.45	77.92	77.89	1.17
	1 : 1	76.95	76.90	82.45	78.76	2.60
	1.5 : 1	79.43	76.83	90.37	82.21	5.87

	2 : 1	81.07	73.94	83.00	79.33	3.90
	0	-	-	-	-	-
OSC	0.8 : 1	30.02	36.57	33.97	33.52	2.69
	1 : 1	30.68	42.37	34.11	35.72	4.91
	1.5 : 1	65.36	80.53	77.19	74.36	6.51
	2 : 1	20.64	28.23	22.29	23.72	3.26
	0	-	-	-	-	-
BSC	0.8 : 1	67.95	35.17	57.67	53.60	13.69
	1 : 1	65.99	60.49	49.92	58.80	6.67
	1.5 : 1	58.04	64.39	57.47	59.97	3.14
	2 : 1	72.15	64.17	66.84	67.72	3.31
Surfactants						
SDS	1.5 : 1	43.96	40.16	46.77	43.63	2.71
Tween® 80	1.5 : 1	48.25	45.28	44.92	46.15	1.49
Poloxamer 188	1.5 : 1	5.22	5.89	5.18	5.43	0.33

Table D.3 The solubility of free 3A.1 and 3A.1 nanosuspensions in buffer solution (pH 1.2, 6.8, and 7.4) and distilled water. UP; undetectable peak in HPLC chromatogram

Formulations	Solubility ($\mu\text{g/mL}$) in buffer pH 1.2			Average	SD
	n1	n2	n3		
Bulk 3A.1	UP	UP	UP	-	-
3A.1 NS-NSC	20.12	25.32	27.51	24.32	3.10
3A.1 NS-OSC	16.26	17.35	18.42	17.34	0.88
3A.1 NS-BSC	17.73	17.65	18.22	17.87	0.25
Solubility ($\mu\text{g/mL}$) in buffer pH 6.8					
Bulk 3A.1	UP	UP	UP	-	-
3A.1 NS-NSC	27.32	28.82	29.31	28.48	0.85
3A.1 NS-OSC	20.21	21.42	21.47	21.03	0.58
3A.1 NS-BSC	21.56	22.30	24.37	22.74	1.19
Solubility ($\mu\text{g/mL}$) in buffer pH 7.4					
Bulk 3A.1	UP	UP	UP	-	-
3A.1 NS-NSC	29.35	31.32	30.81	30.49	0.83
3A.1 NS-OSC	22.27	21.45	22.98	22.23	0.63
3A.1 NS-BSC	23.79	25.01	23.75	24.18	0.58
Solubility ($\mu\text{g/mL}$) in distilled water					
Bulk 3A.1	UP	UP	UP	-	-
3A.1 NS-NSC	30.13	29.43	29.04	29.53	0.45
3A.1 NS-OSC	21.37	22.17	23.60	22.38	0.92

3A.1 NS-BSC 23.75 23.85 24.59 24.06 0.37

Table D.4 The particle size, zeta potential, and %drug content of 3A.1 nanosuspensions stored at a $5 \pm 3^\circ\text{C}$, $60 \pm 5\% \text{RH}$ (long-term condition) for 6 months.

Formulations	Period time (month)	Particle size (nm)	Zeta potential (mV)	%Drug yield
3A.1 NS-NSC	0	185.80 ± 1.14	$(-) 32.00 \pm 0.08$	85.39 ± 5.71
	1	189.07 ± 2.41	$(-) 34.10 \pm 1.14$	77.96 ± 0.81
	2	187.30 ± 0.14	$(-) 30.63 \pm 0.31$	77.22 ± 0.45
	4	181.30 ± 0.36	$(-) 31.50 \pm 0.45$	75.68 ± 0.74
	6	181.87 ± 1.53	$(-) 30.67 \pm 1.32$	75.29 ± 0.77
3A.1 NS-OSC	0	232.77 ± 2.83	$(-) 38.77 \pm 1.01$	74.36 ± 4.24
	1	238.00 ± 1.82	$(-) 38.47 \pm 0.42$	67.97 ± 5.94
	2	240.00 ± 1.47	$(-) 38.53 \pm 0.56$	64.88 ± 5.82
	4	264.00 ± 4.06	$(-) 35.80 \pm 0.83$	63.86 ± 5.60
	6	266.77 ± 0.96	$(-) 35.97 \pm 1.05$	62.84 ± 6.20
3A.1 NS-BSC	0	278.37 ± 0.52	$(-) 33.43 \pm 0.52$	60.97 ± 4.55
	1	289.97 ± 2.10	$(-) 36.43 \pm 2.10$	56.74 ± 6.00
	2	306.27 ± 0.56	$(-) 34.47 \pm 0.56$	56.50 ± 6.65
	4	308.47 ± 0.50	$(-) 32.53 \pm 0.50$	55.13 ± 6.48
	6	317.97 ± 0.17	$(-) 30.87 \pm 0.17$	54.34 ± 6.95

Table D.5 The particle size, zeta potential, and %drug content of 3A.1 nanosuspensions stored at $25 \pm 2^\circ\text{C}$, $60 \pm 5\% \text{RH}$ (accelerated condition) for 6 months.

Formulations	Period time (month)	Particle size (nm)	Zeta potential (mV)	%Drug yield
3A.1 NS-NSC	0	185.80 ± 1.14	$(-) 32.00 \pm 0.08$	85.39 ± 5.71
	1	190.53 ± 0.81	$(-) 32.03 \pm 0.52$	74.29 ± 1.05
	2	207.17 ± 1.14	$(-) 32.93 \pm 0.50$	72.26 ± 1.36
	4	209.43 ± 0.92	$(-) 28.83 \pm 1.33$	71.04 ± 1.71
	6	279.57 ± 2.08	$(-) 27.87 \pm 2.22$	69.92 ± 1.46
3A.1 NS-OSC	0	232.77 ± 2.83	$(-) 38.77 \pm 1.01$	74.36 ± 4.24
	1	319.27 ± 44.43	$(-) 32.20 \pm 1.82$	69.68 ± 4.36
	2	391.53 ± 45.74	$(-) 31.73 \pm 1.41$	66.36 ± 4.28

	4	436.17 ± 63.90	(-) 28.50 ± 1.16	62.35 ± 4.08
	6	544.23 ± 55.50	(-) 25.93 ± 1.19	59.56 ± 4.49
3A.1 NS- BSC	0	278.37 ± 0.52	(-) 33.43 ± 0.52	60.97 ± 4.55
	1	299.37 ± 4.33	(-) 34.03 ± 0.42	55.67 ± 5.80
	2	311.60 ± 3.90	(-) 30.40 ± 1.27	54.07 ± 4.97
	4	325.47 ± 6.04	(-) 30.07 ± 0.40	53.13 ± 4.77
	6	479.27 ± 12.51	(-) 28.30 ± 1.57	51.68 ± 4.22

In vitro cytotoxicity of 3A.1 nanosuspensions

Table D.6 The %cell viability of HCT116 exposed by 3A.1 NS-NSC for 24 h.

Conc. (µg/mL)	%Cell viability					Average	SD
	n1	n2	n3	n4	n5		
Control	105.87	103.04	95.00	101.08	95.00	100.00	4.36
0.1	95.58	97.61	82.46	96.85	90.61	92.62	5.64
0.3	85.06	81.18	87.78	82.28	83.50	83.96	2.30
0.5	68.29	73.49	74.48	69.97	68.75	71.00	2.52
1	24.63	29.09	23.42	30.47	38.97	29.32	5.50
2	14.40	22.03	19.37	24.98	15.96	19.35	3.87
4	14.98	17.64	14.92	16.48	17.98	16.40	1.29
8	13.82	15.50	15.03	21.51	17.52	16.68	2.70
16	13.59	14.22	14.80	10.87	14.22	13.54	1.39

Table D.7 The %cell viability of HCT116 exposed by 3A.1 NS-OSC for 24 h.

Conc. (µg/mL)	%Cell viability					Average	SD
	n1	n2	n3	n4	n5		
Control	99.24	101.31	100.54	98.96	99.95	100.00	0.86
0.1	98.69	93.68	91.99	102.62	94.06	96.21	3.90
0.3	90.63	90.57	90.84	85.18	84.63	88.37	2.84
0.5	65.83	67.52	70.52	69.05	71.72	68.93	2.09
1	63.32	57.55	69.26	70.19	64.25	64.92	4.56
2	24.74	28.01	23.05	22.23	24.63	24.53	1.98
4	19.51	25.78	16.84	18.31	19.40	19.97	3.06
8	18.15	14.88	15.48	16.68	17.93	16.62	1.30
16	13.51	13.84	18.80	19.40	16.78	16.47	2.44

Table D.8 The %cell viability of HCT116 exposed by 3A.1 NS-BSC for 24 h.

Conc. ($\mu\text{g/mL}$)	%Cell viability					Average	SD
	n1	n2	n3	n4	n5		
Control	94.89	103.62	95.90	104.18	101.42	100.00	3.89
0.1	98.71	90.43	93.74	96.90	86.16	93.19	4.51
0.3	87.11	94.14	93.29	90.93	89.27	90.95	2.58
0.5	84.96	86.66	86.56	89.02	83.35	86.11	1.89
1	56.50	63.23	63.03	69.15	60.07	62.39	4.17
2	23.99	16.51	18.47	20.62	16.46	19.21	2.84
4	10.94	14.40	14.90	15.00	12.55	13.56	1.58
8	11.39	12.29	12.44	15.20	11.99	12.67	1.32
16	7.28	7.38	8.13	17.01	8.93	9.75	3.68

Table D.9 The %cell viability of HCT116 exposed by 3A.1 NS-NSC for 48 h.

Conc. ($\mu\text{g/mL}$)	%Cell viability					Average	SD
	n1	n2	n3	n4	n5		
Control	99.37	103.74	98.88	103.43	94.59	100.00	3.36
0.1	93.44	87.68	97.09	100.53	85.94	92.94	5.51
0.3	80.86	77.47	81.93	84.34	77.11	80.34	2.74
0.5	60.57	56.73	61.28	63.24	54.01	59.17	3.33
1	22.75	17.13	17.04	19.85	25.24	20.40	3.20
2	11.64	13.47	12.67	10.39	10.03	11.64	1.31
4	12.13	9.41	8.96	7.54	9.68	9.54	1.49
8	12.09	9.10	8.79	7.98	9.90	9.57	1.40
16	6.87	7.36	7.05	6.56	6.51	6.87	0.32

Table D.10 The %cell viability of HCT116 exposed by 3A.1 NS-OSC for 24 h.

Conc. ($\mu\text{g/mL}$)	%Cell viability					Average	SD
	n1	n2	n3	n4	n5		
Control	93.85	98.65	105.69	98.00	103.82	100.00	4.26
0.1	93.05	97.58	98.88	92.54	99.16	96.24	2.87
0.3	88.72	87.32	93.33	84.29	89.23	88.58	2.93
0.5	67.97	63.26	70.91	69.32	72.07	68.71	3.06
1	29.56	27.51	32.54	28.07	31.38	29.81	1.91
2	14.97	17.95	16.74	17.30	19.72	17.34	1.55
4	13.33	13.66	14.50	14.78	13.57	13.97	0.57
8	10.30	10.82	11.42	11.79	9.79	10.82	0.73

16	7.51	8.21	9.28	8.48	9.23	8.54	0.66
----	------	------	------	------	------	------	------

Table D.11 The %cell viability of HCT116 exposed by 3A.1 NS-BSC for 48 h.

Conc. ($\mu\text{g/mL}$)	%Cell viability					Average	SD
	n1	n2	n3	n4	n5		
Control	101.93	102.42	106.19	94.35	95.11	100.00	4.56
0.1	96.97	98.39	93.02	102.69	94.84	97.18	3.30
0.3	80.74	91.38	86.95	85.79	88.32	86.64	3.49
0.5	66.73	64.96	65.00	76.48	60.08	66.65	5.39
1	22.97	25.45	19.82	24.78	20.79	22.76	2.19
2	14.41	13.83	14.23	16.18	12.55	14.24	1.17
4	9.89	10.06	8.51	8.29	8.20	8.99	0.81
8	9.58	8.38	7.67	8.11	7.80	8.31	0.68
16	4.70	12.77	6.16	12.64	5.59	8.37	3.57

Table D.12 The half-maximal inhibitory drug concentration (IC_{50}) of free 3A.1 and 3A.1-nanosuspensions against HCT116 for 24 h.

Treatments	IC_{50} value ($\mu\text{g/mL}$)			Average	SD
	n1	n2	n3		
Free 3A.1	3.539	3.894	4.103	3.845	0.233
3A.1 NS-NSC	0.654	0.668	0.707	0.676	0.022
3A.1 NS-OSC	0.998	1.000	1.041	1.013	0.020
3A.1 NS-BSC	1.153	1.148	1.128	1.143	0.011

Table D.13 The half-maximal inhibitory drug concentration (IC_{50}) of free 3A.1 and 3A.1-nanosuspensions against HCT116 for 48 h.

Treatments	IC_{50} value ($\mu\text{g/mL}$)			Average	SD
	n1	n2	n3		
Free 3A.1	2.468	2.262	2.587	2.439	0.134
3A.1 NS-NSC	0.563	0.585	0.554	0.567	0.013
3A.1 NS-OSC	0.642	0.666	0.650	0.653	0.010
3A.1 NS-BSC	0.604	0.624	0.619	0.615	0.009

VITA

NAME MR. TEERATAS KANSOM

DATE OF BIRTH 14 October 1990

PLACE OF BIRTH Nakorn Pathom, Thailand

INSTITUTIONS ATTENDED 2015-Present: Doctor of Philosophy, Ph.D. in Pharmaceutical Technology, Faculty of Pharmacy, Silpakorn University, Thailand
2019: Visiting exchange student, Department of Drug Discovery and Development, Harrison School of Pharmacy, Auburn University, Alabama, United States of America.
2009-2014: Bachelor Degree, Doctor of Pharmacy (1st class honors), Pharmaceutical Technology, Faculty of Pharmacy, Silpakorn University, Thailand.

HOME ADDRESS 17 Moo. 8, Huaymonthong, Kampaengsean, Nakorn Pathom, Thailand, 73140

PUBLICATION

1. Teeratas Kansom, Warayuth Sajomsang, Rungnapha Saeeng, Purin Charoensuksai, Praneet Opanasopit, Prasopchai Tonglairoum. Apoptosis induction and antimigratory activity of andrographolide analog (3A.1)-incorporated self-assembled nanoparticles in cancer cells. AAPS PharmSciTech. 2018; 19(7): 3123-3133.
2. Teeratas Kansom, Rungnapha Saeeng, Tanasait Ngawhirunpat, Theerasak Rojanatarata, Prasopchai Tonglairoum, Praneet Opanasopit, Purin Charoensuksai. Effect of semi-synthetic andrographolide analogue-loaded polymeric micelles on HN22 cell migration. Walailak Journal of Science and Technology (WJST). 2018; 17(2), 88-95.
3. Teeratas Kansom, Warayuth Sajomsang, Rungnapha Saeeng, Theerasak Rojanatarata, Tanasait Ngawhirunpat, Prasopchai Patrojanasophon, Praneet Opanasopit. Fabrication and characterization of andrographolide analogue (3A.1) nanosuspensions stabilized by amphiphilic chitosan derivatives for colorectal cancer therapy. J Drug Deliv Sci Tech. 2019; 54: 101287.
4. Teeratas Kansom, Ekachai Dumkliang, Prasopchai Patrojanasophon, Warayuth Sajomsang, Rungnapha Saeeng, Wei Ming Zhu, Praneet Opanasopit. Folate-functionalized amphiphilic chitosan polymeric micelles containing andrographolide analogue (3A.1) for colorectal cancer. Key Engineering Materials. 2019; 819: 15-20.
5. Teeratas Kansom, Warayuth Sajomsang, Arthit

Chairoungdua, Nudchanart Kitcharoen, Prasopchai Patrojanasophon, Praneet Opanasopit. Doxorubicin-loaded N-naphthyl-N,O-succinyl chitosan micelles for colon cancer treatment. Science, Engineering and Health Studies. (In press)

6. Teeratas Kansom and Praneet Opanasopit. Polymeric micelles for tumor targeting, Thai Bulletin of Pharmaceutical Sciences (TBPS), 2019: 14(1), 13-25.

7. Teeratas Kansom and Praneet Opanasopit. Metronomic chemotherapy, Thai Bulletin of Pharmaceutical Sciences (TBPS), 2020: 15(1), 17-30.

AWARD RECEIVED

- The Royal Golden Jubilee (RGJ) Ph.D. Program Scholarship (Grant No. PHD/0077/2558)

- Best poster presentation awards. 9th Thailand Pharmacy Congress : Smart Aging Life & Digital Pharmacy 4.0, 16-17 November 2017, BITEC, Bangkok, Thailand

